Cell cycle heterogeneity as a regulator of epithelial bending during neural tube closure

Katrin Eivindardottir Danielsen

Thesis submitted to University College London for the degree of

Doctor of Philosophy

2016

Newlife Birth Defects Research Centre

UCL Institute of Child Health

London

Declaration

I, Katrin Eivindardottir Danielsen confirm that the work presented in this thesis is my own. Where information has been derived from other sources, I confirm that this has been indicated in the thesis.

K.Danielsen

Abstract

During neurulation, the neural plate bends around the median hinge point (MHP), overlying the notochord. MHP cells spend more time in G1/S-phase of the cell cycle than lateral cells, and this is associated with adoption of a wedged cell shape due to interruption of interkinetic nuclear migration. Clustering of wedge shaped cells in the MHP is suggested to drive midline bending. To determine the mechanism underlying the prolonged cell cycle in the MHP, I examined the mRNA expression of cell cycle inhibitors, and found the cyclin-dependent-kinase-inhibitors (CDKIs), p21, p27 and p57, to be expressed in midline cells. $p21^{-/-}$ mice, which exhibit MHPs, show upregulation of p57 mRNA in midline cells, supporting the hypothesis of a redundant relationship between p21 and p57 during neural plate bending. Detailed cell cycle analysis was performed in $p21^{-/-}$ and $p21^{+/+}$ embryos by sequential injections of two thymidine analogues, IdU and BrdU. $p21^{-/-}$ MHP cells spend significantly less time in S-phase compared to wild-type littermates, suggesting that p21 is responsible for the prolonged S-phase in the MHP. In the absence of p21, S-phase length in the MHP and lateral cells is equivalent. Overexpression of CIP/KIP genes in the midline of cultured embryos did not increase the proportion of basal nuclei, a measure of wedge shaped cells. Electroporation of p57 siRNA abolished p57 mRNA from the neural plate and notochord of $p21^{-/-}$ embryos but did not prevent MHP formation. Collectively, the results indicate that p21 is responsible for the prolongation of S-phase in the MHP but is not necessary for MHP formation. There is possible redundancy between p21 and p57 in the MHP. However, loss of both p21 and p57 is not sufficient to prevent MHP formation. Furthermore, a prolonged S-phase in the midline cells of the neural plate is not necessary for MHP formation.

Acknowledgements

Table of contents

List of Figures

List of tables

Abbreviations

ANOVA	analysis of variance
A-P	anterior-posterior
AS	antisense
BCIP	5-bromo-4-chloro-3-indolyl phosphate
BMP	bone morphogenetic protein
bp	base pair
BrdU	5-bromo-2'-deoxyuridine
cAMP	cyclic adenosine monophosphate
CDK	cyclin dependent kinase
CDKI	cyclin dependent kinase inhibitor
cDNA	complementary DNA
CIP1	Cdk-interacting protein 1
CLE	caudal lateral epiblast
CNH	chordo-neural hinge
C_T	threshold cycle
DAPI	4',6-Diamidino-2-Phenylindole
DEPC	diethyl pyrocarbonate
DIG	digoxygenin
DLHP	dorsolateral hinge point
DMEM	Dulbeco's Modified Eagle Media
DMSO	dimethyl sulphoxide
DNA	deoxyribonucleic acid
DNAse	deoxyribonuclease
dNTPs	deoxynucleotide triphosphates
E	embryonic day
EdU	5-ethynyl-2'-deoxyuridine
Fab	Fragment antigen binding
FBS	fetal bovine serum
GAPDH	glyceraldehyde-3-phosphate dehydrogenase
GFP	green fluorescent protein
GTP	guanosine triphosphate
HCl	hydrogen chloride
HEPES	4-(2-hydroxyethyl)-1-piperazineethanesulfonic acid
HI-SS	heat inactivated sheep serum
IdU	5-iodo-2'-deoxyuridine
IKNM	interkinetic nuclear migration
IP	Intraperitoneal injection
KASH	Klarsicht ANC-1, Syne Homology
kDa	kilodalton
Lat	lateral
LB	Luria Bertani
LHF	late head fold
LIMK	LIM-kinase
MEFs	mouse embryonic fibroblasts
MHP	median hinge point
MT	microtubules

NaOH	sodium hydroxide
NBT	nitro blue tetrazolium chloride
neo	neomycin resistance expression cassette
NMps	neuromesodermal progenitors
NP	neural plate
NSB	node streak border
NTD	neural tube defect
OB	no allantoic bud stage
PBS	phosphate-buffered saline
PBT	phosphate-buffered saline with 0.1% Tween-20
PCNA	proliferating cell nuclear gene
PCP	planar cell polarity
PCR	polymerase chain reaction
Pen/strep	penicillin/streptomycin
PFA	paraformaldehyde
pHH3	phosphohistone H3
pmol	picomol
PNP	posterior neuropore
PS	primitive streak
qRT-PCR	quantitative reverse transcription PCR
Rb	Retinoblastoma
RE	restriction enzyme
RNA	ribonucleic acid
RNA seq	RNA sequencing
RNAi	interference RNA
RNAse	Ribonuclease
ROCK	Rho-kinase
rpm	revolutions per minute
RQ	relative quantification
RT	room temperature
S	sense
SDS	sodium dodecyl sulphate
SEM	standard error of the mean
Shh	Sonic hedgehog
siRNA	small interfering RNA
SS	sheep serum
SSC	saline sodium citrate
SUN	Sad1p Unc84
TBS	tris-buffered saline
TBST	TBS with 1% Triton
TGF β	Transforming growth factor beta
v/v	volume per volume
w/v	weight per volume
WAF1	wild-type p53-activated fragment 1
WISH	whole mount in situ hybridisation

Chapter 1 – General introduction

1.1 Neurulation

Neurulation is the process whereby the future brain and spinal cord are formed in the first 3-4 weeks after fertilisation in humans (Copp et al., 2013; Greene and Copp, 2009). Neural tube defects (NTDs) are a severe group of congenital disorders that arise when neurulation fails and affects approximately 1:1000 established pregnancies worldwide (Copp et al., 2003b; Mitchell, 2005). Neurulation in mice and humans is very similar at the embryonic level (Greene et al., 2009; Greene and Copp, 2009) and as NTD associated genes are discovered in humans, the number of genetic NTD mouse models grows rapidly. To date over 250 genetic mouse mutants have been described (Harris and Juriloff, 2010) in the attempt to find candidate genes for better treatment of NTDs and to improve genetic counselling of people with affected NTD pregnancies.

Neurulation is divided into primary neurulation, which in mice takes place around E8-E10, and secondary neurulation that forms the neural tube at the most caudal region of the spinal cord (Copp et al., 2013). Primary neurulation can further be divided into three distinct morphogenetic events: neural plate shaping, neural fold elevation and neural fold fusion.

1.1.1 Generation of the neural plate

During gastrulation, the embryo transforms from a single layer of pluripotent epithelium to a structure composed of ectoderm, mesoderm and endoderm with the axial organisation of the future embryo (Tzouanacou et al., 2009). In amniote embryos the epiblast comprised of the pluripotent epithelium (Gardner and Rossant, 1979) forms mesoderm and endoderm via ingression through the primitive streak, while surface ectoderm and neurectoderm is formed by cells remaining in the epiblast (Tam and Behringer, 1997). The head and most anterior trunk structures are formed during gastrulation while the embryo continues to elongate

during organogenesis from cells supplied by the posterior neuropore, and later, the tail bud at the caudal end of the embryo (Stern et al., 2006).

The primitive streak (PS) (Figure 1.1, A; white box) in mouse and chick embryos orchestrates much of the early patterning of the embryo during gastrulation (Wilson et al., 2009). Cells of the node streak border (NSB) (Figure 1.1, A; red area), a region comprising the caudal end of the node (Figure 1.1, A; green area) and the rostral 5-10% of the primitive streak (Figure 1.1, A; white box), contribute to the neural tube, somites, and notochord (Cambray and Wilson, 2007) while the neural tube ventral midline is produced by the dorsal part of the node exclusively (Charrier et al., 1999; Selleck and Stern, 1991). Progenitors of the lateral and dorsal neural tube and some somatic tissue are found on either side of the primitive streak in a region known as the caudal lateral epiblast (CLE) (Figure 1.1, A; white circle) (Wilson et al., 2009) with a rostral limit at the NSB, extending caudally to approximately 80% of the primitive streak length in the mouse at the 2-6 somite stage (Cambray and Wilson, 2007). The derivative of the NSB, with a minor contribution from the CLE, is known as the chordo-neural hinge (Figure 1.1, B; CNH) located in the later forming tail bud (TB) rostral to the tail bud mesoderm (TBM) at the junction between notochord (NC) and neural tube (NT). The CNH contains progenitors for the ventral neural tube, somites and notochord (Figure 1.1, B) (Cambray and Wilson, 2007; Wilson et al., 2009). The CNH is continuous with the newly formed neural tube and notochord while somites are produced from the tissue immediately caudal to the CNH (McGrew et al., 2008; Wilson et al., 2009).
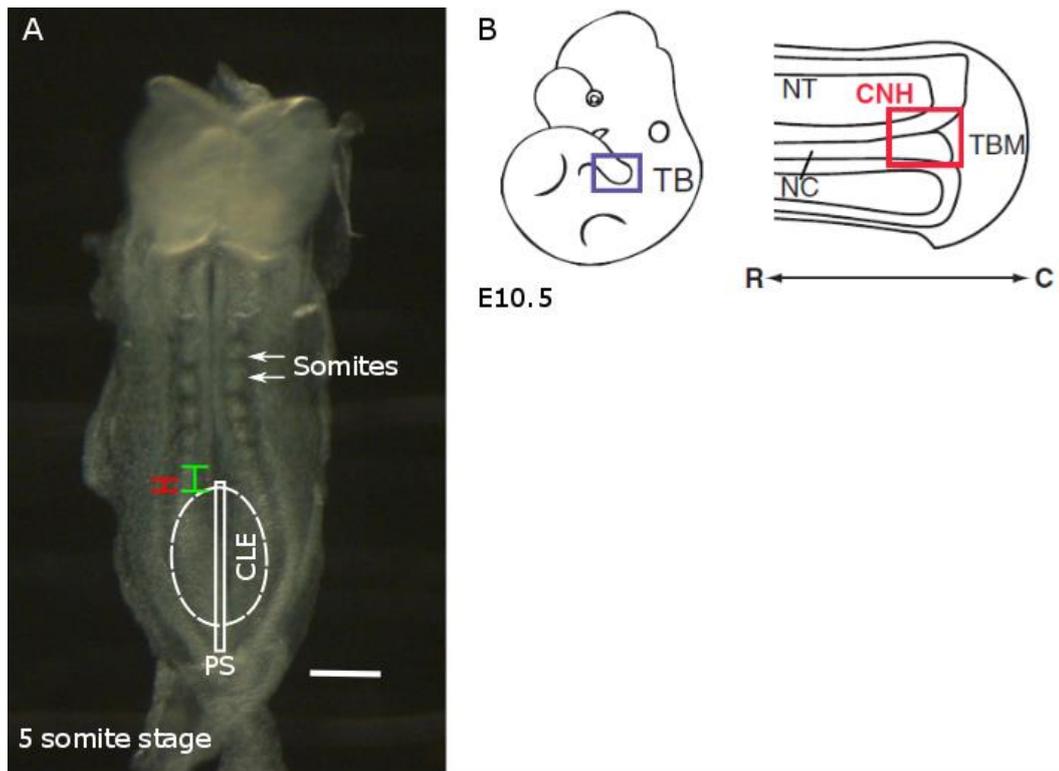
Figure 1.1 - Generation of the neural plate

In the early mouse embryo with 5 somites, the node streak border (red) and caudal lateral epiblast (CLE; white circle) contribute to the spinal cord and the paraxial mesoderm of the extending body axis. The node is shown by the green region and the primitive streak (PS) as the white box (A). At E10.5, the chordo-neural hinge (CNH) has formed with contributions of cells from the NSB and CLE (B). The CNH is situated in the tailbud (TB) rostral to the tail bud mesenchyme (TBM), between the neural tube (NT) and notochord (NC). The CNH contains precursors for the ventral midline from the hindbrain to the tail and the notochord (Henrique et al., 2015; Tzouanacou et al., 2009; Wilson et al., 2009). Figure B is taken from (Wilson et al., 2009). Scale bar = 50 µm.

1.1.2   Neural plate shaping

The first step in primary neurulation is the formation of the neural plate which differentiates from the dorsal midline ectoderm into neuroepithelium. This event is induced by BMP antagonists emanating from the primitive node, underlying the prospective neural plate (Bassuk and Kibar, 2009). Secondly, the neural plate is shaped as it lengthens and narrows. The mechanism behind the shaping is likely to be a combination of the rostro-caudal growth of the embryo and convergent extension movements of cells in the neural plate as they intercalate at the midline, causing the neural plate to converge and extend (Greene and Copp, 2009; Keller,

18

2002). Convergent extension relies on the planar cell polarity (PCP) pathway (Mlodzik, 2002; Zohn et al., 2003) and its importance is highlighted by the severe neural tube defects that arise as a result of the wide neural plate which prevents neural tube closure in several PCP mouse mutants (reviewed by (Greene and Copp, 2009).

1.1.3   Neural fold elevation

The elongated and narrow neural plate undergoes bending as a midline furrow known as the median hinge point (MHP) appears along the rostro-caudal axis in close proximity to the notochord (Figure 1.2). During early neurulation from E8.5 to E9 this is the only point at which the neural plate bends, resulting in the characteristic V-shaped appearance of the neural plate at rostral levels of open neural tube (Figure 1.2 and Figure 1.3, B) while at caudal levels the forming MHP is relatively flat (Figure 1.3, A). At E9, paired dorsolateral hinge points (DLHPs) appear at spinal levels (Figure 1.2; arrowheads) and the neural plate bends around all three hinge points. At the last stage of primary spinal neurulation the MHP is lost and the neural plate bends solely at the DLHPs (Copp et al., 2003b; Greene and Copp, 2009; Shum and Copp, 1996). DLHPs seem necessary for spinal neurulation as mouse embryos with a null mutation in the zinc finger protein Zic2 do not form DLHPs (Ybot-Gonzalez et al., 2007a) and consequently develop fully penetrant and extensive spina bifida (Elms et al., 2003; Nagai et al., 2000). On the other hand, neural tube closure seems to be able to proceed in the absence of MHPs, at least in some mouse models (Greene and Copp, 2009).

In the cranial region, neural plate bending has a slightly different mechanism. During early neurulation the neural folds bend around the MHP as shown in Figure 1.2, but the neural folds then adopt a biconvex appearance where the neural folds face away from the midline before coming together in a biconcave shape in the midline to fuse (Morriss-Kay et al., 1994; Morriss-Kay, 1981). It has been proposed that the convex neural fold elevation is supported by mesenchyme expansion (Morriss-Kay et al., 1986) whereas spinal neural fold elevation is able to proceed in the absence of paraxial mesoderm (Ybot-Gonzalez et al., 2002).
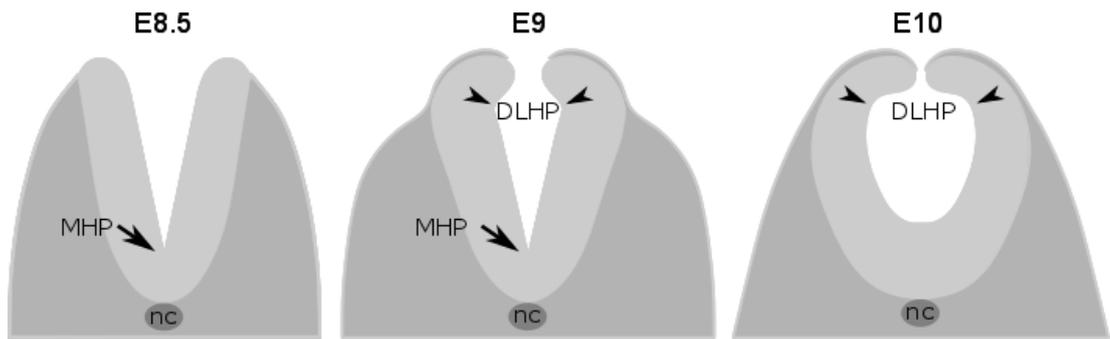
Figure 1.2 - Primary neurulation in the mouse embryo

At E8.5 the neural plate bends around the MHP only (arrows). Later, at E9, paired dorsolateral hinge points (DLHPs; arrowheads) appear and bending occurs at the three hinge points. At the latest stages of primary neurulation the MHP is lost and the neural plate bends solely at the DLHPs. The notochord (nc) is shown in dark grey underlying the MHP.
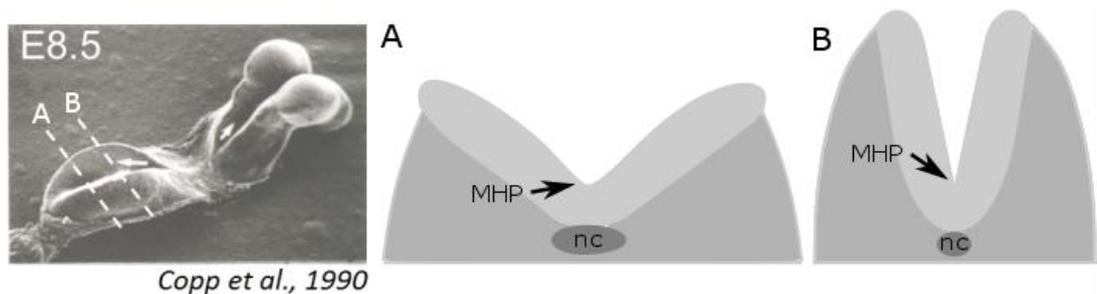
Figure 1.3 - The MHP is flat caudally and sharpens more rostrally

Diagram of transverse sections through the PNP of an embryo at E8.5. At caudal levels the neural plate and the MHP is wide (A). At more rostral levels the MHP is sharp and the neural plate has a V-shaped appearance (B). The notochord (nc) is shown in dark grey.

1.1.4 Neural fold fusion

The last step of primary neurulation is fusion of the neural folds at the dorsal midline. This step seems to depend on cellular protrusions similar to filopodia that extend from the neural fold tips and seem to interdigitate to bring the neural folds into close apposition enabling cell adhesion, remodelling of the epithelia and fusion (Greene and Copp, 2009; Pai et al., 2012; Pyrgaki et al., 2010).

1.1.5 Secondary neurulation

In the tail bud in the caudal region of the embryo, secondary neurulation takes place once primary neurulation is complete. The tail bud hosts a population of stem cells that condense into cell masses and these masses in the dorsal region undergo canalisation whereby the solid neural precursor population is converted into a hollow structure, continuous with the lumen created by primary neurulation (Schoenwolf, 1984). Secondary neurulation thereby creates the lowest part of the spinal cord (Copp et al., 2003b; Copp et al., 2013).

1.1.6 Neural tube closure is a discontinuous event

In the mouse, the first neural tube closure site is observed at the 6-7 somite stage (embryonic day E8.5) at the hindbrain-cervical boundary (closure 1) from where closure propagates bidirectionally to the future brain and spinal cord (Figure 1.4, b) (Copp et al., 2003b; Copp et al., 2013). A second closure is initiated at the forebrain-midbrain boundary (closure 2) approximately 12 hours later and runs in a bidirectional manner, followed by a third closure site (closure 3) which is initiated at the rostral forebrain and proceeds in a caudal direction towards closure 2 (Figure 1.4, c-d) (Copp et al., 2003b; Copp et al., 2013). The open area of elevated neural folds between closures 2 and 3 is called the anterior neuropore and closes up within a few hours, and the open area posterior to closure 1 is called the posterior neuropore (PNP) and has completed closure approximately 48 hours after neurulation has started. Primary neurulation is complete around E10 in the mouse (Copp et al., 2013).

Neurulation in humans is very similar to mouse neurulation (O'Rahilly and Muller, 2002). In the human embryo, neural plate bending is initiated approximately 18 days post-fertilisation at a closure site analogous to closure 1 in mice, although it has been suggested that closure 1 in human embryos is slightly more rostral (Greene and Copp, 2009; O'Rahilly and Muller, 2002). Closure 3 in humans seems to be similar to that of mouse but the presence of a closure 2 site in humans is controversial. Some studies suggest that it exists in humans (Van Allen et al., 1993)

while others do not (O'Rahilly and Muller, 2002). Human cranial neural tube closure is completed by day 25 and PNP closure 26-28 day after fertilisation (Greene and Copp, 2009).
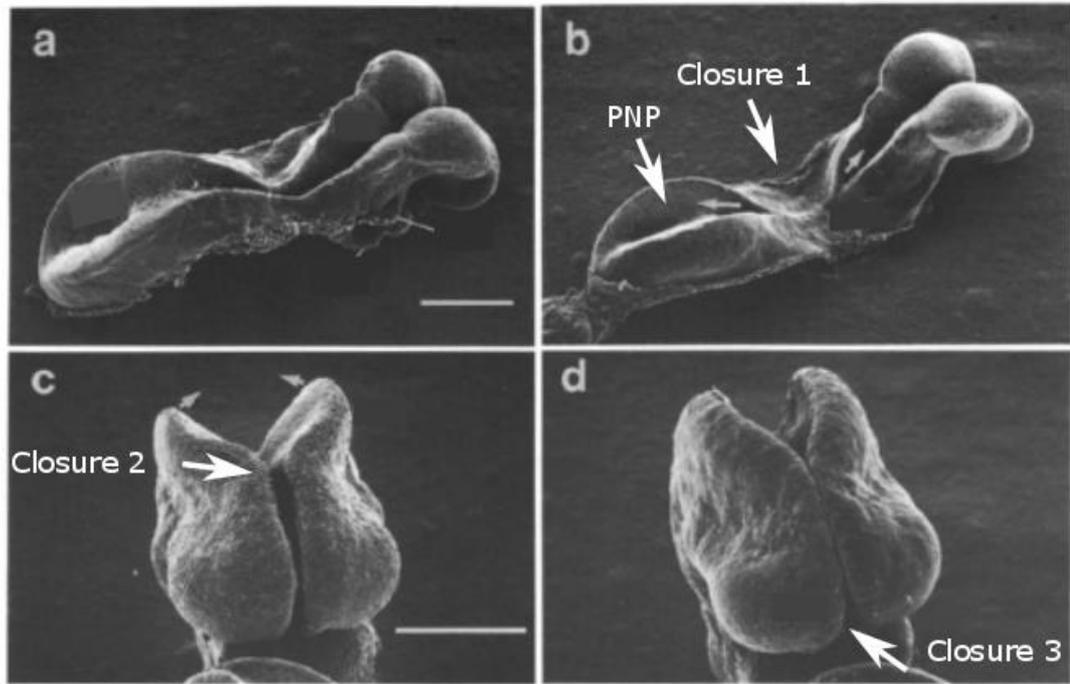
Figure 1.4 - Closure sites during mouse neurulation

Scanning electron micrograph showing the three closure sites in a mouse embryo at E8.5. Closure is initiated at the hindbrain-cervical boundary (b, closure 1) from where closure proceeds bidirectionally. Closure 2 is at the future forebrain-midbrain boundary (c) and closure 3 is observed last at the rostral limit of the future forebrain (d). The posterior neuropore (PNP) is the open region in the caudal embryo (b, PNP). Adapted from (Copp et al., 1990). Scale bars = 250 μm.

1.2   Neural tube defects

Neural tube defects (NTDs) are the second most common birth defects (Copp et al., 2003b; Mitchell, 2005; Stoll et al., 2011). In humans, NTDs occur between three and four weeks after fertilisation and are the result of failure of all or part of the neural tube to close (Bassuk and Kibar, 2009; Copp, 2005; Copp et al., 2013). Numerous types of NTDs have been described and these can be grouped according to the stage of neurulation that fails.

1.2.1 Closure 1

The most severe NTD, craniorachischisis, results from failure of the neural folds to fuse at closure 1 resulting in an entirely open neural tube from the midbrain to the lower spine (Copp et al., 1994). In mouse mutants with craniorachischisis, closures 2 and 3 are generally unaffected (Greene et al., 1998; Murdoch et al., 2003). This is similar to what is seen in human cases and suggests that craniorachischisis in mice closely resembles the condition in humans (Greene and Copp, 2009). Craniorachischisis is not commonly observed in mice as most embryos with NTDs undergo closure 1 successfully with subsequent failure of neurulation in the cranial or rostral region (Copp et al., 2013; Harris and Juriloff, 2010). In fact, from the approximately 250 mouse mutant strains that develop NTDs, only 14 have been reported to develop craniorachischisis (Harris and Juriloff, 2010), suggesting that closure 1 might be a relatively robust event.

Failure of closure 1 to proceed caudally in the spinal region leads to open spina bifida. The two main forms are myelomeningocele where the neural tissue is covered by a meninges-sac, and myelocele where the neural tissue is exposed to the amniotic fluid (Greene and Copp, 2009). Spina bifida is generally compatible with postnatal survival and the severity depends on the axial level at which neurulation stops. Spina bifida can lead to neurological impairment below the lesion, including inability to walk, incontinence, and lack of sensation (Copp et al., 2013). Furthermore, spina bifida is associated with secondary disorders such as hydrocephalus, vertebral deformities and genitourinary and gastrointestinal disorders (Copp et al., 2013).

1.2.2 Closures 2 and 3

Failure of the neural tube to close in the cranial region at closure 2, or failure in the rostral zippering leads to exencephaly where the neural folds remain open and exposed to the amniotic environment. Exencephaly progresses into anencephaly as gestation proceeds and the neural tissue is degenerated by amniotic fluid due to failure of the skull vault to form (Copp et al., 2003b; Greene and Copp, 2009).

Closure defects in the rostral forebrain (closure 3) lead to forebrain anencephaly which is often accompanied by a split phase phenotype (Copp et al., 2003b).

1.2.3 Secondary neurulation defects

NTDs can also arise as a result of incomplete secondary neurulation in the form of closed spina bifida. In this case the neural tube fails to separate from surrounding tissues in the tail bud, leading to tethering of the spinal cord and possible neural damage as the body axis elongates at a different rate than the spinal cord (Greene and Copp, 2009).

1.2.4 Aetiology of NTDs

The aetiology of NTDs is complex and multifactorial. Several genes have been identified that are associated with NTDs and over 250 genetic NTD mouse models are available (Harris and Juriloff, 2010). Among these mouse mutants roughly 80% exhibit cranial defects and only 20% spina bifida (Harris and Juriloff, 2010), suggesting that cranial neurulation is more sensitive to insults compared to the spinal region. This could reflect the more complex mode of closure.

In support of a genetic aspect of NTDs, humans have an increased recurrence risk for siblings: 2-5% compared to 0.1% for the general population. Furthermore, women who have had two or more affected pregnancies have a recurrence risk of approximately 10% (Copp et al., 2013). Environmental factors associated with NTDs include valproic acid, which when taken in pregnancy increases the risk of NTDs (Lammer et al., 1987), maternal diabetes, maternal obesity and a high temperature during pregnancy (reviewed by Copp et al., 2013).

1.3 MHP formation

During neurulation, the early neural plate midline and MHP is formed by cells originating from the node region in the caudal region of the embryo (Patten et al., 2003; Placzek and Briscoe, 2005) and is in close proximity to the underlying

notochord. Although spinal neural tube closure can proceed in the absence of MHPs in some notochord ablated embryos (Ybot-Gonzalez et al., 2002) and at the latest stages of spinal neurulation by bending at DLHPs, the MHP has been shown to be important for cranial neural tube closure in the chick (Eom et al., 2011) and for the positioning of the midline and in establishing a normal morphology of the neural tube (Schoenwolf, 1988; Smith et al., 1994).

The MHP is distinct from the lateral non-bending regions by its cell shape composition. Cells of the MHP are mainly wedge shaped, i.e. are wide at their base, compared to lateral regions of the neural plate where three main cell shapes are found at roughly equal ratios: wedge shaped, spindle shaped (widest in the middle) and inverted wedge shaped (widest at the apex) (Figure 1.5, nuclei in blue) (McShane et al., 2015; Schoenwolf and Franks, 1984). In the flat neural plate, the cell shape composition of the prospective MHP is indistinguishable from the lateral neural plate and the increase in the proportion of wedge shaped cells coincides with midline bending (McShane et al., 2015; Schoenwolf and Franks, 1984; Smith et al., 1994). It has been shown that the position of the nucleus is responsible for the shape of a neuroepithelial cell (Schoenwolf and Franks, 1984). This was originally shown by measuring the greatest diameter of neuroepithelial cells from scanning electron micrographs and comparing it to the diameter of neuroepithelial nuclei from light micrographs. The only place in the cell that was wide enough to accommodate the nucleus was the bulbous part (Schoenwolf and Franks, 1984). Today, this can be easily visualised on transverse sections through the neural plate stained with anti-β-catenin, a marker of neuroepithelial cell membranes, and a nuclear stain.
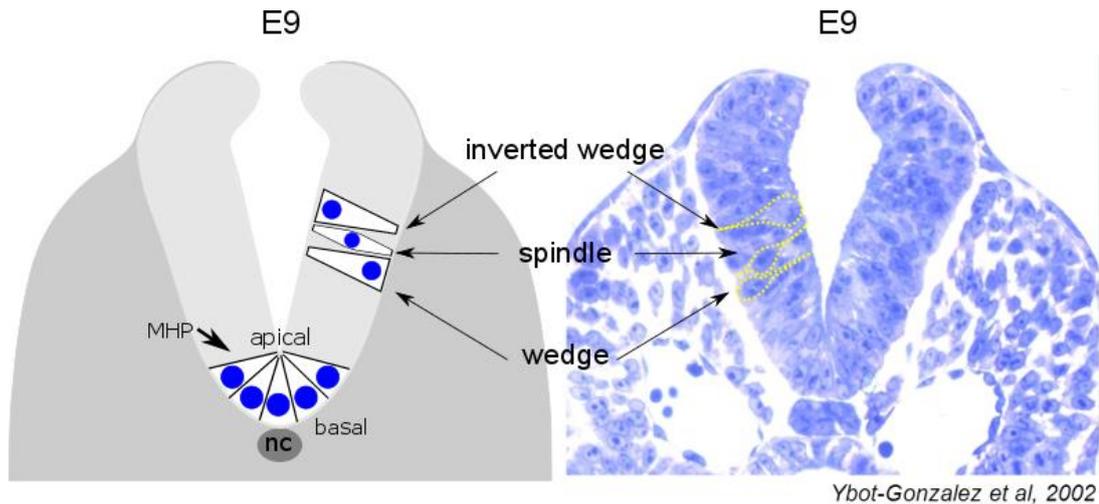
Figure 1.5 - Cell shape composition in the neuroepithelium

In the MHP, the majority of the cells are wedge shaped with basal nuclei (blue) while in the lateral neural folds three cell shapes are found at roughly equal ratios: inverted wedge shaped cells with apical nuclei, spindle shaped cells with nuclei in the centre region of the neuroepithelium, and wedge shaped cells. The notochord (nc) is indicated in dark grey.

It has long been speculated that the cell shape changes in the MHP are important for bending at the neural plate midline and the idea that bending was driven by changes in cell shape was first proposed by Glaser in 1914 (Schoenwolf and Franks, 1984). The question has, however, always been whether MHP cell wedging is an intrinsic process due to apical constriction or basal expansion, or whether it depends on extrinsic forces such as surrounding tissues. Furthermore, are the shape changes the result of neural plate bending, or do the cells change shape in order to cause bending?

1.3.1 Intrinsic forces

1.3.2 Apical constriction

Apical constriction of MHP cells is a popular theory regarding how the cells become wedge shaped. The theory is based on findings by Baker and Schroeder in 1967 (Schoenwolf and Smith, 1990). By transmission electron microscopy, they showed that circumferential microfilament bands were present in the apices of *Hyla regilla*

and *Xenopus laevis* during neural plate bending (Schoenwolf and Smith, 1990). Similar findings were later reported by many other groups in amphibians, birds, mammals, and in the cells of developing systems with similarities to neural tube formation, e.g. optic vesicle and pancreatic bud (reviewed by Schoenwolf and Smith, 1990). The microfilaments found were considered to be contractile, thereby providing force for the bending of the neural plate. Some of the research supporting the theory included the findings that circular bands of apical microfilaments were dense during neural plate bending (Burnside, 1971), that the apical microfilaments were able to bind heavy meromyosin, thereby suggesting actin similar properties (Nagele and Lee, 1980), that active forms of actin, myosin and other contractile proteins were found apically in neuroepithelial cells (Lee et al., 1983; Nagele and Lee, 1980; Sadler et al., 1982), and the fact that calcium, which is required for microfilament contractility, was found in vesicles in the apices of neuroepithelial cells which was released during neurulation (Moran, 1976; Nagele et al., 1981). Furthermore, preventing the release of calcium using papaverine inhibited neural plate bending, while A23187 induced stimulation of calcium transport and release, and accelerated neural plate bending (Moran and Rice, 1976). Later it was shown that Cytochalasin D, which disrupts actin polymerisation, led to neural tube defects in the chick (Schoenwolf et al., 1988). In chick, actin and myosin has been found to be most intense in regions with the highest degree of bending, i.e in the MHP, which coincides with dense packing of microfilaments and highly constricted cell apices (Lee and Nagele, 1985). The intense staining of actin and myosin was seen to decline after neural tube closure (Lee and Nagele, 1985). In the chick midbrain it has more recently been shown that Rho, which regulates actomyosin constriction and cytoskeletal reorganisation, generally accumulates in apices of ectodermal cells where a sheet of columnar cells is bending or invaginating, that actin and activated myosin are slightly more intense in the MHP, and that Blebbistatin, Y27632 and Cytochalasin D all disrupt midline bending of the neural plate (Kinoshita et al., 2008). Mouse embryos treated with the same inhibitors do, however, show normal midline bending during early neurulation (Escuin et al., 2015).

Importantly, cells of the MHP become, and remain, wedge shaped in the absence of microfilaments, and furrowing and bending at the midline proceeds as usual while dorsolateral wedging, furrowing, and neural fold convergence are blocked (Schoenwolf et al., 1988; Ybot-Gonzalez and Copp, 1999). Combined, these studies suggest that there might be a role for microfilaments in neural fold elevation and fusion, while the first events of neurulation: cell wedging, furrowing and bending are independent of microfilaments.

1.3.3   Basal expansion

Basal expansion of neuroepithelial cells is an equally old theory. It was originally thought that the basal expansion observed in neuroepithelial cells resulted from increased water uptake by their bases (Glaser, 1914). Proving this theory was unsuccessful, and when the apical constriction theory came along, the basal expansion theory took a backseat for some decades (Schoenwolf and Smith, 1990).

In 1935 Sauer proposed that the pseudostratified epithelium of the neural plate undergoes interkinetic nuclear migration (Sauer, 1935). That is, nuclei migrate to the basal site during S-phase of the cell cycle and migrate to the apical site during M-phase. This was later confirmed by others (Fujita, 1962; Martin and Langman, 1965; Sauer and Walker, 1959; Sidman et al., 1959). Due to IKNM, cells undergoing S-phase adopt a wedged cell shape as the nuclei are situated at the basal surface. It was later shown that MHP cells are transformed from spindle shaped cells to wedge shaped cells immediately prior to furrowing and bending of the neural plate (Schoenwolf and Franks, 1984). It was proposed that basal expansion occurred in orchestration with the cell cycle due to IKNM as the cell cycle phase determines the shape of the cell (Schoenwolf and Franks, 1984). Thus, it was thought that wedge shaped cells could be generated by cell cycle alterations.

Indeed, Smith and Schoenwolf found that a prolongation of the MHP cell cycle coincided with an increase in the number of wedge shaped cells during neural plate bending in the chick embryo (Smith and Schoenwolf, 1987). The prolonged S-phase was not observed in cells of the lateral regions or in the flat prospective MHP in

younger embryos (Smith and Schoenwolf, 1987). Furthermore, all phases of the cell cycle except M-phase, when nuclei are apical and cells inverted wedge shaped, were prolonged in the MHP (Smith and Schoenwolf, 1988). In fact, the length of M-phase in the MHP shortened as bending proceeded. It has been suggested that nuclei of all regions are apical during M-phase (inverted wedge shaped), apical or central during the transition from G1- to S-phase and during late G2-phase (spindle shaped), and basal during S- and most of G2-phase (wedge shaped). It was therefore predicted that the non-S-phase part of the cell cycle that is prolonged in the MHP is G2 phase, when cells are mostly wedge shaped (Smith and Schoenwolf, 1987; Smith and Schoenwolf, 1988).

The mechanisms behind the altered cell cycle in the MHP are still unknown. A suggested mechanism is that the underlying notochord induces cells to prolong S-phase (and possibly G2). In support of this theory, the proportion of wedge shaped cells in the MHP does not increase following notochord ablation and, as a consequence, furrowing and bending at the MHP is lost (Smith and Schoenwolf, 1989). On the other hand, notochordal fragments transplanted into the lateral region of the neural tube are able to convert overlying (lateral) neuroepithelial cells to 'MHP-like' cells (Smith and Schoenwolf, 1989). Further evidence for this theory comes from work showing that notochordal transplants in the lateral region of the neural tube leads to a reduction in the mitotic index of the cells in contact with the notochord compared to a control region in the opposite neural fold (van Straaten et al., 1988). The authors conclude that the notochord induces floor plate like structures and diminishes proliferation in the overlying neural plate (van Straaten et al., 1988).

1.3.4 Extrinsic forces

1.3.5   Surrounding tissues

MHP cells that have been surgically separated from lateral tissues become wedge shaped and form a MHP indicating that wedging is not secondary to neural plate bending due to extrinsic forces (Alvarez and Schoenwolf, 1992; Schoenwolf, 1988).

Similarly, in mouse embryos, PNP closure proceeds in isolated neural tubes and plates that have been separated from lateral tissues that could otherwise exert extrinsic forces on neural plate bending and elevation (van Straaten et al., 1993).

Interestingly, surgical removal of the lateral neural fold region on one side of the prospective MHP does not change the position of the MHP. That is, cell wedging and bending occurs in the original MHP which is off centre due to loss of one of the lateral regions (Schoenwolf, 1988). Furthermore, the side of the neuroepithelium that is still intact elevates and bends around the original furrow, even though the apposing neural fold is missing (Schoenwolf, 1988). This suggests that an important role for the MHP is to determine the site at which bending and elevation will occur, ensuring that the neural tube forms with the right morphology.

It is difficult to dissect wedge shaping and furrowing from each other as they take place simultaneously. However, the fact that furrowing occurs when midline cells have been separated from all lateral tissues that could have exerted extrinsic forces to cause bending (Schoenwolf, 1988) suggests that the intrinsic, active event of cell shape changes in the MHP causes initial furrowing. Furthermore, furrowing occurs roughly 4 hours prior to neural fold elevation in the chick embryo (Schoenwolf and Franks, 1984), suggesting that cell wedging is not a secondary effect of bending and cell crowding.

1.3.6 Molecular mechanisms of MHP formation

BMP inhibition has in recent years been suggested to be important for MHP formation in the chick midbrain (Eom et al., 2012). pSmad1,5,8 which is a readout of canonical BMP signalling, is found at low levels in the chick midline due to the expression of the BMP antagonists Chordin and Noggin (Eom et al., 2012). Electroporation of overexpressing Noggin-, or dominant negative BMP receptor-constructs into the midline exacerbated the MHP, while overexpression in the lateral neural folds in some cases led to indentation of the neural plate, or an ectopic hinge point (Eom et al., 2012). Moreover, electroporation of a constitutively active BMP receptor led to a flat neural plate, i.e. abolished MHP formation and

resulted in failure of the neural folds to elevate and fuse, suggesting that BMP antagonist mediated MHP formation is necessary and sufficient for neural tube closure (Eom et al., 2012). BMP blockade also led to an increase in apical constriction and an overall trend towards more basal nuclei in the MHP due to a reduction in the levels of apical tight junction proteins and an increase in the apical levels of basolateral proteins (Eom et al., 2012).

BMP inhibition was previously shown to be important for DLHP formation in the mouse embryo (Ybot-Gonzalez et al., 2007a). BMP signalling is both necessary and sufficient for the inhibition of DLHPs while BMP antagonism, in the form of Noggin, is necessary and sufficient to induce DLHPs (Ybot-Gonzalez et al., 2007a). At rostral levels DLHPs do not form as Shh signalling from the notochord inhibits Noggin in the dorsal neural folds. Caudally, however, Shh signalling from the notochord is weaker and unable to inhibit Noggin, leading to DLHP formation (Ybot-Gonzalez et al., 2007a).

1.3.7   Notochordal role in MHP formation

Notochordless chick embryos do not form a MHP and cell wedging, apico-basal cell shortening and midline furrowing is abolished (Smith and Schoenwolf, 1989). Furthermore, the increase in the proportion of wedge shaped cells and the prolongation of the cell cycle in the MHP is only observed after the notochord has formed and established contact with the chick MHP (Smith and Schoenwolf, 1989).

In some notochordless embryos the neural folds elevate but do not fuse, and the cross section is U-shaped rather than V-shaped. In other embryos closure occurs but the cross sectional morphology is abnormal with a broad ventral midline region and a small lumen (Smith and Schoenwolf, 1989). Thus, it seems that the notochord and MHP are dispensable for neural fold elevation and fusion, but are important for the spatial regulation of bending, and the proper cross sectional V-shaped morphology (Smith and Schoenwolf, 1989).

1.3.7.1 Notochordal factors

As described above, BMP antagonists have been implicated in MHP formation in the chick. Noggin and Chordin are BMP antagonists that bind to several BMPs including BMP2 and BMP7 (McMahon et al., 1998) that are expressed in the dorsal neural tube in the mouse (Ybot-Gonzalez et al., 2007a). In the mouse embryo, Noggin is expressed in the node at E7.5 and is later expressed along the rostro-caudal length of the notochord underlying the MHP (McMahon et al., 1998; Ybot-Gonzalez et al., 2007a). In agreement with a role in BMP antagonism, Noggin mutants have ectopic BMP4 expression in the MHP compared to Noggin heterozygous mice but the MHP seems to be normal (McMahon et al., 1998). Thus, the phenotype of BMP overexpressing chick embryos (Eom et al., 2012) is not reproduced in a Noggin mouse mutant (McMahon et al., 1998).

Chordin is expressed in the node and notochord underlying the MHP in the mouse (Bachiller et al., 2000; Ybot-Gonzalez et al., 2007a). Unlike Noggin mutants, Chordin mutants develop normally (Bachiller et al., 2000) while Noggin-Chordin double mutants exhibit holoprosencephaly, a single nasal pit and a cyclopic eye; phenotypes that resemble those observed for Shh null mice (Bachiller et al., 2000). Furthermore, Noggin-Chordin double mutant mice lack Shh in the rostral midline similarly to Shh mutants (Bachiller et al., 2000; Chiang et al., 1996) and develop a notochord which is degenerated after E8.5, suggesting that Noggin and Chordin are required for the maintenance of the notochord (Bachiller et al., 2000).

1.4   Interkinetic nuclear migration

Interkinetic nuclear migration (IKNM) was first identified in the chick and pig neuroepithelium by Sauer in 1935 (Sauer, 1935) and is characteristic of all pseudostratified epithelia (Lee and Norden, 2013). During IKNM, nuclei migrate between the apical and the basal side of the epithelium depending on the phase of the cell cycle, undergoing mitosis at the apex and DNA synthesis basally (Figure 1.6) (Spear and Erickson, 2012b). IKNM has been suggested to be important for shaping of epithelia (Spear and Erickson, 2012b) and in several pseudostratified epithelia IKNM is associated with shape changes (Table 1.1). IKNM has also been suggested to be important for the balance between neurogenesis and maintenance of progenitor pools by regulating the amount of neurogenic and proliferative signals a progenitor cell receives as it traverses through apical and basal expression domains (Del et al., 2008). A third theory is that it allows more progenitor cells to be packed within a limited surface area (Spear and Erickson, 2012b). Pseudostratified epithelia allow for a greater density of cells and are associated with highly proliferating tissues (Lee and Norden, 2013). Accordingly, pseudostratified epithelium has been described in a congenital tumour of the ciliary epithelium (Saunders and Margo, 2012). Abnormal pseudostratification has also been implicated in developmental defects of the brain, such as microcephaly, suggesting that it is important for normal brain development (Ge et al., 2010).

The molecular mechanisms underlying IKNM are controversial and likely to be different from system to system. In liver buds, for example, the transcription factor Hex is required for the transition from a columnar to a pseudostratified epithelium but deletion of Hex affects only the liver bud, and not the neuroepithelium (Bort et al., 2006). Some studies conclude that IKNM is a process driven by microtubules and the minus-end-directed microtubule motor protein Dynein, while other studies find IKNM to be dependent on actomyosin forces (reviewed by Spear and Erickson, 2012b). Examples of different systems and IKNM requirements are shown in Table 1.2.

33
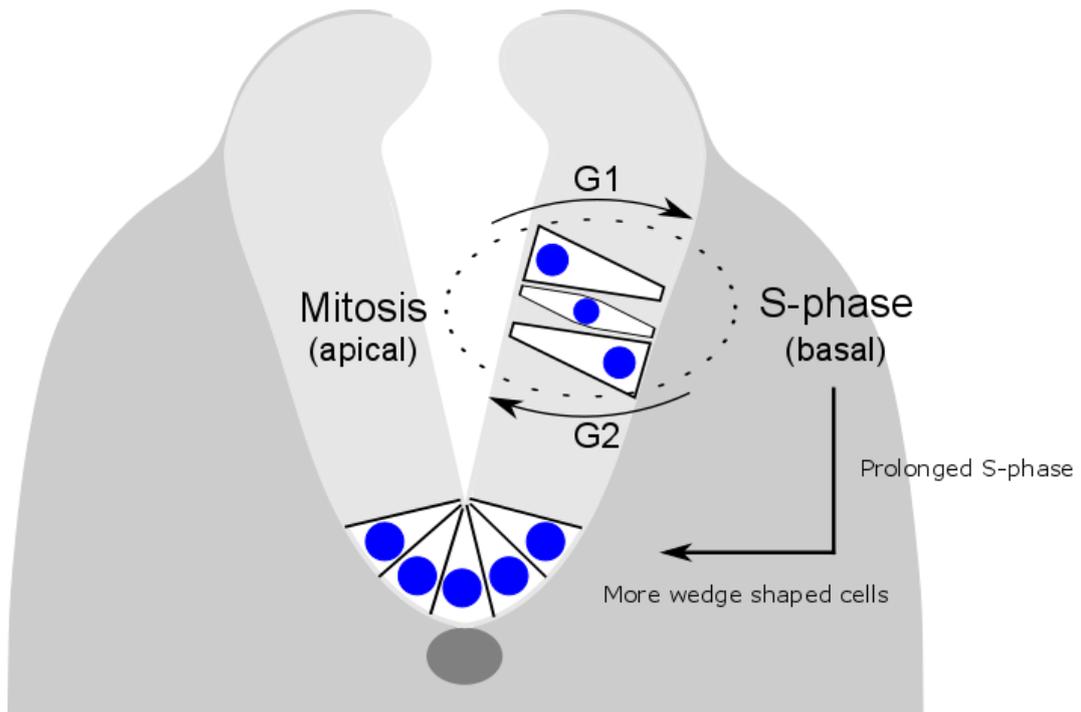
Figure 1.6 - Interkinetic nuclear migration in the neural plate

Nuclei of neuroepithelial cells migrate between the basal surface where they undergo DNA synthesis (S-phase), and the apical surface for mitosis. Cells in the MHP have mainly basal nuclei due to the prolonged time spent in 'basal cell cycle phases'.

Tissue	Reference
Lens placode	(Zwaan et al., 1969)
Liver, lung buds and pancreatic bud	(Bort et al., 2006)
Mouse intestine E12.5-14.5	(Grosse et al., 2011)
Chick somite	(Langman and Nelson, 1968)
Mesonephros	(Sauer, 1935)

Table 1.1 - IKNM in vertebrate embryos is associated with shape change

The lens placode invaginates, and the lung buds, liver bud and pancreatic buds evaginate from the endoderm (Bort et al., 2006; Zwaan et al., 1969).

System	IKNM dependent on:	Reference
Zebrafish retina	MTs and motor proteins play minor roles while most movement is generated by actomyosin activity	(Norden et al., 2009)
Mouse cortex E13.5	Basal to apical regulated by Tpx2. Apical to basal is passive, non-autonomous displacement due to nuclear movement in the opposite direction	(Kosodo et al., 2011)
Chicken neural tube slice culture	Apical migration during G2 microtubule-dependent and cell rounding during mitosis actin-dependent	(Spear and Erickson, 2012a)

Table 1.2 - Requirements for IKNM

Summary of some of the mechanisms proposed for IKNM in the zebrafish retina, the mouse cortex, and in chick slice cultures. MT; microtubules.

1.4.1 Microtubule dependent IKNM

The microtubule-based cytoplasmic motors Dynein and Kinesin have been implicated in IKNM in many systems such as fungi, fruit flies and algae (Baye and Link, 2008). The Dynein motor is referred to as a minus-end directed motor and Kinesin as a plus-end directed motor as they carry cargo in opposite directions: Dynein basal to apical, and Kinesin apical to basal (Figure 1.7) (Baye and Link, 2008). In the mouse and rat cerebral cortex, several studies find a necessary role for microtubules and dynein in IKNM (reviewed by Spear and Erickson, 2012b): Lis1 knock-down (a regulator of Dynein) prevents apical migration and mitosis, and low levels of Lis1 lead to ectopic mitosis away from the apex. NudC (which also regulates Dynein), Cep120 and TACCs (two proteins important for the integrity of the microtubule cytoskeleton), Hook3 and PCM1 (important for the anchoring of microtubules to the centrosomes) and TPX2 (a microtubule associated protein) have all been shown to be essential for IKNM (Spear and Erickson, 2012b). Furthermore, KASH and SUN nuclear membrane proteins, specifically Syne-2 and SUN1 and 2, have been shown to link nuclei of photoreceptor cells to microtubules in the mouse retina, thereby attaching the nuclei to the microtubule motors (Yu et al., 2011). KASH proteins also contain actin-binding sites and could therefore be important in actin and myosin mediated IKNM as well (Baye and Link, 2008).
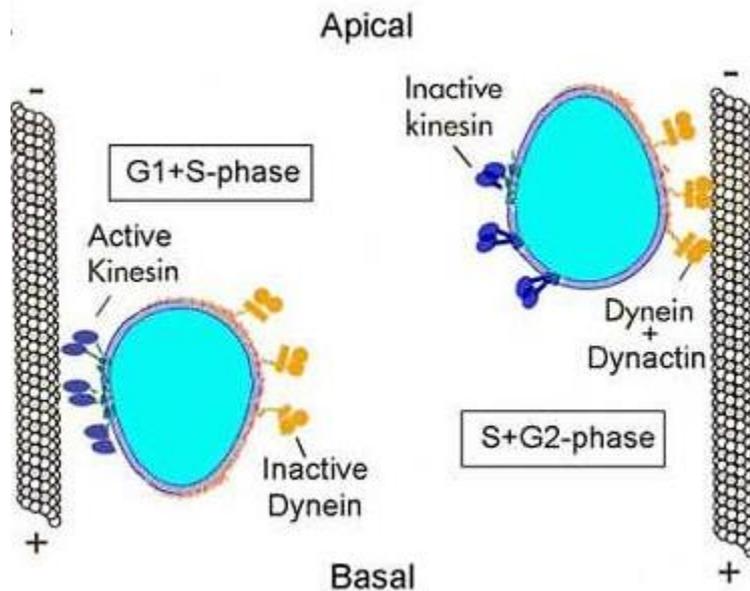
Figure 1.7 - The Dynein and Kinesin motors in IKNM

The microtubule-based cytoplasmic motors Dynein and Kinesin carry cargo in opposite directions: Dynein basal to apical, and Kinesin apical to basal. Taken from Baye and Link, 2008.

1.4.2 Actomyosin dependent IKNM

Other evidence suggests roles for actin and myosin in IKNM. Myosin localises to the basal side of the nucleus during nuclear migration in zebrafish neuroepithelium, seemingly contracting behind the nucleus to push it towards the apex (Leung et al., 2011). Inhibition of non-muscle myosin with Blebbistatin perturbs apical nuclear migration in the zebrafish retina (Norden et al., 2009), Cytochalasin B mediated inhibition of actin polymerisation disrupts IKNM (Murciano et al., 2002) and regulators of the actin cytoskeleton and myosin, including Rho GTPase and Rho kinase (ROCK) affect IKNM (Liu et al., 2010; Meyer et al., 2011; Minobe et al., 2009). In Drosophila, inhibition of ROCK disrupts apical migration, suggesting that ROCK might be an upstream activator of actomyosin contraction during IKNM (Meyer et al., 2011). Furthermore, it has been shown that microtubule depolymerisation in the zebrafish retina does not perturb IKNM (Norden et al., 2009).

36

It is possible that the different outcomes of the studies are linked to morphological differences, as the mouse and rat cortices are vastly wider than the zebrafish retina (Lee and Norden, 2013). Thus, it is possible that over longer distances, as in the rodent developing brain, microtubule motors are required for the steady and directed migration of nuclei to the apex, whereas actin and myosin are sufficient to 'push' nuclei over shorter distances. It remains to be found which system drives IKNM in the mouse neural plate which in width is similar to the zebrafish retina. An alternate theory is that microtubules and actin are both required as suggested by Spear and Erickson in chicken neural tube slice cultures (Spear and Erickson, 2012a). They find that apical migration during G2-phase is microtubule dependent but entry into mitosis occurs some distance away from the apex after which the cell rounds up in an actin dependent manner which is responsible for getting the nucleus the rest of the way to the apical surface (Spear and Erickson, 2012a). Accordingly, colcemide-induced depolymerisation of microtubules prevents apical migration but not mitosis or apical movement of mitotic cells, whereas Cytochalasin B mediated actin depolymerisation prevents mitotic cell rounding and results in ectopic mitoses some distance away from the apex (Spear and Erickson, 2012a).

The apical to basal migration has received less attention and has been suggested to be passive and random for cells in G1- and S-phase in mouse neocortex, zebrafish retina, and zebrafish hindbrain (Kosodo et al., 2011; Leung et al., 2011; Norden et al., 2009). Other studies have found that it depends on actin and myosin (Schenk et al., 2009) or the plus-end directed microtubule motor Kinesin-3 (Tsai et al., 2010).

1.4.3   IKNM is regulated by the cell cycle

IKNM is tightly linked to cell cycle progression in the developing mouse brain but IKNM is not required for cell cycle progression (Kosodo et al., 2011; Murciano et al., 2002; Schenk et al., 2009; Ueno et al., 2006). Through cell cycle block in G2/M-phase or S-phase using the chemical inhibitors 5-azacytidine or cyclophosphamide, respectively, Ueno et al. showed that nuclei fail to undergo IKNM when the cell cycle is blocked (Ueno et al., 2006). Overexpression of the CDK inhibitor p18INK4c has also been used to block the cell cycle at G1-phase and inhibit the apical

migration of nuclei (Kosodo et al., 2011). Moreover, inhibition of IKNM by Cytochalasin B treatment, which inhibits actin polymerisation and disrupts contractile microfilaments, does not affect cell cycle progression (Murciano et al., 2002).

It is not known what triggers apical migration and at what point in the cell cycle this is triggered. In the zebrafish neuroepithelium, using PCNA-GFP constructs, Leung et al found that nuclei in S-phase where found broadly distributed across the centre of the neuroepithelium, and that the apico-basal level of S- to G2-transition varied (Leung et al., 2011). Once nuclei reached G2-phase, apical migration was rapid and directed (Leung et al., 2011). Using a fluorescently tagged myosin together with PCNA-GFP, the group showed that nuclei in G1- and S-phase are surrounded by symmetric myosin which then accumulates at the base of the nucleus once it goes into G2-phase (Leung et al., 2011). The basal myosin then seems to push the nuclei to the apex for mitosis. Finally, Cdk1, which is required for S- to G2-phase transition, was shown to be necessary for apical nuclear migration (Leung et al., 2011). Interestingly, Cdk1 has also been shown to phosphorylate the kinesin microtubule motor, Kif11, and this phosphorylation modulates its interaction with dynactin-1 (Blangy et al., 1997). Another link between the cell cycle and apical migration is through the microtubule binding protein TPX2 that reorganises the microtubule cytoskeleton (Kosodo et al., 2011). TPX2 is contained within the nucleus but relocates to the apical process during G2-phase and could be important for apical migration (Kosodo et al., 2011).

1.5 The cell cycle

The cell cycle is an important regulator of cell behaviour during embryonic development. During neurogenesis the progenitors of neurons undergo G1-phase lengthening which is sufficient to induce neuroepithelial cell differentiation, linking cell fate to the length of the cell cycle (Calegari and Huttner, 2003). Furthermore, alterations of the cell cycle due to loss of negative cell cycle regulators affects cell cycle exit and differentiation in the lens and pituitary during development, leading

to inappropriate proliferation (Bilodeau et al., 2009; Zhang et al., 1998). Moreover, a mouse model with a null mutation in the cyclin-dependent kinase inhibitor, p27, has a neuronal density 30% higher than that of wild-type littermates (Fero et al., 1996) highlighting how de-regulation of the cell cycle can have significant biological implications in development.

The cell cycle is regulated by cyclins and cyclin-dependent kinases (CDK) that form complexes. Cyclins are synthesised and destroyed in a cell cycle dependent manner, thereby regulating kinase activity and ensuring that the cell cycle proceeds in a sequential and orderly fashion (reviewed by Malumbres and Barbacid, 2009). The CDKs that drive the cell cycle consist of three interphase CDKs, namely CDK2, CDK4 and CDK6, and one mitotic CKD, CDK1 (Malumbres and Barbacid, 2009). In addition there are ten different cyclins belonging to four different classes, i.e. A, B, D and E cyclins (Malumbres and Barbacid, 2009). Cell cycle progression is monitored by checkpoints that ensure that DNA replication and chromosome segregation occurs without errors.

Mitogenic signals lead to expression of the D-type cyclins (D1, D2 and D3) that bind and activate CDKs in G1-phase, preferentially CDK4 and CDK6. The cyclin D-CDK4/CDK6 complexes cause partial inactivation of the pocket proteins Rb, RBL1 and RBL2, permitting expression of the E-type cyclins (E1 and E2) which in turn bind and activate CDK2 (Figure 1.8). The cyclin E-CDK2 complexes further phosphorylate and complete inactivation of Rb (reviewed by Malumbres and Barbacid, 2009). Availability of E-type cyclins is under tight regulation and is only permissive during the early stage of DNA synthesis (Malumbres and Barbacid, 2009). During late stages of DNA synthesis, CDK2 is activated by cyclin-A2 to drive transition from S-phase to G2-phase. Lastly, it is thought that CDK1 is activated by A-type cyclins at the end of interphase to allow entry into M-phase. After nuclear envelope breakdown the A-type cyclins are degraded, permitting the formation of cyclin B - CDK1 complexes that drive the cell through Mitosis (Figure 1.8) (reviewed by Malumbres and Barbacid, 2009).
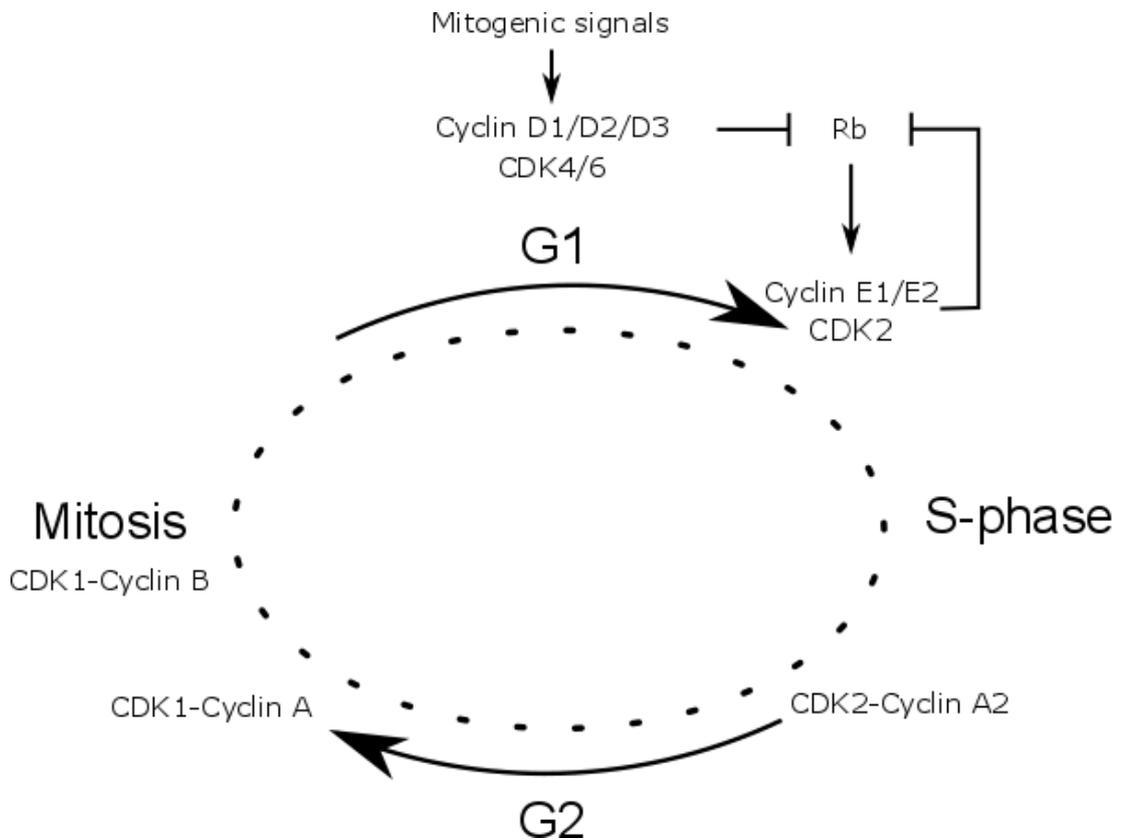
Figure 1.8 - The cell cycle

In mid G1-phase, mitogenic signals induce the transcription of cyclins D which bind and activate CDK4/6, phosphorylating retinoblastoma protein (Rb) to partially inactivate it and release transcription factors from its inhibition. This allows transcription of genes required for G1-S-phase transition including cyclins E which bind and activate CDK2, further inactivating Rb. The availability of cyclins E is limited to early S-phase. In late S-phase, cyclin A activates CDK2 to drive the cell cycle into G2-phase, and at the end of G2-phase, cyclin A activates CDK1 to facilitate the onset of mitosis (M-phase). Once the nuclear envelope has broken down, cyclins A are degraded, and the CDK1-cyclin B complex forms and drives the cell through M-phase.

1.6 CIP/KIP family

The CIP/KIP family consists of three genes, p21 (el-Deiry et al., 1993; Gu et al., 1993; Xiong et al., 1992), p27 (Polyak et al., 1994a; Polyak et al., 1994b; Toyoshima and Hunter, 1994) and p57 (Lee et al., 1995; Matsuoka et al., 1995). They contain a conserved amino-terminal domain responsible for binding of cyclin-CDK complexes and inhibition of CDK protein kinase activity (Harper et al., 1995; Matsuoka et al., 1995; Polyak et al., 1994b) and can all cause cell cycle arrest in G1 when overexpressed (Fero et al., 1996; Harper et al., 1995; Lee et al., 1995). In addition to inhibiting cyclin-CDK complexes, including cyclin D-CDK4/6, p21, p27 and p57 are also involved in assembling catalytically active cyclin D-CDK4/6 complexes (LaBaer et al., 1997).

The CIP/KIP proteins are intrinsically unstructured and adopt tertiary conformations after binding to a wide variety of interacting proteins (Adkins and Lumb, 2002; Esteve et al., 2003; Lacy et al., 2004). Phosphorylation events seem to be important for the binding of CIP/KIP proteins to other proteins and their affinity towards CDKs can be modulated by phosphorylation on specific residues (reviewed by Besson et al., 2008). Furthermore, their subcellular localisation is regulated by phosphorylation events (Borriello et al., 2007; Child and Mann, 2006). Although the CIP/KIP genes are best known as cell cycle regulators, they have a number of other functions, including apoptosis, tumorigenesis, transcriptional regulation and cytoskeletal regulation (Besson et al., 2008).

1.6.1 p21

p21 was first discovered in 1992 as a polypeptide that was detected in anti-cyclin D1, anti-CDK2, anti-CDK4, and anti-CDK5 precipitates (Xiong et al., 1992) but the molecular identity of the protein was not identified until 1993 in a human brain tumour cell line as a gene highly induced by the tumour suppressor gene p53 and was named wild-type p53-activated fragment 1 (WAF1) (el-Deiry et al., 1993). WAF1 was shown to inhibit tumour growth in several tumour cell lines (el-Deiry et al., 1993). In the same issue of Cell in 1993, Harper et al reported the identification of a

gene they called CIP1 (for Cdk-interacting protein) whose product bound to and inhibited cyclin-CDK complexes (Harper et al., 1995). The sequences of CIP1 and WAF1 turned out to be identical (el-Deiry et al., 1993; Harper et al., 1995). Subsequently it was shown that the expression of p21 during embryogenesis as well as during cellular differentiation was not p53 dependent (Macleod et al., 1995; Parker et al., 1995). The best known function of p21 is, however, as a transcriptional target of p53 that mediates G1- and G2-cell cycle arrest following DNA damage (el-Deiry et al., 1993; Gartel and Tyner, 1999). In S-phase, p21 binds PCNA which is a DNA β processivity factor, thereby blocking subsequent DNA synthesis (Luo et al., 1995). p57 has also been shown to bind PCNA in S-phase (Watanabe et al., 1998).

p21 mouse mutants do not develop NTDs (Patterson et al., 2006). However, when double mutant embryos are generated with Gadd45a, another cell cycle regulator, the occurrence of exencephaly is relatively high (30.5%) and spina bifida occurs in 2.9% of embryos suggesting a role for p21 in spinal neurulation (Patterson et al., 2006). In comparison, Gadd45a null embryos develop exencephaly at an occurrence of 8.4% and p53 null embryos develop cranial NTDs with a frequency of 9.1% but no spinal NTDs (Patterson et al., 2006). Although the combinatorial loss of p21 and Gadd45a leads to NTDs, the genes do not seem to be co-expressed during neurulation: at all stages examined Gadd45a seems to be strongly expressed in the tips of the neural folds but not in the neural plate where p21 is expressed (Kaufmann et al., 2011). It is, however, not surprising that there seems to be some cooperation between Gadd45a and p21 since Gadd45a interacting proteins include cdc2/cyclinB1 and PCNA (reviewed by Kaufmann et al., 2011). The roles of p21, Gadd45a and p53 in neural tube closure are unknown.

1.6.2 p27

p27 was identified in 1994 as a p21 related protein that interacted with cyclin-CDK complexes (Polyak et al., 1994a; Polyak et al., 1994b; Toyoshima and Hunter, 1994). As opposed to p21 which has been reported to be expressed mainly in post-mitotic differentiated cells (Brugarolas et al., 1995; el-Deiry et al., 1993; Parker et al., 1995), p27 expression primarily increases in response to extracellular anti-proliferative

signals: p27 protein levels are high in non-proliferating cells, in cells grown to high density, in serum starved cells, as well as in cells treated with anti-mitogenic factors such as cAMP or rapamycin (Coats et al., 1996; Fero et al., 1996; Firpo et al., 1994; Kato et al., 1994; Nourse et al., 1994) suggesting that p27 might be an important element in pathways that connect mitogenic signals to the cell cycle at the restriction point in G1-phase. In G1-phase, p27 has been shown to bind to active cyclin E-CDK2 thereby preventing S-phase entry (Polyak et al., 1994b). Following re-entry into the cell cycle, protein levels are rapidly downregulated (Coats et al., 1996). Moreover, fibroblasts where p27 is blocked with antisense oligonucleotides fail to arrest at the G1-phase restriction point when mitogen starved (Coats et al., 1996).

During lens and pituitary development p27 expression is associated with the timing of cell cycle exit and differentiation as well as to prevent re-entry into the cell cycle of differentiated cells (Bilodeau et al., 2009; Zhang et al., 1998). In both the lens and the pituitary, differentiated cells re-enter the cell cycle in the absence of p27 (Bilodeau et al., 2009; Zhang et al., 1998). As described in detail in Chapter 4, p27 null mice are larger than wild-type littermates, highlighting the role for p27 in the regulation of cell proliferation and differentiation.

1.6.3   p57

p57 was identified in 1995 as a CIP/KIP gene with unique domain structure compared to p21 and p57 in addition to the CDK inhibitory amino-terminal domain (Lee et al., 1995; Matsuoka et al., 1995). p57 is a potent inhibitor of G1-phase CDKs and overexpression leads to G1-phase arrest (Lee et al., 1995; Matsuoka et al., 1995). p57 expression during development is tissue restricted compared to p21 and p27, and is the only CIP/KIP gene that is required for embryogenesis (Lee et al., 1995; Matsuoka et al., 1995). p57 is regulated at the transcriptional level by several factors that are critical during embryogenesis, including Notch/Hes1, MyoD, BMP2- and -6, and p73 (Balint et al., 2002; Georgia et al., 2006; Gosselet et al., 2007; Vaccarello et al., 2006), possibly explaining the importance of p57 in development. In humans, p57 resides on chromosome 11p15 in an imprinted cluster that is

associated with development of Beckwidth-Wiedemann syndrome, a complex overgrowth syndrome with various developmental defects and tumour predisposition (Zhang et al., 1997). In the pituitary and lens, p57 is expressed in proliferating cells during development and seems to be important for cell cycle exit without affecting differentiation. Accordingly, cells proliferate inappropriately in the absence of p57 (Zhang et al., 1998).

1.6.4 CIP/KIPs and regulation of the cytoskeleton

All of the CIP/KIP genes have been implicated in cytoskeletal regulation and cell migration and have been associated with the ROCK/LIMK/Cofilin pathway which is important for cytoskeletal organisation through a net decrease in actin stress fibre formation and regulation of cell shape (Besson et al., 2004a). ROCK activates LIMK which then phosphorylates and inactivates cofilin to promote stress fibre formation (Etienne-Manneville and Hall, 2002). p27 binds RhoA thereby preventing interaction of RhoA with its activators, p21 binds Rho kinase (ROCK) 1 and 2 leading to a decrease in cofilin phosphorylation, and p57 binds to and targets LIM kinase from the cytoplasm to the nucleus, also resulting in decreased phosphorylation and inactivation of cofilin (Besson et al., 2004b; Lee and Helfman, 2004; Tanaka et al., 2002; Yokoo et al., 2003). Further complicating the system, RhoA is implicated in cell cycle regulation, specifically by downregulating p21 and p27 in G1-phase (Olson et al., 1998; Weber et al., 1997). The CIP/KIP genes are all associated with tumorigenesis as is evident from the knock-out mouse models (Chapter 4). However, very rarely are the genes mutated in human cancers. It has been suggested that translocation of the genes to the cytoplasm, rather than mutagenesis, underlies the oncogenic role of the genes through cytoskeletal reorganisation (Besson et al., 2004a; Sherr and Roberts, 1999).

1.7   The INK4 family

INK4 proteins are 15-19 kDa polypeptides, are approximately 40% homologous to one another, and each protein in the mouse is 90% homologous to its human protein counterpart (Malumbres and Barbacid, 2009). The gene family consists of p15INK4b, p16INK4a, p19ARF, p18INK4c and p19INK4d. The INK4a locus in both man and mouse is remarkable and gives rise to two genes encoding two distinct proteins that are immunologically and functionally unrelated, i.e. p16INK4a and p19ARF (Quelle et al., 1995; Stone et al., 1995). p16INK4a is encoded by exons 1α, 2 and 3 while p19ARF is encoded by exon 1β, located 13 kb upstream of 1α, and by exon 2 though an <u>a</u>lternative <u>r</u>eading <u>f</u>rame of exon 2 is used; thereby the name ARF (Quelle et al., 1995; Stone et al., 1995). INK4 proteins, with the exception of p19ARF, specifically inhibit CDK4 and CDK6 with similar affinities in vitro (Hirai et al., 1995; Zindy et al., 1997b). p19ARF does not bind CDKs but instead interacts with mdm2 and leads to cell cycle arrest by stabilising p53 and, interestingly, leading to p53-dependent p21 transcription (Kamijo et al., 1998; Pomerantz et al., 1998). The INK4 family members can all block cell cycle progression in G1 phase when expressed at high levels (Zindy et al., 1997b). p18INK4c and p19INK4d are the only genes in the family to be expressed in utero and are expressed differentially: p18INK4c is associated with proliferating and not differentiated neural cell populations while p19INK4d is expressed in both proliferating and differentiated cell populations (Zindy et al., 1997b). Low levels of p15INK4b and p19ARF transcript have been detected by RT-PCR in all postnatal tissues whereas p16INK4a is only detected in the adult mouse after 15 months (Hara et al., 1996; Serrano et al., 1996; Zindy et al., 1997a).

INK4 proteins bind CDK4 and CDK6 directly regardless if they are bound to cyclin D or not. When they bind to a CDK-cyclin D complex their role is inhibitory towards the kinase whereas binding of INK4 proteins to CDK alone interferes with cyclin D-CDK assembly (Hirai et al., 1995; Parry et al., 1995). p18INK4c and p19INK4d mutant mice develop an apparently normal central nervous system and show no overt phenotypic impairments at one year of age (Zindy et al., 1997b).

As introduced in section 1.3.3, cells of the MHP spend more time in S-phase than cells of the lateral neural plate, resulting in an increase in the proportion of cells with basal nuclei. The increase in cell cycle length coincides with MHP formation (McShane et al., 2015; Smith and Schoenwolf, 1987). The reason underlying the prolonged cell cycle in the MHP is unknown but could be due to cell cycle regulators that inhibit the cell cycle in late G1-phase or S-phase. In sections 1.6 and 1.7 two families of CDKIs were introduced that can inhibit the cell cycle at a relevant point of the cell cycle, i.e. when nuclei would be basal due to interkinetic nuclear migration. Of these two families, one CDKI, p21, has previously been shown to be expressed specifically in MHP cells during neurulation (Rita Carvalho, unpublished). The MHP expression of p21 led to the idea that CDKIs were responsible for the prolonged S-phase in MHP cells, and resulted in the current work on the role of CIP/KIP and INK4 cell cycle inhibitors on MHP formation.

1.8   Thesis aim and objectives

This thesis aims to investigate the reason underlying the prolonged S-phase in MHP cells and to test the hypothesis that cyclin-dependent kinase inhibitors inhibit cells of the MHP in S-phase, thereby leading to a high proportion of cells with basal nuclei due to interruption of IKNM, causing crowding of midline cells and MHP formation (Figure 1.9).

The thesis objectives are to: 1) Analyse the expression of CDKIs during neurulation with focus on the MHP. 2) Analyse the morphology of embryos lacking the CDKI, p21, and examine the possibility of redundancy between CIP/KIP genes in the MHP. 3) Calculate S-phase length in the MHP and lateral neural plate in embryos with a null mutation in p21 and compare it to wild-type littermates. 4) Analyse MHP formation in electroporated embryos with high or low levels of CDKIs.
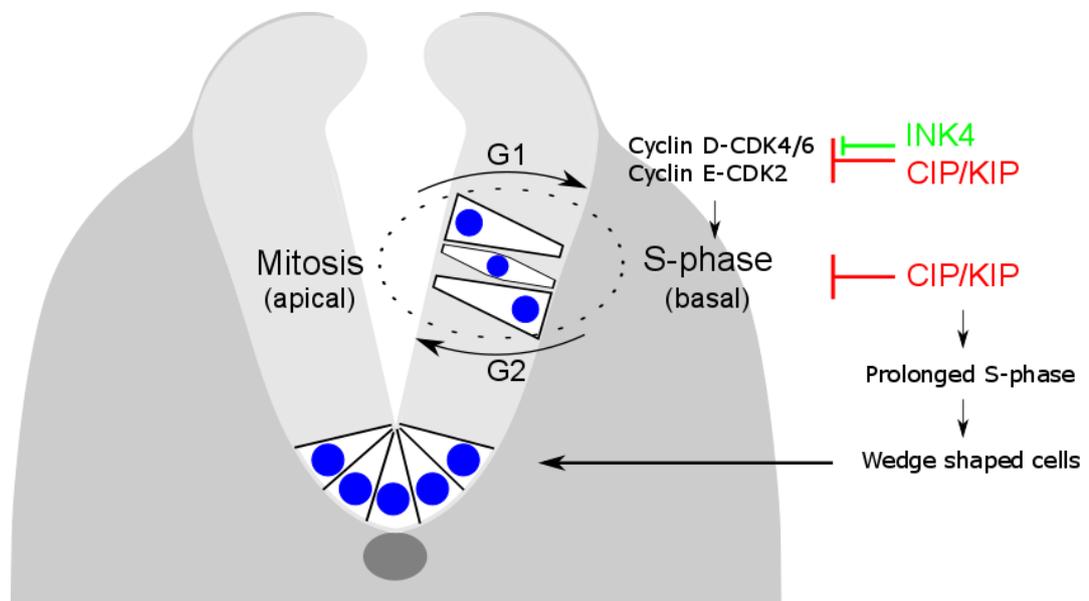
Figure 1.9 – Hypothesis – Cyclin dependent kinase inhibitors prolong S-phase in the MHP

During G1/S-phase transition, cyclin D-CDK4/6 complexes are inhibited by genes of the INK4 family and the CIP/KIP family of cyclin dependent kinase inhibitors. Furthermore, CIP/KIP genes inhibit cyclin E-CDK2 complexes important for G1/S-phase transition, and can in addition block progression through S-phase (reviewed by Besson et al., 2008).

Chapter 2 - Materials and methods

2.1   Animals

Mouse colonies were maintained by Dawn Savery at the Institute of Child Health animal facility, University College London. Animal rooms were kept at 22°C on a 12 hours light/12 hours dark cycle. Females were kept in communal cages from the age of 6-8 weeks and males were kept separately. Standard pelleted food and water was accessible to the mice at all times.

2.1.1   CD1 colony

CD1 random-bred, wild-type mice (Charles River Laboratories International, Inc.) were maintained by the staff at the ICH animal facility.

2.1.2   p21 and p21/p27

$p21^{-/-}$ and $p21^{+/-}$; $p27^{+/-}$ mice were a gift from Dr. Marcos Malumbres (Cell Division and Cancer group, CNIO, Spanish National Cancer Research Centre) and have been previously described as follows. For p21, exons 2 and 3 were replaced with a pgk-neo cassette (Figure 2.1) (Brugarolas et al., 1995). For p27 gene targeting, a neo cassette was inserted within exon 1, leading to an amino-truncated protein that does not inhibit cyclin-dependent kinases (Figure 2.2) (Kiyokawa et al., 1996). The mice were re-derived at the UCL transgenic services and bred onto a C57BL/6J background. p21 mice were maintained as a heterozygous colony and the p21/p27 mice as a p21 homozygous; p27 heterozygous colony.
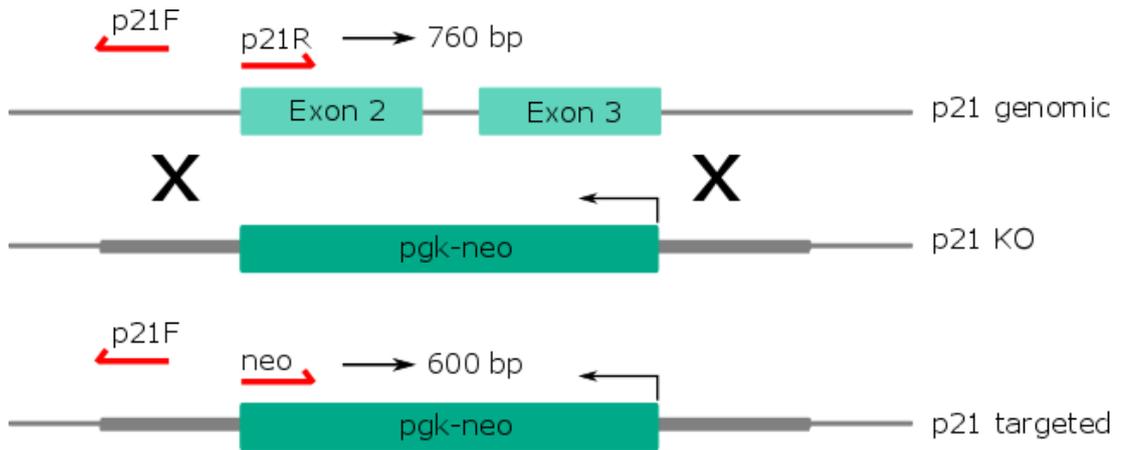
Figure 2.1 - p21 gene targeting

The PCR primers for genotyping are indicated in red. Redrawn from (Brugarolas et al., 1995).
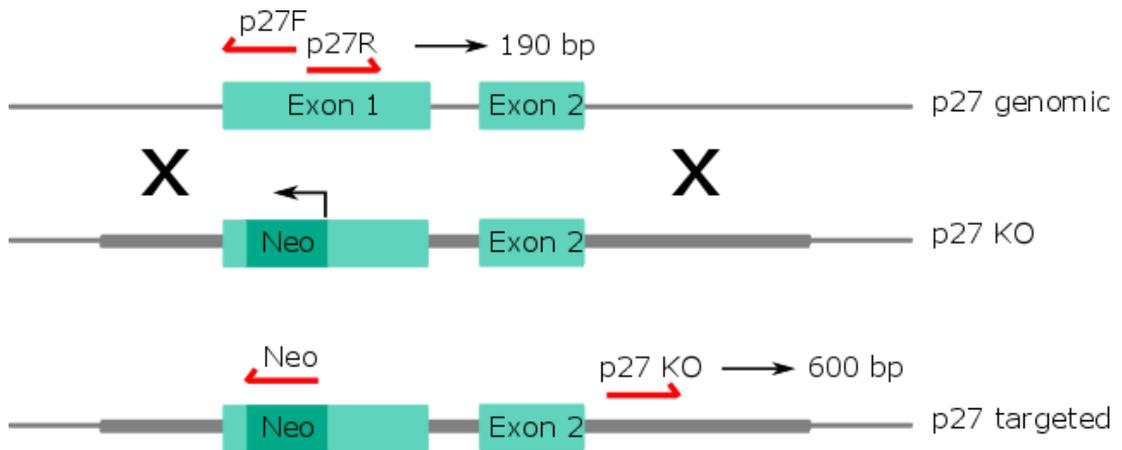
Figure 2.2 - p27 gene targeting

PCR primers for genotyping are indicated in red. Redrawn from (Kiyokawa et al., 1996).

2.1.3   Shh

Shh mice were from Prof. J.P.Martinez-Barbera (Developmental Biology of Birth Defects Section, Institute of Child Health, UCL) and were as described previously (Chiang et al., 1996). They were maintained as a heterozygous colony on a C57BL/6J background.

2.2 Mouse embryology

2.2.1 Embryo collection and dissection

Noon of the day a vaginal plug was found was designated E0.5. Pregnant females were culled by cervical dislocation and the uteri removed by laparotomy into warm (37˚C) dissecting medium: Dulbecco's Modified Eagle's Medium with 25 mM HEPES (DMEM, Invitrogen) supplemented with 10% inactivated foetal bovine serum (FBS, Invitrogen).

The uterus was taken to a stereomicroscope (Zeiss SV6 or SV11), opened along the mesometrial side with two watchmaker's forceps (number 5, Dumont) and the deciduas were gently removed from the uterine wall. The deciduas were opened from the antimesometrial base to expose the embryo which was gently removed, and Reichert's membrane was carefully dissected away with the internally adherent parietal endoderm cells, taking great care not to damage the ectoplacental cone and yolk sac. If the embryos were not to be used for whole embryo culture, the yolk sac was removed, rinsed in ice-cold PBS, and kept at -20°C for genotyping. The embryos were dissected clear of all membranes, somites were counted and they were numbered for future reference. Embryos for in situ hybridisation were fixed in 4% paraformaldehyde (PFA; 4% w/v in PBS-DEPC) overnight for 16-18 hours at 4°C, dehydrated to 100% methanol and stored at -20°C. Embryos for immunohistochemistry were fixed in 4% PFA in PBS on ice for 1 hour, dehydrated to 70% ethanol and stored at 4°C. Alternatively, if the embryos were used for embryo culture, the yolk sac and ectoplacental cone were left intact.

The length of the posterior neuropore was measured using an eyepiece graticule on a stereomicroscope. The length in graticule units was converted to mm: 1 graticule unit corresponded to 0.02 mm with the 5x objective which was used.

2.2.2 Whole embryo culture

After dissection for culture, embryos were cultured in rat serum (0.3-0.5 ml per embryo) in 30 ml plastic culture tubes (Nunc) smeared with silicone grease (Borer Chemie) around the outer rim of the tube to create an airtight seal. The filtered rat serum was gassed with 5% O_2 / 5% CO_2 / 90% N_2 for 1 minute and left to equilibrate for a minimum of 15 minutes at 37°C in a roller incubator (B.T.C Engineering) before the embryos were transferred to the serum using a plastic Pasteur pipette. The serum was then re-gassed with 5% O_2 / 5% CO_2 / 90% N_2 for 1 minute, and re-gassed every 8-14 hours.

2.2.3 Rat serum preparation

Blood serum was collected from adult male rats at UCL Biological Services. Animals were anaesthetised using isofluorane, and anaesthesia was confirmed by pinching one of the paws. The abdomen was surgically opened and, using a syringe, blood was withdrawn from the abdominal aorta until the animal had been exsanguinated. The blood was immediately centrifuged at room temperature (RT) for 5 minutes (10,000 x g) to separate the serum supernatant from the blood. Once the serum had coagulated, the clot was squeezed with flat forceps and the serum was transferred to fresh tubes and centrifuged at 4000 rpm at 4°C for 5 minutes to remove contaminating red blood cells. Any serum that remained pink in colour due to the presence of lysed red blood cells was discarded. The serum was pooled in fresh tubes, heat inactivated for 30 minutes at 56°C, chilled on ice, and aliquoted for storage at -20°C. Immediately prior to whole embryo culture, aliquots were thawed, warmed to 37°C and passed through a Millipore filter (0.45 µm pore size).

2.2.4 Electroporation

Following dissection for culture, E7.5 embryos (CD1 for overexpression, p21 for knock-down) were grouped by developmental stage (OB-LHF) according to the staging system described previously (Downs and Davies, 1993) and separated into equal treatment groups (Figure 2.3, A). For overexpression, all plasmids (Table 2.2) were at a concentration of 3.2 µg/µl in water (Sigma) and were mixed at a 1:1 ratio

for double or triple overexpression together with Fast Green at a final concentration of 0.01%. Alternatively, GFP control and Fast Green (0.01%) were injected for control groups. For siRNA knock-down, all stocks were 20 µM (Table 2.3). p57 or GC matched control siRNA was mixed with the fluorescent oligo at a 3:1 ratio. The fluorescent oligo has a red colour and Fast Green was not required for these experiments.
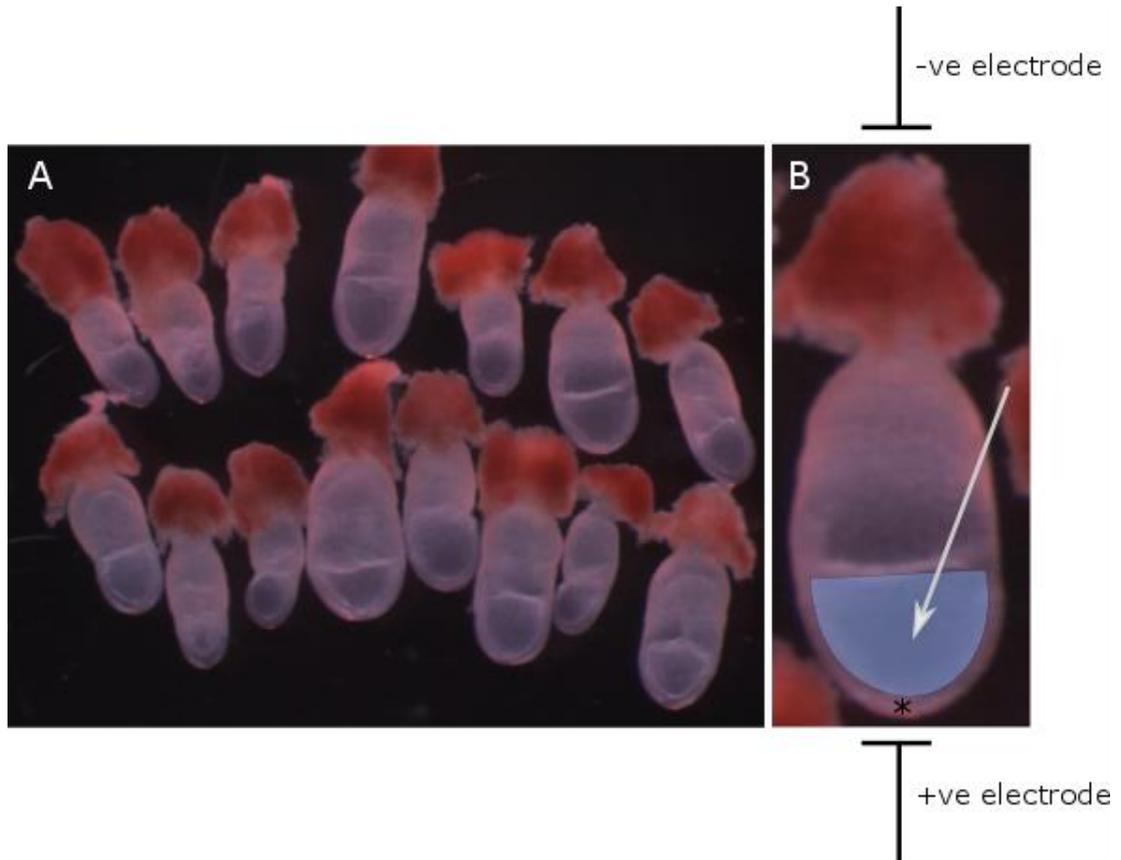
Figure 2.3 - Electroporation of E7.5 embryos

Embryos were divided into equal treatment groups (A), injected into the amniotic cavity (B; blue) and electroporated with the node (*) at the anode.

Embryos were injected one by one into the amniotic cavity (Figure 2.3, B) with a handheld mouth pipetting tube attached to a glass micropipette needle pulled on a Flaming-Brown horizontal pipette puller (Sutter Instrument Co). Approximately 1 µl was injected per embryo and each embryo was immediately transferred to a 55 mm petri dish containing 1% agarose (w/v in DEPC-PBS) with DEPC-PBS, electroporated and transferred back to dissecting medium prior to injecting the next embryo. This

was done to limit the amount of solution that escaped from the amniotic cavity after injection, and to limit the time embryos spent in PBS. Embryos were electroporated between a pair of gold plated 5 mm point electrodes (BTX model 508, Harvard Apparatus) attached to a BTX ECM 830 square wave electroporation system. Embryos were oriented as shown in Figure 2.3 with the node at the positive electrode so that nucleic acids enter cells in the node and the region around the node which give rise to the midline (Catala et al., 1996; Ybot-Gonzalez et al., 2007b). Once all embryos had been electroporated, they were transferred to equilibrated rat serum in culture tubes as described in Section 2.2.3. Electroporation settings were as follows:

Mode	LV
Voltage	20
Pulse length	50 ms
Pulses	5
Interval	950 ms
Polarity	unipolar

Table 2.1- Electroporation settings

Embryos at E7.5 were electroporated with these settings on the BTX ECM 830 electroporation system. LV, low voltage mode; ms, milliseconds.

2.2.4.1   Plasmids and siRNAs

The p27, p57 and GFP control expression plasmids were received from Dr DiCicco-Bloom (Tury et al., 2011). They had been cloned into a modified pCIG vector (Megason and McMahon, 2002) containing an internal ribosomal entry site and the enhanced green fluorescent protein (EGFP) under the control of a chicken β-actin promoter and a cytomegalovirus immediate early enhancer (Tury et al., 2011). The p21 expression plasmid was from Addgene and had been deposited by Bert Vogelstein (el-Deiry et al., 1995). The p21 expression plasmid did not express GFP.

Gene	Region	Plasmid	Reference
pCMW35 p21 (MGI:104556)	All	pBluescript SK	(el-Deiry et al., 1995)
p27 (NM_004064)	466-1062 bp	pCIG2	(Tury et al., 2011)
p57 (U20553)	41-1087 bp	pCIG2	(Tury et al., 2011)
GFP control		pCIG2	(Tury et al., 2011)

Table 2.2 - plasmids used for overexpression studies

The p21 plasmid was a gift from Bert Vogelstein (Addgene plasmid 16478). Other plasmids were received from Emanuel DiCicco-Bloom.

The p57 siRNA was designed using the BLOCK-iT™ RNAi Designer on the Invitrogen website. The highest scoring siRNA (5 stars) was selected. Only the duplexes with the highest probability of success are provided in the designer tool search, with 5 stars being the most likely to achieve high quality results. The p21 siRNA was designed according to the sequence provided by (Ishimura et al., 2012) and had been shown to reduce p21 levels by 80% in MEFs. The GC content of the p57 siRNA was 56% and was used with the matched Hi GC control, designed for siRNAs between 55 and 70%. The p21 siRNA had a GC content of 44% and the low GC control was used (35-45%).

siRNA	Sequence (RNA)	Cat.No.
p57 Stealth RNAi™ (NM_001161624)	S, CCUCCAGCGAUACCUUCCCAGUGAU AS, AUCACUGGGAAGGUAUCGCUGGAGG	-
p21 Stealth RNAi™ (NM_007667)	S, GCCUGACAGAUUUCUAUCACUCCAA AS, UUGGAGUGAUAGAAAUCUGUCAGGC	-
Stealth RNAi™ Negative Control Lo GC	random, unknown	12935-200
Stealth RNAi™ Negative Control Hi GC	random, unknown	12935-400
BLOCK-iT Alexa Fluor® Red Fluorescent Oligo	-	14750-100

Table 2.3 - siRNAs used in the knock-down studies

All siRNAs were from Invitrogen at a concentration of 20 µM.

2.2.4.2   Post culture

At the end of the culture, embryos were transferred to a petri dish in rat serum and rated according to heart beat and yolk sac circulation (Table 2.4). Embryos were then transferred to dissecting medium, dissected and, in p21 litters, yolk sacs were collected for genotyping. Somite number was counted and all embryos were imaged in PBS on a digital camera attached to a fluorescence stereomicroscope (Leica MZ FLIII). Embryos with a high rating (2 or 3; Table 2.4), a round healthy yolk sac and fluorescent midlines were processed for further analysis. Healthy looking young embryos with a strong heart beat and a healthy yolk sac were included in the absence of apparent circulation, as this was often difficult to find in the youngest embryos (5-6 somite stage).

Rating	Heart and circulation
0	Dead.
1	Weak heart beat and no circulation
2	Good heart beat and weak circulation
3	Very good heart beat and strong circulation

Table 2.4 - Scoring system after embryo culture

Embryos were rated according to heart beat and circulation. The appearance of the yolk sac was noted along with somite number. Embryos were imaged on an epifluorescence stereomicroscope with a digital camera. Embryos with a fluorescent midline and a rating of 2 or 3 with a healthy yolk sac were processed for further analysis.

2.2.4.3   Midline dissection

CD1 embryos at E7.5 were electroporated with the p57 siRNA or GC-matched control with the tagged fluorescent oligo and cultured for 24 hours. The midline isolation method was taught to me by Dr. Jean-Marie Delalande and was essentially as previously described (Delalande et al., 2015). In short, embryos with fluorescent midlines were briefly (2-3 minutes) digested in filtered (Millipore filter; 0.45 μm pore size) 2% Pancreatin (w/v in DEPC-PBS). After digestion, embryos were

transferred to dissecting medium with 10% FBS to inhibit enzymatic activity, and the midlines were dissected from the embryos using a tungsten needle, carefully removing all somites (Figure 6.14). The midlines were washed twice in DEPC-PBS and placed on dry ice. For each experiment, the midlines in each treatment group were pooled and stored at -80°C for RNA quantification.

2.3   Cell transfection

The cell transfection was done in duplicate plates, and four wells were used per treatment. 3T3 mouse fibroblasts were plated in a 24 well plate 18-20 hours prior to transfection at a density of $1x10^5$ cells/well in DMEM supplemented with 10% FBS. This resulted in a confluency of approximately 60% at the time of transfection. Appropriate concentrations of plasmid and/or siRNA were diluted in OptiMEM at a volume of 50 µl per well and incubated at room temperature for 5 minutes. Lipofectamine 2000 (3 µl per well) was likewise diluted in 50 µl OptiMEM per well and incubated at room temperature for 5 minutes. The plasmid/siRNA-OptiMEM solution was combined with the Lipofectamine-OptiMEM solution and incubated at room temperature for 20 minutes. The medium of the 24 well plate was removed and 400 µl of fresh DMEM+10% FBS with 100 µl of the plasmid/siRNA-Lipofectamine solution was added per well. Cells were incubated at 37°C and 5 hours post-transfection the media was replaced by DMEM+10% FBS with 1% Pen/Strep antibiotics. At 24 hours post-transfection, RNA was extracted from one plate and the duplicate plate was stained with DAPI for estimation of transfection efficiency.

2.3.1   Transfection efficiency

The medium was removed from transfected cells and cells were washed once in PBS, fixed in 4% PFA for 5 minutes at RT, washed again in PBS and stained with DAPI (1:10,000 in PBS) for 3 minutes at RT. DAPI was removed, images were acquired on a digital camera attached to an epifluorescence inverted microscope (Olympus IX71), and the plate was stored in PBS, covered in foil, at 4°C. Cells were counted

manually in Image J and transfection efficiency was calculated as GFP-positive cells to total stained nuclei (DAPI).

2.4   Quantitative reverse transcription PCR

2.4.1   RNA extraction

For the cell transfections, medium was aspirated, 1 ml TRIzol reagent (Invitrogen) was added to each well and the contents were pipetted up and down 10 times to lyse the cells. The lysed cells in TRIzol were added to an Eppendorf tube and incubated for 5 minutes at RT. For embryonic tissue, caudal and rostral tissue fragments stored at -80°C were pooled as specified in appropriate chapters. TRIzol (500 µl) was added to the first tissue sample in an Eppendorf tube on dry ice, pipetted up and down until the tissue had homogenised, transferred to the next tissue sample on dry ice, and so on. Once the samples had been pooled they were incubated for 5 minutes at RT.

Chloroform was added to each sample (200 µl for cells, 100 µl for tissue) and the tubes were shaken vigorously for 15 seconds, followed by a 3 minute incubation at RT. The Trizol-Chloroform suspension was centrifuged at 12,000 x g for 15 minutes at 4°C and the top aqueous layer containing the RNA was transferred to a new tube. Samples were incubated in Isopropyl alcohol (500 µl for cells, 250 µl for tissue) for 10 minutes at RT to precipitate the RNA, and centrifuged at 12000 x g for 10 minutes at 4°C. The supernatant was poured off, and the pellet was washed with 70% ethanol-DEPC-H_2O (1 ml for cells, 500 µl for tissue), vortexed, and centrifuged again at 12,000 x g for 5 minutes at 4°C. The ethanol was poured off, the pellet was drained upside down, and left to airdry for 10 minutes. The semidry pellet was dissolved in DEPC-H_2O (20 µl for cells, 10 µl for tissue) and put on ice. To remove DNA contamination, 1 µl RNAse inhibitor, 0.5 µl DNAse I, and 2.5 µl 10x DNAse buffer was added (DNA-free Kit, Ambion) and samples were incubated at 37°C for 30 minutes. Inactivating buffer (2.5 µl) was added to stop the reaction and the RNA was incubated at room temperature for 2 minutes and spun at 10.000 rpm for 2

minutes before the supernatant was transferred to a fresh tube. The RNA was measured by spectrophotometry (NanoDrop 100; Thermo Scientific) and stored at -80°C.

2.4.2 Complementary (c) DNA synthesis

First strand cDNA was synthesised using the Superscript VILO cDNA synthesis Kit (Applied Biosystems). RNA (300 ng) was added to RNAse free tubes on ice and DEPC-H_2O was added to make up a volume of 14 µl. A mastermix was made (4 µl 5X VILO Reaction Mix and 2 µl 10X Superscript enzyme Mix per reaction) and 6 µl of the mastermix was added to each tube. The cDNA was synthesised in a thermal cycler with the following programme: 10 minutes at 25°C, 60 minutes at 42°C and 5 minutes at 85°C.

The quality of the cDNA was assessed by amplification in a standard PCR with primers against the house-keeping gene glyceraldehyde-3-phosphate dehydrogenase (GAPDH). The standard PCR conditions are shown in Table 2.5 and the PCR programme in Table 2.6. The samples were subsequently run on an agarose gel to check for the correct size of GAPDH (177 bp).

Reagent	Volume (µl)
10X Reaction buffer (Bioline)	3
dNTPs (Promega)	1.5
50 mM $MgCl_2$ (Bioline)	0.7
10 µM Primer-pair (Forward and reverse)	3
5 U/µl Taq DNA polymerase (Bioline)	0.15
H_2O (Sigma)	20.65
cDNA	1
Final volume	**30 µl**

Table 2.5 - Standard PCR reaction for checking cDNA with GADPH primers

Step	Duration and temperature
1. Heating	5 minutes, 94°C
2. Denaturation	30 seconds, 94°
3. Annealing	30 seconds, 60°C
4. Extension	1 minute, 72°C
5. Final extension	10 minutes, 72°C

Table 2.6 - Standard running conditions for PCR

Steps 2-4 were repeated 35 times.

2.4.3 RNA quantification

RNA quantification was performed on a BIO-RAD CFX96™ Real-Time System C1000 Touch™ Thermal Cycler.

2.4.3.1 Primers

All primers were from Sigma and designed in NCBI Primer-BLAST to amplify between 150-250 bp of the target gene with an optimum temperature of 60°C. The primers were designed to span exons in order to avoid amplification of genomic DNA, and where applicable, detect all transcript variants. The primers used are listed in Table 2.7. β-actin was used as reference gene as GAPDH has been associated with cell cycle regulation, DNA replication, G1-phase arrest, and induction of p21 (Mansur et al., 1993; Phadke et al., 2009; Suzuki et al., 2000; Wang et al., 2013) while significantly fewer modulators of β-actin than GAPDH have been reported (Suzuki et al., 2000). In serum starved cells β-actin levels increase when growth factors are added but GAPDH levels rise even more (Suzuki et al., 2000). However, a link between β-actin and CIP/KIP genes cannot be excluded since β-actin is a major cytoskeletal structural protein and CIP/KIP genes are cytoskeletal regulators as described (section 1.6.4).

Primer	Sequence	Product size (bp)
β-actin	**F**: TCTTTTCCAGCCTTCCTTC **R**: ATCTCCTTCTGCATCCTGTC	175
GAPDH	**F**: ATGACATCAAGAAGGTGGTG **R**: CATACCAGGAAATGAGCTTG	177
p57 (cdkn1c)	**F**: TGCGGCCAATGCGAACGACT **R**: GCTGCCCAGATGCCCAGCAA	202
p27 (cdkn1b)	**F**: TGGCGCAGGAGAGCCAGGAT **R**: CCAGCGTTCGGGGAACCGTC	241
p21 (cdkn1a)	**F**: GCAGACCAGCCTGACAGATTT **R**: AAGACACACAGAGTGAGGGC	154
p15INK4b	**F**: AGACTGCAAGCACGAAGAGG **R**: CGCGTCCTGAAAGGTAGAGG	212
p16INK4a	**F**: ATGGGTCGCAGGTTCTTGG **R**: CGTGAACGTTGCCCATCATC	215
p19ARF	**F**: CGAACTCGAGGAGAGCCATC **R**: TACGTGAACGTTGCCCATCA	182
p18INK4c	**F**: CCTTCTGTCAGCCTCCGATG **R**: CAGCGCAGTTCTCCCAAATC	232
p19INK4d	**F**: GCTCTGAGGCCGGCAAAT **R**: AAGCATAGTGGATACCGGTGG	150

Table 2.7 - Primers used for qRT-PCR

F, forward; R, reverse.

2.4.3.2   Sample preparation and thermal cycling

Designated RNA pipettes, tip boxes and bench area were sprayed down with RNaseZAP (Sigma) before preparing 96 well qRT-PCR plates (BIO-RAD) on ice, taking great care not to contaminate equipment or area with DNA. The components listed in Table 2.8 were thawed at RT, mixed, briefly centrifuged and stored on ice protected from light. All the components except the cDNA were combined in a mastermix for each primer-pair. Each sample was analysed in triplicates for the target gene and the reference gene. cDNA was added to all wells followed by 19 µl of mastermix. Negative controls with mastermix and water instead of cDNA were included for each primer-pair. The plate was sealed with Microseal 'B' adhesive seals (BIO-RAD), briefly vortexed and centrifuged, and loaded onto the thermal cycler. The programme is shown in Table 2.9. Experiments were analysed using the Bio-Rad CFX Manager programme, version 3.1.

Reagent	Final concentration	Volume (µl)
iTaq universal SYBR green supermix (BIO-RAD)	1x	10
Primer-pair 10 µM (F+R) (Invitrogen)	300-500 mM	2.4
H$_2$O (Sigma)	-	6.6
cDNA 300 ng/µl	100 ng – 100 fg	1
Final volume	-	**20**

Table 2.8 - Reaction for gene quantification by qRT-PCR

Step	Duration and temperature
1. Heating	3 minutes, 95°C
2. Denaturation	10 seconds, 95°C
3. Annealing and extension	30 seconds, 60°C
4. Melt curve analysis	0.5 seconds 60°C and 5 seconds 95°C

Table 2.9 - Programme for qRT-PCR

Steps 2 and 3 were repeated 39 cycles.

2.5 Cell cycle analysis

2.5.1 Injections

For BrdU-pHH3 cell cycle analysis in CD1 mice, embryos were collected on ice at exactly 15, 30, 45, 60, 90 or 120 minutes after injection of 50 mg/kg BrdU intra-peritoneally (IP) into E8.5 pregnant mice. Embryos were collected into ice-cold DMEM supplemented with 10% heat-inactivated FBS, dissected in cold medium and fixed within 20 minutes of collection in 4% PFA. Cold medium was used to limit the extent of BrdU labelling that continued after embryo collection.

For IdU/BrdU double labelling experiments, pregnant p21 mice at E8.5 were injected (IP) with IdU and BrdU (Table 2.10) at concentrations of 57.75 mg/kg (IdU) and 50 mg/kg (BrdU) to achieve equimolar amounts. IdU was injected at time 0 followed by BrdU exactly 2 hours later. Precisely 15 minutes after the BrdU injection, embryos were collected as described above for CD1 embryos, and fixed within 20 minutes to reduce variability in IdU/BrdU uptake between litters.

All embryos were fixed for 1 hour in 4% PFA on ice, yolk sacs were collected for genotyping (p21 embryos), and embryos were dehydrated to 70% ethanol and stored at 4°C.

Thymidine analogue	Dissolved in	Concentration	Supplier	Cat.number
BrdU	PBS pH 7.4	50 mg/kg	Sigma	B5002
IdU	1N NH4OH	57.75 mg/kg	Sigma	I7125

Table 2.10 - Thymidine analogues used for cell cycle studies

2.5.2 Length of S-phase

2.5.2.1 Experimental design

As described above, p21 mice were injected with IdU and BrdU and embryos were collected and fixed. All embryos were genotyped and divided into two stage-matched groups: Six p21$^{-/-}$ embryos and seven p21$^{+/+}$ embryos. At this stage all the embryos were blinded and given new numbers (that were not made available to me) by another member of the laboratory. The embryos were subsequently paraffin embedded, sectioned, stained with antibodies, and all analysis (S-phase length, cell phase distribution, and nuclear position) was performed blinded. At the end, embryos were grouped by genotype for graphs and statistical analysis.

2.5.2.2 Calculating S-phase length

IdU and BrdU are incorporated into the DNA during S-phase of the cell-cycle. Therefore, the two hour interval between the injections results in some single labelled cells that have incorporated IdU but have left S-phase before the BrdU pulse. Other cells will have stayed in S-phase during both the IdU and BrdU pulse. Because the cells cycle asynchronously, the ratio of the number of cells in one phase (e.g. S-phase) in proportion to the number of cells in another phase (e.g. G2-phase) is directly proportional to the ratio of the time between the two pulses (i.e. T_i) to the length of S-phase (Martynoga et al., 2005). Therefore, S-phase can be calculated by this formula:

$$S = Ti\ (2\ hours)/\left(\frac{L\ cells\ (single\ labelled\ (IdU))}{S\ cells\ (double\ labelled\ (IdU\ and\ BrdU))}\right)$$

where S is S-phase length, T_i is the interval between the injections, L_{cells} are cells labelled with IdU but not BrdU (i.e. have left S-phase during the experiment) and S_{cells} are cells labelled with both IdU and BrdU (i.e. have been in S-phase throughout experiment).

The IdU and BrdU labelled cell populations were counted on imaged sections following immunohistochemistry with antibodies that detect IdU and BrdU, or only BrdU. A cell nucleus in the centre of the MHP was selected based on IdU/BrdU staining in the green channel and five nuclei were selected on either side of the centre nucleus to give a region of approximately 11 cells in the MHP (Figure 2.4, A; box 1.). Regions of approximately 11 nuclei were similarly selected in the left and right lateral neural plate regions based on IdU/BrdU staining, approximately halfway between the MHP and the surface ectoderm, taking care not to select nuclei in regions of bending (Figure 2.4, A; 2. and 3.). All IdU-positive nuclei in the regions selected were encircled manually in Image J in the green channel (Figure 2.4, A). The circles were then observed in the red channel and any circle partially BrdU-positive was classified as being a double stained nucleus (Figure 2.4, B; single stained/double stained nuclei are indicated). The overall morphology of the neural plate is shown with a nuclear stain (Figure 2.4, C). The number of single and double stained nuclei was counted for each region on 5-13 slides per embryo, and S-phase was calculated from the average number of single and double labelled nuclei for each region (Appendix I). An example of calculation of S-phase length is shown for the section in Figure 2.4, D. The two lateral regions were averaged for the graphs, but the raw data (i.e. left and right lateral) was used for SEM and statistical analysis.
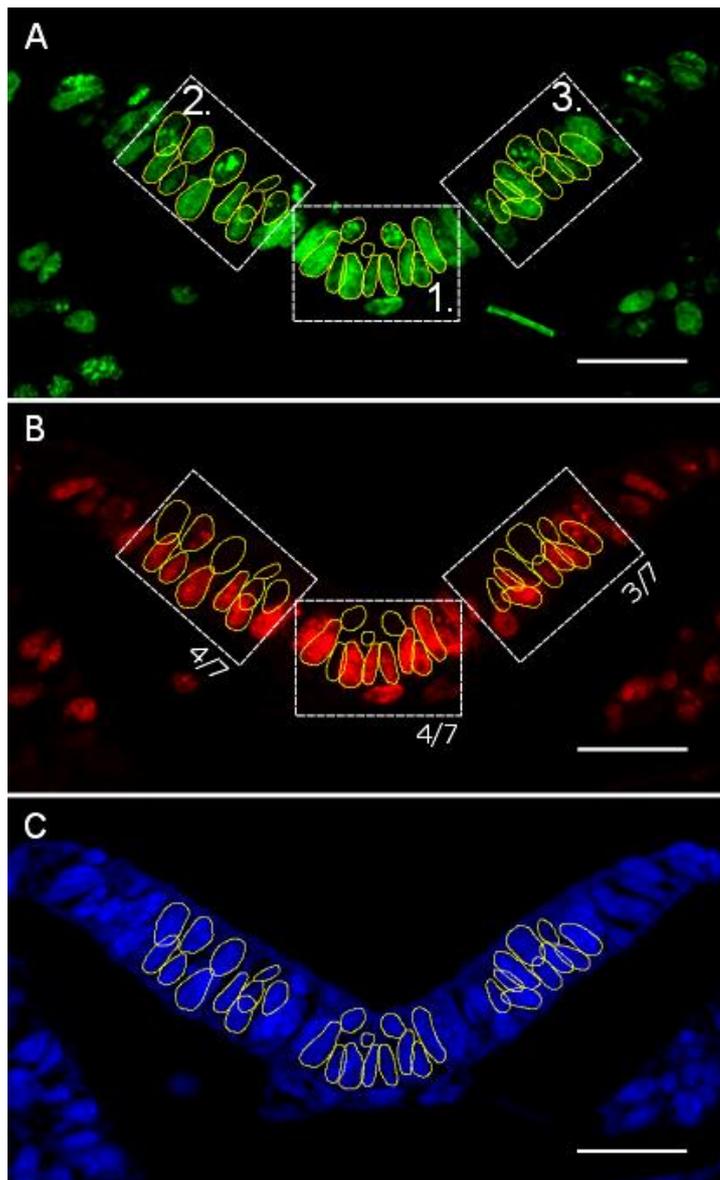
$$\text{Length of S-phase} = T_i \text{ (2 hours)} / (L_{cells}(IdU) / S_{cells}(IdU+BrdU))$$

MHP: S-phase = 2/(4/7) = 3.5 hours

Lateral: S-phase = (2/(4/7)) + (2/(3/7)) /2= 4.1 hours

Figure 2.4 - Counting nuclei for S-phase calculation

IdU/BrdU green positive nuclei were encircled in the MHP (A, 1.), the left lateral region (A, 2.) and in the right lateral region (A, 3.) The number of BrdU-positive nuclei was assessed in the red channel and the number of single labelled and double labelled nuclei was noted (B). Any nucleus partially positive was classified as double labelled. The numbers of single and double labelled nuclei was combined for all sections (5-13) per embryo to calculate S-phase length in each region. The overall morphology is shown in C. Example of S-phase length is shown for section example A-C (D). Scale bars = 30 μm.

2.5.3   Assigning cell cycle phases

2.5.3.1   BrdU and pHH3 (CD1 embryos)

As described in more detail in Section 5.2.2, BrdU and pHH3 immunohistochemistry was used as a tool to determine cell cycle phases in a population of cells, based on the distinct patterns of these during S-, G2-, and M-phase (Hendzel et al., 1997; Zhang et al., 2011). Cells assigned to early S-phase have a uniform BrdU pattern throughout the nucleus and no pHH3 staining. In late S-phase, the BrdU staining is more punctate and no pHH3 staining is observed. In G2 phase, BrdU and pHH3 are both observed in a punctate pattern; for BrdU, this pattern becomes more punctate as G2-phase proceeds, while pHH3 becomes more uniform. In mitosis, BrdU staining is very punctate and pHH3 is dense and bright (Figure 2.5, A-G and A'-G') (Hendzel et al., 1997; Zhang et al., 2011).

2.5.3.2   IdU and pHH3 (p21 embryos injected with IdU and BrdU)

Sections from IdU/BrdU double labelled embryos were stained with an anti-IdU and anti-pHH3 antibody. IdU-positive nuclei were assigned to phases of the cell cycle in the same way as described above for BrdU and pHH3 in CD1 embryos. IdU was in the circulation for 2.25 hours and IdU-positive nuclei were found in S-, G2- and M-phase of the cell cycle.

2.5.3.3   BrdU pattern only (p21 embryos injected with IdU and BrdU)

BrdU pattern was analysed in embryos from IdU and BrdU double injected p21 mice. This analysis was done on immunofluorescence slides stained with anti-IdU and anti-BrdU and pHH3 was therefore not available. BrdU was in the circulation for only 15 minutes and BrdU-positive nuclei were grouped into early/mid S-phase (Figure 2.5, H) or late S-, G2-phase (Figure 2.5, I) based on similarity with the BrdU staining in Figure 2.5, A-G where the phases were revealed by pHH3 staining (Figure 2.5, A'-G').
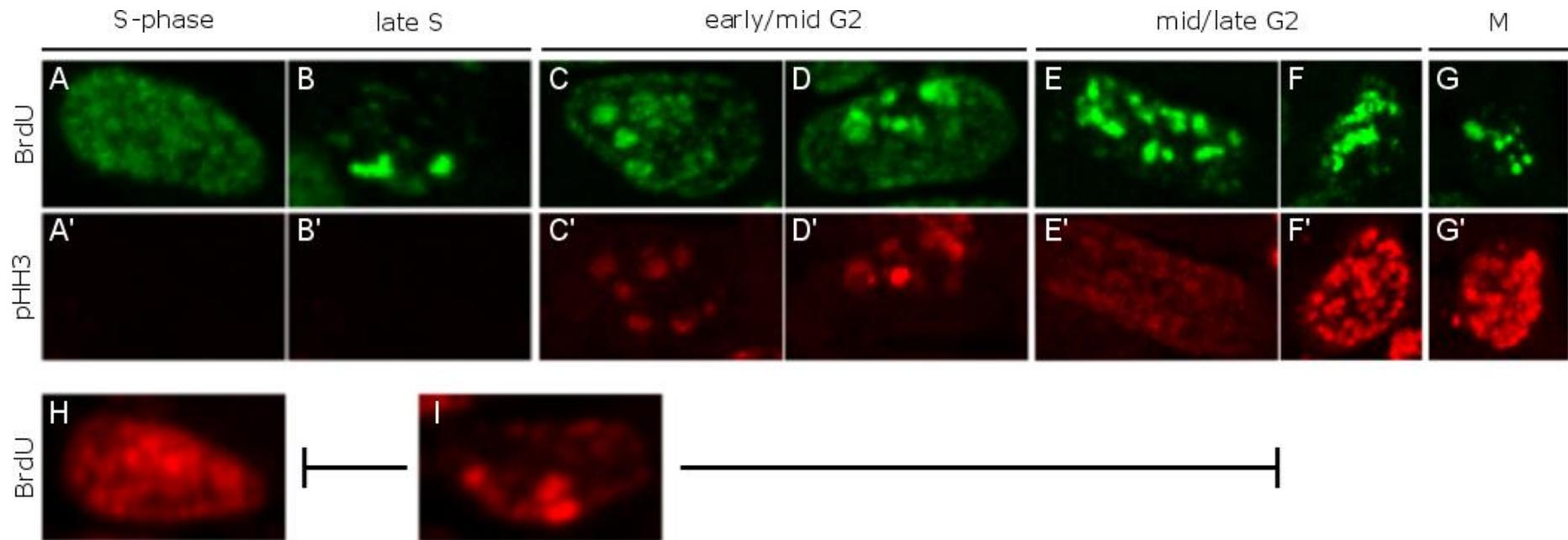
Figure 2.5 - Distinct staining patterns associated with cell cycle phases

BrdU (and IdU) and pHH3 have distinct staining patterns during S-, G2-, and M-phase of the cell cycle that was used to assign cells to different phases of the cell cycle (A-G and A'-G') (Hendzel et al., 1997; Zhang et al., 2011). A-G and A'-G' is the same nucleus viewed in two different channels. The cell cycle analysis that was done with BrdU pattern alone (Section 5.2.6) distinguished between two types of patterns: the distinct early/mid S-phase pattern that is homogenous (H) and similar to (A) which does not have any pHH3 staining (A'). The second type is late S-G2 phase (I) which is similar to the BrdU pattern observed in B-E.

2.5.4 Nuclear position measurements

Neuroepithelial cell shape is associated with the position of the nucleus along the apico-basal axis. That is, a cell with a basal nucleus is widest at the base (wedge shaped). In order to assess whether loss of p21 led to fewer wedge shaped cells, the distance of nuclei from the basal surface was measured (Figure 2.6). The basal distance of nuclei is an indirect measure of how wedge shaped a cell is. A region of at least 10 cells was chosen in the MHP (the centre nucleus and 5 nuclei on each side) and in the two lateral regions, and all IdU- (for IdU nuclear position) or BrdU-positive (for BrdU nuclear position) cells in that region were manually encircled. A macro in Image J, made by Bertrand Vernay, found the centre of the nucleus, and a line was drawn from the centre to the base of the neuroepithelium in the blue DAPI channel. The total thickness of the neuroepithelium was measured at the level of each nucleus, and basal distance was calculated:

$$Basal\ nuclear\ position = \frac{Basal\ distance\ from\ centre\ of\ nucleus}{Neuroepithelial\ thickness}$$

An example of a data sheet is shown in Appendix II.
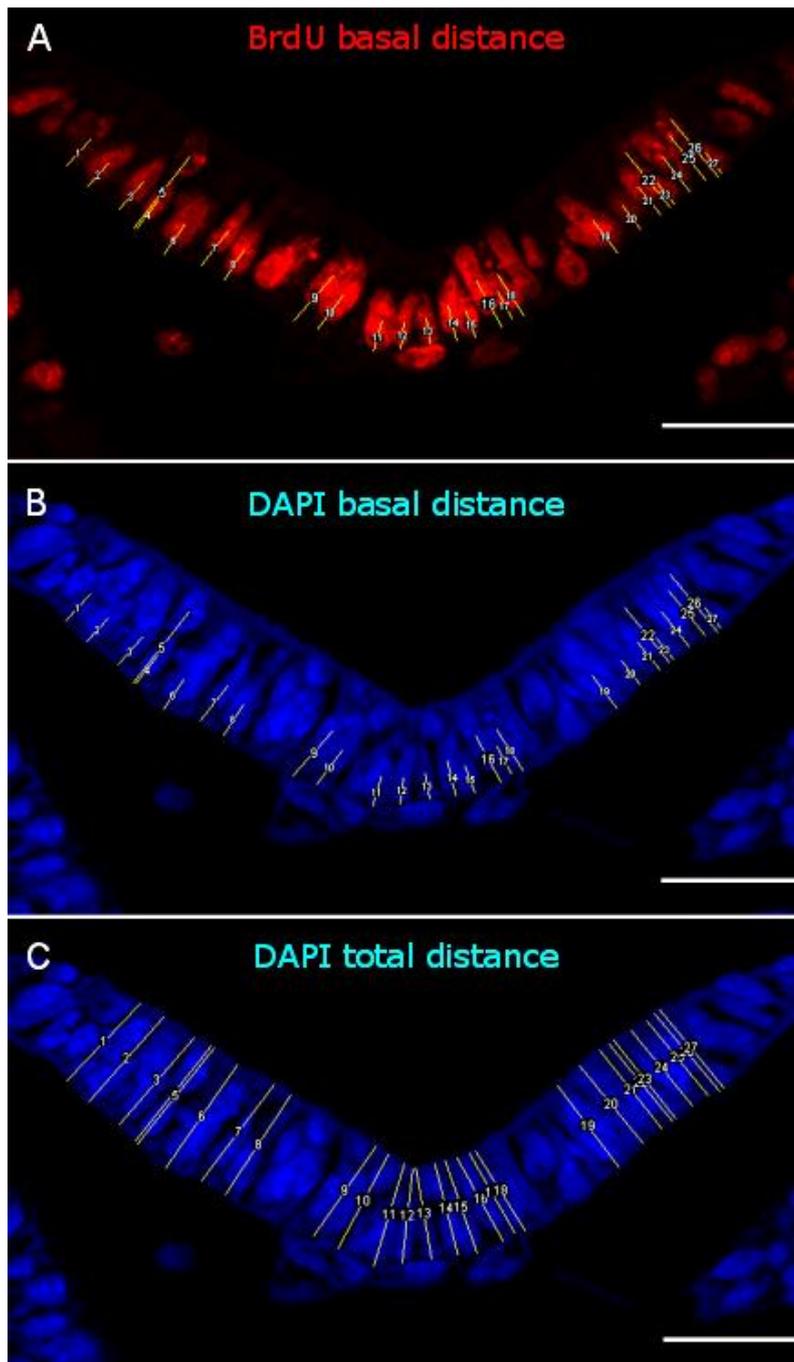
Figure 2.6 - Measuring nuclear position

From manually drawn circles (as shown in Figure 2.4), a macro in Image J was created by Bertrand Vernay to find the centre of the nuclei. A line was then manually drawn in Image J from the centre of the nucleus (A) to the basal surface of the neuroepithelium in the blue DAPI channel (B). The total distance of the neuroepithelium was measured at the level of each nucleus (C) and nuclear position was calculated as basal distance/total distance. Each nucleus has a number for future reference. Scale bars = 30 μm.

2.6   Histology

2.6.1   Wax embedding

PFA fixed embryos in 70% ethanol were washed twice for 30 minutes in 100% ethanol at RT, followed by two 15 minute washes in Histo-Clear (National Diagnostics) at RT in individual glass embedding moulds (Agar Scientific).The first Histo-Clear wash was at RT and the second at 60°C in an embedding oven (ThermoScientific). Histo-Clear was replaced with molten paraffin wax and embryos were incubated at 60°C for 2 hours with exchange of wax every 30 minutes. The embryos were arranged in the appropriate position with heated forceps under a stereomicroscope and left to set overnight at RT.

2.6.2   Microtome sectioning

Wax blocks were placed at -20°C for 20-30 minutes to loosen the wax from the glass mould. The blocks were cut to size and mounted onto wooden cubes using molten paraffin wax. Sections were cut at 5 µm on a microtome (Thermo Scientific) in serial sections (sets of 4) that were subsequently placed on SuperFrost Plus slides that were covered in Milli-Q water. Once the sections had flattened out, the water was removed and the sections were left to dry overnight at 37°C.

2.6.3   Gelatin/albumin embedding

Embryos that had been processed for in situ hybridisation were embedded in gelatin/albumin for vibratome sectioning. Gelatin (45% w/v; Sigma, type A) was dissolved in heated PBS and bovine albumin (27.3% w/v; Sigma) was added once the solution had cooled down to RT. Aliquots were stored at -20°C and thawed immediately prior to use. Whole mount in situ embryos stored in PBT were allowed to submerge in gelatin/albumin at 4°C. Small plastic moulds (capacity of ~330 µl) were filled up with gelatin/albumin and glutaraldehyde (2.3% v/v) was mixed in very rapidly. Embryos were added to the mix (one per mould), oriented, and the block was left to set for an hour. The solid gelatin/albumin block was stored in PBS at 4°C.

2.6.4 Vibratome sectioning

The mould was attached to the specimen disc of the vibratome (Leica) with super glue. The tray was filled with PBS and the specimen disc was secured. Sections were cut at 40 μm and placed on SuperFrost Plus slides in order, going from rostral to caudal or vice versa. The sections were mounted in 50% glycerol (v/v in Milli-Q water) with glass cover slides (#1.5, Thermo Scientific) which were sealed with nail varnish. Sections were stored at 4°C and images were acquired on a AxioCam HRc camera (Zeiss) attached to a compound microscope (Zeiss).

2.7 Whole mount in situ hybridisation

2.7.1 Plasmid DNA templates

Plasmid DNA templates for in situ hybridisation RNA probes are listed in Table 2.11. The p27 probe was cloned in the laboratory with following primer sequences: Forward: GCCCCTGGAGGGCAGATACGA, Reverse: CAGCCCAGATGGGGTGTCAGTTT. The INK4 probes were distributed to us by Prof. Andreas Kispert (Institut fur Molekularbiologie, Medizinische Hochschule Hannover, Germany) with permission from Prof. Charles Sherr (Tumor Cell Biology, St. Jude Children's Research Hospital, US).

2.7.2 RNA probe preparation

Competent DH5α cells were transformed with the plasmid DNA templates according to standard protocols and plated on LB agar (Invitrogen) plates containing 50 μg/ml ampicillin (Sigma). Negative control plates with competent cells but no plasmid were included in each experiment. Colonies were picked from the plates and bacterial cultures were grown in 15 ml falcon tubes containing 8 ml LB broth +ampicillin and incubated shaking at 37°C overnight. Bacterial cultures were spun down at 4,600 rpm for 20 minutes at 4°C and plasmid DNA was purified using a mini prep kit (Qiagen) according to manufacturer's protocol (QIAprep spin Miniprep Kit using a microcentrifuge). All plasmids except p21 were sequenced for verification

and then linearised, purified and transcribed in a reaction containing DIG labelling mix (Roche) using the restriction enzymes (RE) and RNA polymerases listed in Table 2.11. The transcribed probe was purified in a Chroma Spin-100 DEPC-H_2O column (Clontech) and 40 μl formamide and 1 μl RNAse inhibitor was added to the approximately 50 μl of DIG-labelled, single stranded RNA probe. Probes were stored at -20°C.

2.7.3   In situ hybridisation

2.7.3.1   Tissue pre-treatment and hybridisation

All steps were performed for 20 minutes shaking on ice unless otherwise stated. All solutions prior to hybridisation were DEPC treated to prevent degradation of RNA by RNAses.

Embryos were rehydrated from 100% methanol in a series of methanol – PBT washes (75%-50%-25%) followed by two PBT washes. Embryos were bleached in 6% hydrogen peroxide (30% stock solution, Sigma) in PBT for 1 hour followed by three 10 minute PBT washes, treated with proteinase K (5 μg/ml in PBT) for 1 minute (E7.5-8) or 1.5 minutes (E8.5) at RT to aid entry of the probe into the tissues, followed by 1 minute in glycine (2 mg/ml in PBT) at RT to inactivate proteinase K. Embryos were rinsed once in PBT, fixed for 20 minutes in 0.2% v/v glutaraldehyde (25% stock) in 4% PFA, and washed twice for 10 minutes in PBT. The embryos were transferred to 1 ml of pre-hybridisation mix (50% Formamide, 5xSSC pH 4.5, 50 μg/ml yeast RNA, 1% SDS, 50 μg/ml heparin in DEPC-H_2O) pre-heated to 70°C and incubated for 2 hours. DIG labelled RNA probes were added (approximately 1 μg/ml final volume) and the embryos were hybridised at 70°C overnight in an HB-1000 Hybridizer oven (UVP).

2.7.3.2   Post-hybridisation and immunohistochemistry

On the following day, embryos were transferred to solution I (50% formamide, 5x SSC pH 4.5, 1% SDS in ddH_2O) for a quick wash and then washed twice for 20 minutes at 70°C in solution I, followed by two 20 minute washes in solution II (50%

formamide, 2x SSC pH 4.5, 1% SDS in ddH$_2$O) at 65˚C. Embryos were taken to RT and washed three times for 10 minutes in Tris-buffered saline containing Tween-20 (TBST; 140 mM NaCl, 2.7 mM KCl, 25 mM Tris-HCl (pH 7.5), 2 mM tetramisole hydrochloride, 1% (v/v) Tween-20) followed by blocking at RT in 10% heat inactivated sheep serum (HI-SS) in TBST for at least 1 hour to block unspecific antibody binding sites. Embryos were incubated in 1:2000 alkaline phosphatase-conjugated sheep anti-DIG Fab fragments (AP-anti-DIG, Roche) in 1% HI-SS at 4˚C shaking overnight.

2.7.3.3   Post-antibody washes and development

Unbound antibody was washed off in TBST (3 x 5 minutes RT, 5 x 1 hour RT) and left washing in TBST shaking overnight at 4˚C. For developing, embryos were washed three times for 10 minutes in NTMT (100 mM NaCl, 100 mM Tris-HCl pH 9.5, 50 mM MgCl$_2$, 1% Tween-20) and the colour was developed using a reaction for the colorimetric detection of alkaline phosphatase activity with 4.5 µl/ml nitro blue tetrazolium chloride (NBT, Roche) and 3.5 µl/ml 5-bromo-4-chloro-3-indolyl phosphate (BCIP, Roche) in NTMT at RT. Alkaline phosphatase catalyses the hydrolysis of BCIP generating a compound that is oxidised by NBT to produce an insoluble, blue precipitate. To stop development, embryos were washed three times in PBT, post fixed for 1 hour in 4% PFA at RT, washed again in PBT and stored in PBT at 4°C until embedded in gelatin/albumin for vibratome sectioning.

Probe	Vector	Insert size (bp)	RE and RNA polymerase AS probe	RE and RNA polymerase S probe	Source	Reference
p21	pGEM®-T Easy	612	NCoI, SP6	SalI, T7	A.Hoshino	-
p27	pGEM®-T Easy	446	NsiI, T7	NcoI, SP6	new	-
p57	unknown	668	Not linearised, T3	Not linearised SP6	A.Suzuki-Hirano	(Suzuki-Hirano et al., 2011)
Shh	pBluescript SK (-)	640	HindIII, T3	PstI, T7	N.D.E.Greene	(Greene et al., 1998)
Brachyury	M13	1660	SacII, T7	-	R.Beddington	(Wilkinson et al., 1990)
p15INK4b	pBluescript KS (-)	1300	SpeI, T3	-	C.Sherr	(Ludtke et al., 2009)
p16INK4a/ p19ARF	pBluescript KS (+)	1100	NaeI, T3	SalI, T7	C.Sherr	(Ludtke et al., 2009)
p18INK4c	pBluescript SK	510	NotI, T7	SalI, T3	C.Sherr	(Ludtke et al., 2009)
p19INK4d	pBluescript SK	500	NotI, T7	SalI, T3	C.Sherr	(Ludtke et al., 2009)

Table 2.11 - Plasmid DNA templates for in situ hybridisation RNA probes

2.8 Immunofluorescence on tissue sections

All protocols were performed on 5 μm paraffin sections and imaged with epifluorescence on an inverted LSM710 confocal system mounted onto an Axio Observer Z1 microscope (Carl Zeiss Ltd, UK). The Alexa-488 secondary antibodies were excited by a 488 nm line of Argon laser and the Alexa-568 by a 561 nm diode laser. Z-stacks, counting, measurements, and image processing (brightness and contrast only) were done in Image J.

All steps were performed shaking at RT in plastic troughs with a capacity of 200 ml unless otherwise stated. For the DAPI-, PFA fixation-, antigen blocking-, and antibody incubation steps, slides were laid out horizontal in a humidified chamber with tissue soaked in MilliQ-water.

2.8.1 IdU and BrdU

2.8.1.1 De-waxing, rehydration and antigen retrieval

Paraffin was removed in two 5 minute washes in Histo-Clear (National Diagnostics) and rehydrated in a series of 5 minute ethanol washes (2x 100%, 90%, 80%, 70%, 50% and 25% in MilliQ-water) followed by 5 minutes under running dH_2O water. Antigen unmasking was achieved by boiling the slides in 0.01 M citric acid buffer in MilliQ-water (adjusted to pH 6.0 with NaOH) for 8 minutes in a 1000 W microwave at the highest setting. Slides were allowed to cool at RT for at least 30 minutes and were then washed 4x 10 minutes in PBS with 0.1% Triton.

2.8.1.2 Pre-fixation

Nuclei were stained with 4',6-diamidino-2-phenylindole (DAPI) 1:10,000 in PBS for 3 minutes (1 ml per slide) prior to DNA denaturation as DAPI binds single stranded DNA very poorly. Slides were washed four times in PBS for 5 minutes and fixed in freshly made 4% PFA (w/v in PBS) for 50 minutes at RT (500 μl per slide, covered by Parafilm) to fix DAPI.

2.8.1.3 Post-fixation

Slides were washed twice in PBS and the DNA was denatured in 0.1 M HCl for 30 minutes at RT followed by a 2 M HCl solution for 30 minutes at 37°C. The slides were neutralised in 0.1 M Sodium borate buffer pH 8.5 for 10 minutes at RT and washed twice in PBS for 5 minutes. The slides were blocked in 10% heat inactivated sheep serum (HI-SS) in blocking buffer (0.2% BSA, 0.15% glycine and 0.1% triton in PBS) for at least 1 hour at RT (300 µl per slide + Parafilm). The blocking solution was replaced by mouse anti-IdU/BrdU and rat anti-BrdU at a 1:100 dilution in 10% HI-SS in blocking buffer (200 µl per slide + Parafilm) and incubated at 4°C overnight.

Following day slides were washed three times in PBS + 0.1% triton and incubated in secondary antibodies: anti-mouse Alexa-488 and anti-rat Alexa 568 at a 1:200 dilution in 10% HI-SS in blocking buffer (200 µl per slide + Parafilm) for 1 hour at RT. Slides were washed three times in PBS + 0.1% triton and mounted in Mowiol 4-88 mounting medium (Sigma; prepared with glycerol and 0.2 M Tris-HCl pH 6.8).

2.8.1.4 IdU and pHH3

Slides were de-waxed, rehydrated and antigens were unmasked exactly as described above (Section 2.8.1.1). Subsequently, slides were blocked in 10% HI-SS in blocking buffer for 1 hour at RT (300 µl per slide + Parafilm) and then incubated with rabbit anti-pHH3 (1:250) in 5% HI-SS in blocking buffer for 1 hour at RT. Slides were washed three times for 10 minutes in PBS + 0.1% triton and incubated with anti-rabbit Alexa-568 secondary antibody (1:500) in 10% HI-SS in blocking buffer for 1 hour at RT (200 µl per slide + Parafilm). The antibody was washed off in three 10 minute PBS + 0.1% triton washes, incubated with DAPI 1:10,000 for 3 minutes at RT, washed 3 times with PBS + 0.1% triton and fixed in fresh 4% PFA for 50 minutes at RT. The rest of the protocol was exactly as described above for IdU (Section 2.8.1.3), excluding the primary rat anti-BrdU antibody and the secondary anti-rat Alexa-568 antibody.

2.8.1.5   GFP (overexpressing slides)

De-waxing, rehydration and antigen retrieval were as described in Section 2.8.1.1. Sections were blocked in 10% HI-SS in blocking buffer for at least 1 hour at RT and incubated with chick anti-GFP primary antibody (1:300) in 5% HI-SS in blocking buffer at 4°C overnight.

The following day, slides were washed 3 x 10 minutes in PBS + 0.1% triton and incubated with anti-chick Alexa-488 secondary antibody (1:500) in 5% HI-SS in blocking buffer for 1 hour at RT. Slides were then washed 4 x 10 minutes in PBS + 0.1% triton, incubated with DAPI 1:10,000 for 3 minutes at RT, washed twice in PBS and mounted in Mowiol.

2.8.1.6   β-catenin (knock-down slides) and p21

Sections were de-waxed with two Histo-Clear washes (10 minutes) and rehydrated in a series of washes of decreasing ethanol concentrations (2 x 100%, 90%, 80%, 70%, 60%, 50% and 25%) followed by 5 minutes under running dH_2O. Antigens were retrieved by adding slides to cold 1 x Declere solution (Cell Marque) in a plastic trough and boiling 60 minutes in a kitchen steamer. After the first 30 minutes the slides were transferred to a new trough with fresh, heated Declere. Sections were allowed to cool at RT for at least 30 minutes, washed three times with PBS + 0.1% triton, and blocked with 5% HI-SS in blocking buffer for at least 1 hour. Slides were incubated with rabbit anti-β-catenin (1:500) or mouse anti-p21 (1:100) in 5% HI-SS in blocking buffer overnight at 4°C. Slides were washed three times in PBS + 0.1% triton, incubated 1 hour in anti-rabbit Alexa-488 for β-catenin (1:500), or anti-mouse biotin for p21 (1:250) in 5% HI-SS in blocking buffer. β-catenin slides were washed three times in PBS + 0.1% triton, stained with DAPI 1:10,000 for 3 minutes, washed in PBS and mounted in Mowiol. p21 slides were incubated for 1 hour in Streptavidin-555 (1:300) in 5% HI-SS in blocking buffer before the final washes, DAPI staining, and mounting.

2.8.1.7   Antibodies

Target	Raised in	Dilution	Supplier	Cat.No.
Anti-phospho Histone H3 (Ser10), Mitosis marker	Rabbit (polyclonal)	1:500	Millipore	06-570
BrdU (not IdU) [BU1/75 (ICR1)]	Rat (monoclonal)	1:100	abcam	Ab6326
BrdU (and IdU) clone B44	Mouse (monoclonal)	1:100	BD Biosciences	347583
p21 (F-5)	Mouse (monoclonal)	1:100	Santa Cruz	sc-6246
p27 (Kip1)	Mouse (monoclonal)	1:200	BD Transd.lab.	610241
p57 (Kip2)	Rabbit (polyclonal)	1:250	abcam	ab4058
GFP	Chicken (polyclonal)	1:300	abcam	ab13970
β-catenin	Rabbit (polyclonal)	1:500	abcam	ab16051

Table 2.12 - Primary antibodies

Target	Raised in	Conjugate	Dilution	Supplier	Cat.No.
Rat IgG (H+L)	Goat	Alexa Fluor 568	1:200	Thermo Fischer	A-11077
Mouse IgG (H+L)	Goat	Alexa Fluor 488	1:200	Thermo Fisher	A-11001
Mouse IgG (H+L)	Goat	Alexa Fluor 568	1:500	Thermo Fisher	A-11004
Rabbit IgG (H+L)	Goat	Alexa Fluor 568	1:500	Thermo Fisher	A-11011
Rabbit IgG (H+L)	Goat	Alexa Fluor 488	1:500	Thermo Fisher	A-11008
Chicken (H+L)	Goat	Alexa Fluor 488	1:500	Thermo Fisher	A-11039

Table 2.13 - Secondary antibodies for immunofluorescence

2.9   Genotyping

Ear clips and yolk sacs were genotyped by polymerase chain reaction (PCR) amplification of DNA. The DNA was extracted using DNA lysis buffer (Invitrogen) with 0.5 mg/ml added proteinase K. PCR reagents, primers and programmes are shown in the tables below for p21, p27 and Shh genotypes.

2.9.1   p21 genotyping

Reagent	Volume (µl)
10X Reaction buffer (Bioline)	2
dNTPs (Promega)	2
50 mM MgCl$_2$ (Bioline)	0.6
40 µM Primer (Forward, Reverse and Neo)	3 x 0.12
5 U/µl Taq DNA polymerase (Bioline)	0.2
H$_2$O (Sigma)	13.84
DNA	1
Final volume	**20**
F primer: ACCCAGCAAAGCCTTGATTCT **R primer**: CAGGTCGGACATCACCAGGAT **Neo primer**: CCTTCTATCGCCTTCTTGACGA	

Table 2.14 - p21 PCR reaction

Product size: p21 wt 760 bp, p21 KO 600 bp.

Step	Duration and temperature
1. Heating	5 minutes, 94°C
2. Denaturation	1 minute, 94°
3. Annealing	1 minute, 60°C
4. Extension	90 seconds, 72°C
5. Final extension	10 minutes, 72°C

Table 2.15 - PCR programme for p21 genotyping

Steps 2-4 were repeated 35 times.

2.9.2   p27 genotyping

2.9.2.1   p27 wild-type PCR

Reagent	Volume (µl)
10X Reaction buffer (Bioline)	2.5
dNTPs (Promega)	2.5
50 mM MgCl$_2$ (Bioline)	0.5
Betaine 5 M	2.5
40 µM Primer pair (Forward and Reverse)	0.5
5 U/µl Taq DNA polymerase (Bioline)	0.2
H$_2$O (Sigma)	15.3
DNA	1
Final volume	**25**
F primer: GATGGACGCCAGACAA**G**C **R primer**: CTCCTGCCACTCGTATCT	

Table 2.16 - p27 wt PCR reagents

PCR product size: 190 bp.

Step	Duration and temperature
1. Heating	5 minutes, 95°C
2. Denaturation	30 seconds, 95°
3. Annealing	30 seconds, 55°C
4. Extension	45 seconds, 72°C
5. Final extension	10 minutes, 72°C

Table 2.17 - p27 wt PCR programme

Steps 2-4 were repeated 40 times.

2.9.2.2   p27 knock-out PCR

Reagent	Volume (µl)
10X Reaction buffer (Bioline)	2.5
dNTPs (Promega)	2.5
50 mM MgCl$_2$ (Bioline)	0.75
Betaine 5 M	2.5
40 µM Primer pair (Forward and Reverse)	0.5
5 U/µl Taq DNA polymerase (Bioline)	0.2
H$_2$O (Sigma)	15.05
DNA	1
Final volume	**25**
F primer: TGGAACCCTGTGCCATCTCTAT **R primer**: CCTTCTATCGCCTTCTTGACG	

Table 2.18 - p27 knock-out PCR reagents

Primers detect the Neo insert. PCR product size: 600 bp.

Step	Duration and temperature
1. Heating	5 minutes, 95°C
2. Denaturation	1 minute, 95°
3. Annealing	1 minute, 57°C
4. Extension	90 seconds, 72°C
5. Final extension	10 minutes, 72°C

Table 2.19 - p27 knock-out PCR programme

Steps 2-4 were repeated 40 cycles.

2.9.3 Shh genotyping

Reagent	Volume (µl)
10X Reaction buffer (Bioline)	2
dNTPs (Promega)	2
50 mM MgCl$_2$ (Bioline)	0.6
25 µM Primer pair Neo or wt (F+R)	2
5 U/µl Taq DNA polymerase (Bioline)	0.2
H$_2$O (Sigma)	12.2
DNA	1
Final volume	**20**
F primer: TGGAACCCTGTGCCATCTCTAT **R primer**: CCTTCTATCGCCTTCTTGACG	

Table 2.20 - Shh PCR reaction

The Neo primer pair detects the Neo/deleted allele and produces a 500 bp product. The wild-type primer pair detects the floxed (550 bp) and the wildtype allele (500 bp).

Step	Duration and temperature
1. Heating	2 minutes, 94°C
2. Denaturation	30 seconds, 94°
3. Annealing	30 seconds, 60°C
4. Extension	45 seconds, 72°C
5. Final extension	5 minutes, 72°C

Table 2.21 - Shh Neo PCR programme

Steps 2-4 were repeated 33 cycles.

Step	Duration and temperature
1. Heating	5 minutes, 95°C
2. Denaturation	1 minute, 95°
3. Annealing	1 minute, 70°C
4. Extension	1 minute, 72°C
5. Final extension	8 minutes, 72°C

Table 2.22 - Shh wt/floxed PCR programme

Steps 2-4 were repeated 35 cycles.

2.9.4 Agarose gel electrophoresis

PCR products were assayed by agarose gel electrophoresis. The size of the products was compared to molecular weight markers (Bioline Hyperladders). Ladder V was loaded alongside samples with expected PCR products between 25 and 500 bp, and ladder I was used for products between 200-10,000 bp. Gel concentrations were 2-4% w/v agarose in TAE buffer (40 mM Tris acetate and 1 mM EDTA in water). Ethidium bromide was added to the molten agarose to label the DNA. Samples were loaded with loading dye made with Orange G for colour (50% glycerol and 50% 1xTE buffer [10 mM Tris EDTA pH 8]).

2.10 Statistical analysis

Statistical tests were performed in SigmaStat version 3.5. The student's t-test was used to compare a single parameter between two groups, One way ANOVA was used to compare one parameter between more than two groups, and a Two way ANOVA was used to compare two parameters between more than two groups.

Chapter 3 - CIP/KIPs are expressed in the MHP

3.1 Introduction

As introduced in Section 1.3.3, it is thought that basal expansion of cells of the midline is responsible for cell shape changes and MHP formation. This basal expansion could be accounted for by changes in the cell cycle through IKNM, as keeping the nuclei at the base of the neuroepithelium would generate wedge shaped cells. Indeed, the cell cycle of MHP cells has been shown to be longer than that of lateral cells (Langman et al., 1966; McShane et al., 2015; Smith and Schoenwolf, 1987; Smith and Schoenwolf, 1988). In this chapter I examine the expression in wild-type (CD1) mice of negative regulators of the cell cycle, the cyclin-dependent kinase inhibitor (CDKI) families: CIP/KIP and INK4. CDKIs in general can inhibit transition from G1- to S-phase, thereby potentially keeping the nuclei basal. The CIP/KIP family has roles beyond G1- to S-phase transition and can halt the cell cycle in S-phase as well as interrupt S- to G2-phase transition and entry into mitosis (Section 1.6).

Previous work conducted in our laboratory identified the CDKI, p21, as being expressed specifically in the MHP. This finding pointed to p21 and the CIP/KIP family as candidates for cell cycle regulation in the MHP, and provided the impetus for the present study.

3.1.1 CIP/KIP expression

In the literature, p21 expression has been reported from E8.25 in whole embryos by qRT-PCR (Ishimura et al., 2012). In situ hybridisation revealed p21 expression along the midline of the neural tube, hindgut and dermamyotome of somites at E8.5 (Parker et al., 1995). By E10, p21 is expressed in muscle cells of the myotome and, at E13 to E15 p21 is expressed in the nasal epithelium, tongue muscles, hair follicles, the outermost embryonic epidermis, and in the cartilage; sites that all, with

the exception of cartilage, contain post-mitotic, differentiated cells (Matsuoka et al., 1995; Parker et al., 1995).

p21 has been reported to be expressed primarily in post-mitotic differentiated cells (Brugarolas et al., 1995; el-Deiry et al., 1993; Parker et al., 1995). The fact that p21 mice develop normally does however suggest that the role in terminal differentiation must be redundant. Indeed, analysis of the induction of p21 in differentiating myoblasts has shown that p21 induction occurs at a late stage of differentiation after DNA synthesis has stopped, suggesting a role in maintenance of differentiation rather than a role in differentiation itself (Deng et al., 1995).

During mouse embryogenesis, p27 protein is detected in the brain, dorsal root ganglion, lens, retina, lung, cochlea, endocardial cells of the heart, myocardium, kidney, adrenal medulla, liver, skin, thymus, spleen, testis and ovary (Nagahama et al., 2001).

The expression pattern of p57 is similar in human and mouse tissues. During embryogenesis p57 protein is detected in the brain, dorsal root ganglion, lens, lung, endocardial cells of the heart, liver, kidney, skin, palate, pancreas, gut, adrenal cortex, cartilage, and skeletal muscle (Nagahama et al., 2001). Furthermore, mRNA is detected in the neural epithelium, heart, brain, lens epithelium of the eye, lung, kidney, limb buds, palate, skeletal muscle, cartilage and in somites (Matsuoka et al., 1995; Nagahama et al., 2001; Westbury et al., 2001; Yan et al., 1997; Zhang et al., 1997). The mRNA and protein expression of p57 in the mouse is in general consistent with tissues affected in Beckwith-Weidemann syndrome (BWS) in humans (Matsuoka et al., 1995; Westbury et al., 2001). There are, however, tissues that do develop normally in patients with the syndrome that express high levels of p57 in the mouse, i.e. the gonads, lungs and the brain (Westbury et al., 2001). p57 is associated with cells that have left the cell cycle, i.e. post mitotic differentiated cells although, interestingly, p57 is also expressed in many tissues whose cells are not terminally differentiated but instead are undergoing shape changing. Examples of these include the pituitary infundibulum, the lung columnar cells, and the kidney

(Westbury et al., 2001). p57 expression mainly ceases before birth whereas p27 expression is sustained into adult life (Nagahama et al., 2001).

3.1.2 Embryonic expression of INK4 genes

Published work from Northern blots of whole, wild-type embryos has shown that p18INK4c and p19INK4d are expressed in the mouse embryo from E7, while p15INK4b, p16INK4a and p19ARF are not detected at embryonic stages (Zindy et al., 1997a). By in situ hybridisation, however, none of the INK4 genes could be detected during early (<E11.5) mouse embryonic development, and their location during neurulation has therefore not been described (Zindy et al., 1997b). p19INK4d was detected from E11.5 and p18INK4c from E13.5. p15INK4b, p16INK4a and p19ARF were not detected at any embryonic stage by in situ hybridisation consistent with the Northern blot data (Zindy et al., 1997b).

In the developing mouse cortex, the presence of p18INK4c mRNA transcripts are associated with a lengthening in G1-phase of the cell cycle as there is a switch from symmetrical cell divisions to asymmetrical cell divisions. Once neuronal differentiation has occurred, p18INK4c mRNA expression is lost (Zindy et al., 1997b). p19INK4d and p27 have been shown to be co-expressed in the developing mouse cerebral cortex (Zindy et al., 1997b).

3.2 Results

3.2.1 CIP/KIP expression in wild-type (CD1) embryos

As mentioned, p21 had been shown to be expressed specifically in the MHP. p21 is well known as a cell cycle regulator able to prevent cells from entering S-phase, as well as blocking cells going from S-phase into G2-phase (Deng et al., 1995). Thus, p21 could be responsible for prolonging the time nuclei in the MHP spend at the basal neuroepithelium during S-phase, and possibly late G1-phase. To test this, I analysed the expression of p21 and the related genes, p27, p57 and the INK4 genes, in neurulation stage embryos.

The p21 and p27 in situ hybridisation probes were designed in the laboratory and the p57 probe, received from Dr Shimogori at the RIKEN institute, has been published (Suzuki-Hirano et al., 2011). The specificity of the probes was tested in CD1 embryos with p21, p27 and p57 in situ probes transcribed in the sense direction (Figure 3.1). The majority of embryos (4/5) hybridised with the p21 sense probe showed some staining in the rostral part of the embryo while no transcripts were ever detected in the caudal region, where transcripts were apparent with the antisense probe (Figure 3.1, A and B). No expression was detected in embryos hybridised with the p27 or p57 sense probes (Figure 3.1, C-F).

In CD1 embryos, p21 is expressed in the PNP beginning at the 5 somite stage and is observed until the 19 somite stage which was the latest stage tested (Figure 3.2; arrows). At the 11 somite stage, p21 expression is detected in the head and primordium of the limb and from the 13 somite stage expression is observed in the ventral midbrain, branchial arches, and 'oldest' somites (Figure 3.2, D-F). To see which exact regions in the PNP express p21, the embryos were subsequently sectioned at 40 μm.

At the 8 somite stage, sections reveal that p21 is strongly expressed in the PNP in caudal, relatively flat regions and is not specific to the midline (Figure 3.3, F-G; arrows). At more rostral levels p21 expression becomes restricted to the midline (Figure 3.3, D-E), gets weaker and is eventually lost just caudal to the closing neural tube (Figure 3.3, B-C).

In embryos at the 19 somite stage, p21 is not expressed in the closed neural tube but is observed in the underlying dorsal hindgut (Figure 3.4, B). Posterior to the closed neural tube, p21 is expressed specifically in the MHP (Figure 3.4, C). This expression is strong and more widespread at posterior levels of newly formed neural plate (Figure 3.4, D). p21 is expressed in the hindgut at all levels, ventral at first and more uniform at posterior levels (Figure 3.4, B-D).
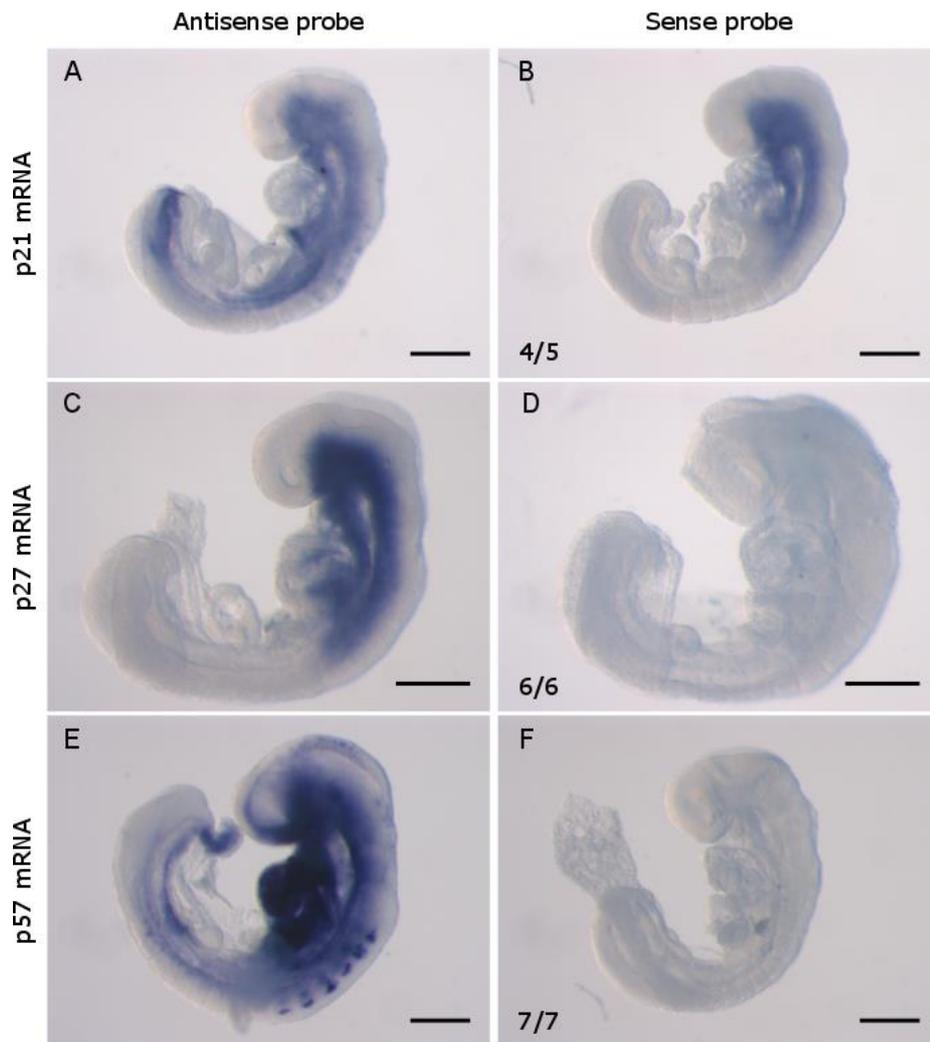
Figure 3.1 - Specificity of CIP/KIP probes

Whole mount in situ hybridisation of E8.5 CD1 embryos with p21, p27 and p57 antisense (A, C, E) or sense (B, D, F) probes reveals non-specific p21 staining in the rostral region of the embryo (B). The staining observed in the caudal region for p21 with the antisense probe is not detected with the sense probe (A-B). The p27 and the p57 probes are specific and no apparent expression is observed (D and F). Scale bars = 100 μm.

Next, the expression of other CIP/KIP gene family members was analysed. p57 is strongly expressed in the heart at all stages analysed, starting at the 5 somite stage (Figure 3.5, A-F). At the 9 somite stage, p57 is expressed in the notochord (Figure 3.5, C; inset) and midbrain. At later stages, p57 expression is observed in the notochord, head, branchial arches, heart, limb buds and somites (Figure 3.5, C-F). Although p57 was not detected at the prospective closure 1 site at the 6 somite stage, it is expressed in the closed neural tube from 16 somites onwards.

p27 expression is not seen at the 8 somite stage (Figure 3.6, A) and is later observed in the ventral region of the anterior neural tube, the midbrain, and the branchial arches (Figure 3.6, B-C). At the 26 somite stage, p27 expression is widespread and seen in most regions of the head, branchial arches, limb buds and ventral neural tube. Note that p27 expression is excluded from the dorsal neural tube, the heart, and is weak, or excluded, from the notochord (Figure 3.6; arrow).

CIP/KIP expression was further examined in the PNP of CD1 embryos at 12 and 15 somites. At the 12 somite stage, p21 is expressed caudally in a wide region of the ventral neural plate including a region with more intense expression in the MHP (Figure 3.7, A-A''). At more rostral levels p21 expression is restricted to the MHP and is weakest in the closed neural tube (Figure 3.7, A'''-A''''). At the most caudal level, p27 is detected in the midline tissues underlying the neural plate and is detected in the ventral region of the neural plate at more rostral levels (Figure 3.7, B'-B''''). In the closed neural tube the expression of p27 looks similar to that of p21. p57 is expressed in the V-shaped neural plate in a broad domain covering almost the entire dorso-ventral axis (Figure 3.7, C''-C'''), the notochord and in the entire closed neural tube with possible exception of the dorsal-most region (Figure 3.7, C'''').

At the 15 somite stage, p21 is strongly expressed in the PNP at all anteroposterior levels with a broad expression domain in the forming MHP (Figure 3.8, A'; arrow) that is more specific as the MHP sharpens, nearer to the closure point (Figure 3.8, A''; arrow). In the closed neural tube p21 expression is relatively weak. Similarly to embryos at the 12 somite stage, p27 and p57 are expressed throughout most of the V-shaped neural plate at 15 somites, with no difference in intensity between the MHP and lateral neural folds (Figure 3.8, B'' and C''; arrows). However, they are not strongly expressed at very caudal levels (Figure 3.8, B' and C'). p57 expression is strong in the notochord while p21 and p27 are weakly expressed, or excluded (Figure 3.8, A''', B''', C''; arrowheads). Note that p21, p27 and p57 are all expressed at the same axial level in the MHP at the 12 and 15 somite stage (Figure 3.7, A'''-C''' and Figure 3.8, A''-C'').
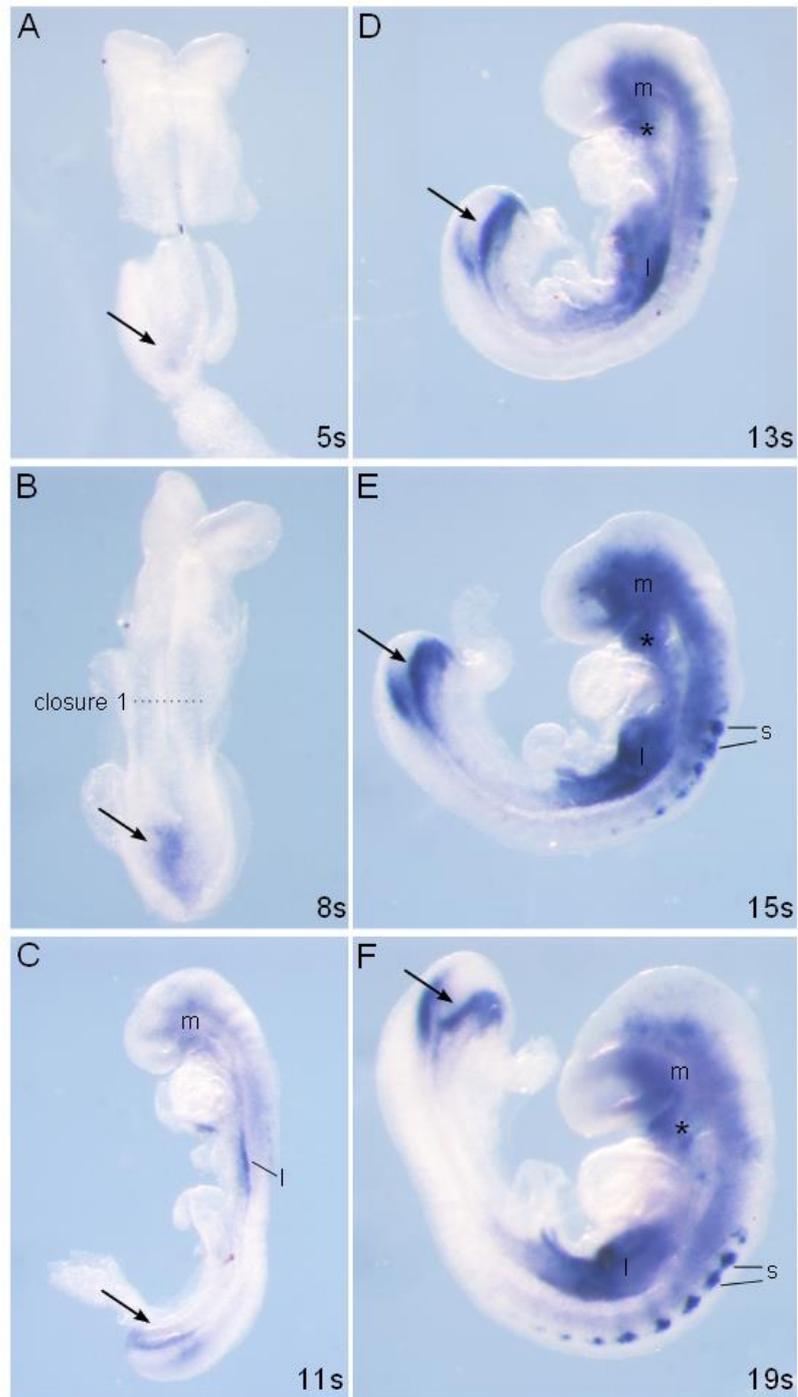
Figure 3.2 - p21 gene expression in whole mounts at the 5-19 somite stage

p21 expression in CD1 embryos by in situ hybridisation. Expression is first observed in the PNP at 5 somites and this domain remains positive until 19 somites (A-F, arrows). p21 is not expressed at the level of closure 1 (B). At 11 somites, expression is observed in the ventral midbrain (m) and in the primordium of the limb (l) (C). From the 13 to 19 somite stage, p21 is expressed in the ventral midbrain (m), branchial arches (*), limb buds (l), somites (s) and in the PNP (arrow) (D-F).
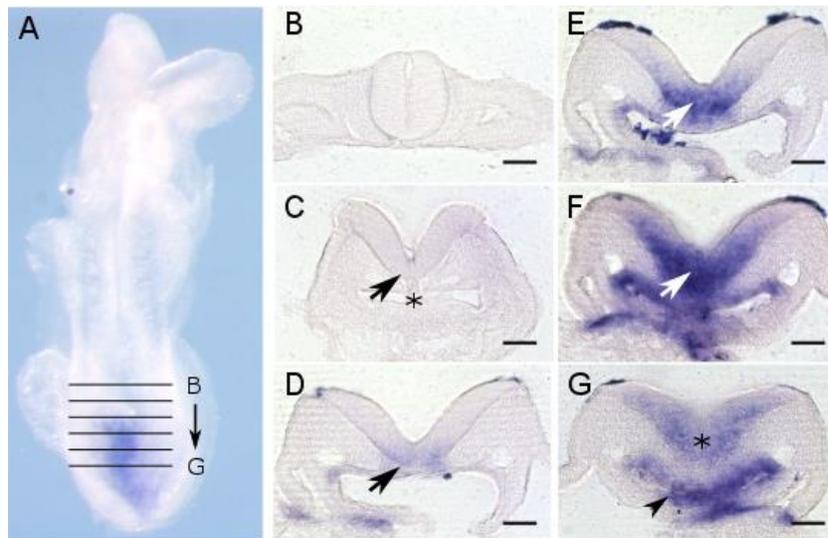
Figure 3.3 - p21 expression in a sectioned embryo at 8 somites

p21 expression at 8 somites as detected by in situ hybridisation. The plane of sections B-G is indicated on the whole mount in situ embryo (A). Section B is rostral and G is caudal (A). p21 is not expressed in the closed neural tube or in the sections immediately caudal to the closed region, including the region overlying the notochord (B-C; *). p21 expression is strong at caudal levels of MHP formation (E-G) and becomes weaker at more rostral levels (D; arrow). In the bent neural plate (D-E) p21 expression is specific to the MHP (arrows) whereas this expression domain is more diffuse caudally (F-G). At very caudal levels of the embryo, where the neural plate is more flattened, p21 expression is observed throughout the newly formed neural plate and is strong in the roof of the hindgut (arrowhead), and the notochordal plate (*) (G). Scale bars = 50 μm.
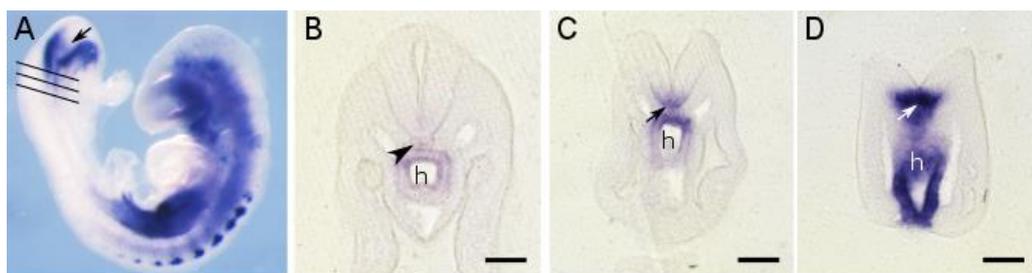
Figure 3.4 - p21 expression in a sectioned embryo at 19 somites

p21 expression at 19 somites as detected by in situ hybridisation. The plane of sections B-D is shown in A; B is rostral and D caudal (A). p21 expression is not observed in the closed neural tube but is present in the roof of the hindgut (B-C; h). In the open neural tube, p21 expression is weak and very specific to the MHP (C; arrow). At more caudal levels expression is stronger and broader but still specific to the midline (D; arrow). p21 is expressed in the hindgut (h) at all planes examined. In the rostral sections this expression domain is limited to the roof of the hindgut and becomes stronger and wider to include all of the hindgut in the caudal most section (B-D). Scale bars = 50 μm.
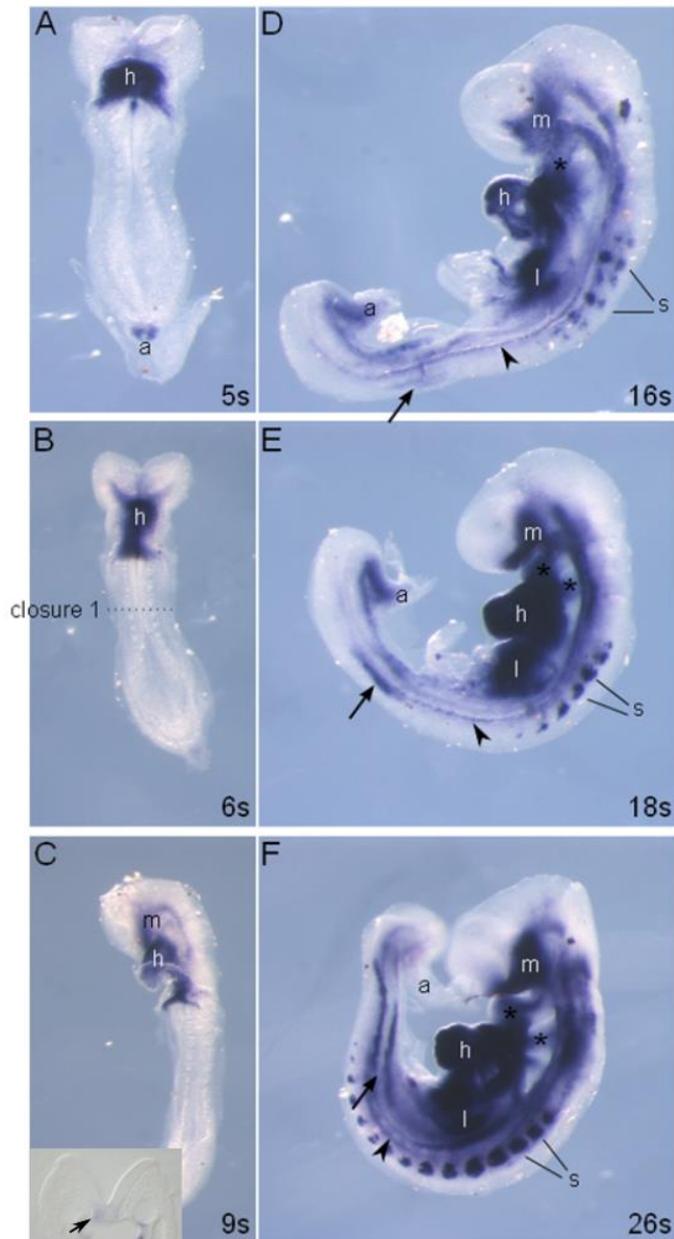
Figure 3.5 - p57 mRNA expression in whole mount neurulation stage embryos

p57 expression in mouse embryos from 5 to 26 somites detected by in situ hybridisation. At 5-6 somites p57 is strongly expressed in the heart (h) and the allantois (a) but not at the level of closure 1 (A-B). Expression in the heart is very strong at all stages examined (A-F). At 9 somites p57 expression has spread to the ventral midbrain (m) and this expression is maintained until 26 somites (C-F). p57 is also observed in the notochord (C, inset, arrow) at this stage. At 16-26 somites, p57 is expressed in the ventral midbrain (m), branchial arches (*), heart (h), limb buds (l), somites (s), notochord (arrowhead), neural tube (arrow), and allantois (a) (D-F). This expression pattern is maintained through to the latest stages examined, with exception of expression in the allantois (a) which is lost by 26 somites (F).
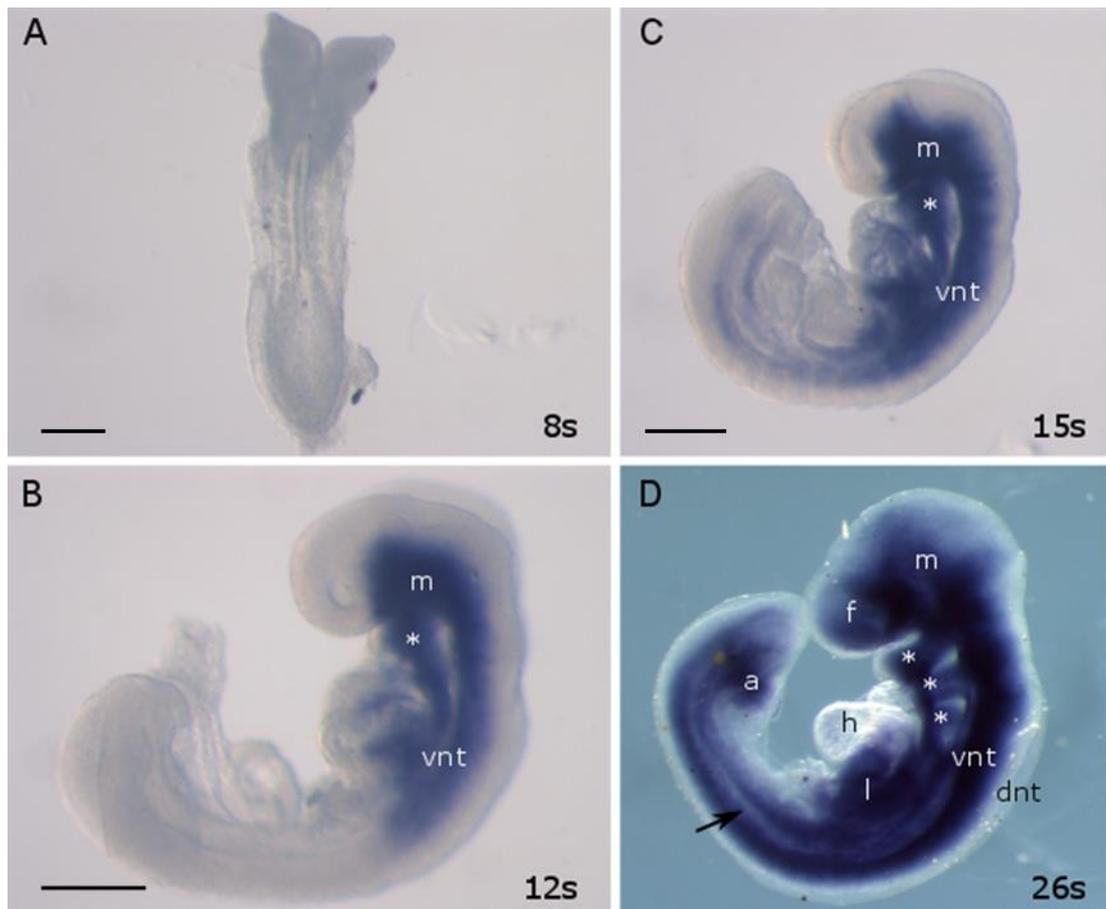
Figure 3.6 - p27 expression in whole mount neurulation stage embryos

p27 expression in mouse embryos from 8-26 somites as detected by in situ hybridisation. p27 is not detected at the 8 somite stage (A). At 12-15 somites p27 is expressed in the ventral midbrain (m), the anterior ventral neural tube (vnt), and in the first branchial arch (*) (B-C). At the 26 somite stage p27 is expressed in most tissues except the dorsal neural tube (dnt), the heart (h), and possibly the notochord (arrow) (D). Scale bars = 100 μm.
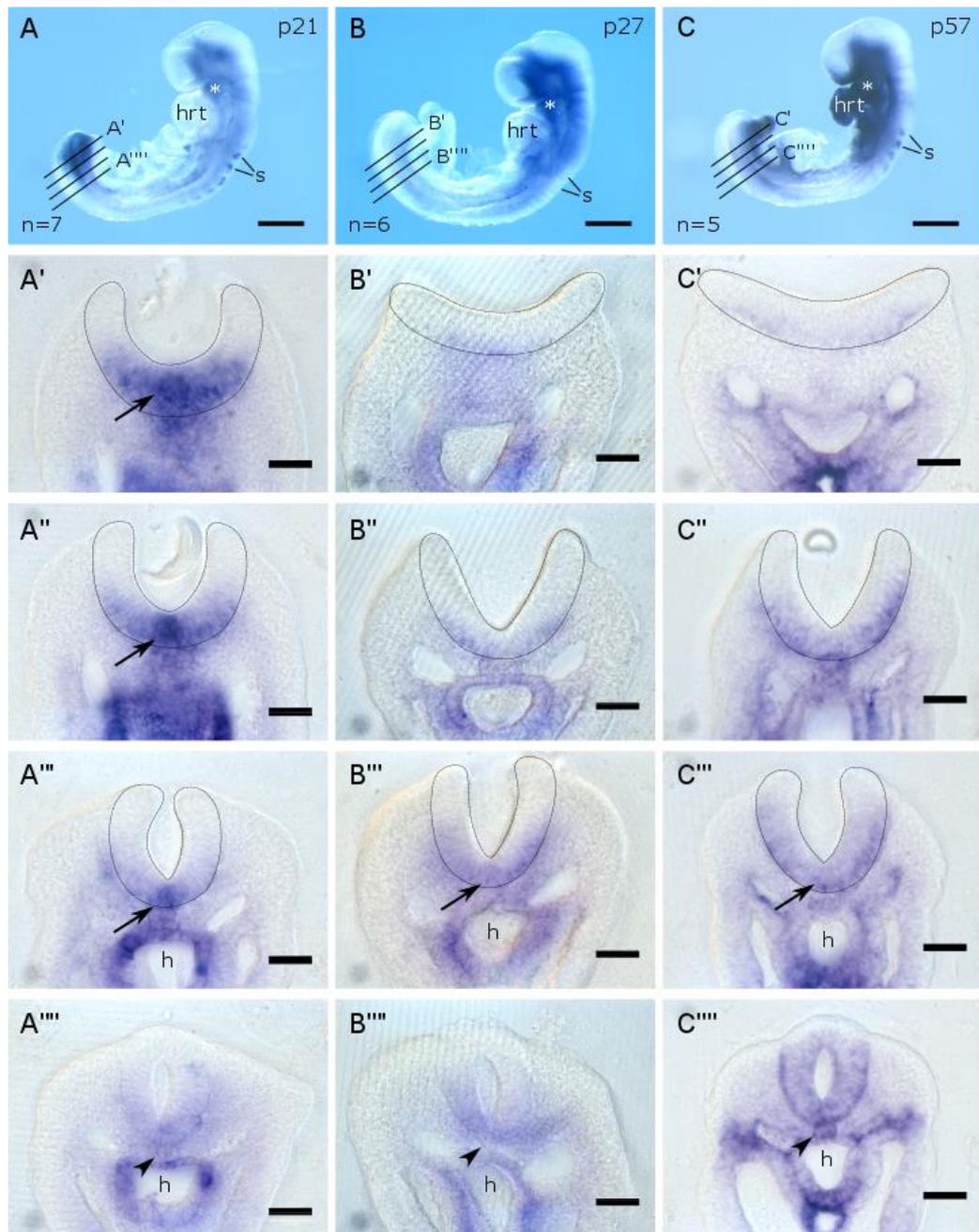
Figure 3.7 - Expression of p21, p27 and p57 in the PNP region of 12 somite stage embryos

In situ hybridisation shows that p21 is expressed across the neural plate width at caudal levels and more specifically in the MHP at a more rostral level, nearer to the closure point (A'-A'''). p21 is also expressed in the roof of the hindgut (A'-A''''). p27 transcripts are detected in the V-shaped neural plate, closed neural tube and the entire hindgut (h) (B''-B'''). p57 expression is similar to p27 in the V-shaped neural plate but covers a wider dorso-ventral area and is strongly expressed throughout the neural tube and notochord (arrowhead) (C''-C'''). Neither p27 nor p57 is expressed as intensely as p21 in the V-shaped neural plate and, unlike p21, do not show regional differences between the MHP and the lateral neural plate (A''', B''' and C'''; arrows). Scale bars = 300 µm (whole mounts) and 100 µm (sections).
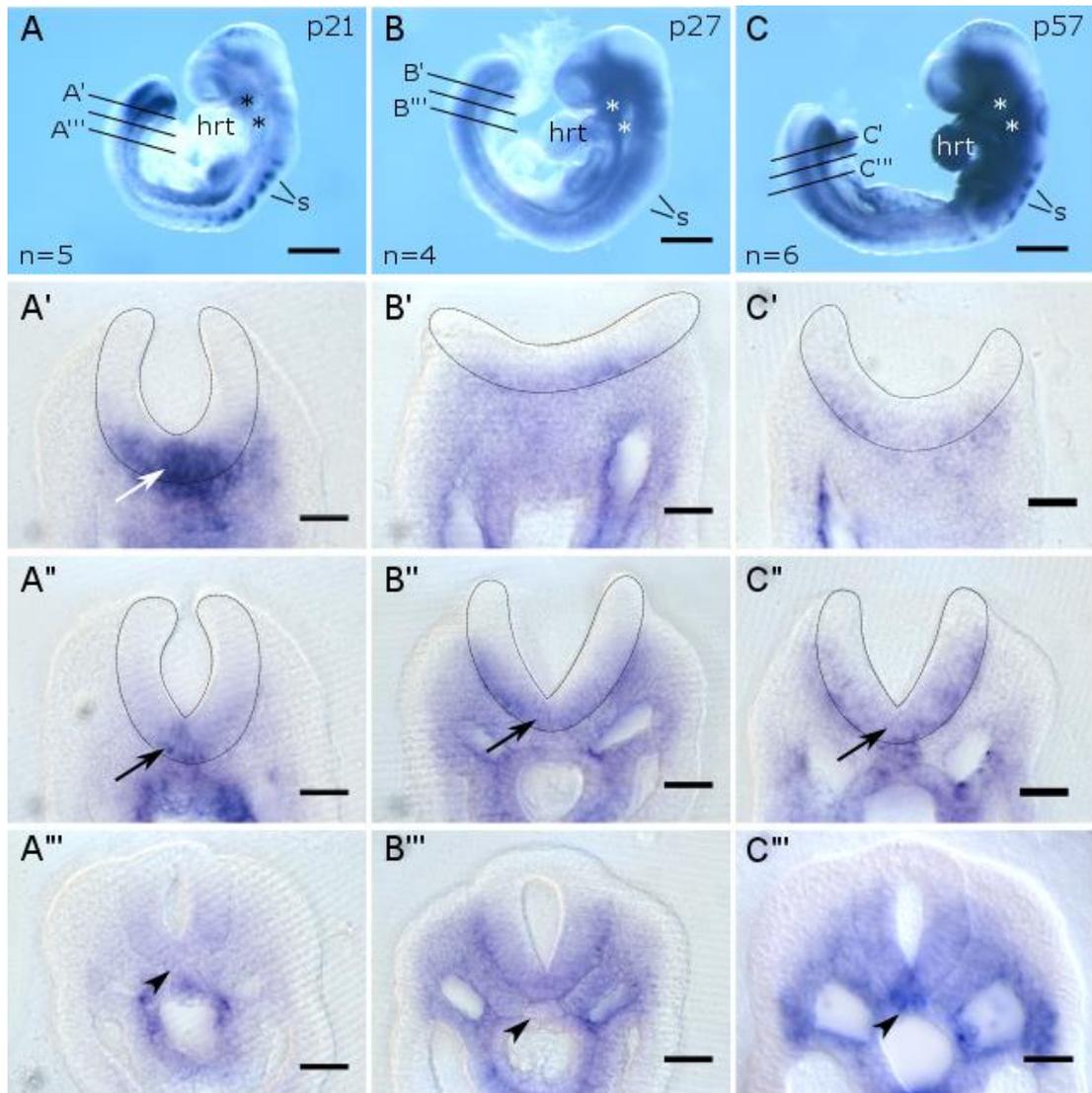
Figure 3.8 - Expression of p21, p27 and p57 in the PNP region of 15 somite stage embryos

At the 15 somite stage p21 is expressed at all levels of the PNP examined (A-A'''). The expression is broad in the forming MHP (A') and more specific in the mature MHP with weaker expression extending throughout the ventral neuroepithelium (A''). In the closed neural tube, p21 expression is relatively weak (A'''). p27 and p57 expression is detected in midline tissues underlying the PNP at caudal levels (B'-C') and in the ventral V-shaped neural plate at more rostral levels with the same level of intensity in the MHP and more lateral regions (B'' and C''). p27 and p57 are expressed throughout most of the closed neural tube (B''' and C'''). In the notochord, p21 and p27 show weak or no staining while p57 is strongly expressed (A'''-C''', arrowheads). Note that p21, p27 and p57 are co-expressed in the MHP at the same approximate level (A''-C''; arrows). Scale bars = 300 μm (whole mounts) and 100 μm (sections).

To summarise the expression of the CIP/KIP genes in the PNP at 8-15 somites, p21 is strongly expressed in the caudal most region of the neuropore and becomes weaker and more specific to the MHP at more rostral levels close to the point of neural tube closure. p27 and p57 are faintly expressed in the flat and forming neural plate and become widely expressed in the V-shaped neural plate, with the same level of intensity for the MHP as the lateral regions. Thus, p21 is the only of the CIP/KIP genes to exhibit an expression pattern suggestive of a specific role in MHP formation. Nonetheless, all three genes are expressed in the MHP at the same approximate level at the 12 and 15 somite stage.

I have established that p21, p27 and p57 are expressed in the MHP during PNP closure following the onset of neurulation at closure 1. Next, I investigated in more detail the expression of p21 and p57 prior to MHP formation and initiation of closure 1. p27 expression was consistently not observed in embryos at the 8-9 somite stage (n=5) and p27 was therefore not included in further analysis. I repeated the analysis of CD1 embryos between the 5 and 8 somite stage, allowing the in situ hybridisation colour development process to proceed for longer to detect low levels of mRNA. I found that p21 and p57 are indeed expressed from the 5 somite stage in the posterior neural plate, in a very specific 'dotted' domain of the midline (Figure 3.9, A'-B'; arrows) just posterior to the point where the neural folds are apposed (Figure 3.9, A'-B'; dashed lines). At the 6 somite stage, this dotted domain of midline expression of p21 and p57 is still visible, but is more posterior in relation to the point where the neural folds are apposed, so that it is now located in a relatively flat region of the neural plate, midway along the neuropore (Figure 3.9, C'-D'; arrows). At the 8 somite stage p21 expression is strong in the caudal part of the PNP and the specific dotted domain in the midline is visible within this larger expression area (Figure 3.9, E'; arrow). p57 expression is widespread at the 8 somite stage and the expression seems to be strongest in the hindgut (Figure 3.9, F; arrowhead) with some expression in the notochord (Figure 3.9, F; between white dashed lines). The dotted p57 domain is no longer visible at 8 somites.
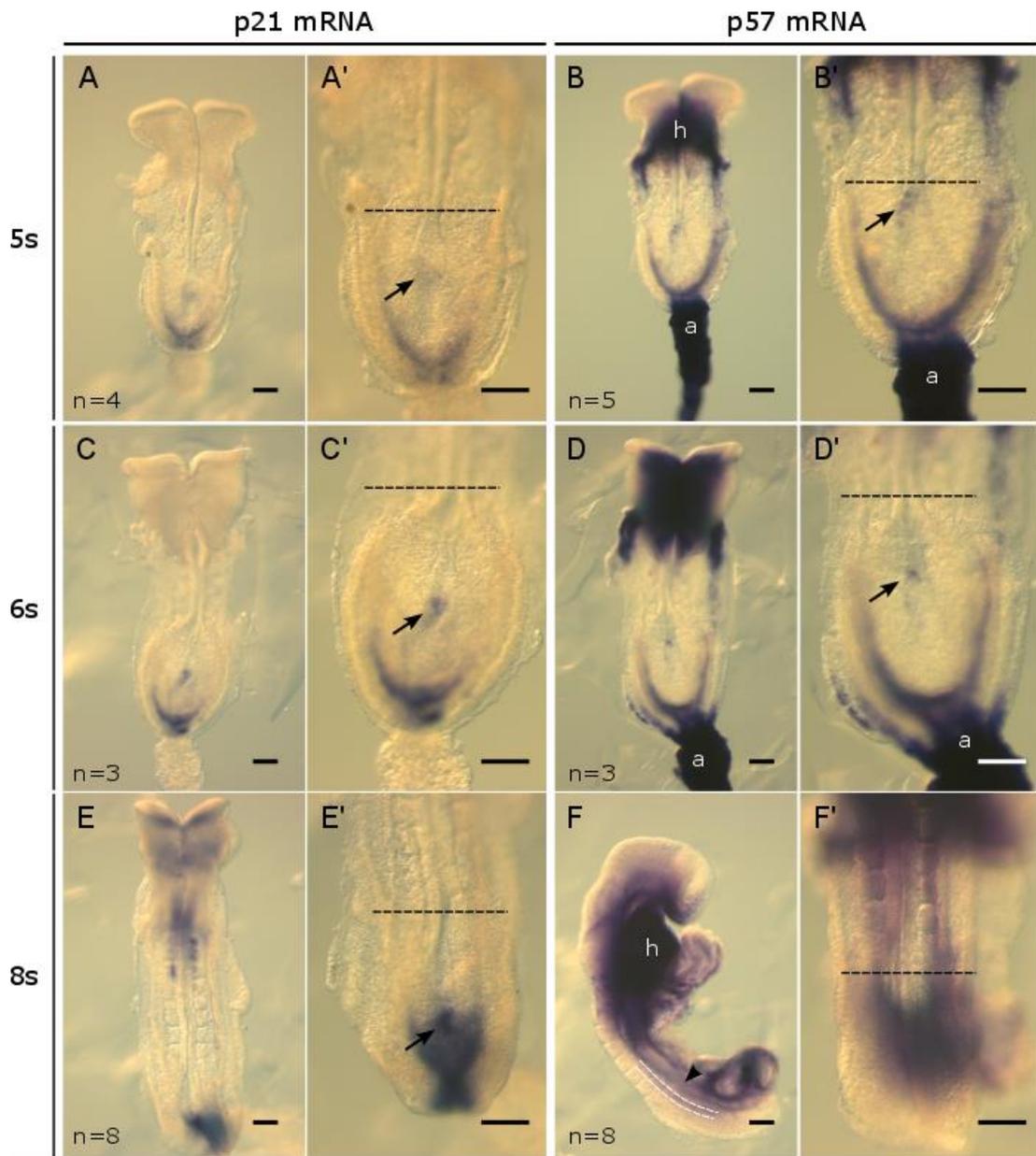
Figure 3.9 - p21 and p57 are expressed in the midline from the 5 somite stage

p21 and p57 are first observed at 5 somites in CD1 embryos in a specific 'dotted' domain of the midline (A'-B'; arrows) close to where the neural folds are apposed (A'-B'; dashed line). At the 6 somite stage the specific dotted midline domain is slightly stronger and is relatively more caudal to the apposed neural folds in what seems to be a flat region of the neural plate (C'-D'; arrows). At the 8 somite stage p21 and p57 expression is stronger and more widespread (E-F). Note the specific dotted domain is still observed for p21 (E'; arrow). p57 expression is very intense in the heart (h) and allantois (a) at all stages examined. Scale bars = 300 μm.
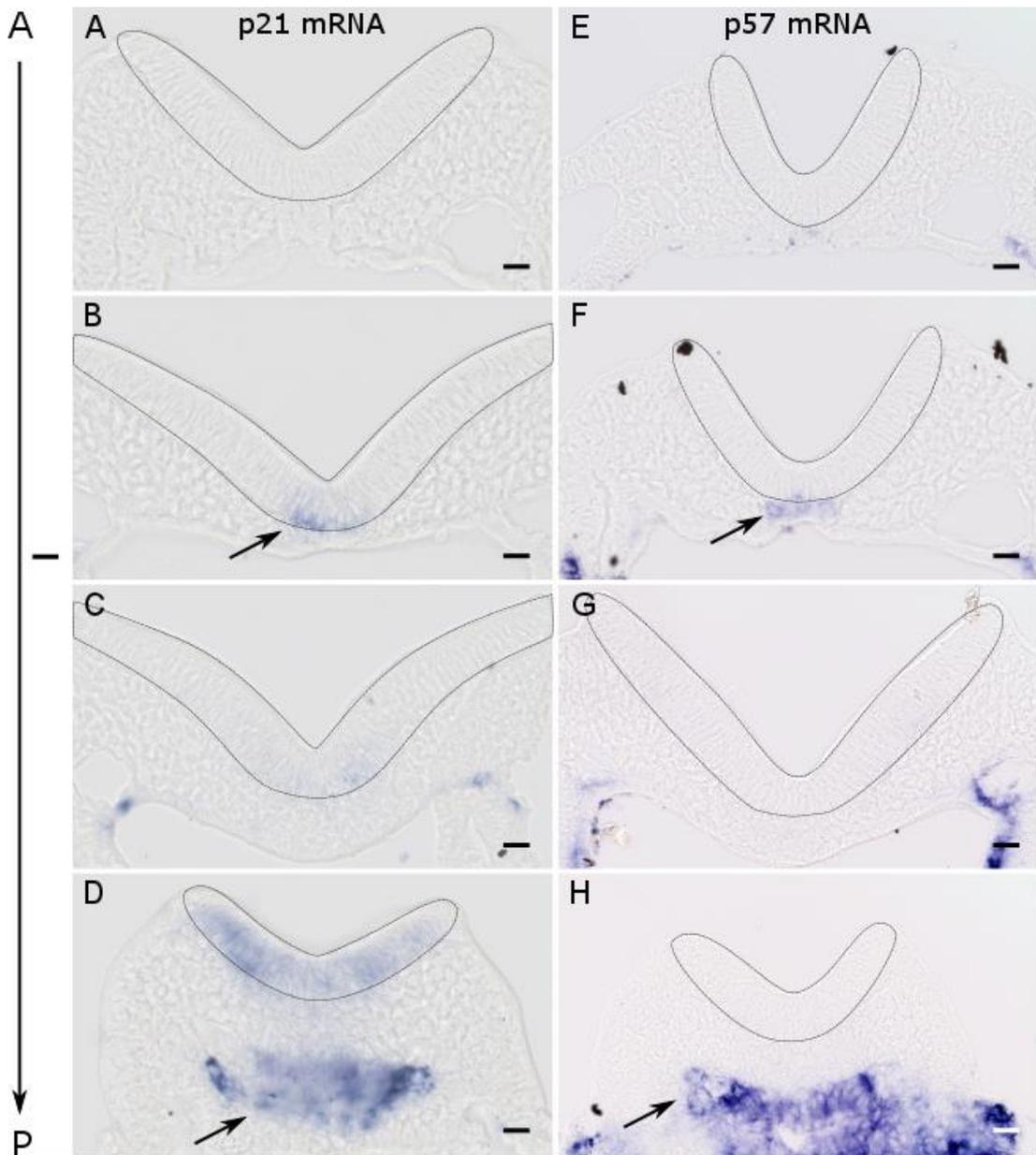
Figure 3.10 - p21 is expressed in the MHP and p57 in the underlying notochord at 6 somites

Whole mount embryos were sectioned at 40 µm and imaged. p21 mRNA expression at 6 somites (A-D) and p57 mRNA (E-H) is shown going from anterior (A) to posterior (P). Note that p21 is expressed in the neural plate midline (B, arrow) while p57 is expressed in the underlying notochord (F; arrow). p21 and p57 are not expressed close to the point of neural fold closure and not in the region caudal to the dotted domain (A, E; C, G). p21 is expressed throughout the neural plate and hindgut at the very caudal end of the embryo while p57 is expressed only in the hindgut (arrow). Scale bars = 50 µm.

The 5-8 somite stage embryos were subsequently sectioned at 40 μm to determine whether the dotted expression domain of p21 and p57 was in the neural plate. Consistent with the images in Figure 3.9, p21 and p57 are not expressed anterior or posterior to the dotted midline domain (Figure 3.10, A, E; C, D). The specific dotted domain localises to the prospective MHP for p21 (Figure 3.10, B; arrow) and to the underlying notochordal plate for p57 (Figure 3.10, F; arrow). At the caudal end of the embryo, p21 is expressed throughout the neuroepithelium and in the hindgut (Figure 3.10, D) while p57 is expressed in the hindgut only (Figure 3.10, H). Figure 3.11 summarises p21 and p57 expression at the 5-8 somite stage. The expression of both genes is specific and located in the forming MHP region, caudal to neural fold closure. p21 is expressed in the forming MHP and p57 in the underlying notochordal plate.
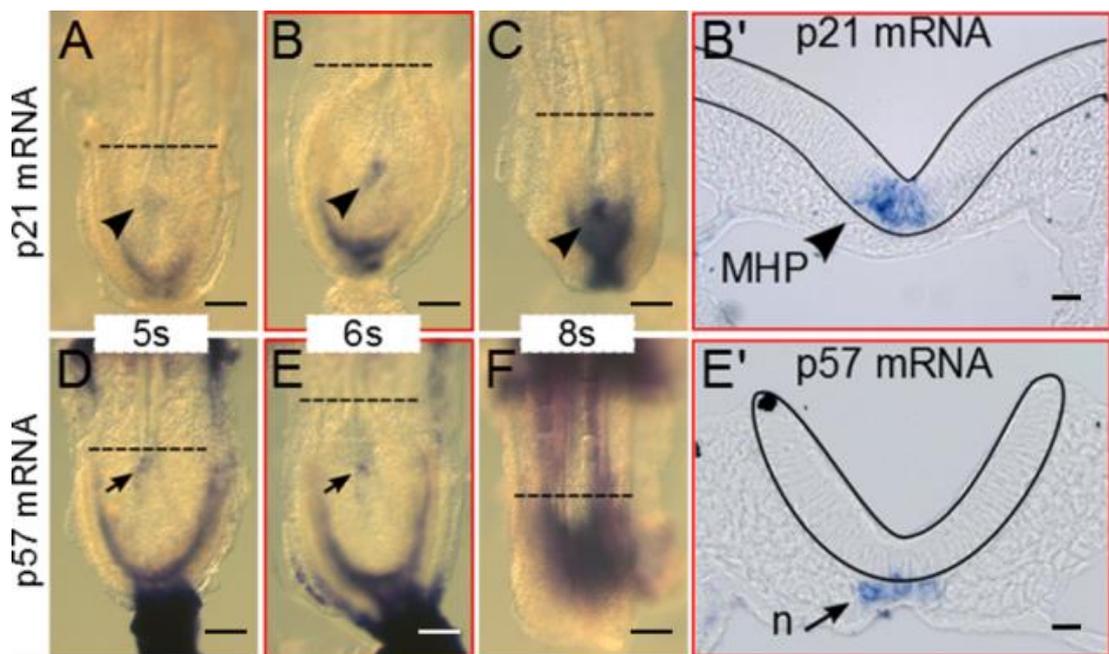
Figure 3.11 - Summary of early p21 and p57 expression

p21 and p57 expression is similar with a specific 'dotted' domain in the forming MHP at a similar anteroposterior level. The p21 'dot' is in the MHP, mid-way along the neural plate, while p57 is expressed in the underlying prospective notochord at the same axial level. Dashed lines show the closure point of the PNP in each embryo. Scale bars = 300 μm (A-F) and 50 μm (B' and E').

CIP/KIP family genes were not studied at the protein level due to lack of suitable antibodies. Two p21 antibodies were tested (F-5 and C-19, Santa Cruz). One of them worked in somites which, based on the in situ hybridisation data (Figure 3.2), express high levels of p21 (Figure 3.12, C-E). The antibody revealed a few positive cells in the dorsal hindgut on a single occasion (Figure 3.12, A-B). The antibody was subsequently tested on sections from embryos deficient in p21. The staining pattern is very similar in both genotypes although the staining is stronger in wild-type embryos (Figure 3.12, G-I). The antibody was also tested on embryos and cells overexpressing p21 by electroporation or transfection with consistent negative results. The p27 and p57 antibodies were validated in pituitary tissue where they are routinely used (J.P Martinez-Barbera's group), but these also failed to detect cells in the E8.5 mouse neural plate.

I have shown that p21 and p57 are expressed in the relevant region at a relevant time during MHP formation and neurulation. In order to assess whether genes of the other family of cyclin-dependent kinase inhibitors, the INK4 family, could be important for MHP formation, their expression was analysed in CD1 embryos at E8.5.

3.2.2 INK4 expression in CD1 embryos

I analysed expression of the INK4 gene family members in CD1 embryos at E8.5 by whole mount in situ hybridisation with probes that had been previously published (Ludtke et al., 2009). p15INK4b and p16INK4a/p19ARF do not appear to be strongly expressed at this stage, and show no specific localisation of transcripts (Figure 3.13, A-B). p18INK4c and p19INK4d expression is more intense and both genes show specific mRNA localisation in the dorsal neural folds (Figure 3.13, C-D; arrows). None of the genes show strong or specific expression in the midline of the PNP. If anything, the expression of p19INK4d in the PNP is weaker than in surrounding tissues (Figure 3.13, D; white dashed outline). Sections through the embryos from Figure 3.13 do not show any staining in the MHP for any of the genes and the expression between the lateral neural folds and the MHP is identical (Figure 3.14, A-

D). p19INK4d is expressed specifically at the dorsal tips of the neural folds (Figure 3.14, D; arrow).

To check the effectiveness of the in situ hybridisation probes, positive control experiments were attempted on E12.5 and E14.5 midsagittal sections through wild-type embryos. However, results were inconclusive and not repeated. Because previous studies showed that p18INK4c and p19INK4d were detectable by Northern blot, but not by in-situ hybridisation from E7, I decided to examine the expression of the CIP/KIP genes as well as the INK4 genes at the mRNA level by qRT-PCR.

CD1 embryos at the 8-10 somite stage were collected and the caudal and rostral parts were separated at the level of the 3rd somite pair. The expression of p27, p57, p15INK4b, p16INK4a, p19ARF, p18INK4c and p19INK4d was analysed in caudal regions relative to the expression of p21 (Figure 3.15). I chose p21 as the control as it was known to be expressed at this stage and it was the most likely candidate for involvement in MHP formation. p27 expression is approximately two thirds of p21 expression and p57 level is approximately three-fold that of p21. None of the INK4 genes are expressed at levels comparable to the CIP/KIP genes with mean Ct values of 30.8, 27.9, 32.4, 30.9, and 28.9 for p15INK4b, p16INK4a, p19ARF, p18INK4c and p19INK4d, respectively. In comparison, p21, p27 and p57 have mean Ct values of 22.9-25.2.
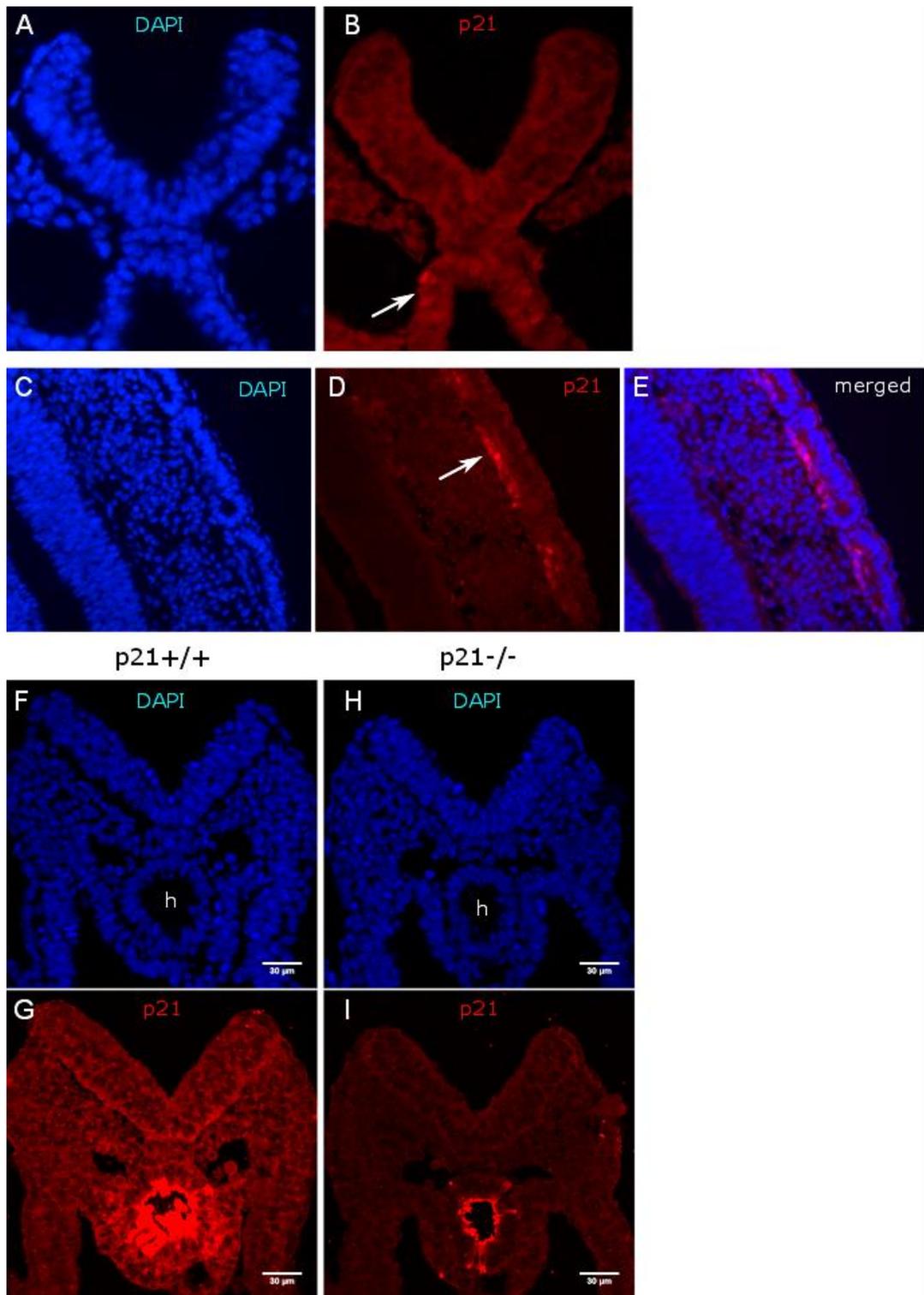
Figure 3.12 - Difficulty in detecting p21 protein in E8.5 embryos

The p21 antibody detected some cells in the wild-type embryo in the neural plate (B) and somites (D; arrows). The antibody was tested on p21$^{+/+}$ and p21$^{-/-}$ embryos (F-I). The staining is stronger in the wild-type embryo but seems solely cytoplasmic (G). The same staining pattern is observed in the mutant embryo with weaker staining (I). The intense hindgut (h) staining is trapping (G-I). Scale bars = 30 μm.
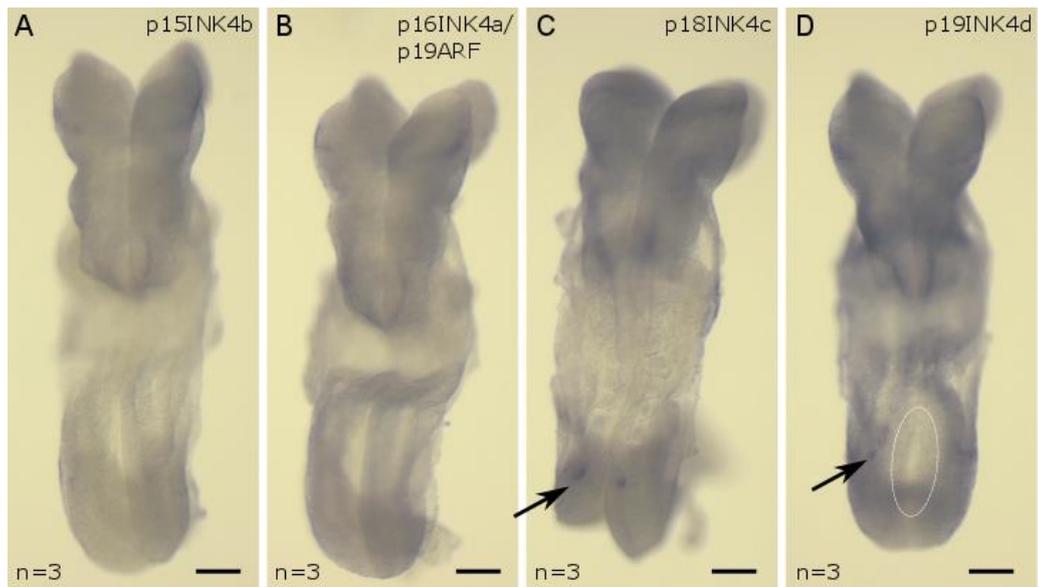
Figure 3.13 - None of the INK4 genes are expressed specifically in the neural tube at E8.5

Whole mount in situ hybridisation shows that p15INK4b and p16INK4a/p19ARF are expressed at low levels, or not at all, throughout the embryo (A-B). p18INK4c and p19INK4d are expressed at higher levels throughout, with slightly stronger expression at a specific axial level on the dorsal tips of the neural folds (C-D; arrows). None of the genes show strong or specific expression in the neural plate midline. If anything, there is weaker expression in the PNP (D; white dashed outline). Scale bars = 300 µm.
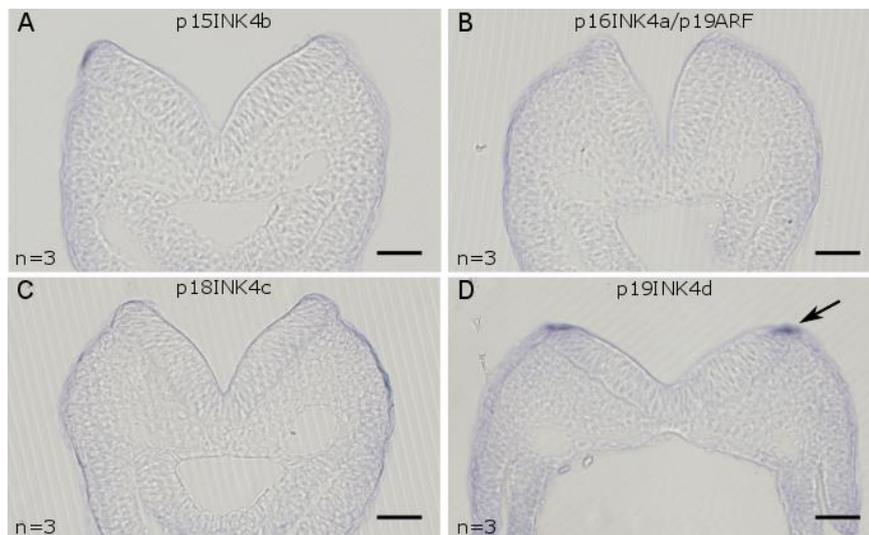
Figure 3.14 - The INK4 genes are not expressed in the MHP at E8.5

Sections of whole mount in situ hybridised embryos shows that p15INK4b, p16INK4a/p19ARF, p18INKc and p19INK4d are not expressed in the MHP. There is no difference in expression of any gene between the MHP and the lateral neural folds. Note the p19INK4d expression in the dorsal neural folds (D, arrow). Scale bars = 50 µm.
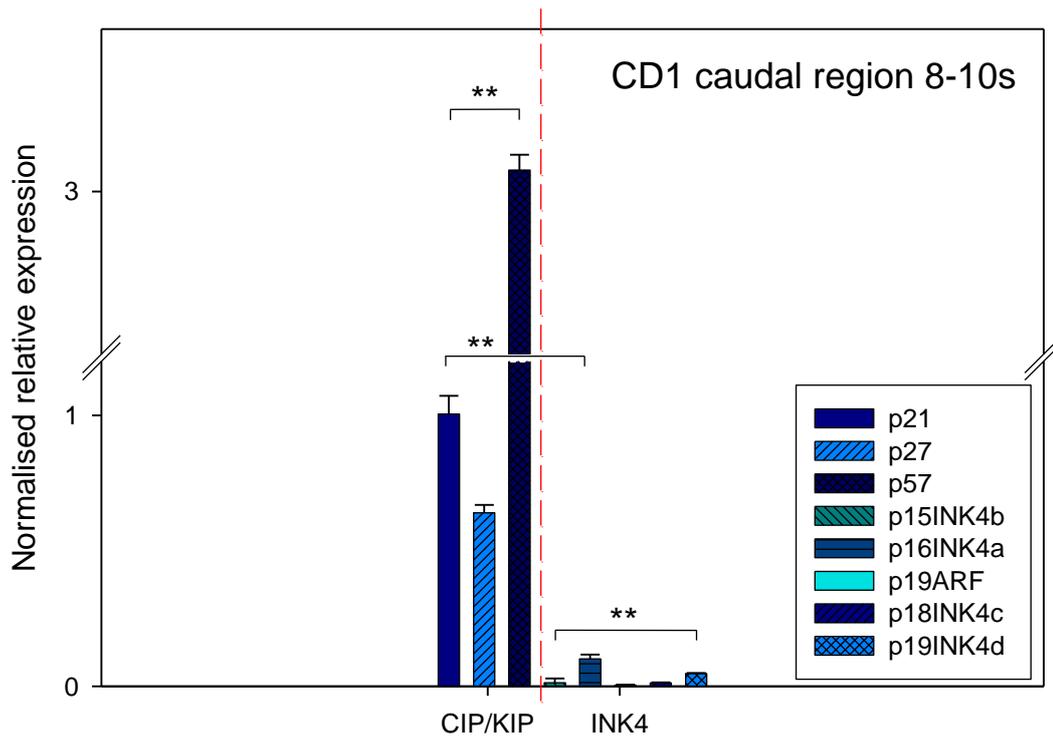
Figure 3.15 - INK4 gene expression is low in the caudal region during MHP formation

Quantitative RT-PCR analysis of gene expression, presented as the expression of CIP/KIP and INK4 genes relative to that of p21 in the caudal embryonic region at 8-10 somites. p27 is expressed at approximately 2/3 the level of p21, while p57 expression is 3-fold that of p21. None of the INK4 genes are expressed at significant levels (Mean Ct values 27.9 - 32.4). Two caudal regions were pooled per sample, and three samples were assayed per gene. There is a statistically significant difference between gene expression among the CIP/KIP as well as the INK4 gene family (One way ANOVA). The difference in the level of the expression of p21 and the highest INK4 gene, p16INK4a, is statistically significant (t-test). **$p < 0.001$.

It has been shown that the protein levels of p15INK4b, p16INK4a, p18INK4c and p19INK4d increase in mouse embryonic fibroblasts (MEF), isolated from embryos at E13.5, as the cells are passaged; a feature associated with cell senescence (Hara et al., 1996; Zindy et al., 1997a). After 2 to 4 passages of the MEFs the proteins are all detectable by Western blot even though p15INK4b and p16INK4a are not detected in embryos (Hara et al., 1996; Zindy et al., 1997a). To check that the INK4 primers detect the relevant genes in the CD1 embryo samples, the levels of p15INK4b, p16INK4a, p19ARF, p18INK4c and p19INK4d were analysed in MEFs that had been isolated from E13.5 wild-type embryos and passaged 3 times. All of the INK4 genes are expressed in the MEF sample (Figure 3.16) showing that the low values seen in the CD1 caudal regions are due to low expression. p19INK4d is expressed at higher levels in the CD1 caudal region compared to the MEF sample. This is due to the relatively low expression of p19INK4d in the MEF sample compared to the other genes and is consistent with previous studies (Zindy et al., 1997a).

INK4 expression was analysed in CD1 embryos at the 11-13 somite stage to see whether the INK4 genes are expressed at a slightly later stage than the CIP/KIP genes. All five genes are expressed at very low levels, in the caudal as well as in the rostral region (Figure 3.17). Thus, it is unlikely that the INK4 genes are important regulatory genes during MHP formation and neurulation in the mouse. At the 11-13 somite stage, p57 is expressed at much higher levels than p21 in the caudal region, approximately 8-fold. p27 expression is only slightly lower than p21 at this stage, possibly reflecting the caudal 'movement' of p27 gene expression in the neural tube (refer to Figure 3.6).

Rostral and caudal p21, p27 and p57 expression was compared in CD1 embryo fragments at the 8-10 and 11-13 somite stage. The results are presented as the normalised expression relative to the expression of each gene in CD1 caudal regions at the 8-10 somite stage. That is, rostral p57 expression at either stage is presented relative to caudal p57 expression at the 8-10 somite stage, and p27 relative to caudal 8-10 somite p27 expression (Figure 3.18). As expected from the in situ hybridisation data, p21 expression is higher in the caudal, rather than rostral, region

of the embryo at 8-10 somites and at the 11-13 somite stage (Figure 3.18). In both stages examined, p27 expression seems slightly higher in the rostral part of the embryo (Figure 3.18). This is consistent with the in situ hybridisation study. p57 expression is very high in the rostral part of the embryo at both stages compared to the caudal region of the embryo. This is likely to reflect the very high expression of p57 in the heart (Figure 3.18).

To conclude, p21, p27 and p57 are expressed in the caudal region of the embryo at the 8-10 somite stage supporting the in situ hybridisation data on the expression in the neuroepithelium, the notochord, and the hindgut. INK4 gene expression is not significant in the caudal embryo by either in situ hybridisation or qRT-PCR quantification. Lastly, the expression levels of p21, p27 and p57 in the rostral compared to the caudal region seems in accordance with the in situ hybridisation data.
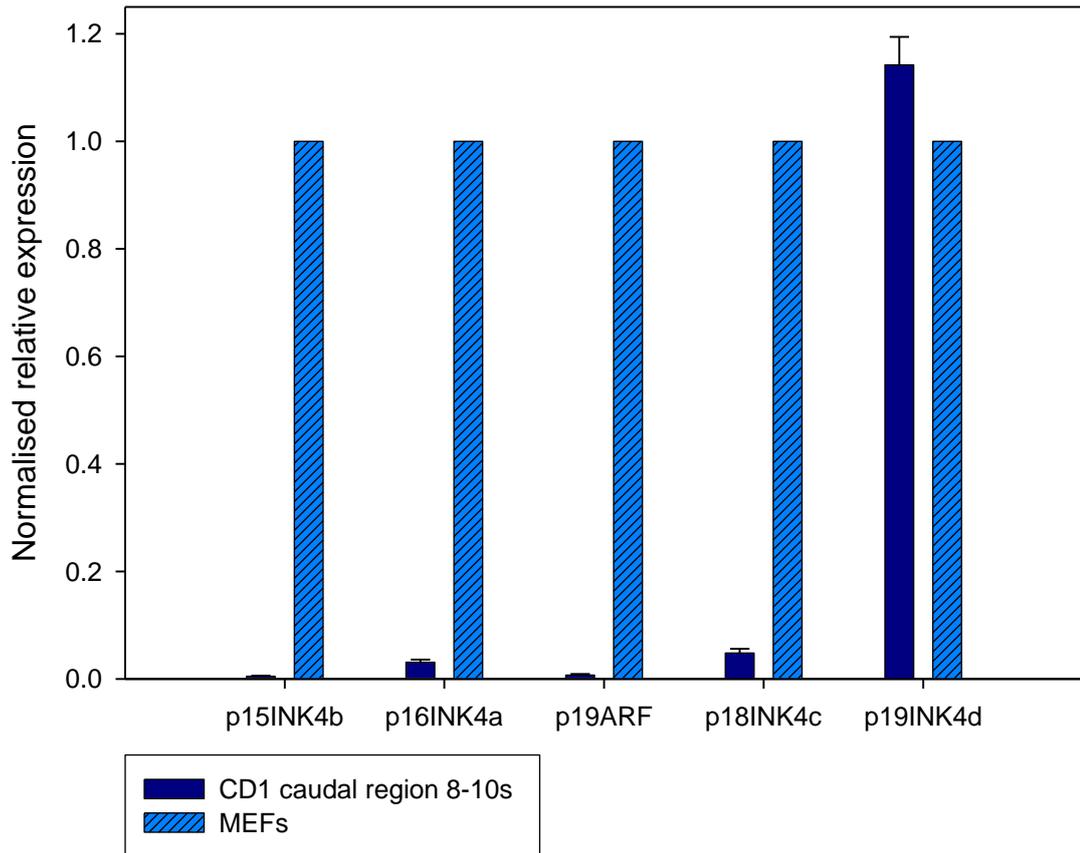
Figure 3.16 - All INK4 genes are detected in MEFs by qRT-PCR

p15INK4b, p16INK4a, p19ARF, p18INK4c and p19INK4d were analysed in MEFs that had been passaged 3 times. The results are presented as the expression in CD1 caudal regions 8-10s relative to the expression in the MEFs. Only one MEF sample was run per gene and thus no error bars were calculated. All the INK4 genes are detected in the MEFs. p19INK4d is expressed at higher levels in the CD1 caudal region than in the MEFs and this reflects that p19INK4d had the lowest expression in the MEFs (Ct=27.5 cycles) compared to the other genes (21.61-24.9 cycles). Two CD1 caudal regions were pooled per sample, and three samples were assayed per gene.

107
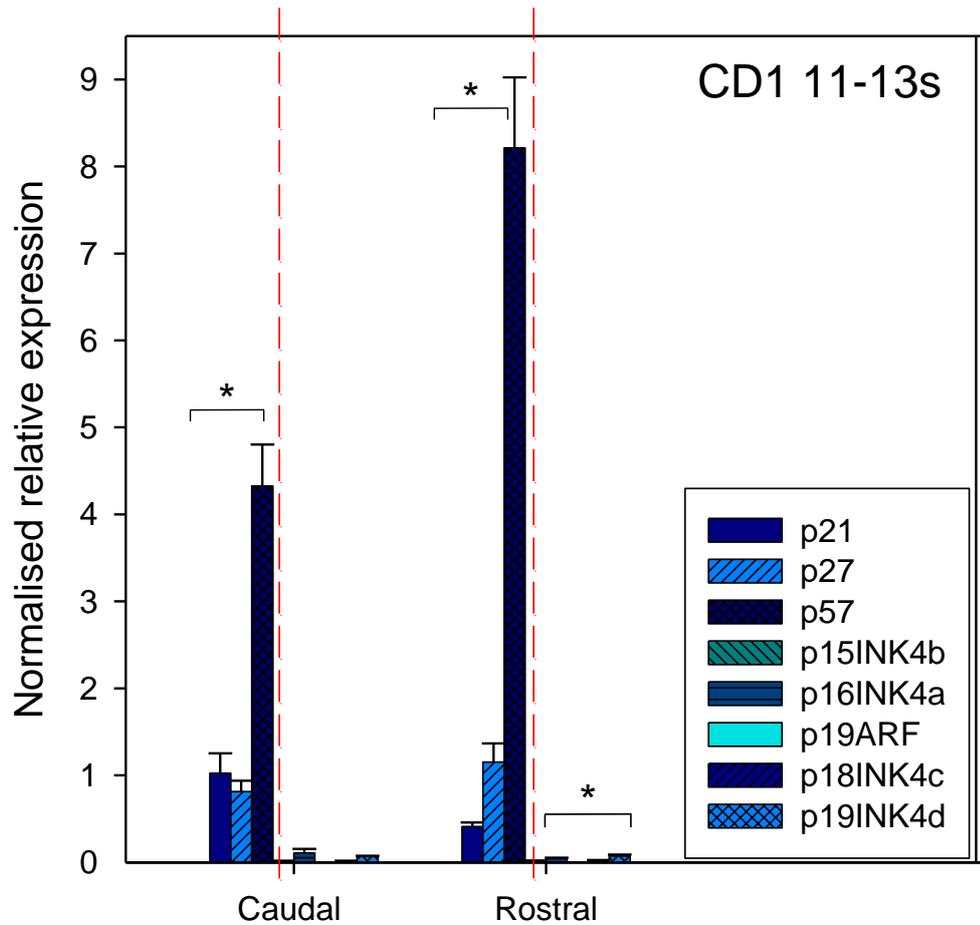
Figure 3.17 - CIP/KIP vs INK4 expression at the 11-13 somite stage

The normalised expression levels of CIP/KIP and INK4 genes are presented relative to p21 expression in CD1 caudal regions at the 11-13 somite stage. As for the 8-10 somite stage, p21 expression is highest in the caudal region, whereas p27 and p57 are expressed at higher levels in the rostral region. The INK4 genes are expressed at low levels, suggesting that they are unlikely to be required for MHP formation. *$p < 0.05$, One way ANOVA.
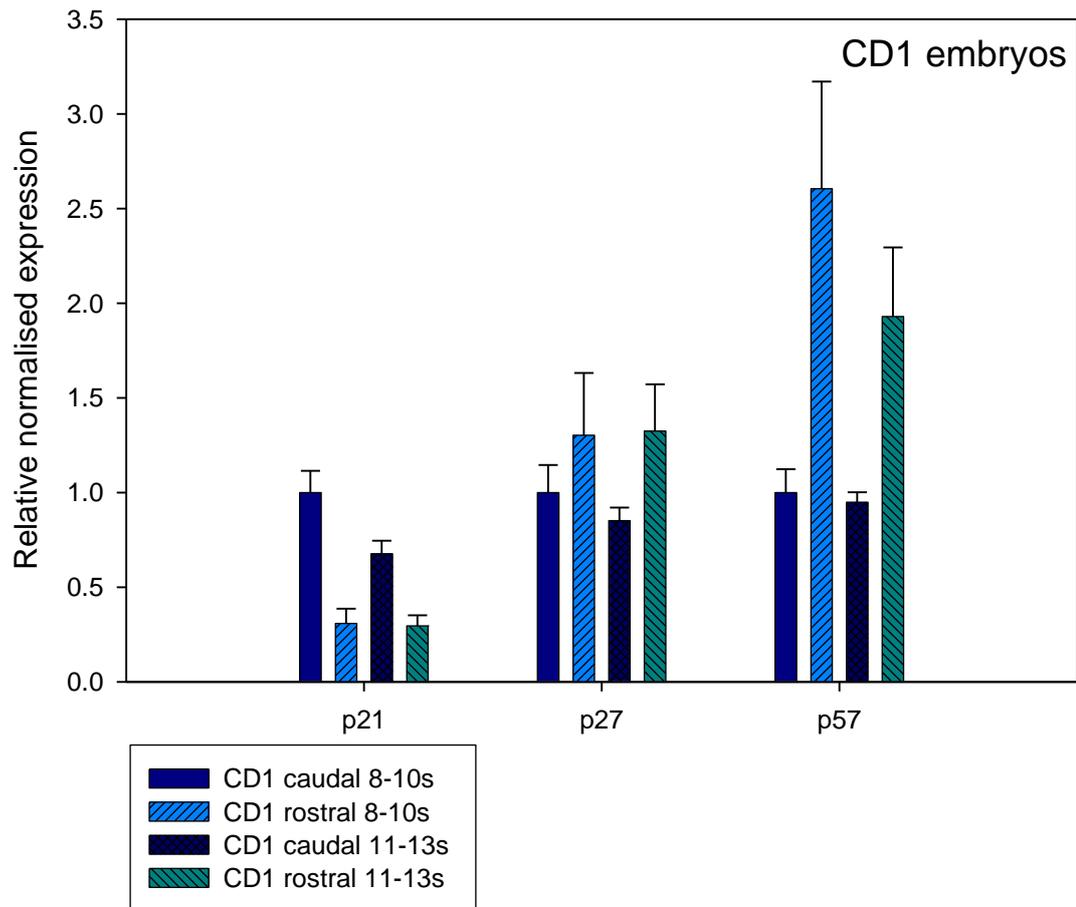
Figure 3.18 - Comparison between anterior and posterior expression of p21, p27 and p57

Expression of p21, p27 and p57 is shown relative to the expression of each gene in 8-10 somite CD1 caudal regions. p21 expression is highest in the caudal region at 8-10 and 11-13s while the expression in the rostral region is similar at both stages. p27 seems expressed more strongly in the rostral part of the embryo than caudal at 8-10s and 11-13s. p57 expression is strongest in the rostral part of the embryo at 8-10s and 11-13s, most likely due to the strong expression in the heart. Two CD1 regions were pooled per sample, and three samples were assayed per gene.

3.3 Discussion

3.3.1 CIP/KIP and INK4 expression in the MHP

p21 mRNA has been reported to be found primarily in tissues containing post-mitotic differentiated cells (Parker et al., 1995; Sherr and Roberts, 1999). This is not true for the neuroepithelium, however, where p21 is widely expressed, as all the cells are proliferating and non-differentiated prior to neural tube closure (Copp et al., 1988; McShane et al., 2015). I have shown that p21 expression in the caudal neural plate is dynamic and is observed predominantly in the flat neural plate at the 6-8 somite stage where the MHP is forming. The temporal and spatial expression of p21 is in agreement with a role for p21 in shaping of the neural plate from flat to bending, i.e. a role in the forming of the MHP. p21 expression is strongest and widest in the most caudal region of the embryo at all stages examined, with expression becoming restricted to the midline in the V-shaped neuroepithelium. In the V-shaped neural plate just caudal of neural tube closure and in the closed neural tube p21 expression is weak or lost, suggesting that p21 is not important for maintaining the MHP.

p57 is expressed in the notochord from the 6 somite stage and is later detected in the overlying neuroepithelium. It is curious that p21 and p57 are both expressed in very specific domains in the flat neural plate almost suggesting they are 'paving the way' for midline bending. It has been shown that notochordal factors are important for MHP formation (Smith and Schoenwolf, 1989) and it is tempting to speculate that p57 in the notochord could be involved in the induction of p21 expression in the overlying neural plate at this early stage. Furthermore, the fact that p21, p27 and p57 are co-expressed in the neuroepithelium at later stages could mean that there is redundancy between the CIP/KIP genes in neural tube formation, explaining why the p21, p27 and p57 knockout mice develop apparently normal neural tubes (Deng et al., 1995; el-Deiry et al., 1993; Fero et al., 1996; Kiyokawa et al., 1996; Yan et al., 1997; Zhang et al., 1997).

The expression pattern of p21 and the other members is somewhat surprising as I would expect them to be expressed at the hindbrain/cervical boundary immediately prior to closure 1, i.e. at the prospective closure 1 site at the 5-8 somite stage. The rationale behind this expectation is the hypothesis that cell cycle regulators are responsible for cell wedging in the midline and that this produces the MHP prior to closure 1. I have not been able to detect p21, p27 or p57 in the prospective MHP at the site of closure 1. Alternatively, the MHP might not be required for closure 1 as the MHP is more pronounced in the PNP following the closure 1 event. RNAseq experiments conducted in our laboratory on prospective closure 1 tissue collected between somites 3 and 6 in wild-type embryos at E8 has failed to detect p21 transcripts. Interestingly, and contrary to my in situ data, low levels of p27 and p57 were found in the prospective closure 1 region (Oleksandr Nychyk, unpublished). The discrepancy between the studies most likely lies in the high sensitivity of the RNAseq method compared to the in situ hybridisation technique. It is also possible that the mRNA is degraded in embryos used for RNA in situ hybridisation as whole litters were dissected before the embryos were fixed (30-60 minutes) whereas embryos were snap-frozen one by one for the RNAseq experiment. It is interesting that p27 is found to be expressed in the prospective closure 1 site in the RNAseq experiment and at relatively high levels in the qRT-PCR experiments I conducted on CD1 caudal regions at the 8-13 somite stage, whereas I failed to detect p27 mRNA in these regions prior to 12 somites by in situ hybridisation. These results suggest that the p27 in situ probe is not very efficient in detecting p27 mRNA at low levels and highlights the importance of quantification of gene expression.

The expression of p21, p27 and p57 is complementary as seen in Figure 3.7 and Figure 3.8. In particular, cells of the very caudal neural plate express high levels of p21 but not p27 or p57, and cells at more rostral levels express lower levels of p21 while the levels of p27 and p57 are higher. It is interesting to speculate that the caudal cells switch of expression of p21 and instead start expressing p27 and p57 as the cells move rostrally, laying down the neural plate midline. Alternatively, it could seem as though p21, p27 and p57 are oscillating in a manner similar to that observed during somitogenesis in sense of the differential rostro-caudal expression

of the genes (Hubaud and Pourquie, 2014). However, the fact that I do not see variation in the rostro-caudal positioning of the gene expression pattern between embryos makes this theory unlikely.

An important consideration in the analysis of CIP/KIP expression in this thesis is that it has only been examined at the mRNA level. I have not looked at the protein levels of p21, p27 or p57 in the MHP as the antibodies were not sufficiently good. I was able to detect p21 protein in the somites where expression is much stronger but nothing was detected in the neural tube in at least 3 separate experiments. The p27 and p57 antibodies were validated in the mouse pituitary where they are routinely used (Gaston-Massuet et al., 2011) but again did not detect anything in the neural tube. The p21 protein has a half-life of approximately 2 hours (Roy et al., 2007) and as I have shown that the expression is dynamic, the protein could be present in the MHP during closure 1 a couple of hours after expression had been switched off. Moreover, the CIP/KIP genes are known to be tightly regulated at the posttranscriptional and posttranslational level leading to ubiquitination and degradation (Blagosklonny et al., 1996; Li et al., 1996; Schwaller et al., 1995; Starostina and Kipreos, 2012). In fact, it has been shown that the half-life of p27 protein in proliferating cells is shorter than in quiescent cells, a change that is concomitant with a smaller amount of p27 ubiquitinating activity in quiescent cells (Pagano et al., 1995). Furthermore, targeted disruption of Skp2, the substrate recognition subunit of the SCF ubiquitin ligase, leads to abnormal accumulation of p27 protein (Nakayama et al., 2000). Thus, the gene expression studies, although informative, would ideally need to be backed up by immunohistochemical examination as post transcriptional mechanisms could alter the actual content of p21, p27 and p57 in the MHP.

The INK4 in situ probes were provided by Prof. Charles Sherr and they have been validated and published previously. I did not detect INK4 expression in the neural plate midline of CD1 embryos at E8.5. As mentioned previously, the cell cycle is prolonged in the midline of embryos during neurulation. Thus, it is likely that the genes that play a role in this prolongation of the cell cycle are differentially

expressed between the MHP and the lateral neural plate regions. There is no difference between the expression of the INK4 genes in the MHP and in the lateral neural folds. The INK4 genes p18INK4c and p19INK4d have previously been detected by Northern blot in embryos at E7 (Zindy et al., 1997a). I have presented the expression of the two genes in the dorsal neural folds of embryos at E8.5.

3.3.2 Quantification of CDKI levels during neurulation

In general, the in situ hybridisation data corresponds to the gene quantification in CD1 embryos at the 8-13 somite stage. The levels of p57 in the caudal region of embryos at the 8-10 and the 11-13 somite stage are higher than p21 which was not apparent from the in situ hybridisation data. The allantois was removed from the embryos for the qRT-PCR analysis, but it is possible that some allantoic tissue remained, causing the high levels of p57 expression in caudal embryonic fragments. Consistent with the in situ hybridisation data the INK4 genes are expressed at very low levels and are unlikely to play roles in MHP formation.

If time permitted it I would have done the qPCR analysis on isolated neural tubes. This would allow me to assess gene expression specifically in the neuroepithelium without other tissues such as the hindgut and would give a better idea of redundancy in the neural plate. I would include p18 and p19 in this analysis to exclude expression in the neural plate.

In conclusion, p21 expression revealed by in situ hybridisation is in agreement with a role in MHP formation as it is expressed widely in the neural plate as the MHP forms, with an intense expression domain in the prospective MHP that becomes more specific as MHP formation proceeds. p27 and p57 are expressed in the MHP at the same axial level as p21, suggesting that there could be redundancy between the genes. There is, however, no regional difference in the expression of p27 and p57 as revealed by in situ hybridisation, between the MHP and the lateral neural folds as would be expected if they were involved in prolonging the cell cycle specifically in the MHP. Post-translational modifications of p27 and p57 might result

in regional differences between the MHP and lateral regions that I have been unable to detect.

In order to analyse MHP formation more closely in relation to the CIP/KIP genes, p21$^{+/-}$ and p21$^{-/-}$; p27$^{+/-}$ mouse lines were acquired and analysed as described in the next chapters.

Chapter 4 - p21 mutant embryos develop MHPs

4.1 Introduction

4.1.1 p21 mutant mouse model

In 1995 two mouse models of p21 deficiency were generated and both groups reported mice at expected Mendelian ratio that developed normally with no histological abnormalities (Brugarolas et al., 1995; Deng et al., 1995; Hosako et al., 2009; Patterson et al., 2006). Despite being associated with tumour suppression in relation to p53, p21 null mice do not develop spontaneous malignancies in the first 7 months of life (Brugarolas et al., 1995; Deng et al., 1995). In comparison, over 60% of mice lacking p53 develop tumours spontaneously by the age of 6 months (reviewed by Kiyokawa et al., 1996). Yet, p21 deficient fibroblasts are defective in undergoing G1 arrest following DNA damage (Brugarolas et al., 1995; Deng et al., 1995). In addition, the mouse models revealed that p21 is necessary for efficient p53 dependent cell cycle arrest in G1-phase following DNA damage and nucleotide depletion, but is not required for p53 dependent apoptosis or for the operation of the mitotic spindle checkpoint (Brugarolas et al., 1995; Deng et al., 1995). Thus, p21 is only responsible for a subset of known p53 functions.

Neural tube defects including exencephaly and spina bifida are not seen in p21 null mice although a p21-null allele was found to significantly increase the frequency of exencephaly in double mutants with Gadd45a-null, and also produced 3% spina bifida, unlike p53-null which only produced exencephaly in double mutants (Patterson et al., 2006). This shows that p21 is required for cranial and spinal closure in some genetic backgrounds. Overexpression of p21 in hepatocytes in vivo leads to dramatic inhibition of proliferation resulting in a reduction in the number of hepatocytes and aberrant tissue organisation, highlighting the importance of correct levels of CDKI during development (Wu et al., 1996).

4.1.2 p27 mutant mouse model

Three p27 deficient mouse models were published in the same issue of Cell in 1996 and all report homozygotes that are viable, without gross morphological abnormalities, and found at the expected Mendelian frequencies (Fero et al., 1996; Kiyokawa et al., 1996; Nakayama et al., 1996). p27 deficient mice are larger and weigh approximately 20-40% more than wild-type littermates from 2 weeks of age. This increase in size is due to an overall increase in skeletal growth, carcass, and organs in proportion to body size with no histological abnormalities, and due to an increase in cell number rather than cell size (Fero et al., 1996; Kiyokawa et al., 1996; Nakayama et al., 1996). An exception to this is the thymus, spleen and pituitary that are disproportionally large in the mice. While the pituitary growth is due to neoplastic growth resulting in pituitary adenomas, the thymic and spleen hyperplasia observed is not associated with any histological abnormalities (Fero et al., 1996; Kiyokawa et al., 1996; Nakayama et al., 1996). Interestingly, these regions of disproportionate growth express p27 at highest levels suggesting a role for p27 in regulating growth of many organs (Fero et al., 1996; Kiyokawa et al., 1996; Nakayama et al., 1996). The overall increase in size of p27 mutant mice is gene dose-dependent as shown by the intermediate size of heterozygous animals (Fero et al., 1996; Kiyokawa et al., 1996; Nakayama et al., 1996). There is no disproportionate level of body fat in the p27 mutant mice and problems with growth hormone (GH) or insulin-like growth factor 1 (IGF-1) signalling, common reasons for overgrowth, were ruled out in all three studies (Fero et al., 1996; Kiyokawa et al., 1996; Nakayama et al., 1996). In thymocytes isolated from p27 mutant mice, CDK2 activity is 2-10-fold higher than in wild-type controls, suggesting that p27 is an important inhibitor of CDK2 (Fero et al., 1996; Nakayama et al., 1996). Thus, p27 deficiency might allow continued proliferation in a situation where mitogenic stimuli are low or absent, resulting in general hyperplasia of the animals.

Female p27 mutant mice are infertile (Fero et al., 1996; Kiyokawa et al., 1996; Nakayama et al., 1996). Even though they are capable of mating, although infrequently, and undergo ovulation and fertilization they are unable to carry

pregnancies to full term and in most cases implantation fails. p27 mutant males, on the other hand, are able to impregnate wild-type females (Fero et al., 1996; Kiyokawa et al., 1996; Nakayama et al., 1996). The mutant females have prolonged oestrus cycles and defective formation of the corpus luteum, important for maintaining a pregnancy (Fero et al., 1996; Kiyokawa et al., 1996; Nakayama et al., 1996). However, transplantation of morulas from pregnant p27 mutant females into pseudopregnant wild-type females develop to full term giving rise to normal sized litters (Fero et al., 1996; Kiyokawa et al., 1996).

The phenotypes reported for all three existing p27-null models are very similar. The p27 mouse model used in this thesis contains a truncated protein lacking only the cyclin-CDK binding amino terminal domain of p27 (Kiyokawa et al., 1996) as opposed to deletion of the entire coding region in the other two models (Fero et al., 1996; Nakayama et al., 1996). This strongly suggests that it is the cell cycle regulatory role of p27 that is responsible for most, if not all, of the abnormalities observed in p27 deficient mice.

4.1.3 p57 mutant mouse models

The CDKIs play important roles during development and tumour formation. However, most CDKI mutants develop normally, i.e. p21 (Brugarolas et al., 1995; Deng et al., 1995), p27 (Fero et al., 1996; Kiyokawa et al., 1996; Nakayama et al., 1996), p16INK4a (Serrano et al., 1996), p15INK4b and p18INK4c (Yan et al., 1997) suggesting functional redundancy between CDK inhibitors. p57 mutant mice, on the other hand, have severe developmental defects related to altered cell proliferation, differentiation and apoptosis (Yan et al., 1997; Zhang et al., 1997). Most (>80%) mice die within 1 day of birth (Yan et al., 1997; Zhang et al., 1997) although there is a lot of variability in penetrance. Approximately 10% of p57 mutant pups are normal and live for months (Yan et al., 1997). Common defects include cleft palate (48.9%), a shortened and abnormal intestine (40%) and shortened limbs in all affected mutant pups (Yan et al., 1997). Other defects include abdominal muscle defects leading to occasional omphalocele, skeletal abnormalities resulting from increased proliferation and delayed differentiation of chondrocytes, renal medullary

dysplasia, adrenal cortical hyperplasia and cytomegaly, and lens cell hyperproliferation and apoptosis (Zhang et al., 1997). In addition, brains from p57 deficient animals are larger than those of wild-type mice (Mairet-Coello et al., 2012). p57 is highly expressed in postmitotic lens fibre cells. Accordingly, p57 loss results in inappropriate S-phase entry in lens fibre cells (Zhang et al., 1997). Many of the p57$^{-/-}$ defects are due to increased apoptosis including the cleft palate and GI tract defects (Yan et al., 1997). The apoptotic phenotype is similar to Rb mouse mutants and the phenotypes are normalised in a E2F1 mutant background, suggesting that abnormal activation of E2F1, that is bound and inactivated by Rb, is partly responsible for the increased apoptosis observed in p57 and Rb mutant animals (reviewed by Susaki and Nakayama, 2009).

p57 is an imprinted gene and the paternal allele in the mouse is inactivated by transcriptional repression and methylation (Hatada and Mukai, 1995). Thus, heterozygous mice that inherit a defective maternal allele exhibit the same phenotype as homozygous mutants (Yan et al., 1997).

Loss of p57 is detrimental during embryonic development. But what makes p57 special compared to p21 and p27? And why do p27 mutant mice exhibit phenotypes related to over-proliferation whereas p57 deficiency leads to an increase in apoptosis rather than over-proliferation? A knock-in mouse model where p57 was replaced by p27 under the control of the endogenous p57 promoter answers this question in part. Replacement of p57 by p27 ameliorates the poor survival as well as most of the developmental defects observed in p57 mutant animals and p27 knock-in mice are indistinguishable from wild-type littermates (Susaki and Nakayama, 2009). Thus, p57 is largely replaceable by p27 regarding the embryogenic functions of p57 (Susaki and Nakayama, 2009). This suggests that the differences observed between the p27 and p57 mutant mice models is the result of the spatial and temporal expression patterns of the genes, rather than differences in the genes themselves. Some defects remain in the p27 knock-in model including those of the renal papilla, the placenta and the abdominal wall muscle (Susaki and Nakayama, 2009). The defects that persist seem to be due to tissue specific

expression of p27, possibly resulting from p27 specific protein degradation in those tissues (Susaki and Nakayama, 2009). Importantly, the p27 knock-in model shows that the defects observed in p57 mutant mice are indeed related to the CDKI activity of p57 and can in large part be rescued by p27 (Susaki and Nakayama, 2009). Moreover, detailed studies of p27 and p57 expression have shown that abnormalities in p27 deficient animals are restricted to tissues expressing p27 but not p57 and, vice versa, tissues that are abnormal in p57 deficient mice express p57 but not p27 in the wild-type setting (Nagahama et al., 2001). Examples of this include the adrenal gland where p27 is expressed exclusively in the medulla and p57 in the cortex. p27 mutant mice show hyperplasia of the medulla but not the cortex, and p57 mutant mice show hyperplasia of the cortex but not the medulla (Nagahama et al., 2001). Furthermore, tissues that express both genes, such as the brain, lung, skin and liver are not affected in p27 or p57 deficient mice (Nagahama et al., 2001).

4.1.4 Combined CIP/KIP deficiency

4.1.4.1 p21/p27 double deficiency

A few double mutant mouse models have been generated. Simultaneous loss of p21 and p27 was described in 2011 (Garcia-Fernandez et al., 2011). p21/p27 double mutant mice have a phenotype indistinguishable from wild-type littermates and body and organ weight is unchanged (Garcia-Fernandez et al., 2011). Contrary to previous studies, p27 mutant mice do not show any increase in body size, a difference the authors put down to the different genetic backgrounds used (Garcia-Fernandez et al., 2011). No developmental abnormalities have been reported for the p21/p27 double mutant mice but they have an increased incidence of tumour formation; 72.2% of the mice develop tumours with an average tumour latency of 11.6 months (Garcia-Fernandez et al., 2011). Parallel studies on p21 and p27 single mutant mice showed a tumour incidence of 55% in p21 mice and 50% in p27 mice with latency periods of 15.4 and 12.6 months, respectively (Garcia-Fernandez et al., 2011). Whereas other studies have reported pituitary tumours with an incidence of approximately 50-100% from 12 weeks of age in p27 mutant mice (Fero et al., 1996;

Nakayama et al., 1996), the group behind the p21/p27 double mutant mouse line reported an incidence of pituitary adenomas of 27.7% with a latency of 11.1 months (Garcia-Fernandez et al., 2011). Even though the data is not in full agreement with previous studies it shows that embryonic development proceeds unperturbed in the absence of both p21 and p27 (Garcia-Fernandez et al., 2011).

Simultaneous loss of p21 and p27 has also been analysed in vitro. In neonatal cardiomyocytes knock-down of p21 and p27 stimulates S-phase entry and triples the mitotic index (Di, V et al., 2011). Contrary to what has been reported in muscle myotubes, p21 and p27 knock-down does not affect apoptosis in cardiomyocytes (Pajalunga et al., 2007). Double knock-down of p21 and p27 in cardiomyocytes does not affect the levels of INK4 genes, but leads to upregulation of p57 (Di, V et al., 2011). Triple knock-down of p21, p27 and p57 results in more than twice as many BrdU incorporating cardiomyocytes as compared to p21/p27 double knock-down and an increase in cyclin A, cyclin E, and hyperphosphorylation of Rb while cyclin D levels remain unchanged (Di, V et al., 2011). p57 knock-down on its own does not affect BrdU incorporation in cardiomyocytes whereas p21 and p27 single knock-down leads to a slight increase in BrdU incorporation (Di, V et al., 2011). In adult cardiomyocytes, which do not normally proliferate, knock-down of p21 and p27 results in upregulation of p57 and re-entry into the cell cycle in 12% of cells (Di, V et al., 2011). However, Rb phosphorylation decreased over time even when triple p21, p27, p57 knock-down was sustained suggesting compensatory additional CKI mechanisms in cardiomyocytes (Di, V et al., 2011).

4.1.4.2 p21/p57 double mutant mice

Mice lacking p21 and p57 die in utero mainly due to placental failure, and no live-born mice are observed for p57 null or p21/p57 double null mice (Zhang et al., 1999). The mice do, however, survive to E16.5 where a normal Mendelian ratio is observed. Double mutant mice display severe defects in skeletal muscle development as well as abnormal lung and skeletal development (Zhang et al., 1999). The lung defect is not due to over-proliferation or apoptosis (Zhang et al., 1999). Whereas loss of p57 leads to a delay in ossification and sternum defects, the

overall shape of the skeleton is unaffected in double mutants (Zhang et al., 1997). In the double mutant mice, however, the posture is abnormal and embryos lack the spinal curvature seen in wild-type mice and they have rib cage defects (Zhang et al., 1999). In the absence of p21 and p57, skeletal muscle defects arise as myoblasts fail to withdraw from the cell cycle, leading to over-proliferation, endoreplication and apoptosis (Zhang et al., 1999). The severe phenotype of double mutant mice suggests that p21 and p57 play redundant roles in some tissues. In line with this, p21 and p57 co-localise in myotubes during development (Zhang et al., 1999). The skeletal phenotype observed in the p21/p57 double mutant mice is similar to that of Rb mutant mice, and their phenotype can be rescued by a Rb transgene (Zacksenhaus et al., 1996). Thus, the primary role of p21 and p57 in skeletal muscle is likely to be to down-regulate CDK activity and maintain Rb in a hypophosphorylated, active form (Zhang et al., 1999). Furthermore, p27 and p57 have been implicated in the control of Rb in the pituitary and lens, while p57 has been implicated in the control of the Rb proteins p107 and p130 in chondrocyte differentiation (Zhang et al., 1997).

4.1.4.3 p27/p57 double mutant mouse models

p27 does not have much effect on the phenotype of p57 null embryos as no p57 deficient mice survive past postnatal day 10 irrespective of p27 status (Zhang et al., 1998). However, embryonic lethality between E12 and E16.5 is doubled in p27/p57 double mutant mice compared to p27$^{+/-}$; p57$^{-/-}$ mice (Zhang et al., 1998). Double mutant embryos most likely die from placental failure as the cardiovascular system and erythropoiesis develop normally in p27/p57 double mutant mice (Zhang et al., 1998). Most developmental defects in the double mutant mice are identical to those observed in the p57 single mutant mice with exception of the lens which is more severely affected in double mutant animals (Zhang et al., 1998). Interestingly, the lenses of p27 mutant mice are indistinguishable from those of wild-type littermates (Zhang et al., 1998). p27 and p57 are expressed in the same cells during lens development, suggesting a redundant function of p57 in p27 loss (Zhang et al., 1998). In the lens as well as in the placenta of p27/p57 double mutant mice, proliferation and differentiation is affected resulting in a lens phenotype similar to

that of Rb deficient mice (Morgenbesser et al., 1994). This suggests that the phenotype resulting from loss of p27 and p57 is related to their CDKI activity leading to increased Rb phosphorylation and inhibition of the differentiation promoting activity of (hypophosphorylated) Rb (Zhang et al., 1998).

4.1.4.4 Triple knock-out CIP/KIP mouse

In 2012 a triple knock-out mouse model was generated (Tateishi et al., 2012). Triple mutant embryos die around E13.5 from placental failure which is slightly earlier than the p27/p57 double null mouse (Zhang et al., 1998). Embryos were analysed at E11.5, E13.5 and E15.5. No NTDs were mentioned and the phenotype of the mice was very similar to that of p27/p57 double null mice (Tateishi et al., 2012) suggesting that p21 is more or less dispensable during embryonic development.

In this chapter, my aims were to analyse MHP formation in mice lacking p21 and test the theory of redundancy in p21 null-, and p21/p27 double null mice, by quantitating the levels of p57 mRNA in these backgrounds. Furthermore, the role of the notochordal factor, Shh, in p21 induction was assessed in Shh null mice.

4.2 Results

4.2.1 Development is normal in p21$^{-/-}$ embryos

p21$^{-/-}$ embryos were generated from staged heterozygous matings. p21 null mice have been described before with no reports of developmental abnormalities (Brugarolas et al., 1995; Deng et al., 1995). In our laboratory no abnormalities were observed in p21$^{-/-}$ embryos. They develop normal MHPs (Figure 4.1; arrows) and they grow to become fertile mice. To assess whether p21$^{-/-}$ embryos develop at the same rate as p21$^{+/+}$ embryos, average somite number at E8.5 was compared between genotypes in 65 litters (Figure 4.2). Average somite number for p21$^{+/+}$ and p21$^{+/-}$ embryos at E8.5 was 8.1 while average somite number for p21$^{-/-}$ embryos was 7. The difference was significant between genotypes (One way ANOVA p<0.001) and pairwise testing revealed a significant reduction in somite number of p21$^{-/-}$ compared to p21$^{+/-}$ and p21$^{+/+}$ embryos. To see whether the developmental delay at E8.5 is observed at later stages, a limited number of mice were collected at E9 and E9.5. No difference in average somite number between genotypes was observed at either stage (p=0.82 and p=0.32, respectively) (Figure 4.3).
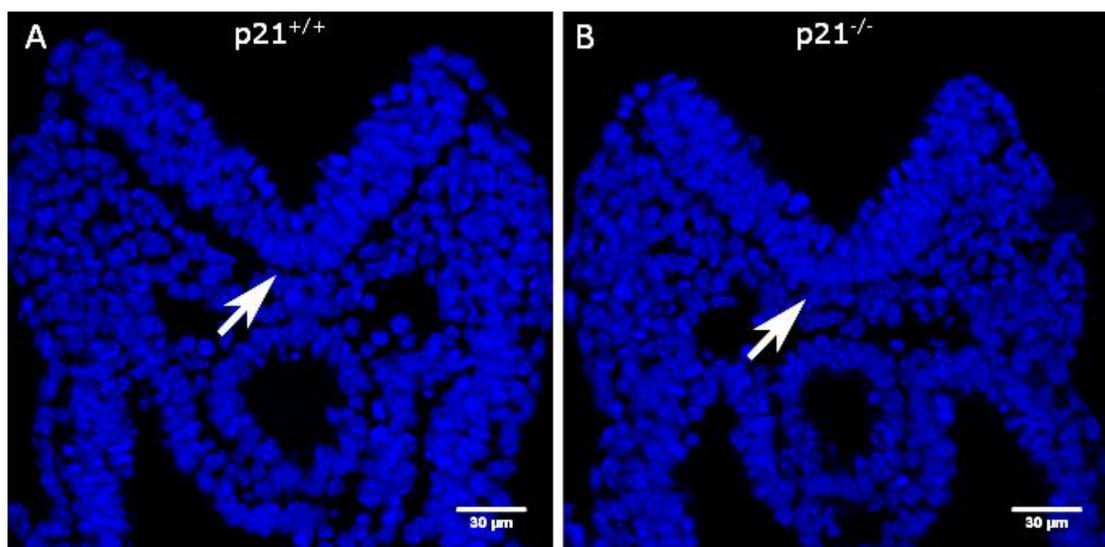
Figure 4.1 – E8.5 p21 deficient embryos develop normal MHPs

There is no morphological difference between the MHP (arrows) of p21$^{+/+}$ (A) and p21$^{-/-}$ embryos (B).

Neurulation was analysed in a small number of embryos. Posterior neuropore length is a measure of the rate at which neurulation proceeds in relation to axial growth and an enlargement of neuropore length can indicate early neurulation defects (Copp, 1985). No significant difference in PNP length was observed between p21 genotypes at E8.5 (Figure 4.4). In order to assess whether the PNP closure rate of p21 deficient mice is slower than that of wild-type littermates, somite number was plotted against PNP length. Due to the relatively small sample number, the correlation is poor for $p21^{-/-}$ and $p21^{+/-}$ embryos. Regression lines do not reveal any apparent differences between the closure rates of p21 genotypes (Figure 4.5). Thus, p21 mutant embryos have, on average, one somite less than heterozygous and wild-type embryos at E8.5 with no delay in neurulation. The developmental delay is not observed at E9 and E9.5 although the number of embryos analysed is smaller. Due to the large natural variation in somite number in embryos at E8.5 (~6-13 somites), the biological significance of a one somite delay is questionable. I therefore conclude that p21 mutant embryos develop normally compared to wild-type littermates. The observed phenotypes do not adhere to the expected Mendelian ratio (p=0.03) but are close, consistent with survival of all, or most, mutant embryos (Figure 4.6).
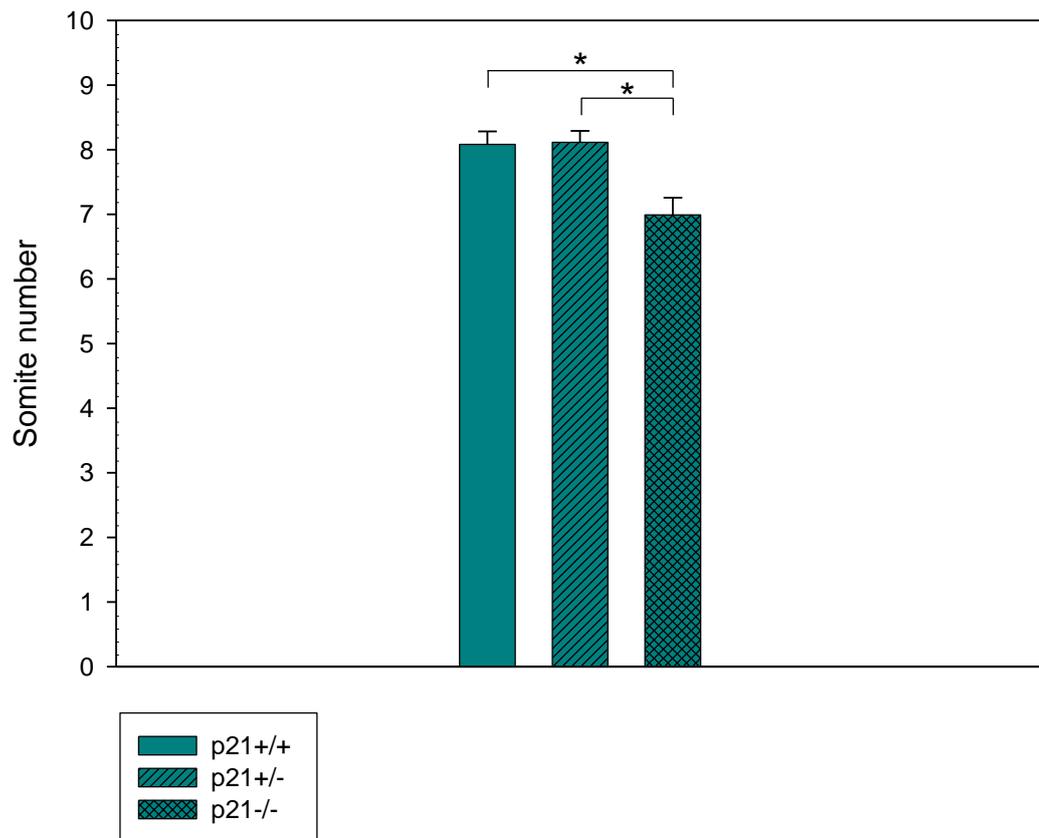
Figure 4.2 - p21 mutant embryos at E8.5 show developmental delay

Average somite number of p21 mutant embryos is significantly lower than wild-type and heterozygous embryos. 134 wild-type, 219 heterozygous, and 94 mutant embryos from 65 litters were analysed. Error bars represent the SEM. One way ANOVA shows that the difference in somite number between genotypes is statistically significant ($p < 0.001$). Pairwise testing (Holm-Sidak method) shows that p21$^{-/-}$ embryos have a significantly lower somite number than p21$^{+/+}$ and p21$^{+/-}$ embryos ($p < 0.05$).
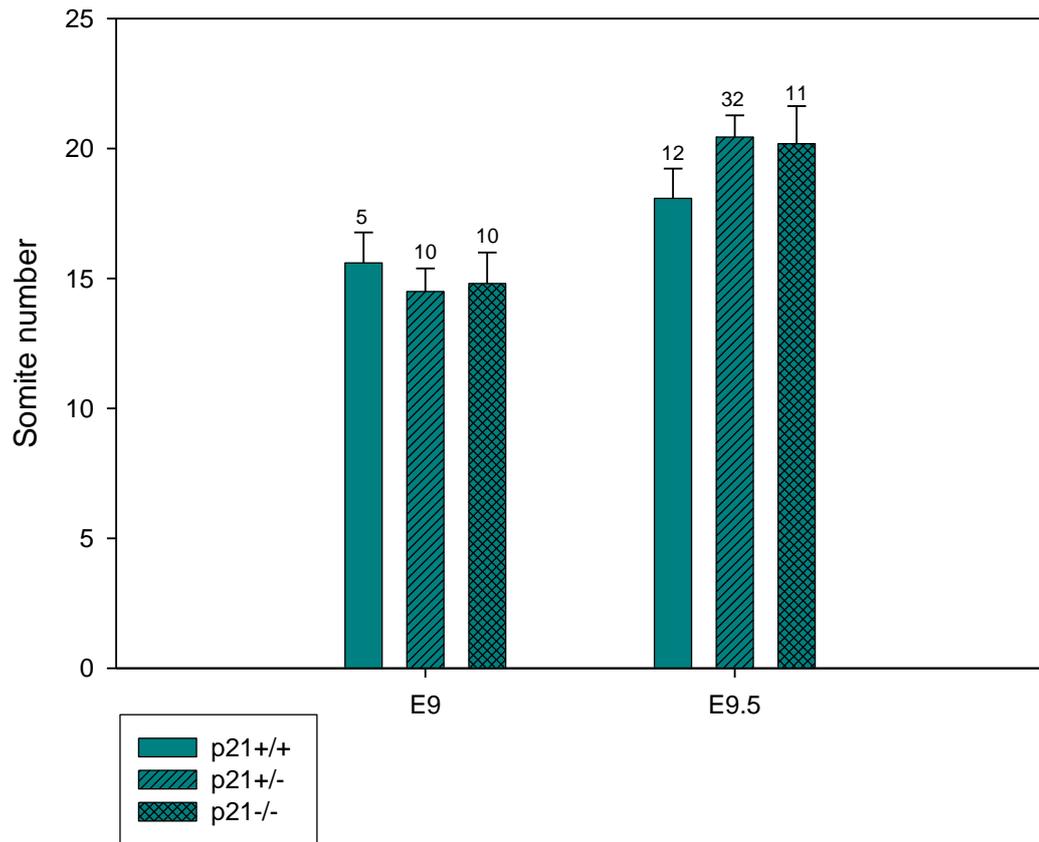
Figure 4.3 - p21 mutant embryos are not delayed at E9-9.5

Somite number in embryos from heterozygous matings was analysed at E9 and E9.5. There is no difference between the genotypes at E9 or E9.5 (p=0.823 and p=0.317, respectively. One Way ANOVA). The number of embryos analysed is shown above the graphs. Error bars represent the SEM.
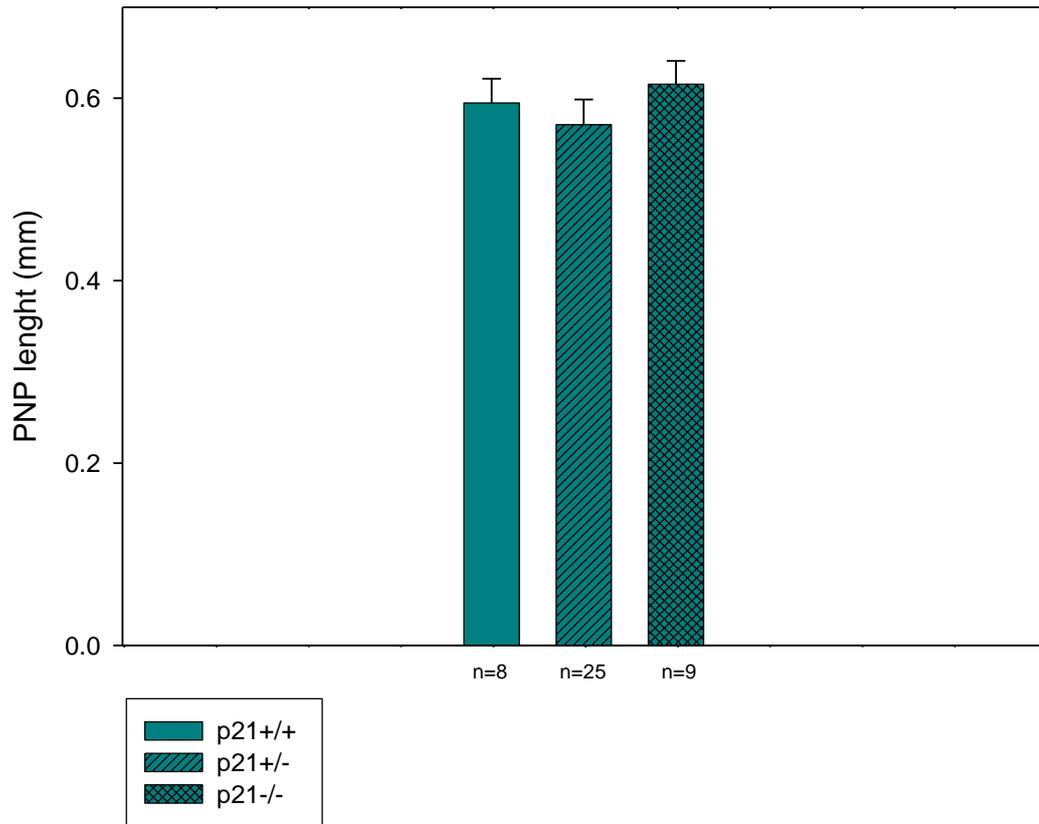
Figure 4.4 - Neurulation is not significantly different in p21 mutant embryos

The length of the PNP was measured in E8.5 embryos. No significant difference was detected between genotypes (p=0.94, One Way ANOVA). Error bars represent the SEM. The number of embryos analysed is shown for each genotype.
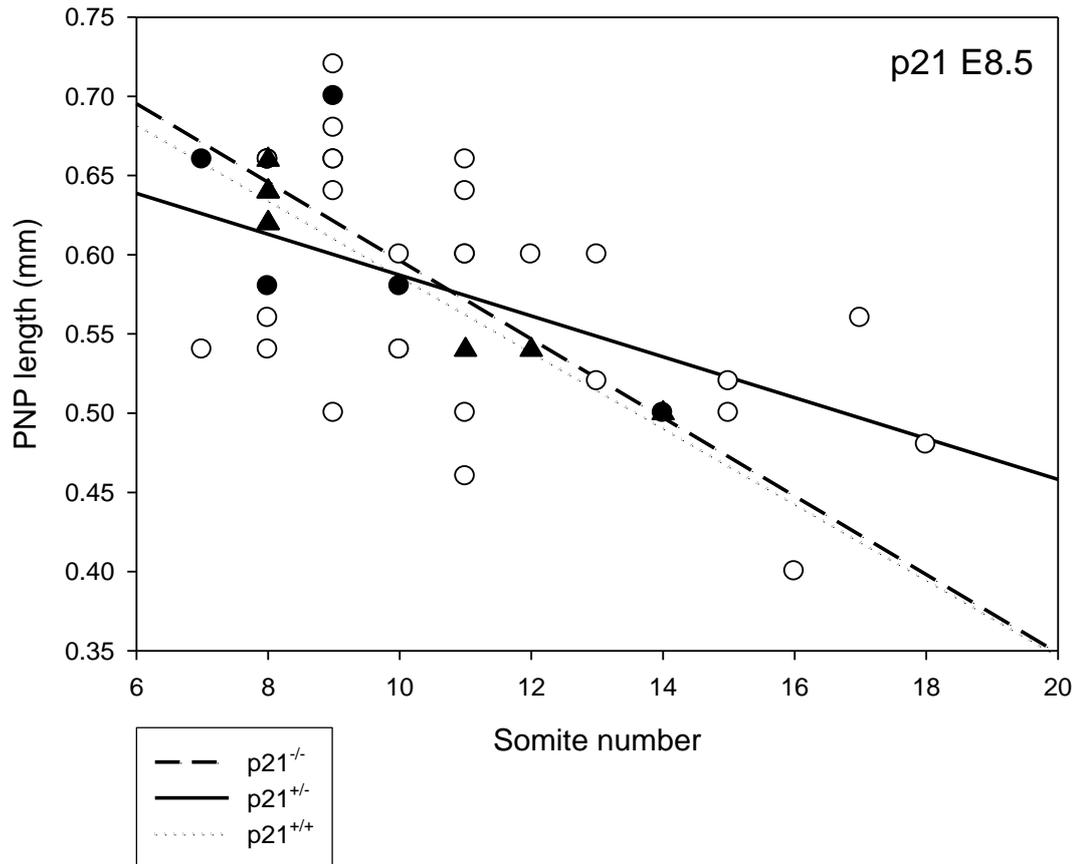
Figure 4.5 - Correlation between somite number and PNP in p21 mice at E8.5

Somite number of the embryos from Figure 4.4 was plotted against PNP length. Regression lines do not reveal delays in spinal neurulation in p21^{-/-} (closed circles) embryos compared to p21^{+/-} (open circles) or p21^{-/-} (triangles). The PNPs of p21^{-/-} shorten as somite number increases, similar to p21^{+/+}. There is a poor correlation for p21^{-/-} (r^2=0.56) and p21^{+/-} (r^2=0.25) but not p21^{+/+} (r^2=0.93).
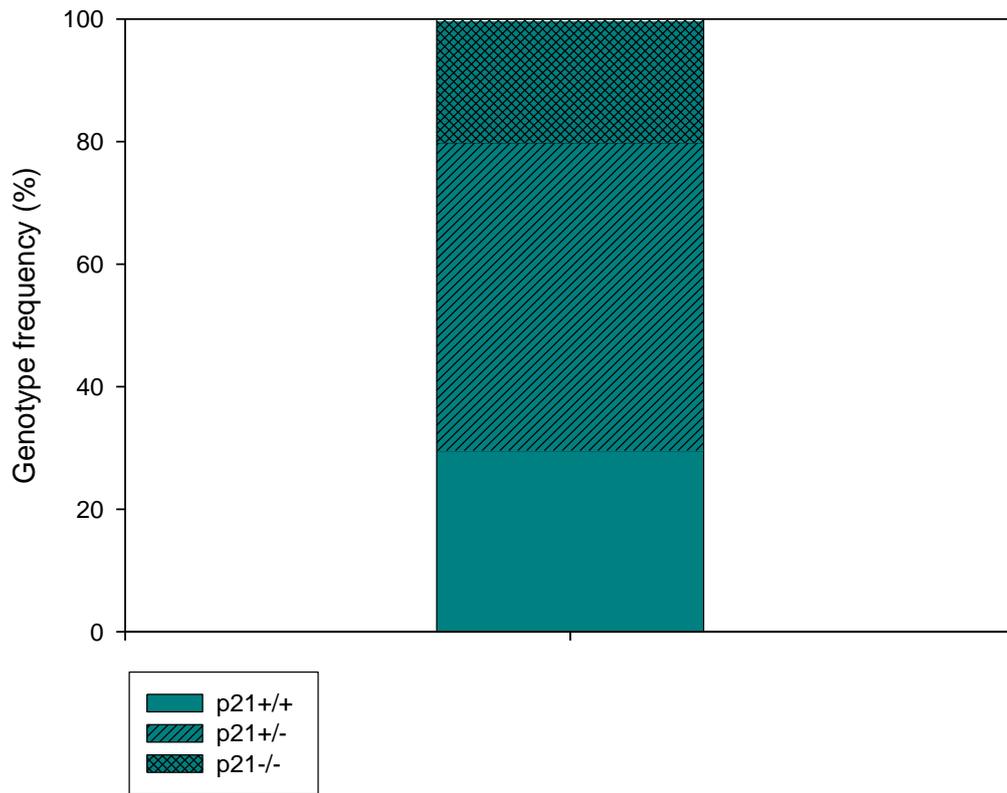
Genotype	Expected		Observed		Chi square
	%	Freq.	%	Freq.	
p21$^{+/+}$	25	112/447	30	134/447	4.32
p21$^{+/-}$	50	223/447	49	219/447	0.07
p21$^{-/-}$	25	112/447	21	94/447	2.89
Deviation from Mendelian ratios:	X^2=7.28 with 2 degrees of freedom (p=0.03)				

Figure 4.6 - Mendelian ratio in the p21-null mouse line

66 litters of embryos from a p21$^{+/-}$ x p21$^{+/-}$ deviate from the Mendelian ratio. p21 null embryos are found at a slightly lower frequency than expected.

4.2.2 p21/p27 double mutant embryos develop normally

p21$^{-/-}$; p27$^{+/-}$ mice did not breed well. Out of 42 plugged females, only 21 (50%) were pregnant at gestational day 8.5. A number of the 21 mice looked like they had been pregnant as they had swollen uterine horns. p27$^{-/-}$ female mice have been shown to be infertile and although they mate and fertilization takes place, they are unable to maintain a pregnancy (Fero et al., 1996; Kiyokawa et al., 1996; Nakayama et al., 1996). Our p21$^{-/-}$; p27$^{+/-}$ females seem to be partially infertile. This has not been mentioned in previous reports with p21/p27 double mutant mice (Cerqueira et al., 2014; Garcia-Fernandez et al., 2011) but was a recognised problem in the laboratory that provided us with the mice (M.Malumbres, personal communication).

In accordance with previous published studies, I do not find that p21/p27 double mutant embryos differ from wild-type littermates (Garcia-Fernandez et al., 2011). Embryos from 18 litters at E8.5 were analysed for average somite number, which ranged from 8.2 to 8.5 for all genotypes. The difference between the groups was not significant (p=0.879; One Way ANOVA) (Figure 4.7). The decrease in somite number I observed for p21$^{-/-}$ embryos at E8.5 is not reproduced in the double mutant embryos.

p21$^{-/-}$; p27$^{+/-}$ matings did not produce genotypes at the expected Mendelian ratios. This could be due to the relatively low numbers of p21$^{-/-}$; p27$^{+/+}$ and p21$^{-/-}$; p27$^{-/-}$ embryos that were collected (Figure 4.8). It is unlikely to be due to embryonic lethality as the wild-type and the mutant embryos are both found at low ratios (Figure 4.8).
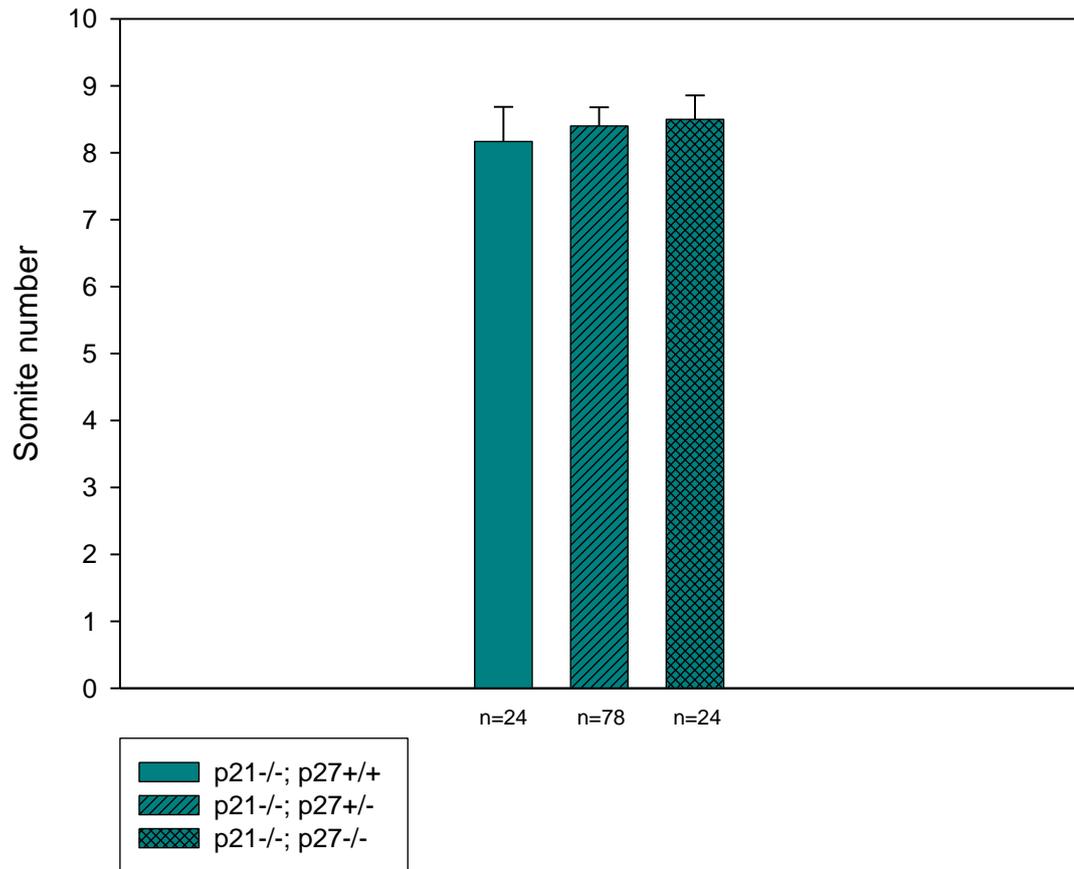
Figure 4.7 - p21/p27 double mutant embryos are not developmentally delayed

Embryos from 18 litters were analysed at E8.5. There is no difference in somite number between genotypes (p=0.879; One Way ANOVA). The number of embryos analysed is shown on the graph. Error bars represent the SEM.
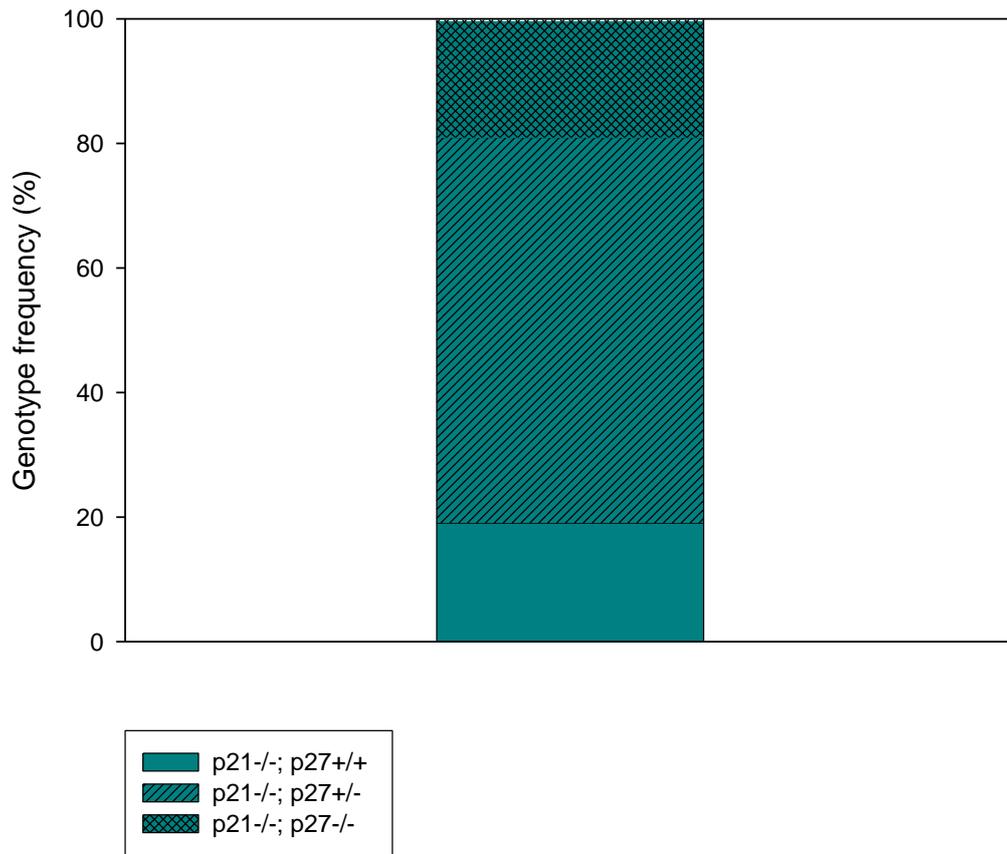
Genotype	Expected		Observed		Chi square
	%	Freq.	%	Freq.	
p21$^{-/-}$; p27$^{+/+}$	25	31.5/126	19	24/126	1.79
p21$^{-/-}$; p27$^{+/-}$	50	63/126	62	78/126	3.57
p21$^{-/-}$; p27$^{-/-}$	25	31.5/126	19	24/126	1.79
Deviation from Mendelian ratios:	X^2=7.15 with 2 degrees of freedom (p=0.03)				

Figure 4.8 - p21$^{-/-}$; p27$^{+/-}$ matings did not produce litters at expected Mendelian ratio

Embryos were analysed from 18 litters. There is a statistically significant deviation from the expected Mendelian ratio.

4.2.3   Are p21 and p57 redundant in the neural tube?

Mice deficient in p27 have been shown to have normal tissue distribution of p21 and p57 protein (Kiyokawa et al., 1996). The mouse models do, however, suggest that there is some level of redundancy between all three genes in other systems. As p21 and p57 are both expressed in the developing neural plate midline, I set out to examine the expression of p57 in p21 deficient embryos.

At the 8 somite stage, p57 is expressed in the notochord and ventral hindgut and expression is similar in mutant and wild-type p21 embryos (Figure 4.9). At the 12 somite stage, p57 is upregulated in the notochord and overlying neuroepithelium of p21 deficient embryos (Figure 4.10, A-C). Furthermore, the notochord in p21 deficient embryos is wider (Figure 4.10, C; arrow). Due to variations in the in situ hybridisation results, it is difficult to draw definite conclusions regarding redundancy based on the in situ hybridisation data alone. Therefore, the caudal region of p21 embryos from the 3rd somite pair was collected for quantitative PCR analysis in order to quantify any change in p57 expression in the absence of p21.

At the 5-7 and 8-10 somite stages, p21 expression corresponded to embryonic genotype with approximately 20-60% p21 mRNA in heterozygous p21 embryos compared to wild-type, and very little expression detected in p21 deficient embryos (Figure 4.11). This confirms that the p21 mutants are complete nulls. p57 expression was very varied as suggested by the large error bars. There is no apparent difference between p57 mRNA levels among the p21 genotypes (Figure 4.11). Thus, I am unable to show upregulation of p57 in the absence of p21 in this analysis. The varied results could be due to inconsistent cutting of the caudal part of the embryo. Since p57 expression is observed in the most rostral somites, some variation in the expression of p57 could have resulted from differences between embryos in the precise position of the cut, to separate the caudal regions. Moreover, the allantois expresses high levels of p57 and was therefore removed from the embryos prior to collection, but it is possible that some tissue remained in some embryos. Lastly, it could be that p57 is upregulated specifically in the neural plate and, as I collected caudal regions that included the hindgut and notochord, which both exhibit high

expression of p57, these areas might have masked any upregulation in the neural plate. Embryos from p21$^{-/-}$; p27$^{+/-}$ matings were also analysed to determine whether p57 is upregulated in the absence of both p21 and p27. There was no difference in p57 mRNA levels between p21$^{-/-}$; p27$^{+/+}$ and p21$^{-/-}$; p27$^{-/-}$ embryos although this could also have been due to inclusion of other tissues that express p57 strongly (Figure 4.12).

Due to the limited number of embryos that could be obtained from the p21$^{-/-}$; p27$^{+/-}$ matings, I was unable to assess specific upregulation of p57 in the neural tube by in situ hybridisation.
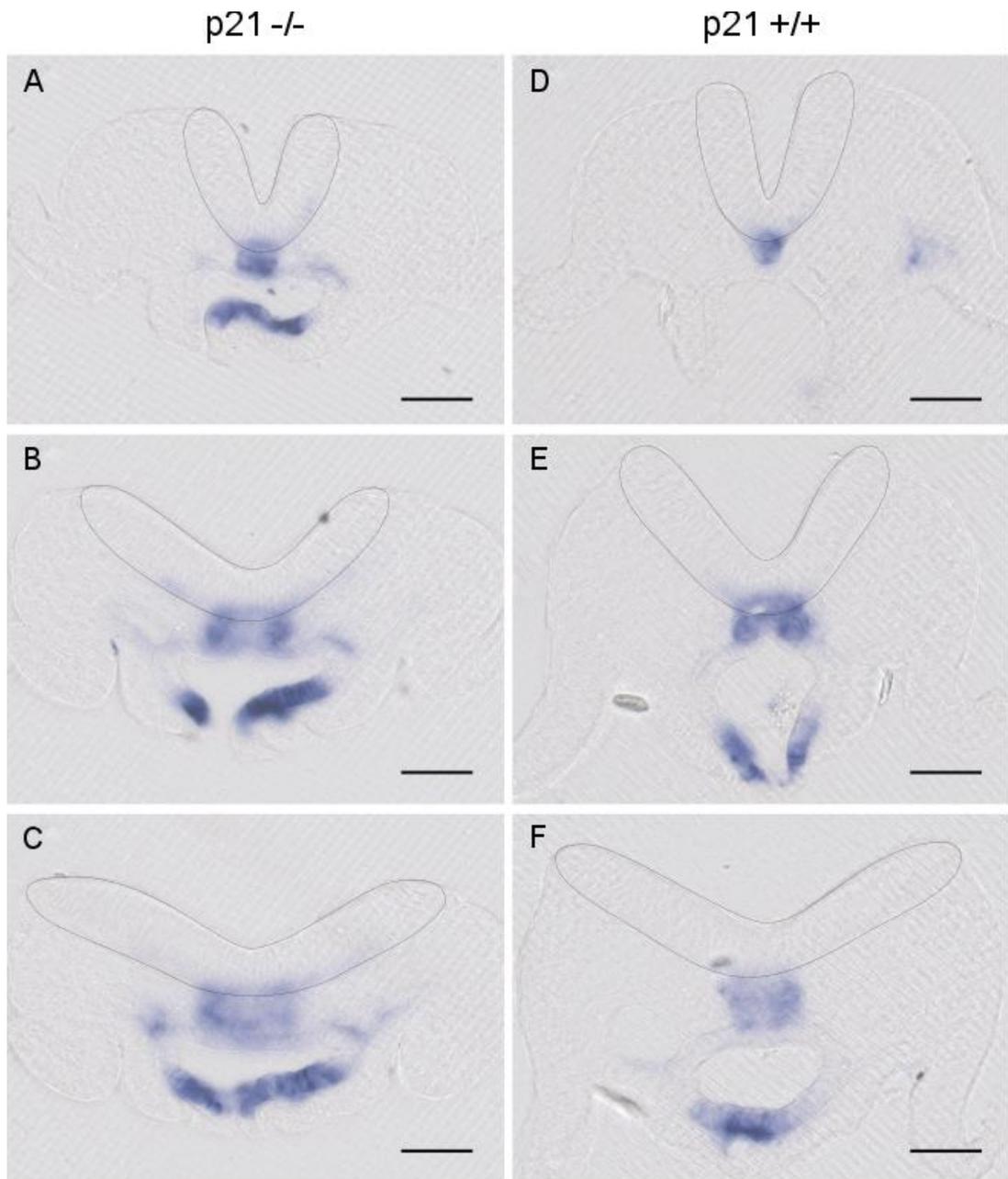
Figure 4.9 - p57 mRNA expression in p21$^{-/-}$ and p21$^{+/+}$ embryos with 8 somites

Whole mount in situ hybridisation was performed, after which embryos were vibratome sectioned. There is no difference between p57 mRNA expression in the MHP of p21$^{-/-}$ (A-C) and p21$^{+/+}$ (D-F) embryos, although the notochord is wider in the p21 mutant. n≥3. Scale bars = 50 μm.
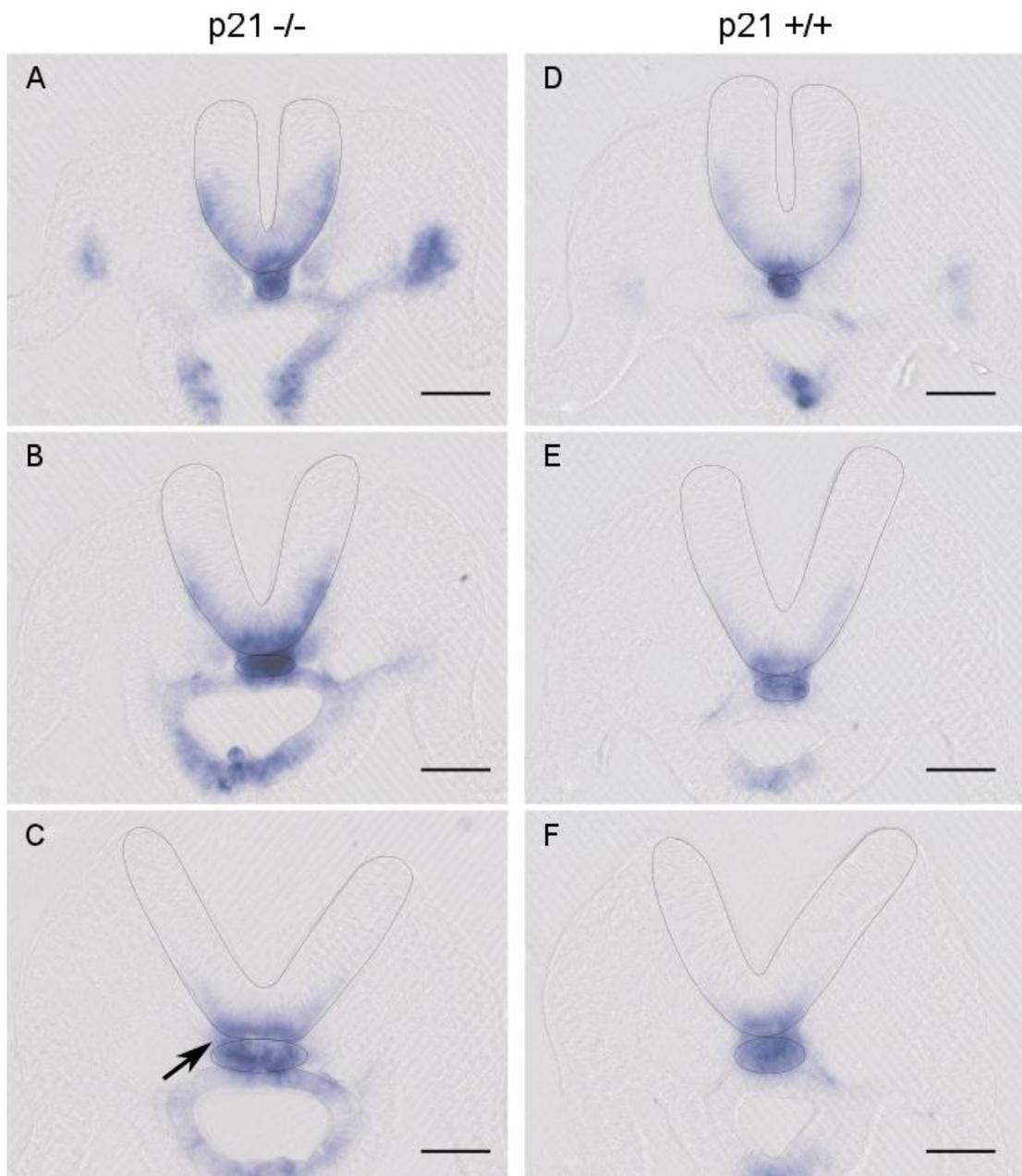
Figure 4.10 - p57 is expressed more intensely in p21$^{-/-}$ compared to p21$^{+/+}$ embryos with 12 somites

Whole mount in situ hybridisation was performed, and embryos were vibratome sectioned. At 12 somites there is upregulation of p57 mRNA in the MHP and basal neuroepithelium of p21$^{-/-}$ embryos compared to p21$^{+/+}$. Note the darker notochord in A-C as well as the very broad notochord observed in C (arrow), corresponding to the findings at 8 somites (Figure 4.9). n≥3. Scale bars = 50 μm.
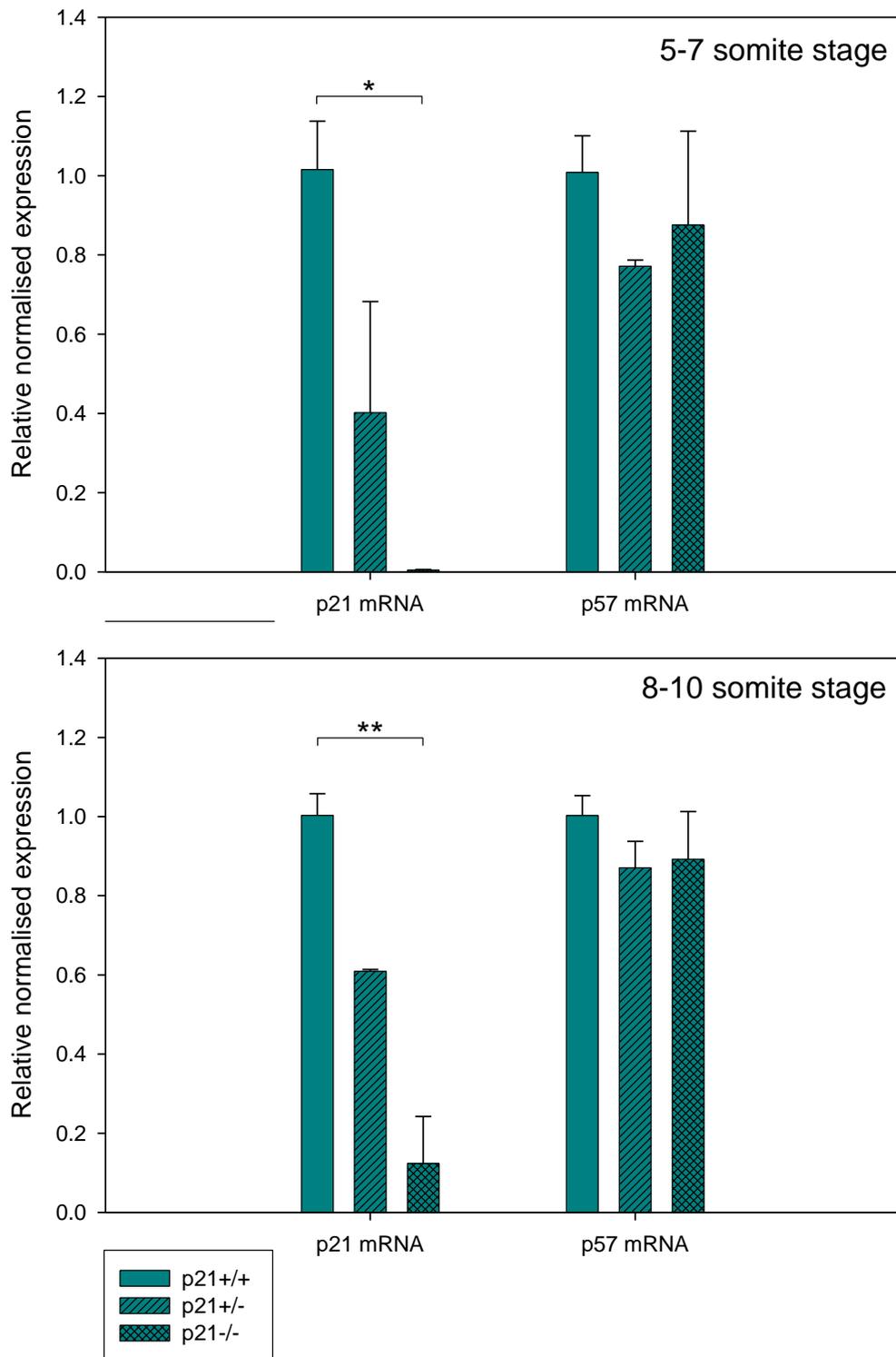
Figure 4.11 - p57 expression in the caudal embryo does not differ between p21 genotypes

Caudal parts from p21$^{+/+}$, p21$^{+/-}$ and p21$^{-/-}$ embryos at E8.5, separated at the 3rd somite pair, were analysed by qRT-PCR. p21 mRNA expression level corresponds to genotype while there is no difference in p57 mRNA between p21 genotypes (p=0.66 and 0.63; One way ANOVA). Caudal regions were pooled for each sample (3 for 5-7s and 2 for 8-10s) and 3-4 samples were assayed per genotype. Error bars represent the SEM. *p<0.05, **p<0.001; One way ANOVA.
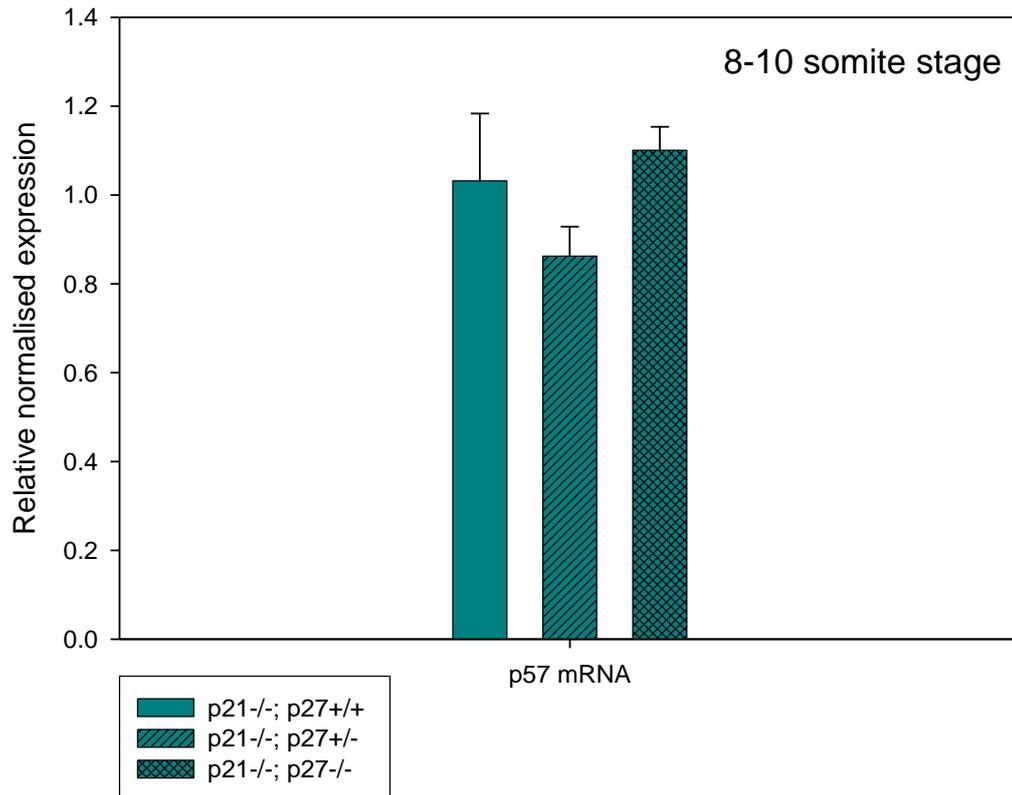
Figure 4.12 - p57 is not upregulated in p21/p27 double mutant embryos with 8-10 somites

Caudal embryonic regions were collected from the 3rd somite pair, pooled two per sample, and p57 mRNA was quantified by qRT-PCR. 4-5 samples were assayed per genotype. p57 is not upregulated in the caudal region of p21/p27 double mutant embryos (p=0.27; One way ANOVA).

4.2.4   Is p21 expression dependent on Shh?

Heat ablation of the notochord during embryonic development results in loss of the MHP in the mouse (Ybot-Gonzalez et al., 2002). Furthermore, notochordal fragments transplanted into the lateral neural tube in chick embryos induce MHP characteristics in the cells overlying the explant (Smith and Schoenwolf, 1989; van Straaten et al., 1988). Thus, it seems that factors emanating from the notochord are important for MHP formation. Shh, Chordin and Noggin are all expressed in the mouse notochord underlying the neural plate midline during neurulation (Ybot-Gonzalez et al., 2002; Ybot-Gonzalez et al., 2007a) but the MHP forms in Shh deficient embryos, indicating that other notochordal factors are required for MHP formation (Ybot-Gonzalez et al., 2002). In order to assess whether notochordal factors are required for the induction of p21 expression in the MHP, p21 mRNA was

examined in embryos deficient in Shh which were expected to develop with no notochord.

Contrary to what was expected, and in agreement with the original work (Chiang et al., 1996), the Shh mutant embryos used in this study form a notochord that appears normal at E7.5 but is subsequently lost in a rostral to caudal manner. This is seen by the discontinuity and loss of Brachyury expression especially in the rostral region (Figure 4.13, A) compared to the strong and continuous expression in wild-type littermates at E8.5 (Figure 4.13, B). Brachyury is required for the differentiation of the notochord and is commonly used as a marker for primitive streak, node and notochord in E7.5 and E8.5 embryos (Herrmann and Kispert, 1994). Note that at E8.5, the notochord looks intact in the PNP where the MHP is forming (Figure 4.13, A-A'; arrow).

The expression of p21 was examined in Shh deficient embryos to see whether Shh is required for p21 expression. The MHP morphology of Shh deficient embryos is indistinguishable from wild-type littermates (Figure 4.14). p21 expression is similar with or without Shh although the expression seems stronger in wild-type embryos (Figure 4.14, E-H). The notochord can be observed in Shh deficient embryos (Figure 4.14, C; arrow) but interestingly, p21 is only expressed in the notochord in the absence of Shh, suggesting that Shh expression in the notochord might repress p21 expression (Figure 4.14, C and G; arrows). Shh is not required for p21 expression. However, the presence of the caudal notochord in the embryos at E8.5 means that the notochord could be responsible for the induction of p21 independently from Shh. Indeed, it has been found that local application of Shh and Chordin together can induce strong expression of p21 in the neural plate (R.Carvalho and A.J.Copp, unpublished). A different model would be required to test whether notochordal factors are required for p21 (and p27, p57) induction in the MHP. For example, node ablation can be achieved using a hot tungsten needle, leading to notochordless embryos (Ybot-Gonzalez et al., 2002). There was insufficient time in this project to carry out notochord ablation experiments.
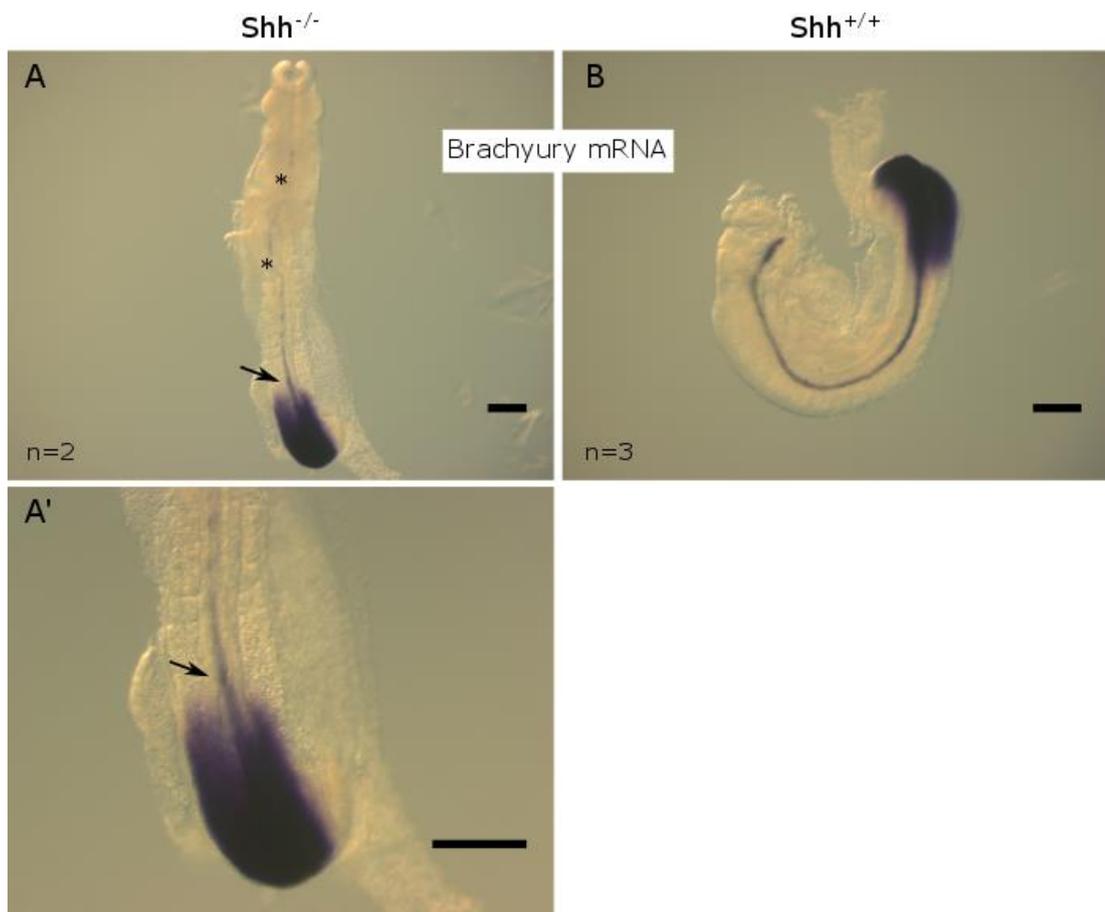
Figure 4.13 - Shh deficient embryos have some notochordal tissue, especially caudally

Embryos at E8.5 were analysed by in situ hybridisation for Brachyury expression, a marker of the notochord. The notochord is almost completely lost in the rostral region of $Shh^{-/-}$ embryos (A-A') compared to $Shh^{+/+}$ (B). The notochord Brachyury signal is strongest in the caudal region and looks intact in the PNP region (A-A'; arrow). Note the absence of notochord at more rostral levels (A-A'; *). Scale bars = 500 μm.

In order to see if p21 has any effect on Shh expression, or if the notochord is wider in embryos lacking p21, Shh expression was analysed by in situ hybridisation in $p21^{-/-}$ and $p21^{+/+}$ embryos. The notochord is wider in $p21^{-/-}$ embryos compared to wild-type littermates while overall MHP morphology and Shh expression is similar (Figure 4.15). Shh is expressed in the notochord and in the ventral hindgut in both $p21^{-/-}$ and $p21^{+/+}$ embryos. Interestingly, p21 is expressed in the dorsal hindgut further indicating that Shh and p21 expression could be mutually exclusive (Figure 4.14 and Figure 4.15).
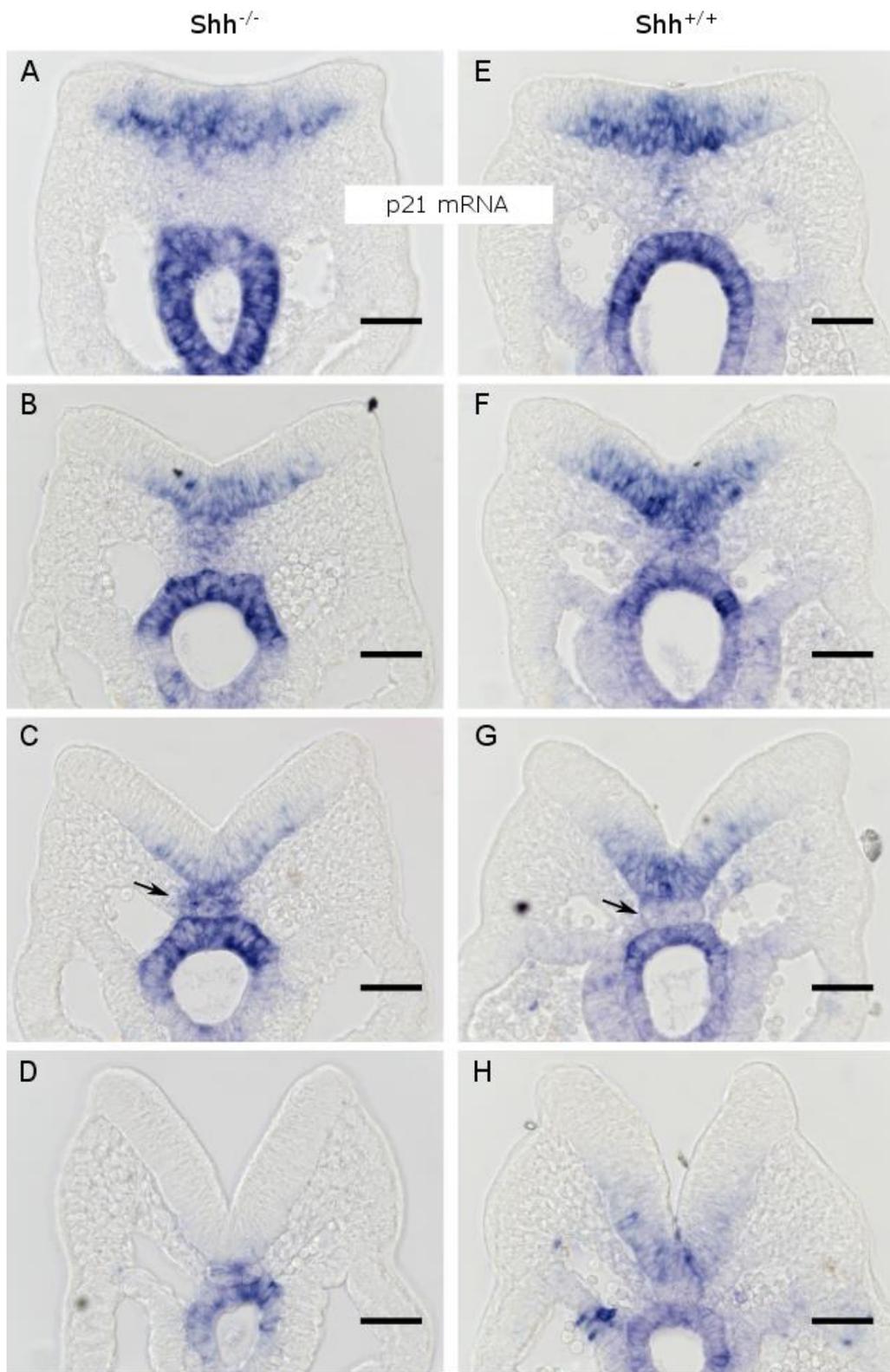
Figure 4.14 - p21 expression is maintained in Shh deficient embryos at E8.5

p21 expression detected by whole mount in situ hybridistaion followed by vibratome sectioning. Expression is maintained in the neuroepithelium of Shh deficient embryos (A-D). Note that p21 is expressed in the notochord only in the absence of Shh (arrows). Scale bars = 50 μm.

141
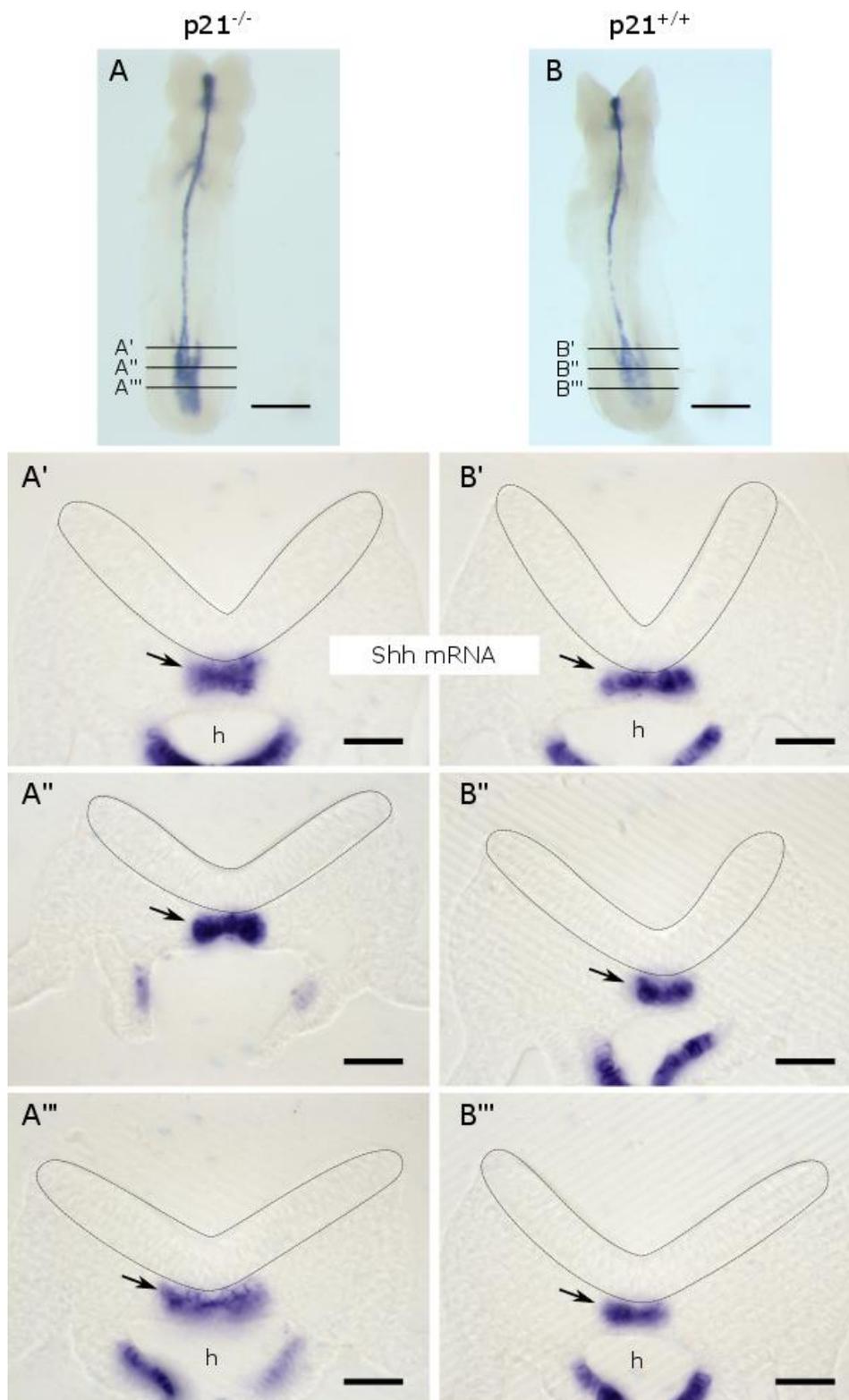
Figure 4.15 - Shh expression is unchanged in the absence of p21 at E8.5

p21$^{-/-}$ and p21$^{+/+}$ embryos were analysed for Shh expression by in situ hybridisation followed by sectioning. There is no difference in neural plate morphology whereas the notochord is wider in the p21$^{-/-}$ embryo (arrows). Shh is expressed normally in the notochord (arrows) and ventral hindgut (h). Scale bars = 300 μm (A-B) and 50 μm. (A'-B'). n=3.

4.3 Discussion

Development of the MHP and the possibility of genetic redundancy between different CDKIs were examined in p21 and p27 mutant mice. p21 deficient mice form normal MHPs, undergo normal spinal neurulation and overall development is unaffected.

The amounts of p21 and p57 mRNA in the caudal region of the embryo, assessed by quantitative RT-PCR varies a lot. The variation in p21 expression could be due to incorrect genotyping of one embryo in a pooled sample, as one of the $p21^{+/-}$ samples at the 5-7 somite stage and one sample of the $p21^{-/-}$ 8-10 somite stage expressed a much higher amount of p21 than the other two or three samples. The source of the variation in p57 expression is unknown but could be due to contamination of samples with allantoic tissue which expresses very high levels of p57, and which I aimed to remove in the dissection.

Due to poor breeding of the $p21^{-/-}$; $p27^{+/-}$ mice I had limited resources of embryos to work with and all were used to quantify p57 mRNA expression in double mutant embryos. Unfortunately I did not get conclusive results from the analysis. It would have been important to analyse the expression of p57 in isolated midline fragments of double mutant embryos by qPCR to exclude background expression from the hindgut and other caudal tissues. Furthermore, examination of MHP and notochord morphology and p57 expression in double mutant embryos by in situ hybridisation would have been informative.

Interestingly, the expression pattern of p57 and Shh are similar in the PNP: i.e. they are both expressed in the notochord and ventral hindgut. In comparison, p21 is excluded from these regions and is instead expressed in the neuroepithelium and neural plate. It is intriguing that p21 expression is found in the notochord of embryos deficient in Shh which might suggest that Shh excludes p21 expression. This does not seem to be the case in the hindgut as p21 expression is localised to the dorsal hindgut in Shh mutant as well as wild-type embryos. Nonetheless, Shh is

143

expressed in the ventral hindgut in rostral regions of the PNP while the expression in the hindgut is lost at very caudal levels (Ybot-Gonzalez et al., 2002). In comparison, p21 expression is ventral in the hindgut underlying the rostral PNP and is uniform throughout the hindgut at more caudal levels. Although p21 and p57 are expressed in separate regions of the hindgut they are both expressed in the neural plate during neurulation. Thus, it is highly unlikely that p21 and p57 exclude expression of each other. On the contrary, they could co-operate in the neural plate to regulate the cell cycle of MHP cells.

Shh and Chordin soaked beads, when implanted in the PNP region, were found to induce expression of p21 in the neural plate as visualised by in situ hybridisation (R.Carvalho and A.J.Copp, unpublished). However, this gain-of-function experiment was performed on wild-type mice where p21 is usually expressed. I have found that the level of expression detected by in-situ hybridisation of all three CIP/KIP genes varies somewhat from experiment to experiment. Thus, in a system where p21 is endogenously expressed, it is difficult to conclude that Shh and Chordin are sufficient for p21 induction based on more intense p21 staining as visualised by in situ hybridisation. With a loss-of-function experiment I have shown that Shh is not required for p21 induction as Shh$^{-/-}$ embryos display a normal distribution of p21 mRNA in the neural plate. This is in agreement with the gain-of-function experiments using Shh soaked beads which did not lead to increased intensity of p21 expression on its own (R.Carvalho and A.J.Copp, unpublished). I cannot conclude whether notochordal factors are required for p21 induction in the Shh mouse model as the notochord is intact in the regions underlying MHP formation in the PNP. To determine this, it would be necessary to repeat the p21 expression analysis on embryos where the notochord had been ablated prior to neurulation (Ybot-Gonzalez et al., 2002). Alternatively, knock-down of Chordin and/or Noggin in the notochord could answer the question as to whether these 'notochordal genes' are required to induce p21 in the MHP. It would also have been informative to determine whether expression of p57 is dependent on Shh expression, as these are expressed in the same region.

In conclusion, the mouse models suggest that there is redundancy between the CIP/KIP genes in various systems. By in situ hybridisation experiments it seems that p57 mRNA is expressed more intensely in the notochord and neural plate in a p21 deficient background, suggesting that in the mouse neural plate, p21 and p57 might be redundant. p21 is expressed specifically in the neural plate midline and could be important for the prolongation of the cell cycle in MHP cells. The MHP of p21 mutant mice develops with a normal morphology, indicating that either p21 is not important for MHP formation, or that p27 and/or p57 in the neural plate have redundant roles. I was unable to conclude whether p57 is upregulated in the neural plate of p21 and p21/p27 double mutant mice and whether the MHP forms in p21/p27 double mutant animals.

There is evidence that the notochord is required for MHP formation. I have shown that Shh, expressed from the notochord, is not required for p21 induction. This suggests that other notochordal factors could be required for p21 induction in the overlying neural plate. Nonetheless, p21 is not necessary for MHP formation in the mouse neural plate.

Chapter 5- Reduced S-phase length in p21$^{-/-}$ mice

5.1 Introduction

5.1.1 The median hinge point is enriched in wedge shaped cells

"Suppose we have a sheet of cells, the elements of which are as wide at their bases as they are at the free surface. If now, as a result of internal forces, the cells are all induced to become thicker at their bases and thinner at their free ends, the result will be that the sheet bends and folds together to form a hollow structure." His, 1894 (Schoenwolf and Smith, 1990).

As described in Section 1.3, median hinge point (MHP) formation is often regarded as a combination of apical constriction and basal cell expansion. It is clear, however, that in the spinal region, disassembly of microfilaments using Cytochalasin D is not sufficient to abolish existing MHPs, nor to prevent new MHP formation (Escuin et al., 2015; Ybot-Gonzalez and Copp, 1999). Therefore, microfilament-dependent apical constriction is not essential for MHP formation, although it remains to be determined whether apical constriction plays more secondary roles in supporting the shape of the neuroepithelium, when this is influenced by other factors.

The cell composition of the MHP in the mouse and chick has been shown to consist of mainly wedge shaped cells (McShane et al., 2015; Schoenwolf and Franks, 1984; Smith et al., 1994). Smith and Schoenwolf published a detailed analysis of the cell shapes found in the mouse neural plate in 1997, and in 2015 members of our lab published an even more detailed study of nuclear position (which is an indicator of cell shape), and cell cycle times in the mouse neural plate (McShane et al., 2015; Smith et al., 1994). In the chick neural plate the cell shape composition has also been studied in detail (Schoenwolf and Franks, 1984). The main findings of these studies are summarised in Table 5.1. The three studies are not directly comparable as two of them were done by rating cell shape while the third measured nuclear localisation as a measure of cell shape. Furthermore, two of the studies were done

146

in mouse and one in chick. However, the studies suggest that, during midline bending, the proportion of wedge shaped cells is higher in the MHP than in the lateral, non-bending region.

One of the main questions has, however, always been whether the cell wedging is an active event preceding bending, or whether the bending of the neuroepithelium at the MHP causes cell shape changes due to compression. Evidence consistent with the wedging-before-bending theory comes from McShane et al, showing that in the flat neuroepithelium there is no difference in the proportion of cells with basal nuclei in the prospective MHP and lateral regions (Table 5.1) (McShane et al., 2015). Furthermore, Schoenwolf and Franks show that in the avian midbrain, the increase in the proportion of wedge shaped cells in the MHP coincides with the formation of the midline furrow while the neuroepithelium is still very flat (Schoenwolf and Franks, 1984) (Figure 5.1). Thus, it is unlikely that compression occurs in the virtually flat neural plate midline causing cell shape changes (Schoenwolf and Franks, 1984). The increase in the proportion of wedge shaped cells is not observed in the lateral neural plate (Figure 5.1). In the avian spinal cord region, cell shapes were quantified after the midline furrow had started to form, and at this stage more wedge shaped cells were observed in the MHP (Schoenwolf and Franks, 1984). These studies show that cell shape changes in the MHP coincide with midline furrowing. No conclusive studies have been published on whether cell changes precede midline furrowing, or if the cell changes occur as a consequence of midline furrowing. As mentioned previously, midline furrowing is thought to be important for the position of the midline and thereby the normal morphology of the closed neural tube (Smith et al., 1994).

	Early/flat NP		Late/elevated NP		
	MHP	Lateral	MHP	Lateral	Reference
Mouse E8	-	-	65.4 W 25.1 S 6.7 IW	31.7 W 40.2 S 21.9 IW	(Smith et al., 1994)
Mouse E9.5	30-40 W 20-30 IW	30-40 W 20-30 IW	60 W 5-10 IW	30-40 W 20-30 IW	(McShane et al., 2015)
Chick HH7-11	59.4 W* 32.0 S 8.5 IW	26.1 W* 56.3 S 17.6 IW	72.0 W 25.7 S 2.2 IW	33.1 W 54.7 S 11.2 IW	(Schoenwolf and Franks, 1984)

Table 5.1 - Cell shape distribution (%) in the MHP and lateral regions

All three studies find a higher proportion of wedge shaped cells in the MHP than in the non-bending lateral region. This increase is seen as soon as the 'early' neural plate starts to show an indent at the midline. Numbers are percentages of cells with each shape. *Note that Schoenwolf and Franks, 1984, did not study the completely flat NE at the spinal level; numbers are from an already furrowing NP, hence the high proportion of wedge shaped cells in the early neural plate MHP. NP= neural plate, W= wedge shaped, S= spindle shaped, IW= inverted wedge shaped.
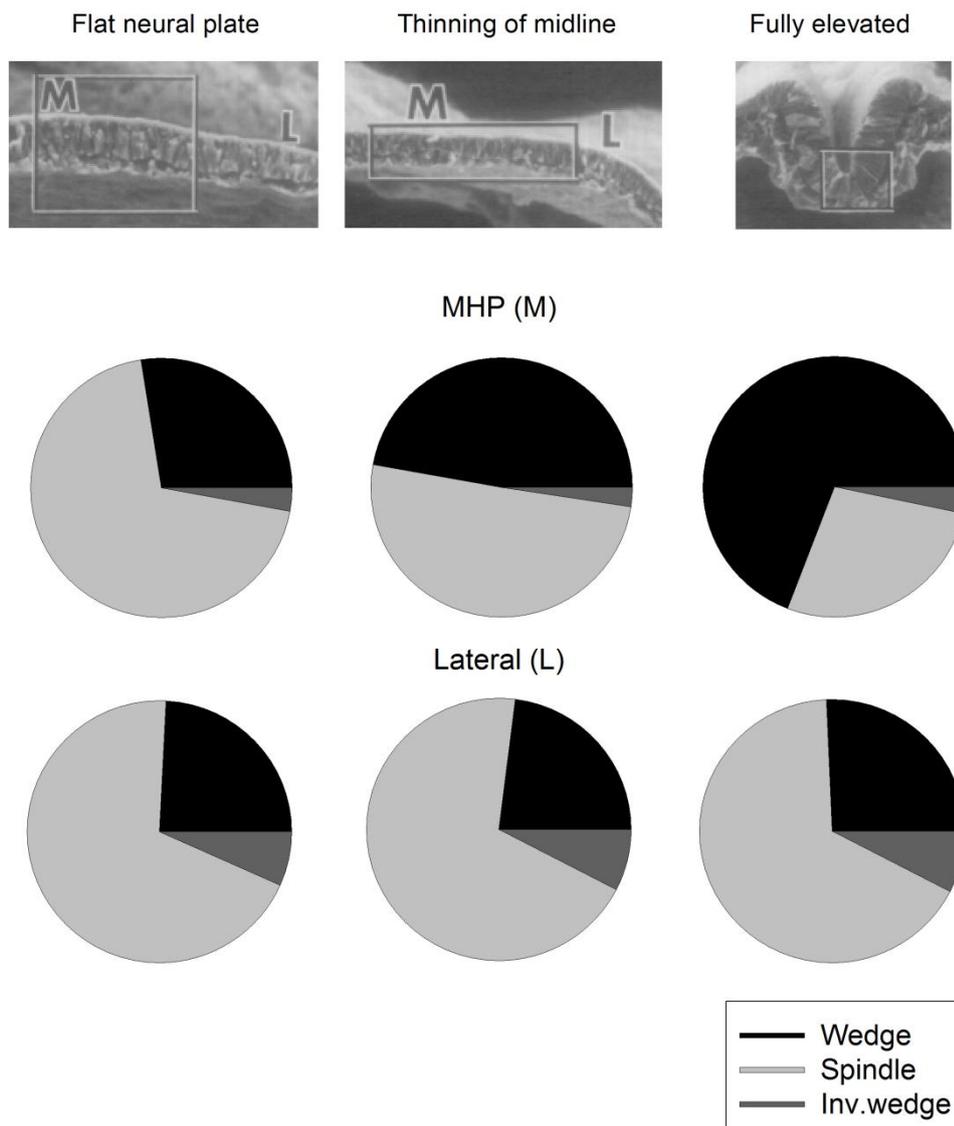
Figure 5.1 - In the avian midbrain wedging precedes initial midline furrowing

Schoenwolf and Franks quantified cell shapes in the completely flat avian neural plate (NP), NP with a thinning midline, and fully elevated NP at HH stages 4-8. The proportion of wedge shaped (black), spindle shaped (light grey) and inverted wedge shaped cells (dark grey) is presented for the MHP (top row) and the lateral region (bottom). Note how the proportion of wedge shaped cells in the MHP increases as the neural plate starts indenting at the midline. The proportion of wedge shaped cells in the lateral region is fairly constant. Redrawn from Schoenwolf and Franks, 1984.

5.1.2 Prolonged cell cycle in the MHP

As it seems a possibility that wedging of MHP cells is important for the correct bending of the neural plate at a restricted site within the neuroepithelium, the mechanism of the shift from a mix of cell shapes to a more uniform wedged cell population in the MHP is a question of much interest. Due to interkinetic nuclear migration, nuclei are located basally during S-phase and apically during M-phase (Langman et al., 1966). As mentioned before, the position of the nucleus determines the cell shape of neuroepithelial cells (Schoenwolf and Franks, 1984). Therefore, basal cell expansion in the MHP could occur by altering the cell cycle so that cells are kept in S-phase for longer periods while other cell cycle phases are shortened, thus reducing the time nuclei spend at the apical site (Eom et al., 2011; Smith and Schoenwolf, 1987).

Early studies in the chick have shown that the cell cycle of MHP cells is around 65% longer than that of cells in the regions outside of the MHP (Smith and Schoenwolf, 1987). Furthermore, the cell cycle times of midline cells not yet differentiated into MHP in the flat neural plate are similar to those of non-bending lateral regions in the mature V-shaped neuroepithelium (Smith and Schoenwolf, 1987). This suggests that the cell cycle of MHP cells becomes longer as the cells become wedge shaped during neural bending. Moreover, Smith and Schoenwolf showed that in the chick neural plate, S-phase, G1-phase, and G2-phase are prolonged in MHP cells while M-phase is 40 % shorter (Smith and Schoenwolf, 1988). Nuclei are basal during S-phase and likely during parts of G1-, and G2-phase as well. Thus, prolongation of S-, G1-, and G2-phase could lead to more basal nuclei overall. Recent work from McShane et al builds onto this evidence showing that the cell cycle in the MHP is significantly longer than in lateral non-bending regions, partly due to prolongation of S-phase (McShane et al., 2015). The findings of the studies mentioned are summarised in Table 5.2 - Length of the cell cycle (hr) in the MHP and lateral regions

In addition to prolonged cell cycle times, MHP cells are found to be shorter apico-basally than lateral cells during bending (McShane et al., 2015; Smith and Schoenwolf, 1988). Together with the longer time spent in basal phases of the cell cycle, this means that nuclei may spend less time moving between the apical and basal side, and spend more time basally as wedged shaped cells. But what causes the prolonged cell cycle, and specifically S-phase in the MHP?

	Early/flat NP		Late/elevated NP		
	MHP	Lat	MHP	Lat	Reference
Mouse E9.5	-	-	6.7 (2.3)	5.5 (1.5)	(McShane et al., 2015)
Chick HH4,7-10	7.7		9.9	6.3	(Smith and Schoenwolf, 1987)
Chick HH5-8+*	-	-	11.6 (3.6)	7.7 (2.4)	(Smith and Schoenwolf, 1988)
Chick 7-10ss**	-	-	8 (5)		(Langman et al., 1966)

Table 5.2 - Length of the cell cycle (hr) in the MHP and lateral regions

Studies that have quantified the length of the cell cycle (hr) show a longer cycle in the MHP compared to lateral regions. In cases where S-phase length was calculated this is shown in brackets. All the studies used thymidine labelling to calculate the cell cycle parameters. *Future midbrain region. **The whole V-shaped NP was analysed, no regional analysis was done, and rostro-caudal level is not clear from the paper.

5.1.3 The role of p21 in S-phase prolongation in the MHP

The use of different thymidine analogues to calculate cell cycle length has been around for some time (Hayes and Nowakowski, 2000; Shibui et al., 1989), and the specific use of IdU and BrdU was described as early as 1989 to estimate S-phase length in human glioma cell lines (Shibui et al., 1989). In 1991, this method was even described in vivo in 5 patients diagnosed with solid tumours (Miller et al., 1991). These patients received intravenous infusions of IdU followed by BrdU prior to removal of the tumours, after which the cell cycle times of their tumours were calculated (Miller et al., 1991). This method has since been modified by several authors.

The method used in this thesis was modified slightly from Martynoga et al (Martynoga et al., 2005) and used to calculate S-phase length in embryos lacking p21 compared to wild-type littermates. The aim was to assess whether loss of p21 lead to shorter S-phase lengths, specifically in the MHP. The method was developed in the mouse telencephalic neuroepithelium which, like the mouse neural plate, contains an asynchronous cell population (Martynoga et al., 2005). In such a population of cells, the number of cells in a particular phase of the cell cycle is proportional to the length of that given phase, in relation to the total length of the cell cycle (Martynoga et al., 2005; Nowakowski et al., 1989).

A few assumptions are made for this model (Nowakowski et al., 1989). Firstly, it is assumed that cells of the asynchronous population under study form a single population with similar cell cycle times and distributions between the cell cycle phases. In my analysis, I have analysed the MHP separately from the lateral regions, and therefore this assumption can be made in my population of cells. Secondly, it is assumed that the cell population is growing at a steady state. McShane et al 2015 showed by cumulative ^{3}H thymidine labelling that the cells of the mouse MHP and lateral regions grow linearly, i.e. steady state (McShane et al., 2015). The data from McShane et al. also shows that the first assumption is true as the linear growth indicates that the proliferating cells comprise a single cell population (Nowakowski et al., 1989). The third assumption is that there are no non-proliferating cells to

consider. This assumption has been proven in the mouse neural plate (Copp et al., 1988; McShane et al., 2015) and in the chick (Langman et al., 1966; Smith and Schoenwolf, 1988).

BrdU and IdU, halogenated thymidine analogues, are incorporated into DNA during DNA synthesis in place of thymidine (Martynoga et al., 2005). The sequential injection of the two analogues enables calculation of cell cycle parameters such as the length of S-phase (Martynoga et al., 2005). Mice at gestational day 8 were injected with IdU at time 0 (T=0), labelling all cells in S-phase at the start of the experiment. After an interval, the mice received an injection of BrdU, which labels all cells in S-phase at the end of the experiment (Figure 5.2, A-B). Embryos were collected 15 minutes after the BrdU injection, and fixed in 4% PFA within 20 minutes (Figure 5.2, A). Because the cell population is asynchronous, some cells will have left S-phase in the interval before the BrdU injection. This is the leaving fraction (L_{cells}: IdU^+BrdU^-) (Figure 5.2, B; green nuclei). Cells that have remained in S-phase throughout the experiment will have incorporated both IdU, which, contrary to what was previous thought (Cronkite et al., 1959; Langman et al., 1966) is not rapidly cleared and is still in the bloodstream (Hayes and Nowakowski, 2000; Martynoga et al., 2005), and BrdU. This is the population in S-phase at the end of the experiment (S_{cells}: IdU^+BrdU^+) (Figure 5.2, B; yellow nuclei). The interval between the injections (T_i) equals the time when cells can incorporate IdU and not BrdU. Because the cell population is asynchronous and growing at a steady state, cells will leave S-phase at a constant rate during the interval (T_i). The cells that have incorporated IdU only can be distinguished from the cells that have incorporated IdU and BrdU using specific monoclonal antibodies. Thus, L_{cells} and S_{cells} can be counted. Because the number of cells in a given phase of the cell cycle equals the length of that phase relative to total cell cycle length (Martynoga et al., 2005; Nowakowski et al., 1989), I can say that the ratio of the length of one phase to another phase is equal to the ratio of the number of cells present in the first phase to the number of cells in the second phase (Martynoga et al., 2005; Nowakowski et al., 1989). Therefore, the ratio between the number of cells in the leaving fraction

(L_{cells}) and the S-phase fraction (S_{cells}) equals the ratio between the interval (T_i) and the length of S-phase (T_s) (Martynoga et al., 2005; Shibui et al., 1989):

$$\frac{Ti}{Ts} = \frac{L\ cells\ (IdU + BrdU-)}{S\ cells\ (IdU + BrdU+)}$$

Thus, the length of S-phase is calculated as:

$$S = Ti\ /\left(\frac{L\ cells\ (single\ labelled\ (IdU))}{S\ cells\ (double\ labelled\ (IdU\ and\ BrdU))}\right)$$

The method by Martynoga et al. complies with other studies in age and tissue matched animals, where cumulative BrdU labelling was used to calculate the cell cycle parameters, with a correlation of p=0.022 (Martynoga et al., 2005). Thus, in the mouse telencephalon, this IdU/BrdU labelling method gives the same results as cumulative BrdU labelling. The advantage is that it requires fewer animals while being very specific.

5.1.4 Purpose of the study

As introduced, several groups have shown that nuclei of MHP cells are mainly basal and have longer cell cycles than cells in lateral regions of the neural plate. I set out to examine if the CIP/KIP family of cell cycle regulators might be responsible for the regional change in cell cycle length observed in the MHP. I showed in Figure 3.3 that p21 is expressed in the forming MHP in the mouse neural plate. The next step was to assess whether loss of p21 resulted in altered cell cycle parameters in the MHP.

5.2 Results

5.2.1 Validating the IdU/BrdU double labelling method

$p21^{+/-}$ males and females were mated to give litters containing $p21^{-/-}$, $p21^{+/-}$ and $p21^{+/+}$ embryos. Pregnant $p21^{+/-}$ mice at gestational day 8 were given an injection of IdU followed by the same dose of BrdU after an interval (Figure 5.2, A). The initial IdU pulse labels all cells in S-phase at the start of the experiment, while BrdU labels all cells in S-phase at the end of the experiment (Figure 5.2, A-B). During the interval between IdU and BrdU, some cells will have left S-phase and have incorporated IdU only. Cells that have incorporated IdU can be distinguished from cells that have taken up IdU and BrdU using specific monoclonal antibodies (Figure 5.2, C-F). The number of nuclei in each group is counted and S-phase is calculated as shown above. Because of their large and reproducible litters, CD1 embryos were used to determine a suitable interval between the IdU and BrdU injections and for validating the antibodies.

In order to check that the BrdU specific antibody does not cross-react with IdU, mice were injected with 56.75 mg/kg IdU on gestational day 8 and embryos were collected after 1.5 hours. Immunohistochemistry was performed with the IdU/BrdU-specific, and BrdU-specific-antibodies on serial sections from the same embryos (Figure 5.3). The BrdU specific antibody does not cross-react with IdU in any of the embryos tested (n=4) (Figure 5.3, A-C). Serial sections stained with the IdU/BrdU antibody reveal clear IdU uptake (Figure 5.3, D-F). The positive phosphohistone H3 staining in (B) serves as an additional control to show that the lack of BrdU staining is not due to problems with the immunohistochemistry protocol.
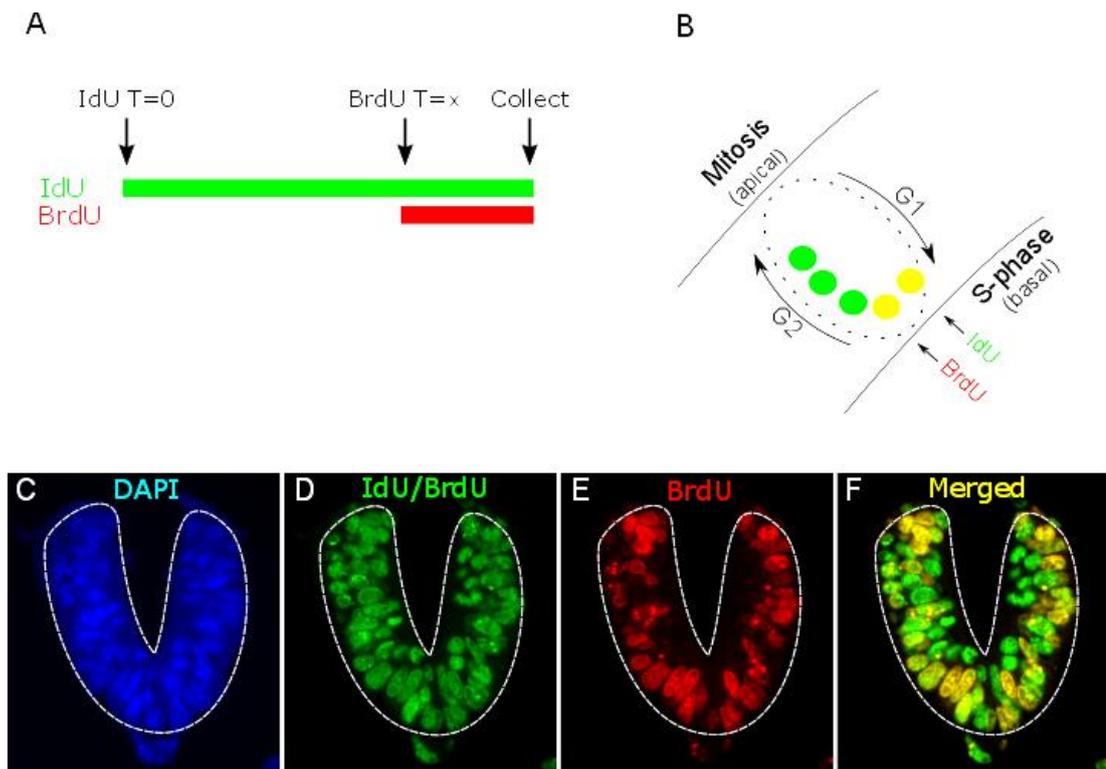
Figure 5.2 - Sequential thymidine analogue labelling to calculate S-phase

p21 mice at E8.5 were injected with IdU at time 0. After an interval BrdU was injected into the mouse and shortly after the embryos were collected (A). IdU and BrdU get incorporated in S-phase when the nuclei are basal during IKNM. Nuclei that stay in S-phase throughout the length of the experiment will be labelled with IdU and BrdU (B, yellow nuclei), while nuclei that have left S-phase before the BrdU pulse will only label with IdU (B, green nuclei). Example of an embryo with an interval of 3 hours between the IdU and BrdU pulse (C-F). The green nuclei (IdU) are found throughout the apico-basal axis of the neuroepithelium (D) while BrdU labelled nuclei (red) are more basal (E-F).
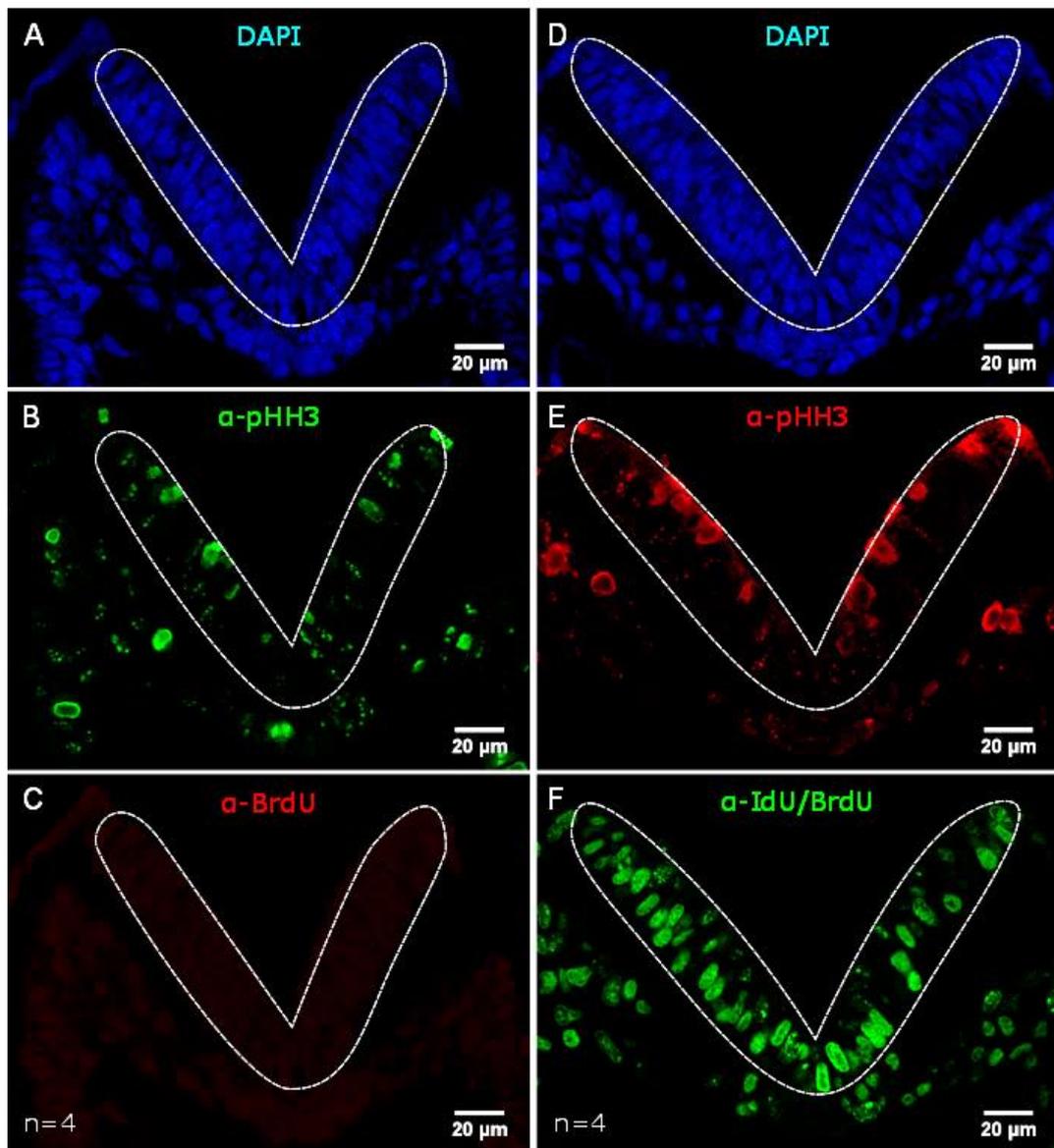
Figure 5.3 - The BrdU specific antibody does not cross-react with IdU

The specificity of the rat anti-BrdU antibody is shown on two representative sections from the same embryo at E8.5. Pregnant CD1 mice were injected with IdU and serial sections from the embryos were stained with either specific BrdU antibody (C) or IdU/BrdU antibody (F). Section A-C and section D-F are 4 microns apart. pHH3 staining serves as a positive control (B). n= 4 embryos.

Having shown that the BrdU specific antibody is truly specific, I wanted to see if both antibodies are equally efficient in localising BrdU labelled cells. If the IdU/BrdU-antibody labelled BrdU cells more efficiently than the BrdU-specific antibody, then the number of IdU^+BrdU^- cells would be overestimated and this, in turn, would underrepresent the length of S-phase.

Two embryos from mice injected with BrdU were collected and processed for immunohistochemistry. Serial sections 4 microns apart were stained with the BrdU-specific antibody (Figure 5.4, A) or the IdU/BrdU antibody (Figure 5.4, B). Six sections were quantified per embryo (3 sections α-IdU/BrdU and 3 sections α-BrdU) and presented as mean BrdU labelling as a percentage of total nuclei estimated by counting all DAPI nuclei (Figure 5.4, C). The efficiency of both antibodies seems similar and with exception of the lowest and highest point on the graph, the other sections show a mean labelling index of between 71 and 81% (Figure 5.4, C). There is not a statistically significant difference between the two antibodies (t-test; p=0.255) although the mean for the BrdU-specific antibody is slightly higher. In the analysis of S-phase length both antibodies detect BrdU positive cells. Therefore, no IdU$^-$BrdU$^+$ cells are ever observed and a higher efficiency of the BrdU specific antibody would not distort the analysis.

Next, the incorporation of IdU and BrdU was assessed. In order for the calculation of S-phase length to be accurate, IdU and BrdU need to be incorporated by comparable numbers of cells. IdU and BrdU uptake was quantified in embryos from mice injected with either IdU, or BrdU. Embryos were processed for immunohistochemistry, and the IdU/BrdU antibody was used to detect IdU and BrdU uptake (Figure 5.5, A-D). Total cell number in the MHP and in two lateral neural fold regions was estimated by counting nuclei stained with DAPI. IdU or BrdU uptake is given as percentage of total nuclei that were labelled with DAPI (Figure 5.5, E). There is a trend towards more IdU positive nuclei in the MHP and in the lateral regions but this difference between uptake of IdU and BrdU is not statistically significant in n≥3 embryos (Figure 5.5, E). The embryos analysed are from different litters and I would need to analyse many more to overcome the possibility of interlitter variation as well as differences in the circulation of IdU or BrdU in the pregnant mice. Thus, I cannot prove that the uptake of the two thymidine analogues is equivalent, but in this small sample number it seems to be comparable.
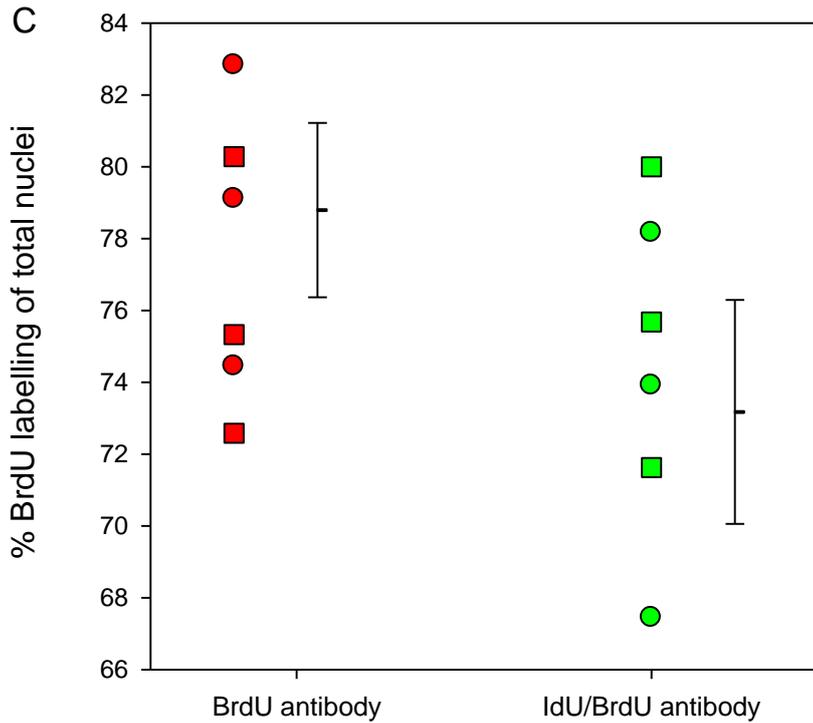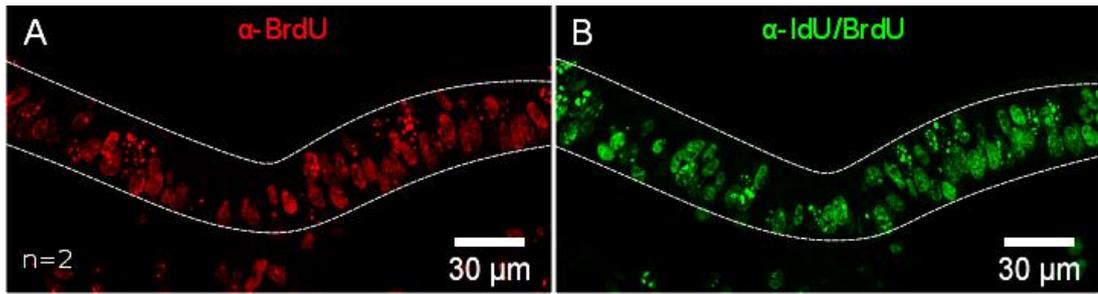
Figure 5.4 - No significant difference between efficiency of the BrdU and IdU/BrdU antibodies

Embryos from BrdU injected CD1 mice at E8.5 were analysed with either α-BrdU (A) or α-IdU/BrdU (B) to see if the two antibodies are comparable in staining efficiency (A-B). Sections A and B are from the same embryo, 4 microns apart. A number of nuclei should be present in both sections as the nuclei span 8 microns. 6 sections from two embryos were counted (3x α-BrdU and 3x α-IdU/BrdU per embryo) and BrdU labelling was quantified as percentage of total nuclei (DAPI) (C). The points represent the % labelling per section from embryo 1 (circles) and embryo 2 (squares). Error bars are +/-SEM. There is not a significant difference between the two antibodies (p=0.255; t-test).
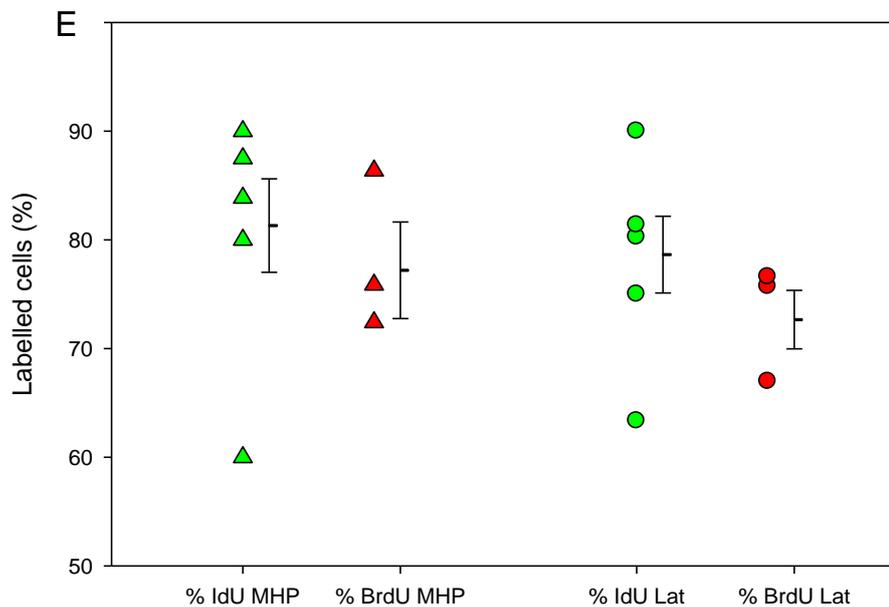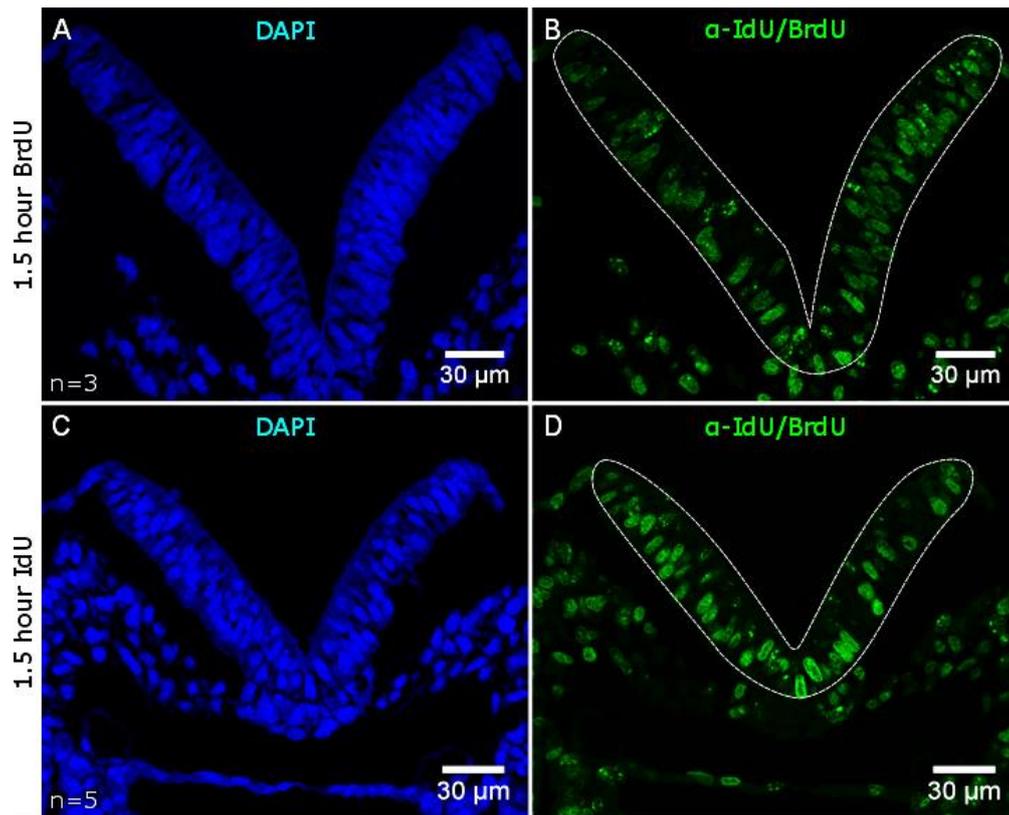
Figure 5.5 - IdU and BrdU uptake is comparable

Embryos from CD1 mice at E8.5 injected with either BrdU (A-B) or IdU (C-D) have comparable levels of labelling using the anti-IdU/BrdU-antibody (E). Each point on the graph represents the average labelling (% of DAPI) for a single embryo, calculated from 3 sections. Error bars are +/- SEM. There is no statistically significant difference between the uptake of IdU and BrdU in either the MHP (p=0.520) or the lateral region (p=0.191).

5.2.2 G2 phase is approximately 2 hours

Published methods using IdU/BrdU labelling to calculate cell cycle length are mostly from the mouse telencephalon or cortex (Mairet-Coello et al., 2012; Martynoga et al., 2005; Quinn et al., 2007; Wu et al., 2014) and all use an interval of 1.5 hours between injections.

In order to test which IdU-BrdU interval is appropriate in the mouse neural plate at E8.5, a series of injections of BrdU were done in CD1 mice at gestational day 8. To account for between-litter variation, embryos were analysed from at least 2 injected mice (Table 5.3). Embryos were collected on ice at 15, 30, 45, 60, 90, and 120 minutes after injection of BrdU, dissected in cold medium, and fixed within 20 minutes. Sections were stained with anti-BrdU antibody, which labels cells in S-phase, and anti-phosphohistone H3 antibody, which labels cells in G2 and M phase (Hendzel et al., 1997). As BrdU and pHH3 give characteristic staining patterns in S-, G2-, and M-phase (Hendzel et al., 1997, Zhang et al., 2011), combining the antibodies is a useful way of assigning cells to specific phases of the cell cycle (Figure 5.6) and thereby estimating the time it takes BrdU labelled cells in S-phase to reach the apical surface and M-phase. It is important that the length of G2+M phase is longer than the interval between the IdU and BrdU injections as after that point single labelled cells will start to divide and this population of cells will be overrepresented (Martynoga et al., 2005). I also wanted to make sure that the interval between the IdU and BrdU injections is shorter than the time it takes cells that were in late S-phase during the IdU pulse to complete the cell cycle, and return to S-phase to be labelled during the BrdU pulse. This would otherwise over-represent the population of double labelled cells and complicate the calculation of the length of S-phase.

At 15 minutes after BrdU injection many BrdU positive cells are observed. Some lateral nuclei have reached the apical surface and are co-labelled with speckled phosphohistone H3 (yellow asterisk), indicative of G2-phase cells. Although these cells are likely to have been in late S-phase during the BrdU pulse, it suggests that either basal to apical interkinetic nuclear migration is very rapid in the E8.5 mouse

neural plate, or that cells are not necessarily completely basal during all of S-phase (Figure 5.7, A; 1st panel). Nuclei labelled with phosphohistone H3 but not BrdU indicate nuclei that have left S-phase prior to the BrdU pulse (Figure 5.7, A; panel 1 and 2, white arrowheads). Nuclei in the MHP are very basal after the 15 minute BrdU pulse compared to the lateral regions. This regional difference in apico-basal position was quantified for two CD1 embryos. In the forming neural plate (Figure 5.7, A; top), nuclei of the MHP are significantly more basal than nuclei of the lateral regions (Figure 5.8, top). Interestingly, there is not a significant difference in nuclear position along the apico-basal axis in the mature, V-shaped neural plate from the same embryos, suggesting that apico-basal migration of MHP nuclei is particularly slow in the forming neural plate (Figure 5.8). This coincides with the strong, wide expression domain of p21 in the forming neural plate (Figure 3.3). Many mitotic cells are seen after a 15 minute pulse of BrdU but none are co-labelled with BrdU (Figure 5.7, A; 1st panel, open arrows).

At 30 and 45 minutes the BrdU pattern looks very similar to that at 15 minutes. Most of the MHP BrdU labelled nuclei are basal while nuclei of the lateral regions tend to be more apical with punctate pHH3 staining, indicative of a cell in G2 (yellow asterisk). Several mitotic pHH3$^+$BrdU$^-$ cells are observed at 30 and 45 minutes (Figure 5.7, A; panels 2 and 3; open arrows). Embryos collected 1 hour after the BrdU injection exhibit many apical nuclei, both in the MHP and in the lateral regions. At this time-point, 22.11% of mitotic figures are BrdU positive, but the majority of mitotic cells are BrdU negative (Figure 5.7, B; 1st panel; open arrow and Table 5.3). 90 minutes after the BrdU injection 85.9% of the mitotic cells are BrdU positive (Figure 5.7, B; closed arrows and Table 5.3) while some BrdU negative cells in late mitosis are seen (Figure 5.7, B; open arrows). At 120 minutes after the BrdU injection almost all (94%) mitotic cells are BrdU positive, suggesting that the approximate time it takes a nucleus to travel through G2 phase is close to 2 hours (Figure 5.7, B; last panel; closed arrows and Table 5.3). At all time-points, very basal nuclei are observed that are labelled with BrdU and punctate pHH3 showing that these cells have entered G2 although very basal (Figure 5.7, turquoise asterisks).

The combined length of G2 and M can be estimated following a BrdU pulse long enough to ensure that all mitotic figures are BrdU positive (Takahashi et al., 1995). Seeing that 94% of mitotic figures are BrdU positive following a 2 hour BrdU pulse (Table 5.3) G2+M phase in the CD1 mouse neural plate at E8.5 is close to 2 hours (T_{G2+M} =2). Therefore, the time it takes a cell to go from S-phase, through cell division, and return to S-phase exceeds 2 hours.

In conclusion, just under a quarter of mitotic figures are BrdU positive after a 1 hour BrdU pulse, while almost all mitotic figures are BrdU positive after a 2 hour pulse (Table 5.3 and Figure 5.9). The 1 hour time-point suggests that a good fraction of cells leave S-phase in a 1 hour interval. Therefore, the IdU/BrdU double labelling method was tested under experimental conditions in the p21 mouse line with a 1 hour interval between the injections.

5.2.3 Calculating S-phase length in p21$^{-/-}$ and p21$^{+/+}$ embryos

In the experiments above, using CD1 outbred mice, almost a quarter of mitotic cells after a 1 hour BrdU pulse are co-labelled with BrdU, suggesting that a fair proportion of cells leave S-phase within a 1 hour interval. On the other hand, it seemed very unlikely that many BrdU-labelled cells would have divided, and their nuclei re-entered S-phase, in this time period. Therefore, 1 hour was chosen as the best interval to use between the IdU and BrdU pulse for subsequent experiments in the p21 mouse, in order to limit the number of IdU^{+}BrdU^{-} dividing cells, and to best avoid including IdU^{+}BrdU^{+} cells that had been labelled in two successive cell cycles.

p21$^{+/-}$ mice were mated, and pregnant females at gestational day 8 were given an injection of IdU followed by the same dose of BrdU 1 hour later. Embryos were collected 15 minutes after the BrdU pulse and processed for immunohistochemistry, exactly as in the CD1 studies above. In the first experiment I noticed that the pattern of IdU and BrdU looked identical in the embryos analysed (Figure 5.10) and when counting the number of single labelled cells in 6 sections from 3 p21$^{+/+}$ embryos I found on average only 1.67 single labelled cells. Thus, a 1

hour IdU-BrdU interval is not sufficient to give enough single labelled cells to calculate S-phase length in p21 mutant mice.

Next, the interval between IdU and BrdU injection was increased to 2 hours (Figure 5.11, A) which resulted in a distinct population of single labelled cells (Figure 5.11, C-E; circled nuclei) that were labelled with IdU (C) but not BrdU (D). The number of single and double labelled nuclei was counted and the length of S-phase was calculated as shown (Figure 5.11, F). S-phase length in the MHP (Figure 5.11, C-E; inside white dotted lines) was compared to a region in each of the lateral neural folds (Figure 5.11, C-E; red boxes).
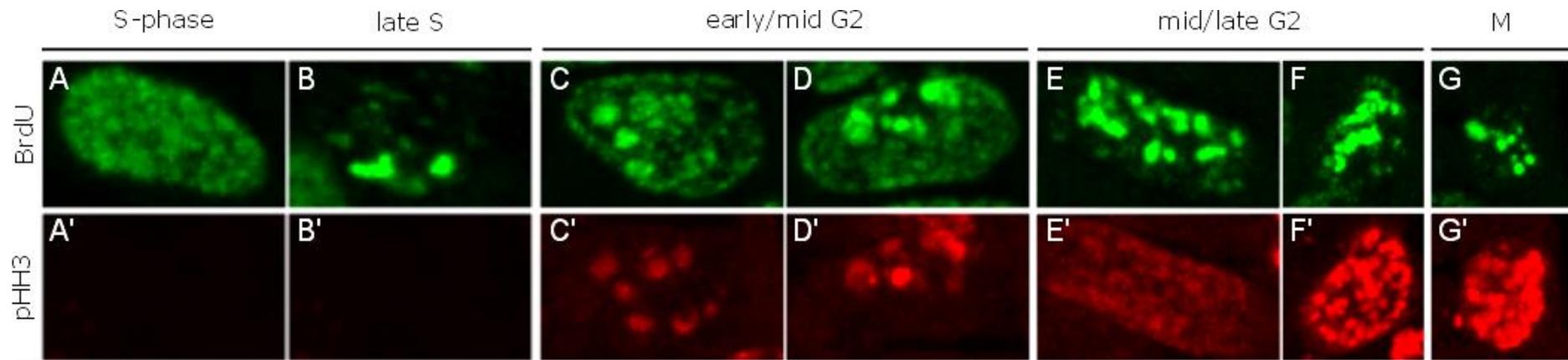
Figure 5.6 - Determining cell cycle phases

The BrdU staining pattern changes in different phases of the cell cycle (Zhang et al., 2011) as shown in Figure 2.5. A-G and A'-G' is the same nucleus viewed in two different channels. In early/mid S-phase the pattern is uniform (A), turning more punctate with an outline of the nucleus visible in the first part of G2 (C-D). In late G2 and through to mitosis (E-G) the staining is punctate with no staining of the nuclear outline (Zhang et al., 2011). pHH3 stains nuclei in G2-phase and mitosis (C'-G'). The pattern starts out very punctate in small nuclear domains (C'-D'), turning more uniform throughout the nucleus in late G2 (E'-F') and is very condensed and strong during mitosis (G') (Hendzel et al., 1997). In a subset of cells the BrdU pattern looks like late G2 but no pHH3 staining is observed (B-B'). These are classified as late S-cells.

A

| | BrdU | pHH3 | Merged | High mag. |

15 minutes (n=5)

30 minutes (n=6)

45 minutes (n=8)

30 µm
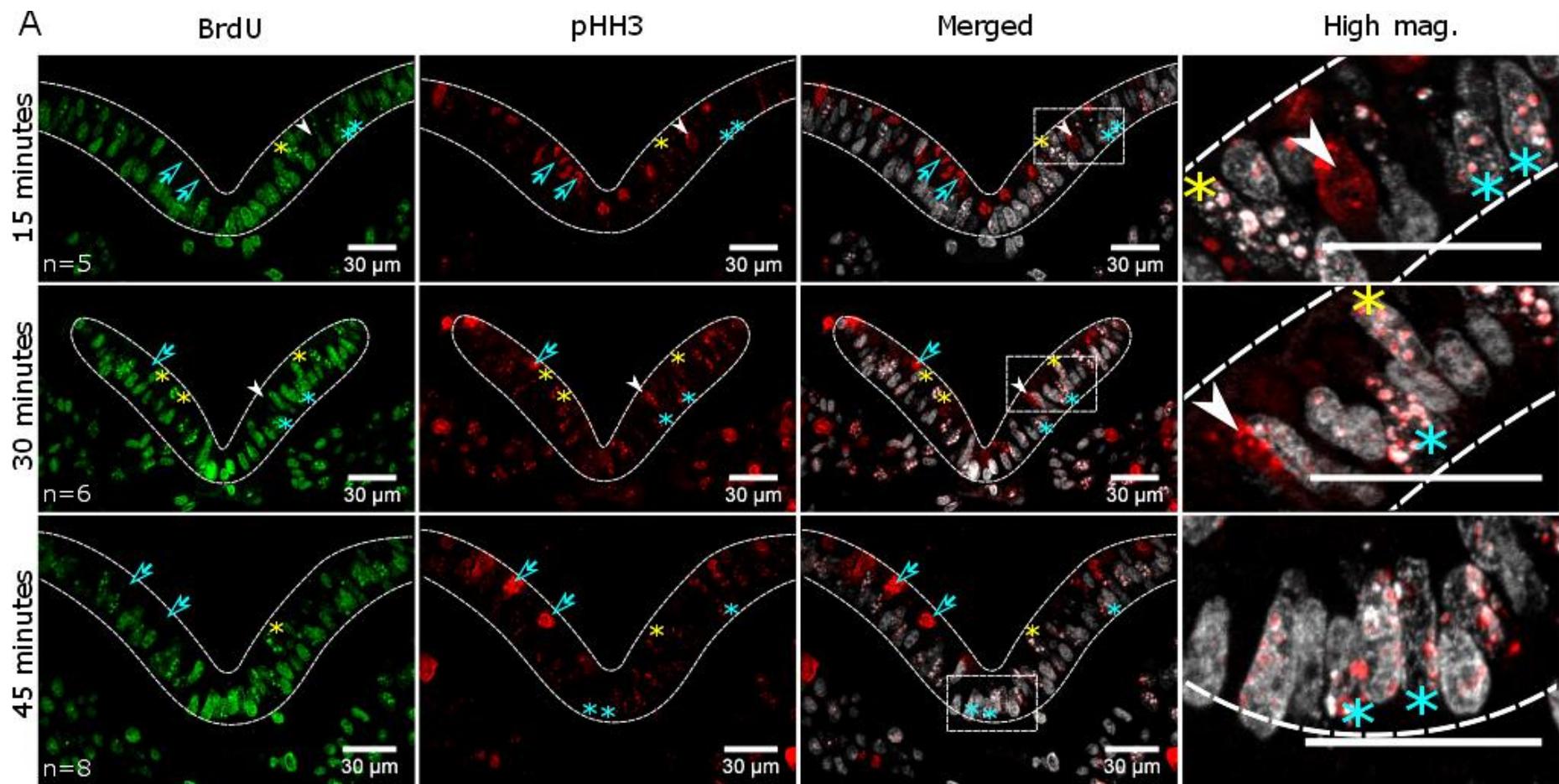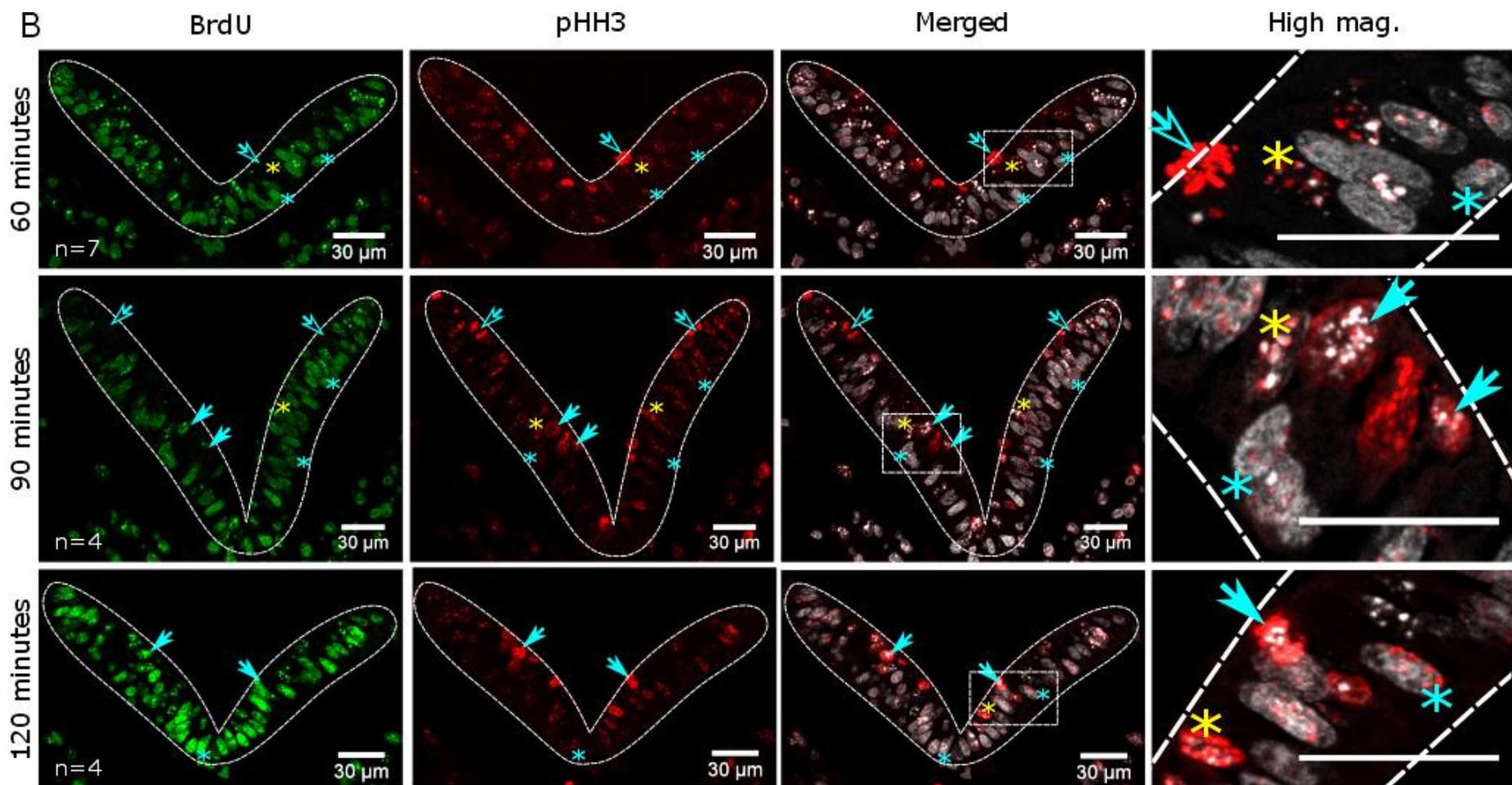
Figure 5.7 - BrdU +ve mitotic cells are observed after 1 hour

CD1 mice at E8.5 were injected with BrdU and left for different time periods before embryos were collected and analysed. Cells labelled with BrdU are observed as soon as 15 minutes after BrdU administration (A; top panel). Mitotic cells labelled with pHH3 are observed at all time-points (pHH3$^+$BrdU$^-$; open arrows, pHH3$^+$BrdU$^+$; closed arrows). The first time at which double pHH3$^+$BrdU$^+$ cells are observed is after 60 minutes. At 90 minutes mitotic cells that are BrdU+ve (B, middle panel, closed arrows) and late mitotic cells that are BrdU-ve (open arrow) are observed along with G2 cells (B, middle panel, *). At 120 minutes most mitotic cells are BrdU+ve (B, bottom panel, closed arrows). Yellow asterisks indicate apical G2 nuclei and turquoise asterisks indicate basal G2 nuclei. White arrowheads indicate G2 nuclei that left S-phase prior to the BrdU pulse. Scale bars = 30 μm.
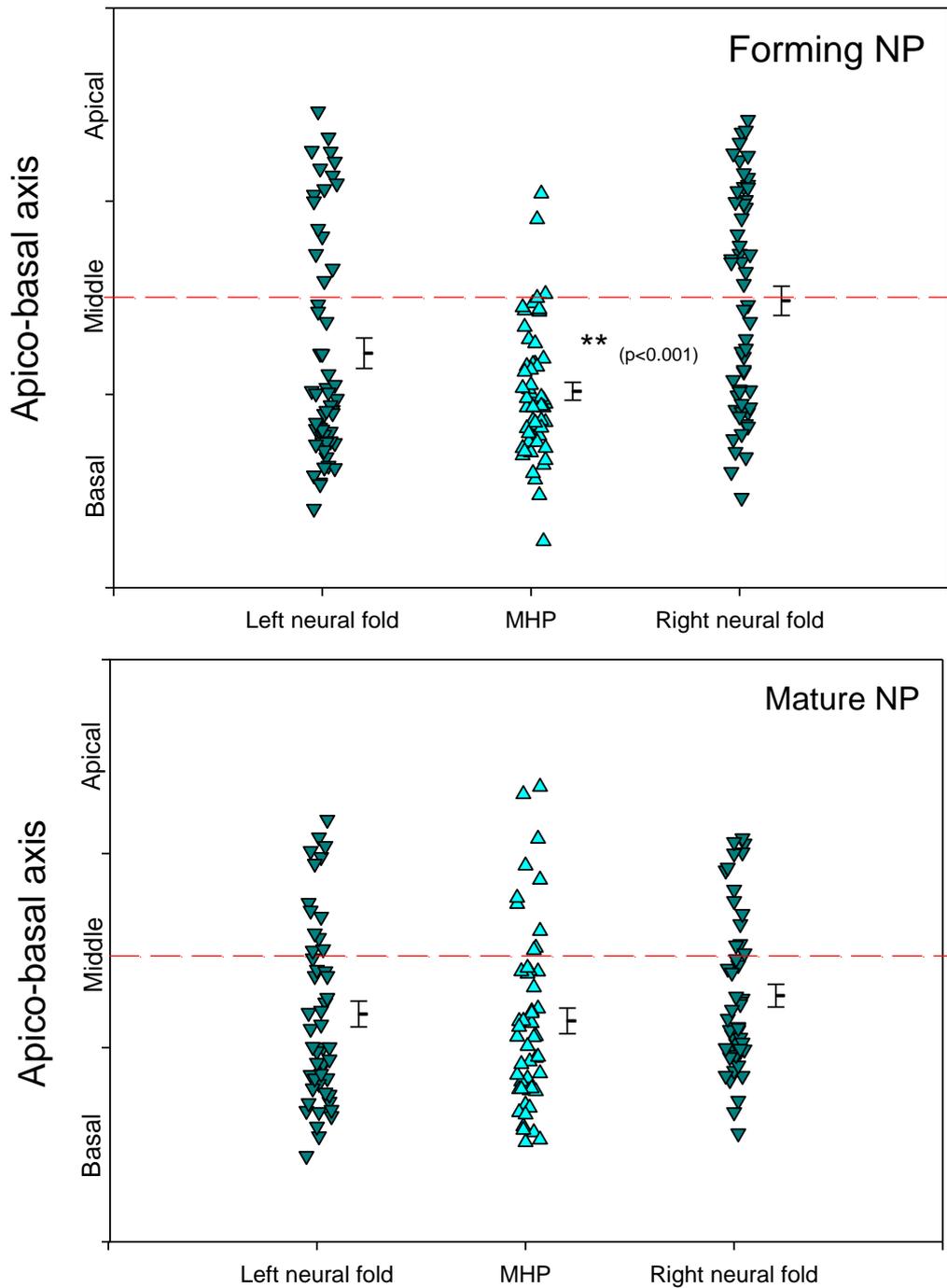
Figure 5.8 – Apical migration of MHP nuclei is slower than that of lateral nuclei

CD1 embryos at E8.5 received a 15 minute pulse of BrdU (Figure 5.7; top panel) and nuclear position along the apico-basal axis was measured. Nuclei of the MHP are significantly more basal in the forming MHP compared to the lateral regions. This significant difference is not observed for the mature, V-shaped neural plate in the same embryos, suggesting that MHP nuclei have the longest 'basal cell cycle phase(s)' in the forming neural plate. Nuclear distance was measured on 6 sections from two embryos. p-value; One way ANOVA. Error bars are +/-SEM.

	Mitotic pHH3⁺BrdU⁺		Embryos	Mice injected
	%	Freq.		
15' BrdU	0	0/97	n=5	2
30' BrdU	0	0/86	n=6	2
45' BrdU	0.8	1/132	n=8	3
60' BrdU	22.1	21/95	n=7	4
90' BrdU	85.9	61/71	n=4	2
120' BrdU	94.0	63/67	n=4	2

Table 5.3 - Almost all mitotic cells in wild-type embryos are BrdU positive after a 2 hour pulse

CD1 mice at E8.5 were injected with BrdU and embryos collected following 15, 30, 45, 60, 90, or 120 minutes. α-pHH3 was used to identify mitotic cells, and α-BrdU to identify cells labelled in S-phase. Mitotic cells co-labelled with BrdU are shown as a percentage of total number of mitotic cells counted on ≥3 sections per embryo.
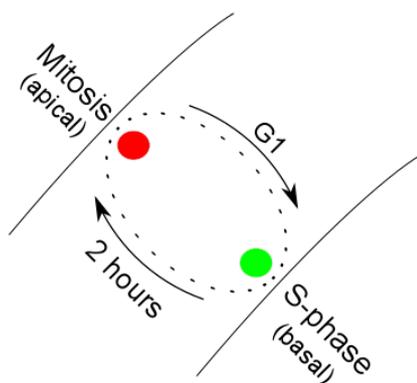
Figure 5.9 – G2 phase is approximately 2 hr

Cells take up BrdU (green) during S-phase at the basal neuroepithelium and pHH3 labels cells in G2-phase and mitosis (red). The earliest mitotic cells that are BrdU+ve are observed after 1 hr, suggesting that some cells that were in late S-phase during the BrdU pulse have reached mitosis. At 2 hours the majority of mitotic cells are BrdU positive, indicating that the time it takes a cell to move through G2 is approximately 2 hours.

Almost all mitotic cells were IdU positive at the end of a 2 hour interval in CD1 mice (Figure 5.7, B and Table 5.3). Assuming p21 mice behave similar to CD1 mice, a 2 hour interval between IdU and BrdU injections is the upper limit for the interval in this p21 mutant experiment to avoid IdU$^+$BrdU$^-$ dividing cells. In order to estimate whether a 1.5 hour interval would suffice, which in theory would reduce the chance of single labelled dividing cells, the number of single labelled cells was counted on all the slides from a 2 hour IdU-BrdU interval in p21 mice as shown in Table 5.4. With a 2 hour IdU-BrdU interval, 11.65% of sections analysed had no single labelled cells in the MHP. Furthermore, 36.89% of sections analysed contained 1 or 2 single labelled cells in the MHP, strongly suggesting that 2 hours is the lower limit for the interval in p21 mice (Table 5.4). Interestingly, the number of sections with no IdU$^+$BrdU$^-$ cells was twice as much for p21$^{+/+}$ compared to p21$^{-/-}$. Thus, cells of p21 wild-type embryos were more likely to stay in S-phase during the 2 hour interval compared to mutant embryos. Furthermore, 2.4 times as many sections from p21$^{+/+}$ embryos had only one or two single labelled cells compared to p21$^{-/-}$. This suggests that nuclei of p21$^{-/-}$ embryos are more likely to leave S-phase during the 2 hour interval compared to p21$^{+/+}$ embryos, indicating that p21$^{-/-}$ cells, in particular MHP cells, might spend less time in S-phase compared to wild-type littermates (Table 5.4).

Furthermore, the number of mitotic cells that are IdU negative was found to be higher for p21$^{+/+}$ than for p21$^{-/-}$ embryos in the MHP as well as in the lateral regions, suggesting that it takes longer for S-phase labelled wild-type cells to reach mitosis compared to mutant littermates (Table 5.5). In CD1 embryos, I showed that 94% of mitotic cells were labelled with BrdU after a 2 hour pulse (Table 5.3). Here, I found in p21$^{+/+}$ embryos, that approximately 91% of mitotic cells co-labelled with IdU, which had been in the bloodstream for 2.25 hours (Table 5.5; between 8.7 and 9% of mitotic cells were IdU-ve). Thus, in p21$^{+/+}$ embryos there is strong evidence that the length of G2+M is more than 2 hours, similar to what I previously suggested for CD1 mice. Moreover, p21$^{-/-}$ embryos hardly show any mitotic cells that are not co-labelled with IdU, suggesting that p21$^{-/-}$ IdU labelled S-phase cells reach mitosis quicker than in the wild-type setting, i.e. almost all (~97.6%) p21$^{-/-}$ mitotic cells are

IdU positive (Table 5.5). For both genotypes, the number of mitotic cells in the MHP is almost half of that observed in the lateral regions (Table 5.5).
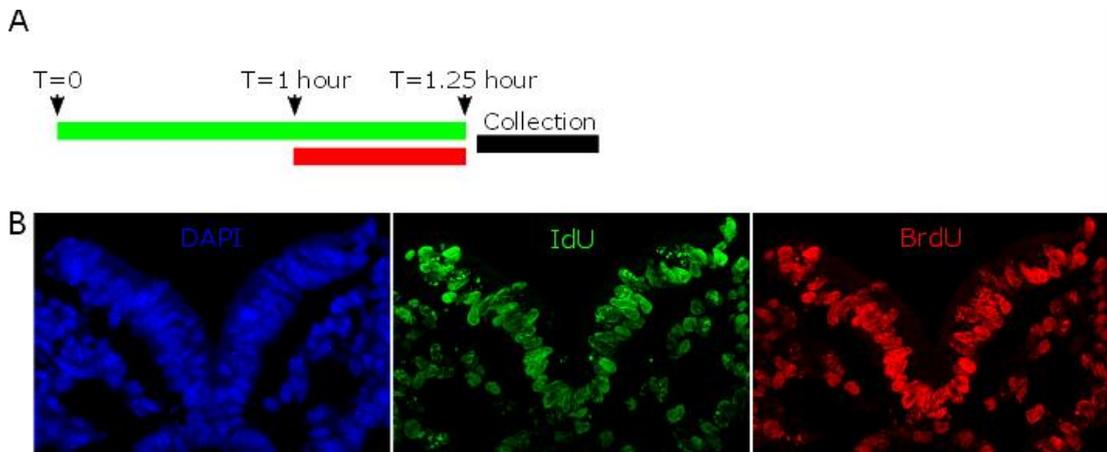
Figure 5.10 – A 1 hour interval is too short for S-phase calculation in p21 mutant mice

Pregnant p21^{+/-} mice at E8.5 were injected with IdU followed by BrdU 1 hour later (A). Embryos were collected and analysed with antibodies for IdU/BrdU and BrdU (B). Nuclei labelled with IdU, but not BrdU, were quantified in 6 sections from 3 embryos. The average number of single labelled cells was 1.67. Note how the IdU and BrdU staining is very similar.
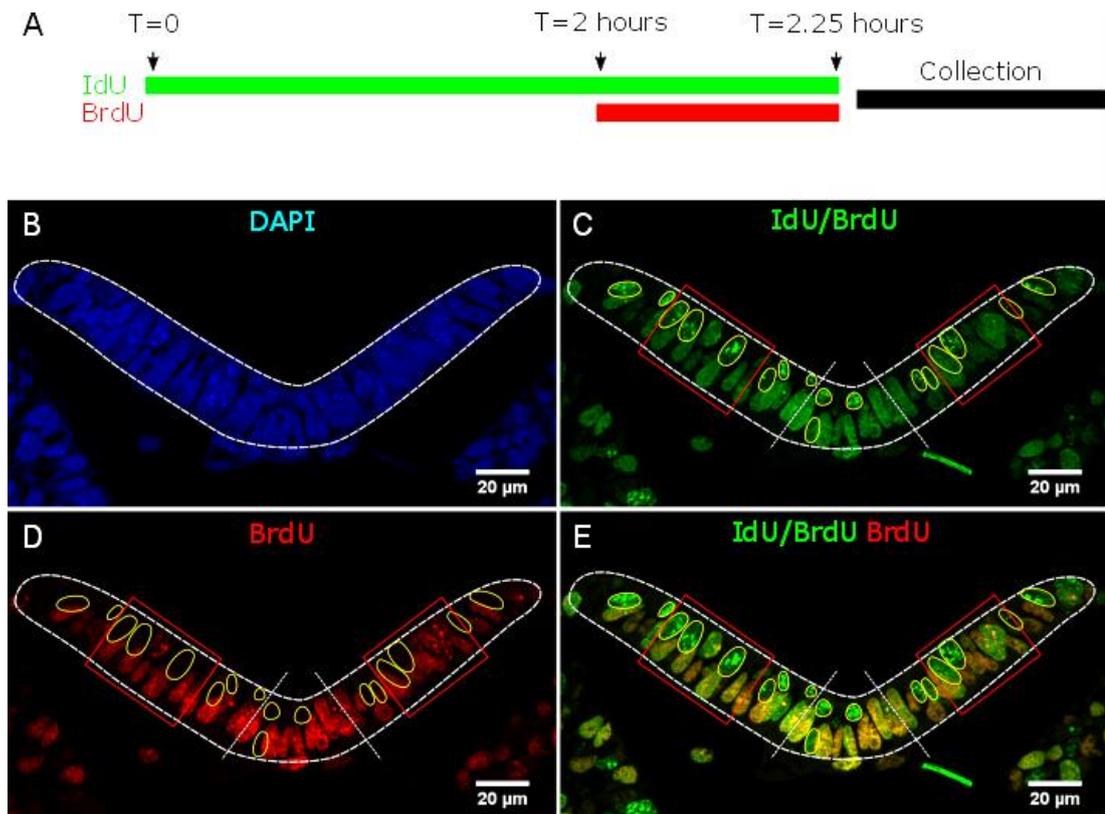
$$\text{Length of S-phase} = T_i / (L_{cells}/S_{cells})$$

T_i = Interval when cells can incorporate IdU but not BrdU (=2 hours)
L_{cells} = Cells that have left S-phase, i.e labelled with IdU but not BrdU
S_{cells} = Cells in S-phase at end of experiment, i.e. labelled with IdU and BrdU

Figure 5.11 - Sequential labelling with IdU and BrdU enables calculation of S-phase length

Pregnant p21^{+/-} mice at E8.5 were given an IP injection of IdU followed by BrdU two hours later. The mice were culled and the embryos collected on ice 15 minutes after the second injection (A). The IdU/BrdU antibody detects both IdU and BrdU (C) while α-BrdU is specific for BrdU (D). Combining the IdU/BrdU and BrdU staining pattern reveals a group of cells that have left S-phase and the basal neuroepithelium (IdU[+]BrdU[-]; yellow circles in C-E) and another group of cells that remain in S-phase at the end of the experiment (IdU[+]BrdU[+]; C-E). S-phase length was calculated in the MHP (inside white dotted lines; C-E) and in the lateral neural folds (red boxes; C-E) using the formula as shown (F).

	#Sections	Embryos	0 L_{cells}	≤2 L_{cells}
p21$^{-/-}$	47	6	3.9%	10.7%
p21$^{+/+}$	56	7	7.7%	26.2%
Total	103	13	11.7%	36.9%

Table 5.4 - A 2 hour IdU/BrdU interval is required for S-phase calculation in p21 mutant mice

Mice at E8.5 were injected with IdU followed by BrdU 2 hours later. Embryos were collected after 15 minutes and analysed with monoclonal antibodies to distinguish cells labelled with IdU and BrdU from cells that had left S-phase prior to the BrdU pulse (L_{cells}; labelled with IdU only). 12 sections out of the total 103 analysed did not have any single labelled cells in the MHP (Sections with 0 L_{cells}; 11.65%). The high number of sections with 1 or 2 single labelled cells in the MHP (≤2 L_{cells}) suggests that a 2 hour interval is required in the early p21 neural plate for S-phase calculation.

		Mitotic cells	IdU-ve mitotic cells	#Sections
p21$^{-/-}$	MHP	23	0/23 (0%)	31
p21$^{+/+}$		23	2/23 (8.7%)	37
p21$^{-/-}$	Lateral	41.5	1/41.5 (2.4%)	31
p21$^{+/+}$		39	3.5/39 (9%)	37

Table 5.5 - Fewer pHH3^{+}IdU^{-} cells in p21$^{-/-}$ than p21$^{+/+}$

The number of mitotic cells in the MHP and lateral regions counted in six p21$^{-/-}$ and 7 p21$^{+/+}$ E8.5 embryos collected 2.25 hours after the IdU injection. For both genotypes almost half as many mitotic cells are found in the lateral regions compared to the MHP. Fewer IdU-ve mitotic cells are observed in p21$^{-/-}$ embryos compared to wild-type littermates.

5.2.4 S-phase is significantly shorter in p21$^{-/-}$ embryos

E8.5 embryos from p21$^{+/-}$ crosses were stained for IdU and BrdU (Figure 5.12 and Figure 5.13). Between 5 and 13 sections per embryo were imaged, the single-labelled L$_{cells}$ and the double-labelled S$_{cells}$ were counted in the MHP and in two lateral regions (Figure 5.11, C-E), and S-phase length was calculated as the mean per embryo, combining the number of single and double labelled nuclei from all the imaged sections (Figure 5.11, F) (Appendix I). Overall morphology was normal in p21$^{-/-}$ embryos, both in the forming, flat neural plate (Figure 5.12) as well as in the V-shaped, elevated neural plate (Figure 5.13).

p21$^{-/-}$ and p21$^{+/+}$ embryos were analysed at two stages of MHP development: the early stage, forming MHP, and the later stage, V-shaped mature MHP (Figure 5.12 and Figure 5.13). This allowed any differences in S-phase length to be detected at different stages of MHP formation. Some embryos appear in both groups as some sections from the embryo were posterior and had a forming MHP morphology, while other sections from the same embryo were more anterior with a V-shaped morphology. Therefore, for each MHP developmental stage, 2-7 sections were analysed per embryo, and average S-phase length per embryo was calculated.

In the forming neural plate, cells in the p21$^{-/-}$ MHP as well as in lateral regions spend significantly less time in S-phase compared to wild type littermates: 3.9 vs 7.1 hours, and 3.4 vs 4.5 hours, respectively (Figure 5.14, forming and Table 5.6). This difference is statistically significant (p=0.009). In the mature neural plate, three embryos had very high S-phase length values as there were no single labelled cells in the MHP in 3 out of 5 sections. Thus, the number of single labelled cells was very low (approx. 2-3) while the number of double labelled cells was as high as for other embryos (approx. 30-50). This resulted in S-phase lengths of 20, 29 and 54 hours. These embryos are shown as red outliers on the graph (Figure 5.14, mature). The difference in S-phase length between genotypes in the mature neural plate was not statistically significant when the outliers were included (Figure 5.14, mature). When the outliers were excluded from the statistical analysis, there was a statistically significant difference between the length of S-phase in p21$^{-/-}$ and p21$^{+/+}$ embryos in

the mature neural plate (p<0.001) (Figure 5.15) with a decrease in length from 8.4 to 3.2 hours in the MHP and from 6 to 3.5 hours in the lateral regions (Table 5.6). The difference between S-phase length in the MHP and lateral regions was not significant (p=0.309). That is, in all regions, and during all stages of MHP formation, p21$^{-/-}$ cells spend significantly less time in S-phase than comparable cells in wild-type littermates.

As the S-phase times were very similar between the forming neural plate and the mature neural plate when the outliers were not considered (Table 5.6) the pooled data were plotted on a graph to determine effect of genotype (Figure 5.16). A significant difference in S-phase length is seen in the MHP as well as in the lateral regions when the outliers are excluded (p=0.005; Two way ANOVA). There is not a significant difference between S-phase length of the MHP and lateral regions (Figure 5.16). The reduction in S-phase length for the pooled data is from 7.7 to 3.9 hours for the MHP and from 5.2 to 3.8 hours for the lateral regions (Table 5.6).

In the MHP, S-phase length is decreased by 49.4% for p21$^{-/-}$ compared to p21$^{+/+}$, and in the lateral region the reduction in S-phase length is 26.9% (Table 5.7). Interestingly, the length of S-phase is decreased in the lateral neural plate regions although this is not where p21 is most strongly expressed (Table 5.7). The decrease in S-phase length in the p21$^{-/-}$ lateral region is smaller than that seen in the MHP. Thus, the effect of p21 deficiency is more pronounced on MHP cells than cells of lateral regions, but the reduction in the lateral region suggests that p21 action is not solely restricted to the MHP. The regional difference in S-phase length between the MHP and the lateral non-bending regions is seen in p21$^{+/+}$ embryos: S-phase in the MHP is 32.5% longer than it is in the lateral region (Table 5.7). This regional difference is essentially abolished in p21$^{-/-}$ embryos with S-phase being 2.5% longer in the MHP than in lateral region, strongly suggesting that p21 is responsible for the prolongation of S-phase in the MHP. The loss of the regional increase in S-phase length in the MHP of p21$^{-/-}$ embryos has no effect on the morphology of the neural plate (Figure 5.12 and Figure 5.13), suggesting that prolongation of S-phase is not necessary for midline bending.
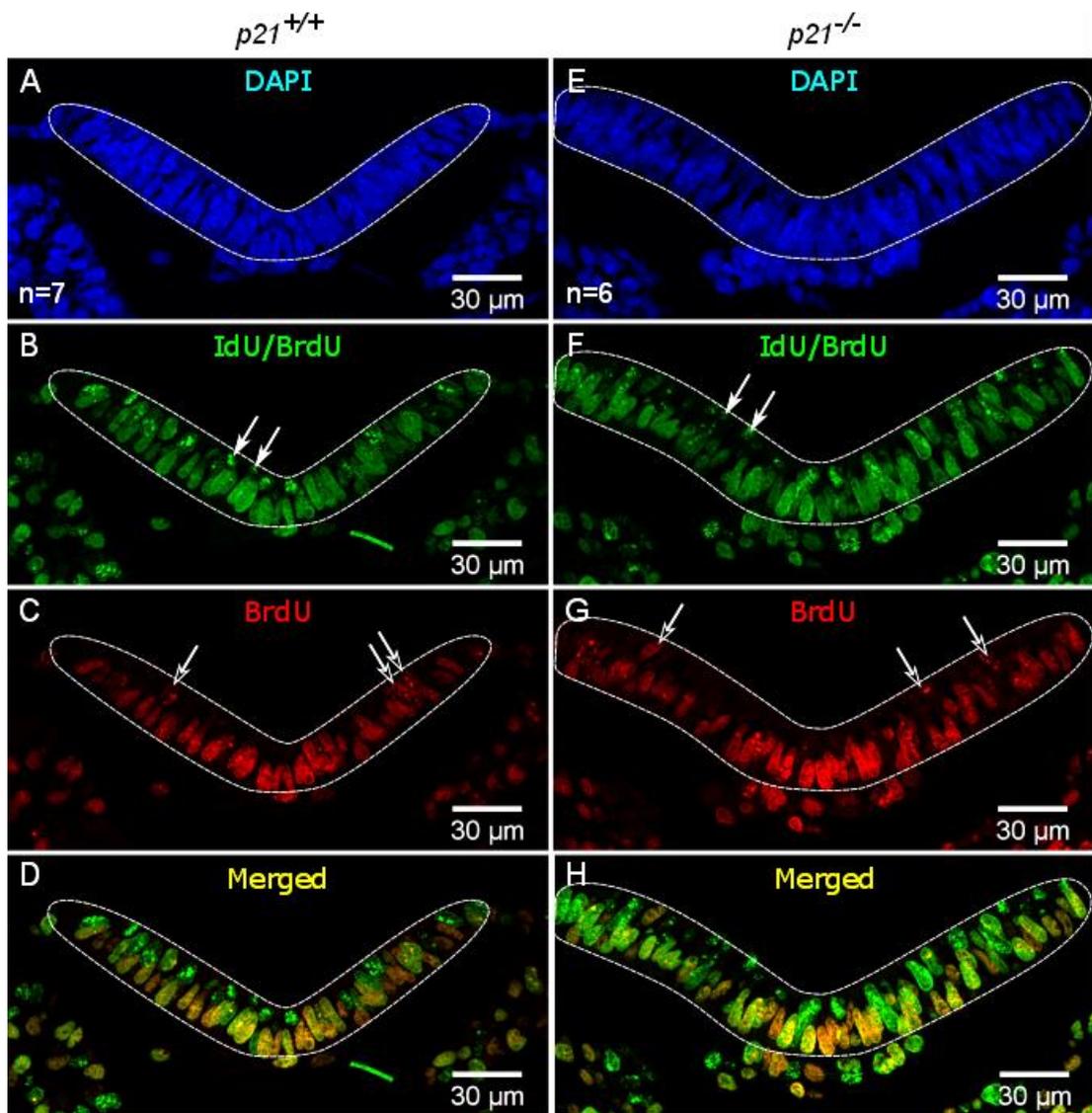
Figure 5.12 - Example sections through embryos at the level of the forming MHP

p21$^{+/+}$ and p21$^{-/-}$ embryos at E8.5 were stained with α-IdU/BrdU (B and F) and α-BrdU (C and G) following injections of IdU and BrdU 2 hours apart. Embryos lacking p21 show the same overall morphology as well as pattern of IdU and BrdU labelling (compare A-D to E-H). In both genotypes IdU labelled nuclei are found throughout the apico-basal axis with some mitotic looking cells at the apex (B and F, arrows). BrdU labelled cells are overall more basal but some apical nuclei are observed, mainly in lateral regions (C and G, open arrows). The overall pattern of staining is comparable between the two genotypes.
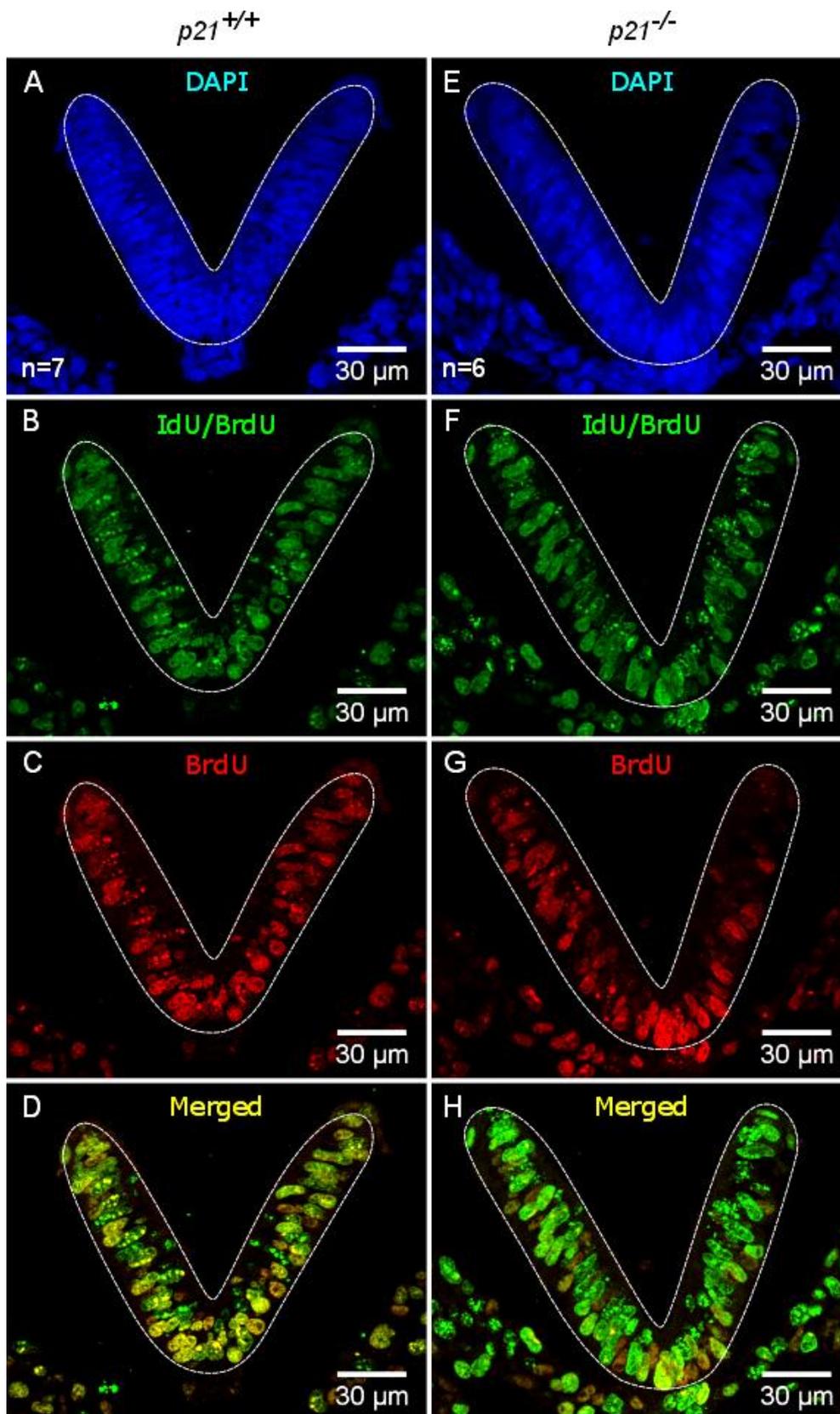
Figure 5.13 – Normal V-shaped MHP formation in p21$^{-/-}$ embryos

There is no apparent difference in MHP formation between p21$^{+/+}$ and p21$^{-/-}$ embryos at E8.5. IdU and BrdU labelling patterns are comparable in the V-shaped neural plate of both genotypes.
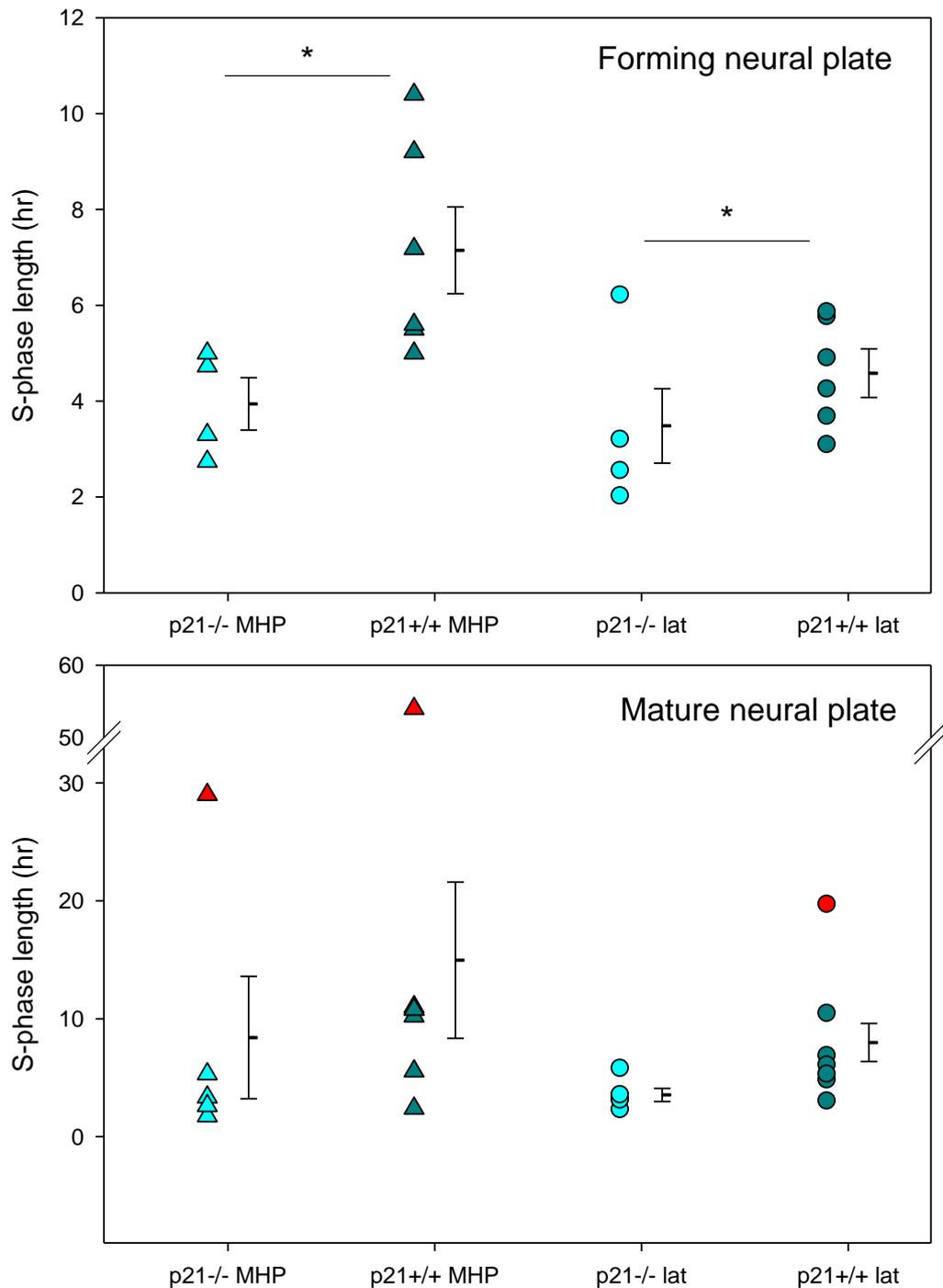
Figure 5.14 - S-phase length is shorter in p21$^{-/-}$ embryos compared to wild-type littermates at E8.5

Neural plate cells lacking p21 have a shorter S-phase than wild-type littermates. This is true for the MHP as well as the lateral neural folds, and for the forming as well as the mature neural plate. Between 4 and 6 embryos were analysed in each group. There is a significant difference between S-phase length between genotypes in the forming NP (p=0.009) while the regional difference in the forming NP fails to reach statistical significance (p=0.06). The difference between S-phase length in the mature neural plate is not statistically significant between genotypes (p=0.116) or regions (p=0.091). p-values were calculated by Two way ANOVA. Error bars are +/-SEM.
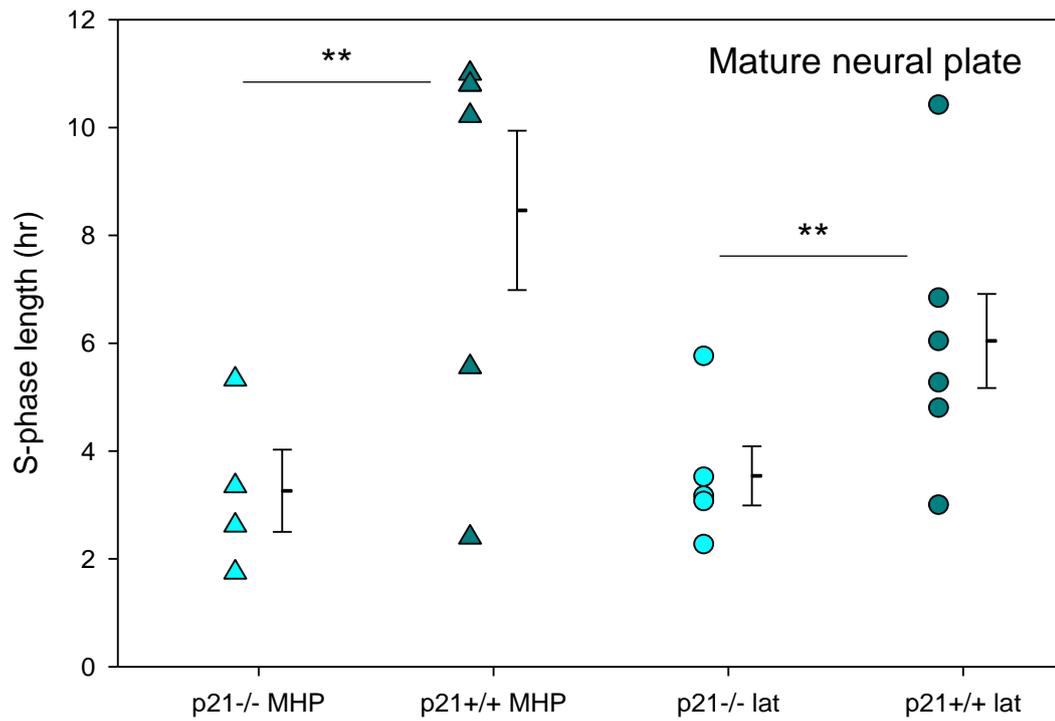
Figure 5.15 - S-phase length is significantly reduced in the p21$^{-/-}$ mature neural plate at E8.5

The same data is shown as above but the outliers are excluded. S-phase length is significantly shorter for p21$^{-/-}$ than p21$^{+/+}$ embryos (p<0.001). Length of S-phase is not significantly different between the MHP and lateral regions (p=0.309). p-values were calculated by Two way ANOVA. Error bars are +/- SEM.
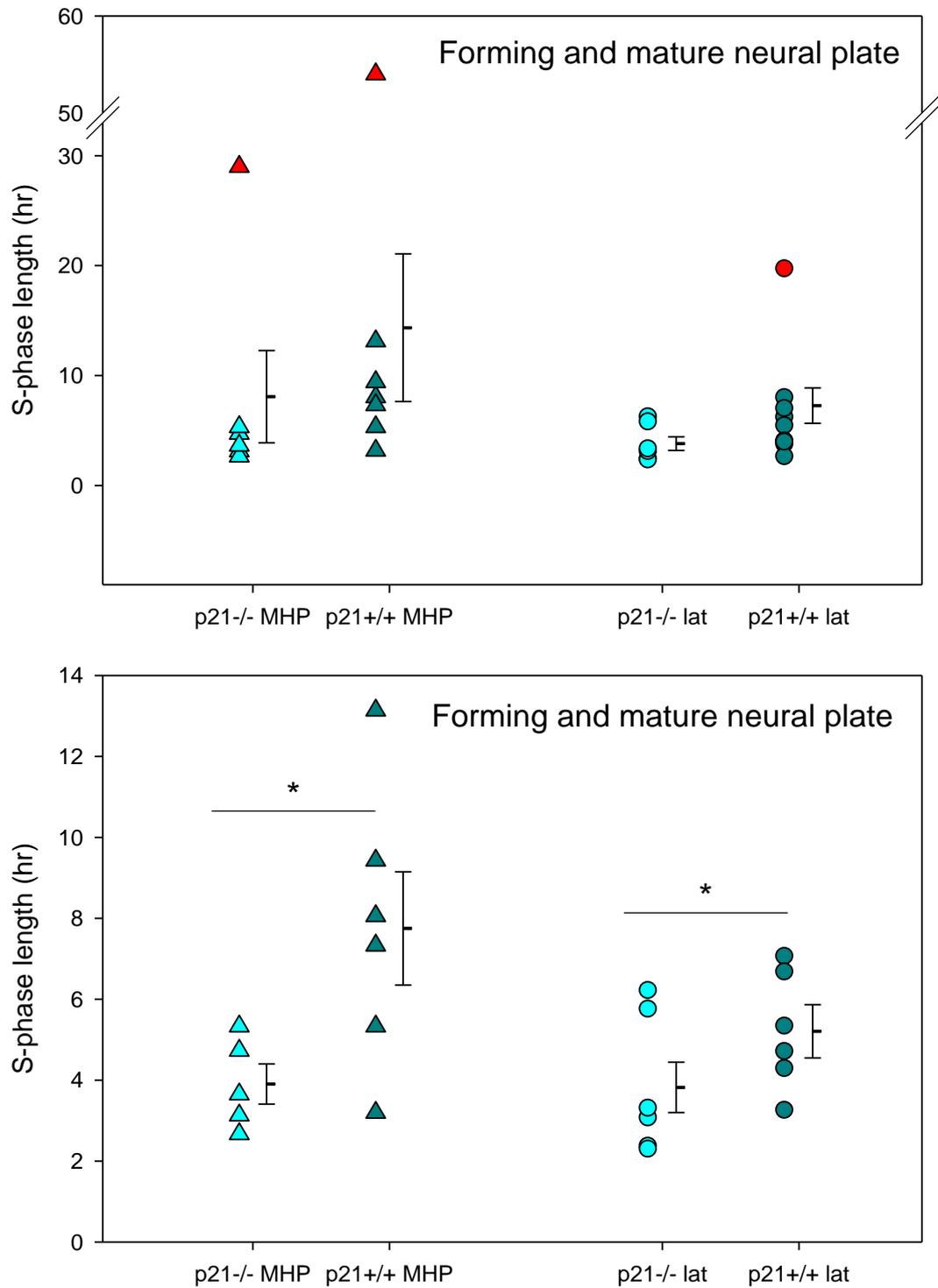
Figure 5.16 - Neuroepithelial cells deficient in p21 spend significantly less time in S-phase

Pooling data from the immature and mature neural plate shows a significant difference between the length of S-phase in p21$^{-/-}$ embryos compared to p21$^{+/+}$ when the outliers (red) are excluded, (p=0.005; Two way ANOVA). At least 6 embryos were analysed per group. There is not a significant difference between S-phase in the MHP and the lateral region when genotype is accounted for (p=0.137). Error bars are +/-SEM.

S-phase length

	MHP		Lateral	
	p21$^{-/-}$	p21$^{+/+}$	p21$^{-/-}$	p21$^{+/+}$
Forming	3.9 (0.55)*	7.1 (0.90)	3.4 (0.94)*	4.5 (0.46)
Mature	3.2 (0.76)**	8.4 (1.48)	3.5 (0.59)**	6.0 (1.02)
Combined	3.9 (0.5)*	7.7 (1.4)	3.8 (0.7)*	5.2 (0.59)

Table 5.6 - S-phase is significantly shorter in p21 null embryos at E8.5

Table showing the mean length of S-phase (hours) (+/- SEM) in the MHP and lateral neural plate of p21$^{-/-}$ and p21$^{+/+}$ embryos. The outliers from Figure 5.14 and Figure 5.16 are not included in the mean. *p=0.005, **p<0.001.

	Mean S-phase MHP		Mean S-phase lateral	
	p21$^{-/-}$	p21$^{+/+}$	p21$^{-/-}$	p21$^{+/+}$
p21$^{-/-}$ vs p21$^{+/+}$	-49.4%		-26.9%	
p21$^{-/-}$ MHP vs p21$^{-/-}$ lat.	+2.5%	-	x	-
p21$^{+/+}$ MHP vs p21$^{+/+}$ lat.	-	+32.5%	-	x

Table 5.7 - Length of S-phase is decreased by 49.4 % in the p21 mutant MHP at E8.5

Percentage differences in mean S-phase length between p21$^{+/+}$ and p21$^{-/-}$ embryos for the MHP and lateral regions based on the numbers presented in Table 5.6. Data for the forming and mature neural plate have been combined in this analysis. S-phase length is decreased by 49.9% in the mutant MHP compared to wild-type, and by 26.9% in the lateral region. In wild-type embryos (last row), S-phase in the MHP is 32.5% longer than in the wild-type lateral region (x). In p21$^{-/-}$ embryos (middle row) S-phase in the MHP and lateral region is essentially the same (x).

5.2.5 Cell cycle phase distribution is slightly altered in p21 mutants

Embryos used in the analysis of S-phase length were sectioned serially. One set of sections was stained with anti-IdU and -BrdU for S-phase length analysis, and the next set 4 microns away was stained with anti-IdU and -pHH3 to estimate cell cycle phase distribution in order to examine whether nuclei of p21$^{-/-}$ were more likely to be found in G2- or M-phase rather than S-phase due to the shorter S-phase.

As with the IdU/BrdU analysis, 5 to 13 sections were analysed per embryo. Approximately 11 IdU positive cells in the MHP were chosen (5 nuclei on each side of the central-most nucleus) and two regions in the lateral regions containing at least 11 positive IdU cells. Cells were assigned to early/mid S-phase, late S-phase, G2 phase, or mitosis depending on the pattern of IdU and pHH3 staining (Figure 5.6 and Figure 5.17). The percentage of cells in each cell cycle phase was calculated as the mean per embryo, calculated from 5-13 sections, based on the total number of cells in the analysis for that embryo (Appendix II).

The percentage of cells in early/mid S-, late S-, G2-, or M-phase was plotted for p21$^{-/-}$ and p21$^{+/+}$ embryos (Figure 5.18). In the MHP as well as in the lateral region there are fewer cells in early/mid S-phase than what is seen in p21$^{+/+}$ embryos. Concurrently, there are more cells in late S-phase in the mutant embryos in the forming as well as the mature neural plate (Figure 5.18 and Table 5.8). This difference is highly significant in the lateral region. In the forming neural plate the number of cells in S-phase in total (early/mid + late) is 34.4% for the mutant embryos while this number is 43.4% for wild-type. In the lateral region there is also a decrease in total cells in S-phase, 30.6% vs 33.6% (Table 5.8). The decrease in cells in S-phase that is observed in the mutant embryos corresponds to an increase in cells in G2-, and M-phase although this does not reach statistical significance (Figure 5.18). In the mature neural plate, there is less difference between the total number of cells in S-phase between mutants and wild-type; 46.4% vs 44.5% in the MHP and 35.2 vs 40% in the lateral region (Table 5.8).

In conclusion, the decrease in S-phase cells in p21$^{-/-}$ embryos corresponds with the decrease in S-phase length as these cells tend to move to G2- and M-phase quicker than cells in the p21$^{+/+}$ embryo.
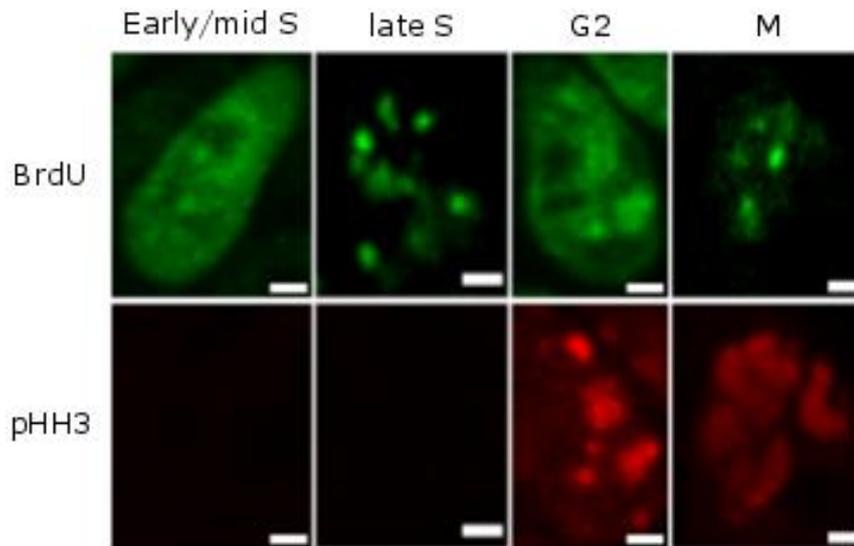
Figure 5.17 - Cell phase distribution based on nuclear pattern

Nuclei were grouped into early/mid S-phase, late S-phase, G2-phase or M-phase based on BrdU (top) and pHH3 (bottom) pattern as described in 2.5.3.2. The same nuclei are shown in two different channels. Scale bars = 2 μm.
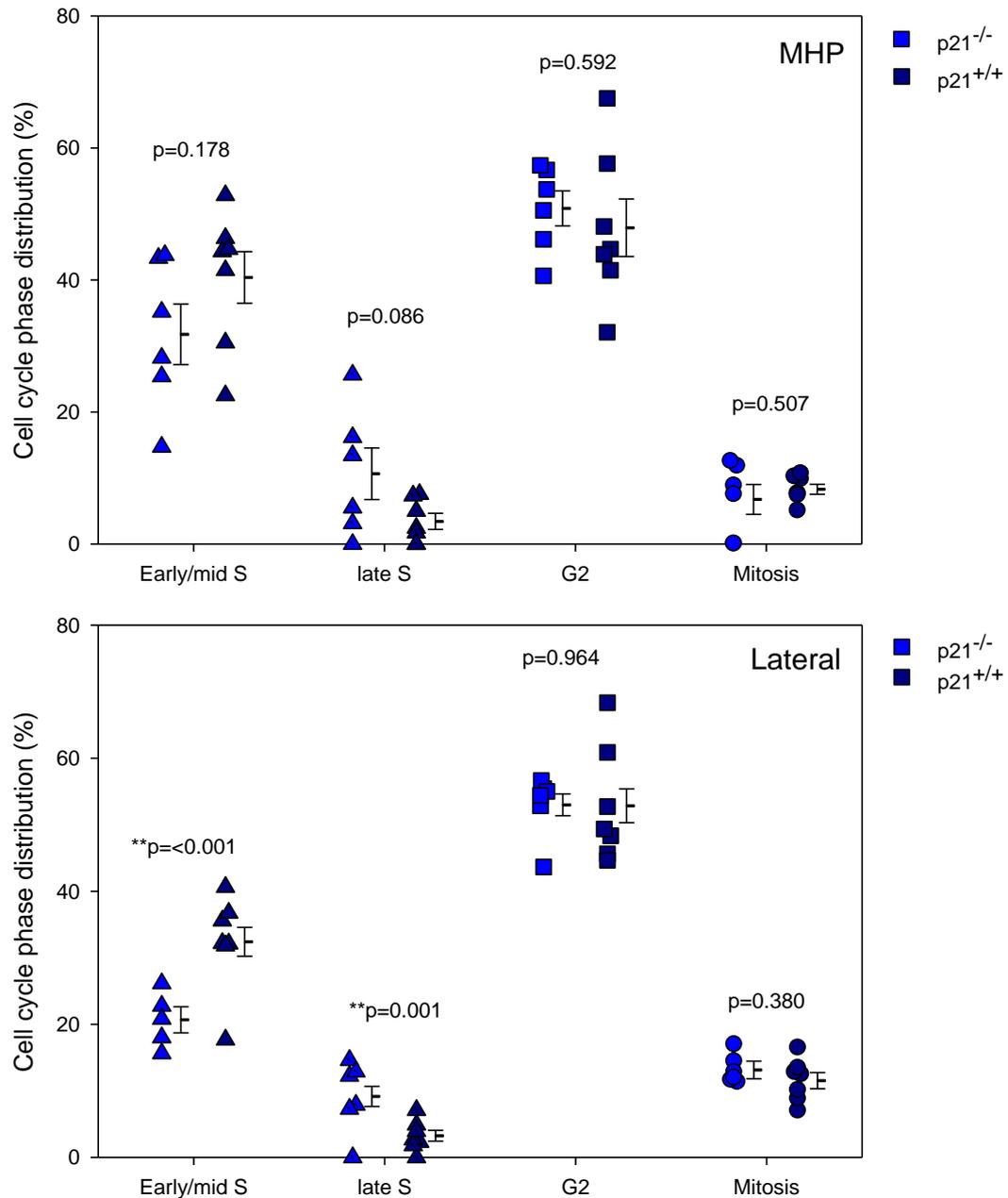
Figure 5.18 – A shift from early to late S-phase in p21 null embryos at E8.5

The distribution of cells in S-, G2, and M-phase, based on the pattern of pHH3 and IdU staining as shown in Figure 5.17, is shown in the MHP (top) and the lateral neural folds (bottom). In both regions there is a shift from early/mid S-phase to late S-phase in p21$^{-/-}$ embryos. In the lateral neural folds this difference is statistically significant whereas in the MHP the same trend is visible, but statistically non-significant. There is no statistically significant difference in the distribution between cells in G2 and M phase between p21$^{-/-}$ and p21$^{+/+}$ littermates. Cell cycle phase distribution was calculated from ≥5 sections from at least 6 embryos per genotype. Percentage of cells was calculated from a total of IdU+ve cells in the MHP and lateral regions. p-values were calculated using the student's test. Error bars are +/-SEM.

Cell cycle phase distribution (%) in the forming neural plate

	MHP		Lateral neural fold	
	p21$^{-/-}$	p21$^{+/+}$	p21$^{-/-}$	p21$^{+/+}$
Early/mid S-phase	27.2	39.6	20.8*	30.7
Late S	7.2	3.8	9.8**	2.9
S-phase total	**34.4**	**43.4**	**30.6**	**33.6**
G2	54.2	47.4	56.9	53.2
Mitosis	11.4	9.2	12.5	13.1

Cell cycle phase distribution (%) in the mature neural plate

	MHP		Lateral neural fold	
	p21$^{-/-}$	p21$^{+/+}$	p21$^{-/-}$	p21$^{+/+}$
Early/mid S-phase	32.6	42.4	27	36.9
Late S	13.8	2.1	8.2*	3.1
S-phase total	**46.4**	**44.5**	**35.2**	**40**
G2	49.5	47.8	51	50.4
Mitosis	4.1	7.7	13.8	10.2

Table 5.8 - Distribution of cells in S-, G2-, and M-phase in p21$^{-/-}$ vs p21$^{+/+}$ embryos at E8.5

Summary of the cell cycle phase distribution data for the forming (top) and mature (bottom) neural plate separately. In the forming neural plate, there are more cells in late S-, G2- and M-phase in the mutants compared to wild-type, and fewer cells in S-phase overall in mutant than wild-type. Total number of cells in S-phase is more similar between mutant and wild-type in the mature neural plate, but there is a shift towards more cells in late S-phase compared to wild-type controls. *p<0.05, **p<0.001.

5.2.6 No change in number of wedge shaped cells in the mutant MHP

As shown in Figure 5.19, neuroepithelial cell shape is directly related to the position of the nucleus (Schoenwolf and Franks, 1984). This can be visualised on tissue sections stained with an antibody against beta-catenin which serves as a marker of the membranes of neuroepithelial cells (Figure 5.19). Nuclei are found at all levels of the apico-basal axis of the neuroepithelium, as a result of interkinetic nuclear migration. Some basal nuclei, visualised with DAPI (blue), are indicated in Figure 5.19. Note the very thin apical process in a cell with a basal nucleus (Figure 5.19; arrow). Because of the relationship between nuclear position and cell shape, measurement of the distance of nuclei from the basal surface of the neuroepithelium is an indirect measure of cell shape.

To see whether $p21^{-/-}$ nuclei are less basal than their wild-type counterparts, nuclear distance was measured as illustrated for BrdU-labelled nuclei in Figure 5.20. More than 10 stained nuclei per section were selected in the MHP (5 on each side of the centre nucleus) and in the lateral regions, nuclei were outlined in image J and a macro was used to find the centre of the nuclei (Figure 5.20, A-B). Lines were drawn from the centre of the nuclei to the basal surface (Figure 5.20, C) and basal distance was calculated as a proportion of total neuroepithelial thickness, at the level of each nucleus (Figure 5.20, D-E).

Firstly, nuclear position was measured using IdU-labelled nuclei in $p21^{-/-}$ and $p21^{+/+}$ embryos from the IdU/BrdU double labelling experiment. Again, 5-13 sections were analysed per embryo, for at least 6 embryos per genotype. The average distance of nuclei from the basal surface per embryo is presented in Figure 5.21. IdU was given 2.25 hours prior to embryo collection and the nuclei are expected to be scattered along the apico-basal axis with many cells undergoing mitosis. In both the MHP and the lateral region, $p21^{-/-}$ nuclei appear slightly more apical than those of $p21^{+/+}$ although this is not statistically significant (Figure 5.21).

Next, nuclear position was quantified for BrdU positive nuclei. This measurement is more interesting, as the embryos were collected 15 minutes after the BrdU pulse

and therefore any instant changes can be identified. Based on the data presented so far, I expected that nuclei of the mutant MHP might be more apical than wild-type MHP nuclei in this snapshot. As shown in Figure 5.22, there is no difference in nuclear position in the MHP or lateral regions between mutants and wild-types. The forming neural plate and the mature neural plate are represented separately and for that reason the number of embryos on each graph is relatively small. In the mature neural plate, mutant MHP nuclei are more basal than wild-type although not statistically significant (Figure 5.22). This was un-expected as p21$^{-/-}$ MHP cells spend less time in S-phase.

The forming and mature neural plate data were combined to show the overall basal position of BrdU positive cells in the MHP and lateral region of p21$^{-/-}$ and p21$^{+/+}$ with greater numbers. Nuclei are significantly more basal in the MHP than in the lateral regions (p=0.02) showing that the apico-basal movement of nuclei is more rapid in the lateral neural plate compared to the MHP (Figure 5.23). This was also shown in Figure 5.7, A and Figure 5.8. In the MHP, p21$^{-/-}$ nuclei are slightly more basal than wild-type nuclei although this is by very little, 0.36 vs 0.38. In the lateral region there is no difference between p21$^{-/-}$ and p21$^{+/+}$. Thus, the changes seen in cell cycle phase distribution and overall nuclear position as measured for IdU is not evident after 15 minutes of BrdU labelling.

In order to get more information about the cell cycle phase distribution of the BrdU positive cells, and to see if p21$^{-/-}$ MHP nuclei were more likely to have a BrdU pattern indicative of late S-, or G2-phase, nuclei were assigned to either early/mid S-phase or late S/G2 phase based on BrdU staining pattern alone (see Section 2.5.3.3). pHH3 staining was not used in this analysis, as it was not available on the IdU/BrdU slides used for S-phase analysis. In the MHP, there is no difference between the distribution of cells in early/mid S phase or late S/G2 between the genotypes (Figure 5.24, left). In the lateral region, there are significantly more cells in early/mid S-phase for p21$^{-/-}$ embryos compared to p21$^{+/+}$ and fewer cells in late S/G2 phase (Figure 5.24, right). This is completely opposite from what I saw in the

IdU/pHH3 analysis and again suggests that the changes I see in S-phase length between p21$^{-/-}$ and p21$^{+/+}$ are not instantaneous.
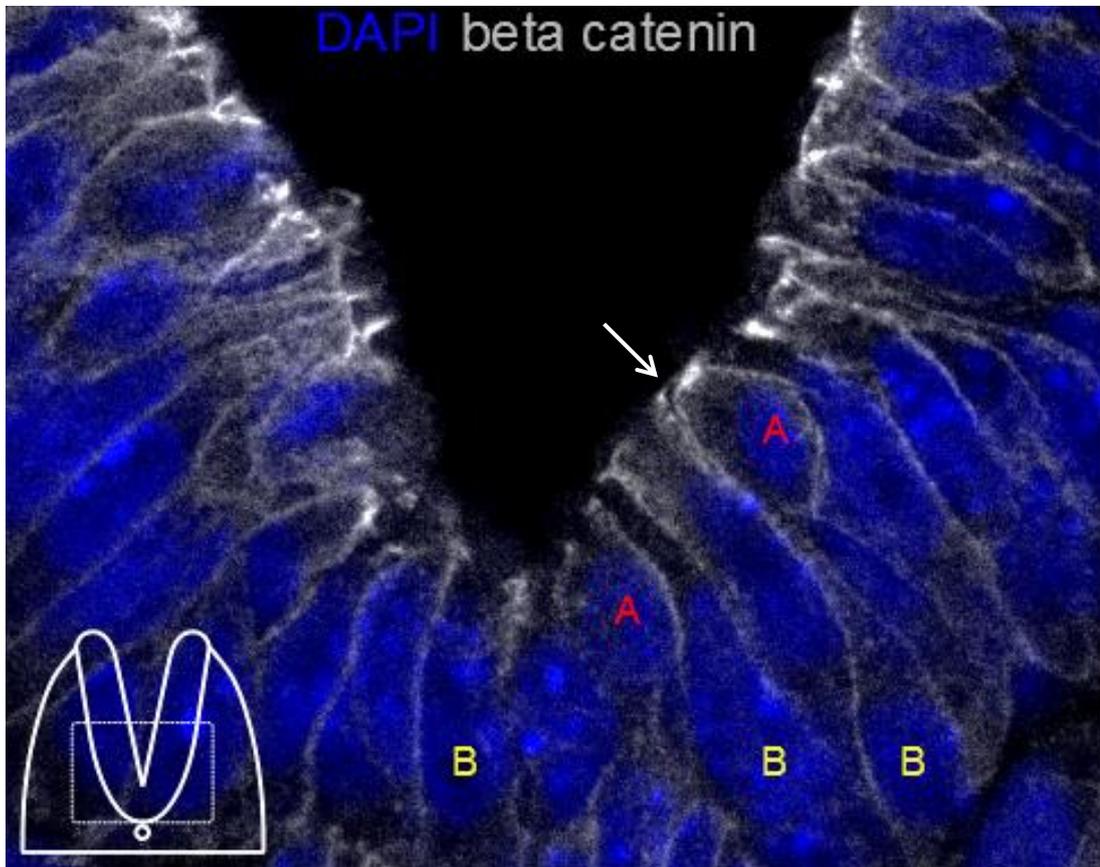
Figure 5.19 – Nuclear position determines cell shape in the neuroepithelium

Nuclei (DAPI) are found throughout the apico-basal axis in the neuroepithelium due to interkinetic nuclear migration. Beta catenin is a marker of the cell membrane and shows the outline of the cells. Apical (A) and basal (B) nuclei are indicated. Note the very thin apical process in a wedge shaped cell with basal nucleus (arrow).
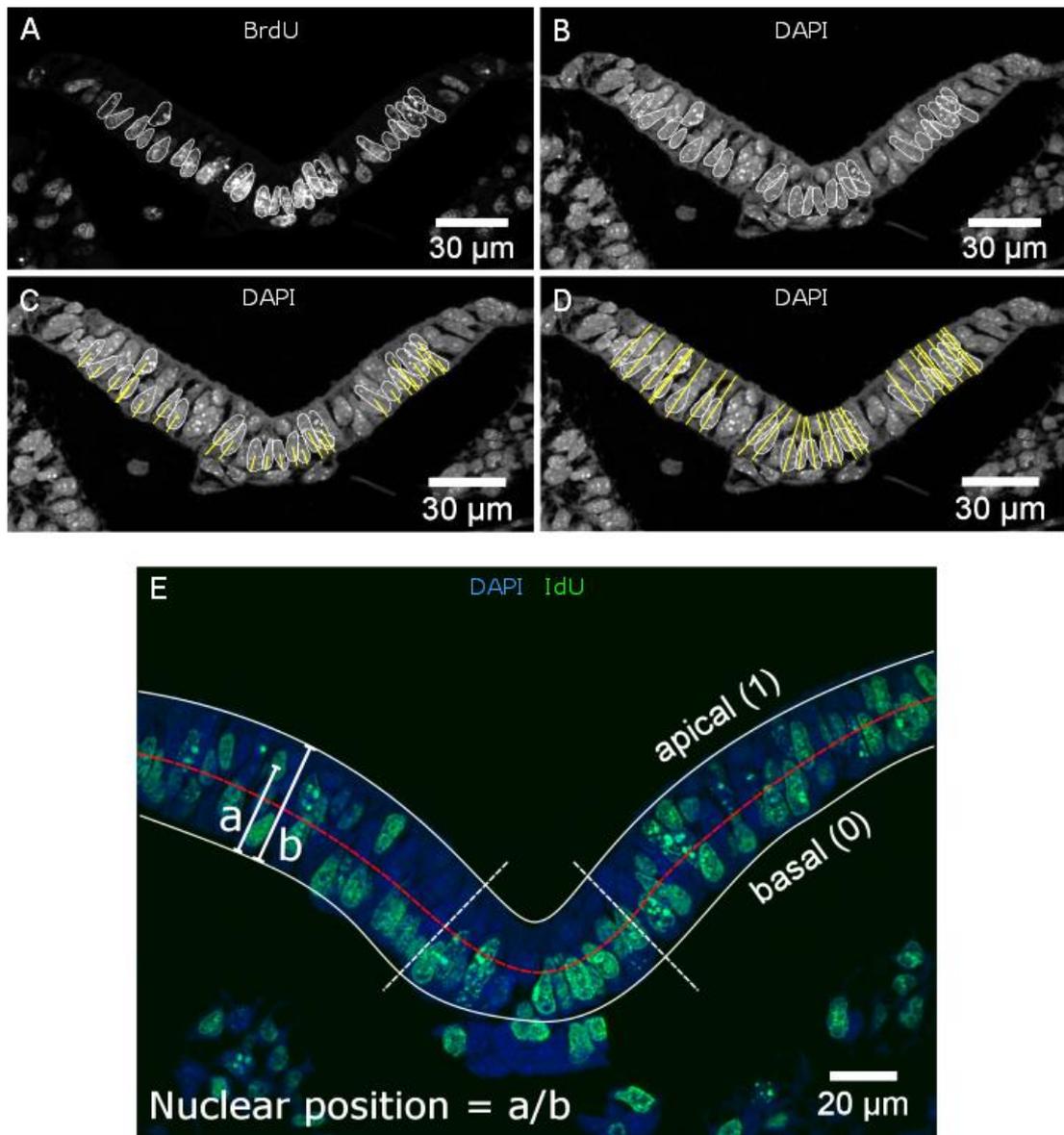
Figure 5.20 – Apicobasal nuclear position as a measure of cell shape

Basal nuclear distance was measured from BrdU labelled cells to the base of the neuroepithelium. In image J, BrdU positive nuclei were circled (A-B) and a macro was used to find the centre of the drawn circles. A line was subsequently drawn from the nuclear centre to the basal surface (C) and total neuroepithelial thickness was measured at the level of each nucleus (D). Basal distance is shown as a proportion of total neuroepithelial thickness where a value of 1 represents an apical nucleus, and 0 a basal, wedge shaped, nucleus (E). The MHP (inside white dotted lines) was compared to the lateral neural plate. The red dotted line indicates the division between the lower and upper half of the neuroepithelium.
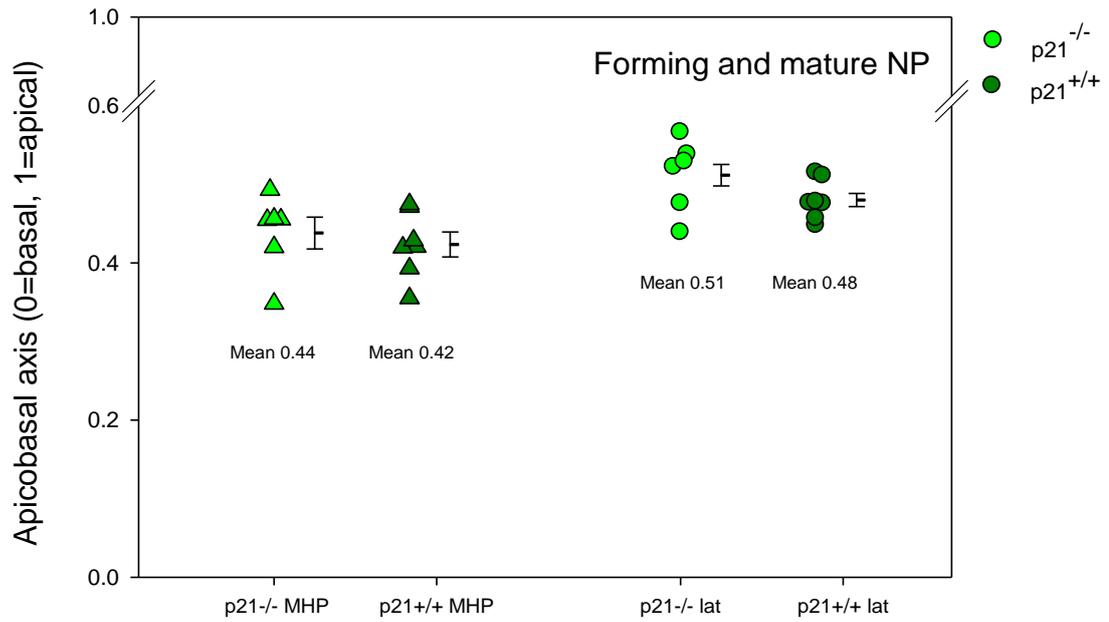
Figure 5.21 - Apico-basal position of IdU+ve nuclei is similar between p21$^{-/-}$ and p21$^{+/+}$ embryos

The apico-basal nuclear position was measured for IdU positive cells in the MHP and the lateral neural folds of at least 6 p21$^{-/-}$ and p21$^{+/+}$ embryos at E8.5. Each dot represents the sample average for a single embryo. Error bars are +/-SEM. The difference between nuclear apico-basal position is not statistically significant between genotypes (p=0.11) but is highly significant between the MHP and lateral region (p<0.001). Two way ANOVA.
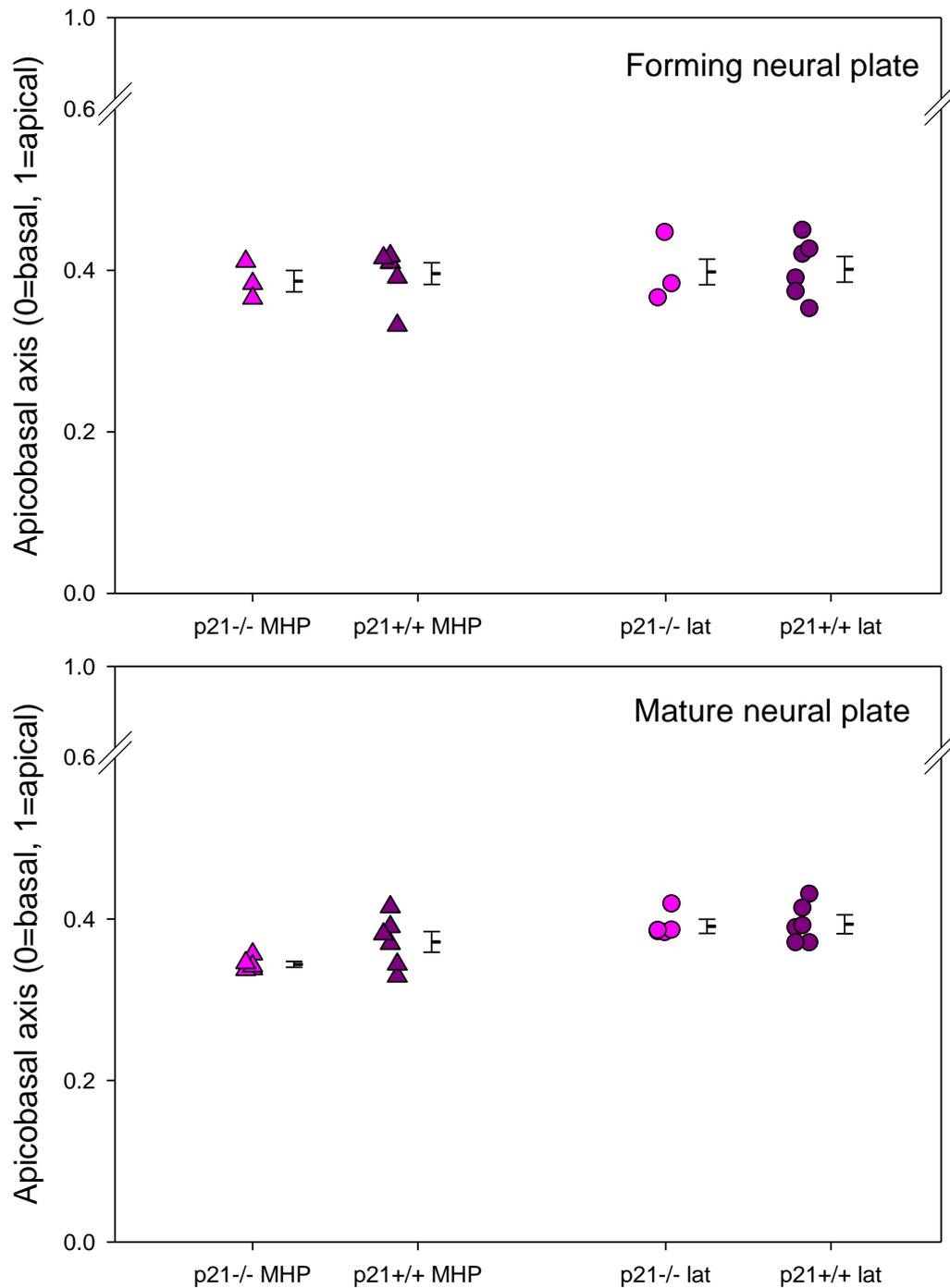
Figure 5.22 - Apicobasal position of BrdU +ve nuclei 15 minutes after injection at E8.5

Distance to the basal surface of BrdU+ve nuclei in the forming MHP (top) and in the mature neural plate (bottom). There is no statistically significant difference in the apico-basal positioning of nuclei between $p21^{-/-}$ and $p21^{+/+}$ in the forming or mature neural plate (p>0.21) although $p21^{-/-}$ nuclei in the mature MHP are slightly more basal than $p21^{+/+}$ embryos. For the mature neural plate, nuclei are significantly more basal in the MHP than in the lateral region (p=0.007). This difference is not significant in the forming neural plate (p=0.68). Each point represents the mean for each of at least 3 embryos. Error bars are +/- SEM. p-values were calculated by Two way ANOVA.
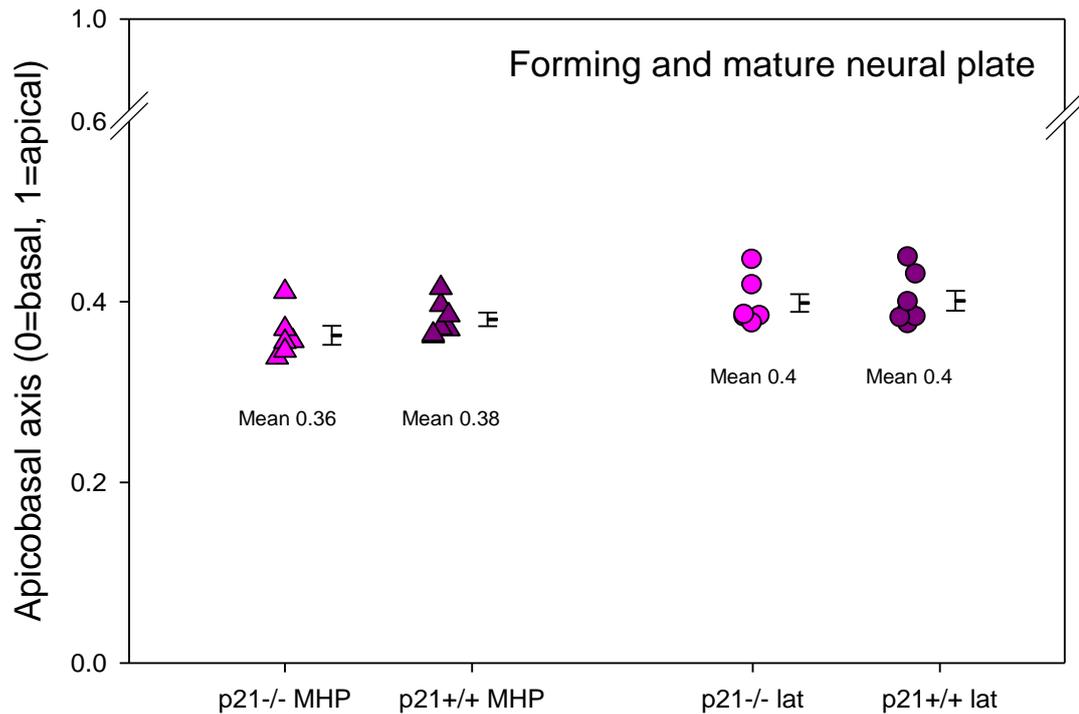
Figure 5.23 - Similar apico-basal position of BrdU+ve nuclei in p21$^{-/-}$ and p21$^{+/+}$ at E8.5

Data were combined from forming and mature stages of neural plate bending to determine whether there is an overall difference in nuclear basal position between p21$^{-/-}$ and p21$^{+/+}$ neuroepithelial cells. In the MHP, there is a very small, statistically non-significant difference, i.e. 0.02 points, with p21$^{-/-}$ MHP cells being more basal. In the MHP and lateral regions, there is no difference between genotypes (p=0.39) but MHP nuclei are significantly more basal than nuclei of the lateral regions (p=0.02). p-values were calculated by Two way ANOVA. Error bars are +/-SEM. At least 5 embryos were analysed per genotype.
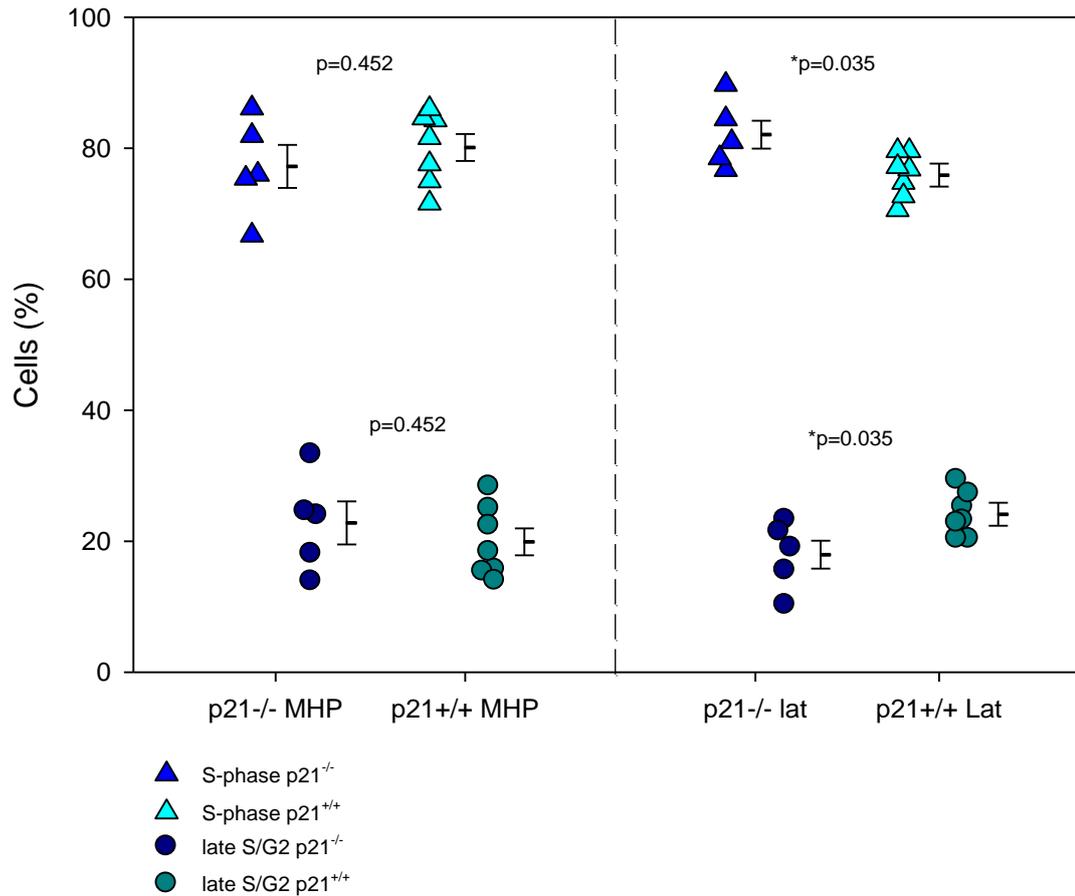
Figure 5.24 - p21$^{-/-}$ and p21$^{+/+}$ embryos have similar cell phase distribution in a 15 minute snapshot

Embryos at E8.5 were given a 15 minute pulse of BrdU before being collected on ice. BrdU positive cells in the MHP and lateral neural folds were rated for being in early/mid S-phase or late S/G2 phase, based on the staining pattern of BrdU (see Figure 2.5). In the MHP, the number of cells in the two categories is very similar. In the lateral neural folds there are significantly more cells in early/mid S-phase and fewer in late S/G2 phase in the p21$^{-/-}$ embryos than p21$^{+/+}$ littermates. Five p21$^{-/-}$ and 7 p21$^{+/+}$ embryos were analysed.

5.3 Discussion

5.3.1 Reliability of methods

The most important prerequisites for the IdU/BrdU double labelling method are that the antibodies are specific, enabling accurate counts of single and double labelled cells, and that the thymidine analogues are incorporated into equal numbers of cells. I have shown that IdU is incorporated into a slightly higher number of cells than BrdU in a small sample number. In the original method by Martynoga, and several other IdU/BrdU studies, the same amount of IdU and BrdU was injected without concerns about their molecular weights (Mairet-Coello et al., 2012; Martynoga et al., 2005; Quinn et al., 2007; Wu et al., 2014). It has, however, been shown that administration of equivalent wt/vol concentrations of the thymidine analogues IdU and CIdU leads to distorted results as the compounds are not taken up by equal numbers of cells, whereas injection of equimolar amounts co-labels all cells (Vega and Peterson, 2005). Other studies have used equal, not equimolar, amounts of IdU and BrdU and found that the number of IdU cells was within 5-7% of the number of BrdU positive cells (Bauer and Patterson, 2005). To account for any differences in uptake due to differences in molecular weight, I have used IdU and BrdU in equimolar amounts, i.e. 56.75 mg/kg and 50 mg/kg, respectively. As the molecular weight of the compounds is close, this modification of the method should not make a big difference to the incorporation of IdU into cells and should not cause the slightly higher uptake of IdU observed. Because the embryos analysed for IdU and BrdU incorporation were from different mothers and potentially from different days, I would need to collect many more litters to do a proper comparison. Another complication is the difficulty of locating nuclei reliably as DAPI does not stain the single stranded DNA very well. Therefore, the total number of nuclei in the analysis cannot be given with 100% confidence.

If it is true that IdU is incorporated more easily than BrdU at equimolar amounts, then the number of single labelled cells will be overrepresented in all the embryos,

and all regions. Thus, the comparison between S-phase length in the MHP and lateral regions, as well as comparisons between genotypes is still reliable.

5.3.2 BrdU and pHH3 staining as cell cycle phase markers

In order to get detailed information about the cell cycle progression in the MHP and in the lateral regions of the mouse neural plate, BrdU and pHH3 antibodies were used as tools to determine cell cycle phases of neuroepithelial cells. Wild-type CD1 embryos were analysed at different time-points following BrdU injection of the mother. Strikingly, there is a wide apico-basal range of BrdU$^+$ nuclei 15 minutes after the BrdU injection, suggesting that some (mainly lateral) nuclei move very rapidly between basal and apical neuroepithelial regions during, or soon after, completion of DNA synthesis. The range of BrdU staining patterns observed suggests that BrdU labels cells that have just entered S-phase, as well as cells that are in late S-phase. Furthermore, many nuclei, both basal and apical, are co-stained with punctate pHH3, indicating that these cells have already entered G2-phase (Hendzel et al., 1997). The cells in G2-phase are likely to have been in late S-phase during the BrdU pulse. The very basal position of many G2-phase cells suggests that during parts of G2-phase, nuclei are basal.

Smith and Schoenwolf have suggested that in the chick, S-phase cells can adopt all cell shapes. That is, DNA synthesis is not necessarily restricted to the basal neuroepithelium (Smith and Schoenwolf, 1988). They proposed a model whereby nuclei of all regions are apical during M-phase (inverted wedge shaped), apical or central during the transition from G1 to S-phase and during late G2 (spindle shaped), and basal during S-phase and most of G2 phase (wedge shaped). Based on that model they predicted that the non-S-phase part of the cell cycle that is prolonged in the MHP is G2 phase, when cells are mostly wedge shaped (Smith and Schoenwolf, 1987; Smith and Schoenwolf, 1988). The model proposed by Smith and Schoenwolf that cells in S-phase can have any shape, i.e. any nuclear position, is very interesting and could explain the number of BrdU-positive nuclei I observed at the apex 15 minutes after the BrdU injection. More recently, it has been shown in the zebrafish neuroepithelium by live imaging that S-phase cells are found at all

levels of the apico-basal axis, and that S- to G2-phase transition occurs at all levels (Leung et al., 2011). This is in agreement with my findings.

In line with other studies (Hayes and Nowakowski, 2000) BrdU labelled cells are observed shortly after IP injection. I show here that a 15 minute pulse is sufficient to label a large population of cells in the mouse neural plate. Assuming that cells are basal during S-phase, and that it takes approximately 5 minutes for the embryos to start incorporating BrdU, this suggests that basal to apical migration is extremely rapid in the E8.5 neural plate. Alternatively, supposing Smith and Schoenwolf's model is true in the mouse, some cells undergoing S-phase might not be basal. It will be difficult to test which of these is true. I could collect the embryos 5 and 10 minutes after the injection to see if this would limit the amount of apical nuclei and thereby support the theory of rapid apical migration. Based on the model by Smith and Schoenwolf, G2 is the main non-S-phase that is increased in the MHP. It would be very interesting to compare the length of G2-phase in the $p21^{-/-}$ embryos compared to $p21^{+/+}$ to see if G2 phase is decreased alongside S-phase in p21 mutant embryos.

Using BrdU and pHH3, I show that 2 hours after a BrdU pulse almost all mitotic nuclei are also BrdU-positive. Because the time when all mitotic nuclei are BrdU positive equals the time it takes for G2+M phase (Takahashi et al., 1995), this shows that G2 and M phase together are close to 2 hours in CD1 as well as p21 mice. Thus, I can estimate that it takes nuclei approximately 2 hours to go from basal S-phase to mitosis at the apical surface. The presence of BrdU labelled basal nuclei in embryos collected 2 hours after injection suggests that BrdU does indeed stay in the bloodstream for at least 2 hours, labelling new cells entering S-phase. Alternatively, the cells might be stalled in S-phase, or be in a basal G2-phase. As mentioned previously, it has been suggested in the chick neural tube that cells in G1-phase are mostly inverted wedge shaped or spindle shaped while cells in G2-phase are mainly wedge shaped (Smith and Schoenwolf, 1988). This suggests that G1-phase and G2-phase do not proceed in the same manner. Thus, my estimation of the time it takes cells to go from the basal surface through G2 to the apical surface, is not necessarily

representative of the time it takes the cell to get back from the apical surface to the base (Smith and Schoenwolf, 1988). In line with this, it has been suggested that apical to basal INKM is a passive process as opposed to basal to apical INKM, suggesting that the two movements should not be assumed to be regulated in the same way (Kosodo et al., 2011). However, as I estimate that the length of G2+M is close to two hours, and as published studies of the cell cycle in the avian and mouse neural plate estimate the cell cycle to be 9.9 and 6.7 hours, respectively (Table 5.2) (McShane et al., 2015; Smith and Schoenwolf, 1987), I am confident that the double labelled population I observe does indeed represent cells that have been in S-phase during both pulses, and have not returned to undergo a second S-phase, after one cell division.

5.3.3 S-phase length

I have used a double thymidine labelling technique to directly calculate S-phase length in the neuroepithelium. By modifying the method by Martynoga et al. by increasing the interval between IdU and BrdU injection to two hours, I have managed to calculate the length of S-phase in p21 mutant embryos. It is notable that a 1 hour injection interval in p21 mice is not enough to get a population of single labelled IdU$^+$BrdU$^-$ cells when I see many apical cells in BrdU timepoint experiments in CD1 mice where embryos were collected 15-45 minutes after BrdU injection. This difference is likely to be strain dependent and is further highlighted by the fact that it seems to take longer for p21 mice to reach 100% IdU-positive mitotic cells than it does CD1 mice. That is, in CD1 embryos 94% of mitotic nuclei co-labelled with BrdU after a 2 hour pulse, while p21 embryos, after 2.25 hours, showed 91% co-labelling of mitotic nuclei. However, the MHP is the region with the longest S-phase, as previously suggested, and even in CD1 mice I do see very few apical nuclei in the MHP at 15-45 minutes after BrdU injection. At 1 hour after the BrdU injection 22.1% of mitotic cells are BrdU+ve in the neuroepithelium, and the majority of these are found in the lateral regions. Thus, the IdU$^+$BrdU$^-$ cell population after a 2 hour interval in p21 mice does, largely, fit with the BrdU time-point experiments conducted in CD1 embryos.

I have found that in the forming neural plate, which does not have a distinct MHP, as well as in the mature V-shaped MHP, S-phase length in the midline is decreased in the absence of p21. As shown in Chapter 3, p21 is strongly expressed in the forming MHP as well as in the V-shaped MHP. Surprisingly, loss of p21 also leads to a decrease in S-phase length in lateral regions, away from the strong expression domain normally observed in the midline. This result suggests that p21 action is not restricted to the midline but rather extends further up through the neural folds. This is in line with the lateral p21 expression I occasionally observed by whole mount in situ hybridisation. Loss of p21 essentially abolishes the difference in length of S-phase between the MHP and lateral regions compared to the wild-type situation. Thus, p21 is strongly implicated by these findings as being required for the prolongation of S-phase in the MHP. Importantly, the MHP still forms with no apparent morphological differences in the absence of a prolonged S-phase in the MHP. It would be interesting to examine differentiation in the floor plate to assess whether increased proliferation in the MHP in the absence of p21 causes aberrant subsequent differentiation. Unfortunately, due to problems of mouse breeding, I had insufficient time to calculate S-phase length in $p21^{-/-}$; $p27^{-/-}$ embryos that we had available in the laboratory. It would have been important to see if the loss of p27 had any additional effect on the length of S-phase or MHP morphology, in p21 mutants.

The length of S-phase I have found varies from other work recently published on the cell cycle in the mouse neural plate. I find that S-phase is longer in the wild-type setting than was reported by McShane et al.; namely 7.7 hours in the MHP and 5.2 hours in the lateral region compared to 2.3 and 1.5 hours, respectively, reported by McShane et al. (McShane et al., 2015). The reason for the discrepancy between the two studies could be that I have done my analysis in the forming and newly formed MHP at E8.5 whereas the previous work by McShane et al. was done in the closing neural tube at E9.5. Furthermore, different techniques were used to calculate the cell cycle parameters. I have used a relatively new technique to directly calculate S-phase while, in the study by McShane et al., cell cycle time and S-phase was estimated by cumulative ^{3}H thymidine labelling in cultured embryos, followed by

linear regression analysis (McShane et al., 2015). Martynoga et al. have shown that in the telencephalon, the IdU/BrdU double labelling method produces cell cycle lengths that correlate significantly with values published for the same tissue and at the same stage, using cumulative BrdU labelling (Martynoga et al., 2005). Thus, the two methods should in theory be comparable in the developing mouse neural plate as well, although there might be differences in using BrdU and ^{3}H thymidine. The correlation between S-phase length calculated by ^{3}H thymidine cumulative injections and IdU/BrdU double labelling was not assessed by Martynoga, and it is also possible that differences lie in the calculation of S-phase in the two methods, although ultimately all were based on the work by Nowakowski (Nowakowski et al., 1989).

A way to validate the IdU/BrdU method in the forming neural plate would be to compare the total length of the cell cycle using IdU/BrdU to parallel experiments with cumulative BrdU labelling. This was not done for a few reasons. Firstly, nuclei that have undergone the stringent IdU/BrdU immunohistochemistry protocol are left with single stranded DNA which binds DAPI, and Hoechst, very poorly. Thus, I was unable to consistently and accurately count the number of total nuclei using DAPI in my experiments and therefore unable to calculate total cell cycle length. Secondly, it would require a lot of mice to do the cumulative labelling, and as this had been done previously in our lab in the early mouse neural plate using ^{3}H thymidine (McShane et al., 2015), I decided not to do this.

5.3.4 Do dividing IdU positive cells distort the analysis?

The original method by Martynoga et al. used an interval of 1.5 hrs between IdU and BrdU injections. I found, at 1 hour there were only 1-3 single labelled cells per sample, which was not enough to calculate S-phase as the formula in most samples would be:

$$S = Ti \ (1 \ hour) / \left(\frac{single \ labelled \ (0)}{double \ labelled \ (n)} \right)$$

Increasing the interval to 2 hours did, in the majority of cases result in a reproducible number of single labelled cells in all regions, although there were 12 MHP sections with no single labelled cells that led to very high values for average S-phase length in 3 embryos. Following a 2 hour IdU pulse, 94% of all mitotic figures were co-labelled with IdU in CD1 embryos while the first IdU$^+$ mitotic figures were observed after a 1 hour pulse. Therefore, I cannot exclude the possibility that the number of single labelled cells in p21 embryos is overestimated when the embryos are collected at 2.25 hours, as a proportion of IdU$^+$ cells might have recently gone through cell division. This problem is difficult to overcome and might be quite specific to the mouse neural plate during early development due to the very short apico-basal length of the neuroepithelium, the shortening of this axis in the MHP (McShane et al., 2015; Smith and Schoenwolf, 1988), as well as the relatively long S-phase. Adapting this method to a shorter interval between injections, e.g. 1.5 hours, could possibly have limited the number of dividing IdU$^+$ cells. However, the proportion of mitotic IdU$^+$ cells in CD1 embryos only fell from 94% to 85.9% when the pulse was reduced from 2 hours to 1.5 hours. Moreover, a 1.5 hour interval would probably not produce enough single labelled cells in the p21 mouse line for the analysis. Single labelled cells, i.e. IdU$^+$ cells that have left S-phase, should theoretically increase linearly during the interval between the injections (Hayes and Nowakowski, 2000). I have shown in CD1 and p21 embryos that 2 hours is below the limit for 100% IdU$^+$ mitotic figures, i.e. close to the length of G2+M. Therefore, a two hour interval should still be in the linear phase before the slope doubles as IdU labelled daughter cells are produced by mitosis (Hayes and Nowakowski, 2000). Importantly, an over-representation of single labelled cells would result in a shorter calculated S-phase length whereas, as I discussed above, my analysis of S-phase gave higher S-phase length values than were described before (McShane et al., 2015). This suggests that dividing IdU-labelled cells was not an over-riding problem in the current study.

5.3.5 Cell cycle phase distribution

Cell cycle phase distribution was quantified in the p21$^{-/-}$ and p21$^{+/+}$ embryos using the IdU and pHH3 staining pattern as a tool. I have shown that S-phase is reduced by almost half in the MHP of p21$^{-/-}$ embryos compared to wild-type. Therefore, I expected there to be fewer cells in S-phase in the mutant MHP. I do, indeed, see fewer cells in S-phase in the forming neural plate and to a lesser extent in the mature neural plate. Interestingly, in the mutant embryos, a relatively high proportion of cells have a nuclear IdU pattern similar to that seen in G2-phase but with no pHH3 staining. These cells, which I classified as late S-phase, were very rarely seen in the wild-type neuroepithelium.

One possible reason for finding so many p21$^{-/-}$ cells in late S-phase could be because the cells become stalled in late S-phase in the absence of p21. However, this seems unlikely considering that S-phase length was found to be reduced significantly in p21 mutants. Another possibility is that there are just many more cells that are ready to leave S-phase in mutant embryos compared to wild-type and that this phase is only truly picked up in the mutant setting. It is surprising that the changes in cell cycle phase distribution in the MHP do not reach significance when considering how much S-phase length is decreased. In the lateral region there are significantly fewer early/mid S-phase cells and significantly more cells in late S-phase. Statistics are generally more powerful for the lateral regions because I analysed two regions, one on each side, and averaged these. This generates larger n-values and the standard error is generally smaller than in the MHP where I have a smaller population of cells with greater variation (e.g. compare the size of SEM values between MHP and lateral in Figure 5.18). Hence, the different findings between MHP and lateral regions may be a reflection of sample size and statistical power.

Based on the analysis of S-phase length I would expect there to be a trend towards more cells in G2 and M-phase for p21$^{-/-}$ embryos compared to p21$^{+/+}$. I do see more cells in late S-, G2-, and M-phase but the results are not very striking. A larger dataset would have painted a clearer picture.

In conclusion, p21$^{-/-}$ mutant MHP and lateral region cells both show a trend towards an increased proportion of cells in late S-, and G2- phase while fewer cells are observed in early/mid S-phase compared to wild-type. This finding correlates with the observed decrease in S-phase length in both regions of p21$^{-/-}$ embryos.

5.3.6 Nuclear position measurements

I analysed nuclear position to get an idea of whether there are fewer basal nuclei in p21$^{-/-}$ embryos, consistent with the decreased S-phase length and number of cells in S-phase. Analysis of nuclear position in IdU positive cells showed that, in the MHP and lateral regions of p21$^{-/-}$ embryos, there is a small increase in the number of apical nuclei compared to wild-type. This difference was not statistically significant. The IdU-positive cell fraction contains many cells that were in S-phase for variable periods of the 2.25 hours of labelling in the experiment. This therefore gives an overall picture of nuclear position in the two genotypes. To get a snapshot of nuclear position immediately after injection, the position of BrdU-positive nuclei was analysed in embryos that had been exposed to BrdU for only 15 minutes. Nuclei should all be, or have been, in S-phase just prior to collection. In the MHP as well as the lateral regions, p21$^{-/-}$ nuclei were slightly, but not significantly, more basal than wild-type. In the V-shaped neural plate this same trend was seen. When combining the forming and mature plate, I found that p21$^{-/-}$ nuclei in the MHP were slightly more basal than p21$^{+/+}$ whereas in the lateral region no difference was seen. To conclude, there is not a big difference in nuclear position between mutant and wild-type embryos at this early phase, and changes in S-phase length and overall nuclear apico-basal position (IdU) observed later are likely to take more time than 15 minutes to occur. Considering that the reduced S-phase length in the MHP of p21$^{-/-}$ embryos is still 3.2-3.9 hours, 15 minutes is a very short time to see any differences. Calculating overall nuclear position in the MHP and lateral regions with DAPI would be informative, but was not possible due to technical difficulties with the DAPI staining.

Lastly, cell cycle phase distribution of BrdU positive cells was estimated to see if there were fewer cells in early/mid S-phase in the mutant setting. As for the nuclear

position of BrdU positive cells, 15 minutes is likely to be too short to see a difference as cell phase distribution was very similar in the p21$^{-/-}$ and p21$^{+/+}$ MHP. Surprisingly, p21$^{-/-}$ nuclei in the lateral region tended to be in early/mid S-phase and not in late S or G2 phase as seen in the wild-type embryos. This analysis was done by approximation only, by looking at the BrdU staining pattern, and is therefore not very reliable. It does, however, give an idea of the overall trend of the cell phases.

In conclusion, I have shown that S-phase is significantly reduced in the absence of p21, and that p21 is strongly implicated as being responsible for the regional difference in S-phase length between the MHP and lateral non-bending regions, as this difference is abolished in the absence of p21. I have not detected changes in MHP morphology or major changes in the apico-basal position of MHP nuclei. It is possible that there is redundancy between p21 and p27 and/or p57 in the MHP and that these other genes keep the nuclei at a basal position, independently of cell cycle prolongation. The fact that the long S-phase in the MHP is abolished upon loss of p21 suggests that: 1) the role of p21 in prolonging S-phase specifically in the MHP is not redundant, and 2) prolongation of S-phase in the MHP is not necessary for MHP formation and neural tube closure. The long S-phase might be the result, rather than the cause, of the cell shape changes occurring in the MHP during neural plate bending. However, it is hard to imagine how cell shape changes would be due to cell-cycle-independent changes in IKNM, resulting in secondary effects on the length of S-phase, since IKNM does not affect cell cycle progression (Ueno et al., 2006).

Chapter 6 - CIP/KIP genes are redundant in MHP formation

6.1 Introduction

Electroporation of developing mouse embryos enables gene manipulation that is relatively cheap with the possibility of knocking down several genes at once, avoiding the problem of genetic redundancy often observed in genetic mutant mice, or overexpressing several genes locally. The development of culture methods of intact mouse embryos provides the means to study neural tube development (Cockroft, 1990) following gene manipulation by electroporation. Gene knock-down can be achieved with RNA interference (RNAi), which was discovered in *C.elegans* and in plants in the late 1990s (Calegari et al., 2004) and is based on double stranded RNA molecules that can silence the expression of genes with complementary sequences. Overexpression can be achieved with plasmids that express any gene of interest.

In Chapter 3 I showed that p21, p27 and p57 are expressed in the MHP region during early neurulation. In the present chapter, I aimed to test whether the CIP/KIP genes are necessary or sufficient for MHP induction. I electroporated siRNAs to achieve knock-down, or plasmids to overexpress CIP/KIP genes in the neural plate.

The aim was to abolish CIP/KIP genes in the MHP to see if loss of the inhibitors led to a shorter S-phase, fewer wedge shaped cells, and a broader MHP (Figure 6.1, A). On the other hand, I planned to overexpress the genes in the lateral neural tube to see if a high local concentration of p21, p27 and p57 would be sufficient to cause an ectopic hinge point. Due to technical difficulties it was not possible to routinely target the lateral neural plate, and instead I targeted the MHP to examine whether the midline bend would be sharper with more basal nuclei in an overexpressing setting (Figure 6.1, C).

For the knock-down experiments, a p57 siRNA or a GC-matched control siRNA was electroporated into neural plates of $p21^{+/+}$ and $p21^{-/-}$ embryos, using a tagged fluorescent oligo to trace the electroporated siRNA. For the overexpression, p27 and/or p57 cDNA in bi-cistronic expression plasmids that also expressed EGFP (Tury et al., 2011), were electroporated into the neural tube together with a plasmid expressing p21.
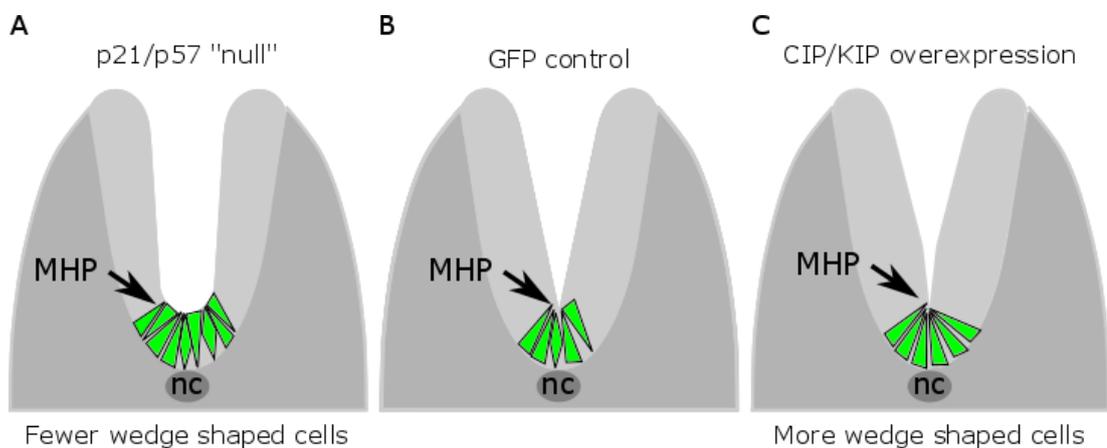
Figure 6.1 - Manipulating CIP/KIP gene expression by electroporation

In order to achieve a scenario where CIP/KIP genes are downregulated or overexpressed, siRNAs or plasmids were electroporated into the neural plate at E7.5 (A-C). The hypothesis was that downregulation of CIP/KIP genes in the MHP would lead to a shorter S-phase, fewer basal cells, and a broader MHP (A). Overexpression of CIP/KIP genes in the MHP was hypothesised to lead to a prolongation of S-phase, cause an enrichment of basal cell nuclei, and exaggerate the MHP (C). Green wedges represent electroporated fluorescent cells.

6.2 Results

6.2.1 Validating siRNA and plasmid in cell culture

Prior to starting the work on genetic mouse mutants (Chapter 4), I attempted to manipulate p21 levels specifically in the neural tube by electroporation. I obtained two anti-p21 antibodies (p21 C-19 and p21 F-5, both from Santa Cruz Biotechnology) but found they did not detect p21 protein in immunohistochemistry of the embryonic neural tube. Hence, it was difficult to validate the siRNA and plasmid actions directly in electroporated embryos and so, as an alternative method, I used a cell culture system. For gene knock-down experiments, mouse 3T3 fibroblasts were transfected with a p21 siRNA plus a GFP plasmid or a GC-matched siRNA control with a random sequence +GFP. For overexpression experiments, the 3T3 cells were transfected with a p21 plasmid plus a GFP plasmid or with the GFP plasmid alone. A standard approach was taken using the widely available transfection reagent, Lipofectamine-2000. RNA was extracted from the cells 24 hours after transfection and p21 levels were quantified by qRT-PCR. The transfection efficiency was estimated by calculating the ratio of GFP transfected cells to total nuclei.

Following transfection with p21 siRNA +GFP, a dose dependent decrease in p21 expression was observed for 10 pmol and 25 pmol concentrations of siRNA compared to transfection with GFP alone (Figure 6.2). p21 knock-down with a higher dose, i.e. 50 pmol siRNA, did not reduce p21 expression further. The reduction in p21 expression was not observed with the GC-matched siRNA control +GFP or GFP alone (Figure 6.2). p21 expression was significantly decreased in cell transfected with p21 siRNA compared to siRNA control ($p < 0.001$; Two way ANOVA) although the difference between the concentrations of p21 siRNA was not statistically significant. Transfection of cells with the p21 plasmid +GFP led to a 3-fold overexpression of p21 mRNA levels compared to GFP on its own (Figure 6.2). It was found that transfection of cells with GFP alone consistently led to higher expression levels of p21. To assess if this was a specific response to the GFP plasmid

or a stress response to the transfection procedure itself, a random plasmid (Msx2) of the same size as GFP was transfected into the cells. Msx2 transfection resulted in an up-regulation of p21 gene expression, similar to that observed for GFP alone, compared to untreated cells (Figure 6.2). The difference in p21 expression following transfection with GFP only or Msx2 was not significant (p=0.147; One way ANOVA). Furthermore, the transfection reagent, Lipofectamine-2000, led to slight up-regulation of p21 gene expression compared to non-treated cells (Figure 6.2).

The transfection efficiency of the different treatments was roughly equal as estimated by the amount of GFP-positive cells (Figure 6.3). GFP-positive cells and DAPI stained nuclei were counted manually in three random fields of view in Image J to estimate transfection efficiency, calculated as the percentage GFP-positive cells to total nuclei (Figure 6.4). The cells were confluent at the end of transfection, making it difficult to distinguish GFP positive cells from one another and get an accurate number (Figure 6.3). For that reason the efficiency presented in Figure 6.4 is probably an underestimate of the actual efficiency. The efficiency ranged from 32% to 45% with SEM values ranging from 1.4 % to 7.9 % (Figure 6.4). While perhaps not accurate, the transfection efficiency indicates that the failure of the highest concentration of p21 siRNA to further knock-down p21 gene expression was not due to lower transfection efficiency. Statistically, there was no significant difference between the treatments (p=0.178; One-way ANOVA).

Relative expression of p21
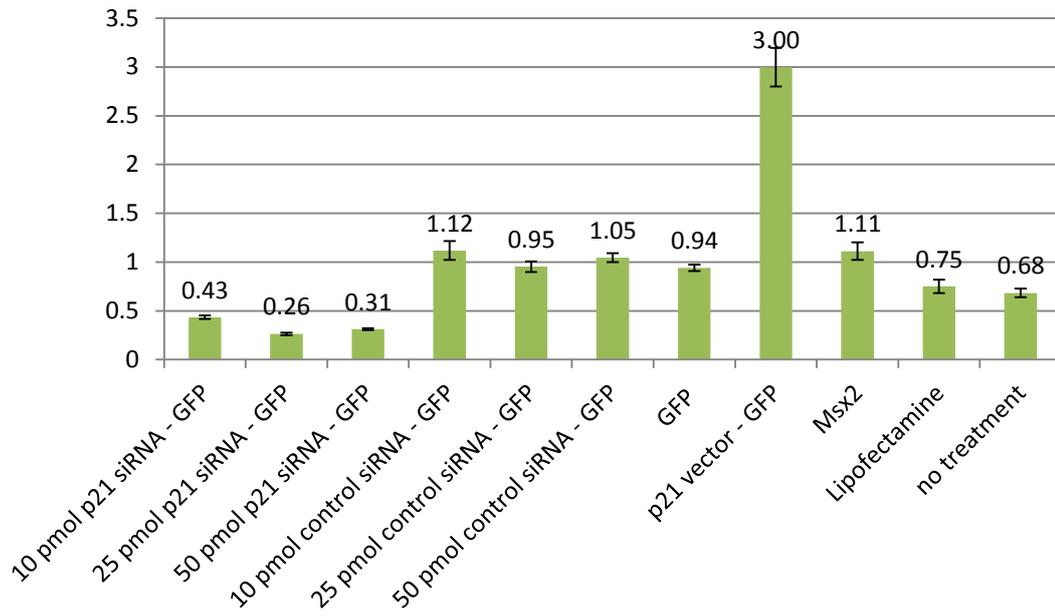
Figure 6.2 – p21 levels can be manipulated in cell culture

A 3T3 fibroblast cell culture system was used to validate knock-down by the p21 siRNA and overexpression by the p21 plasmid. p21 siRNA +GFP caused a significant, dose dependent reduction in p21 gene expression compared to siRNA control (p<0.001; Two way ANOVA). The reduction in p21 mRNA levels was not observed with the control siRNA +GFP. The p21 plasmid +GFP resulted in a 3 fold increase in p21 expression compared to GFP alone. Furthermore, an unspecific upregulation of p21 expression was observed with GFP alone, the random plasmid Msx2, or Lipofectamine compared to untreated cells. Error bars are +/-SEM. Three samples were assayed per treatment group.
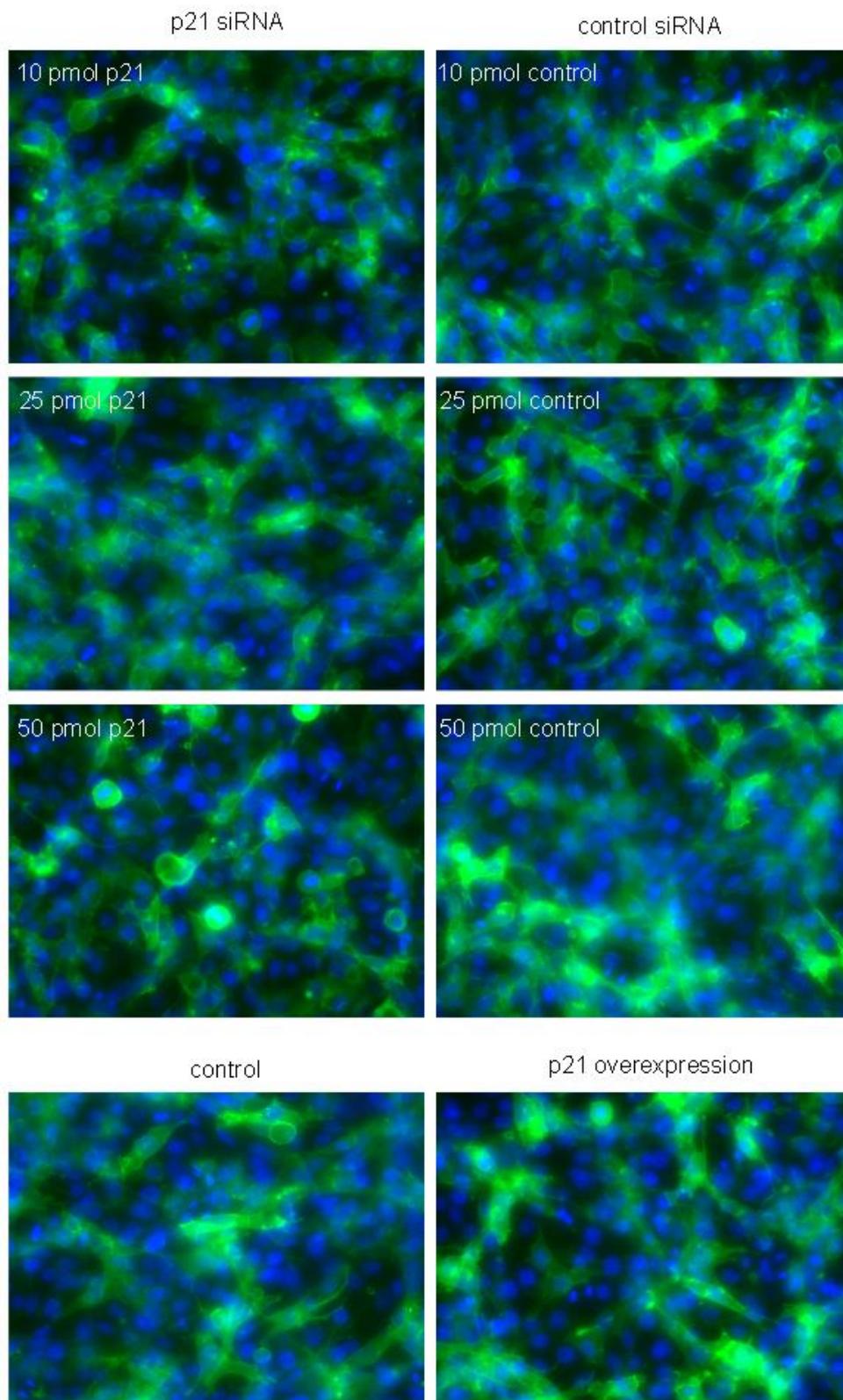
Figure 6.3 - Transfection efficiency of siRNA and/or plasmids in 3T3 cells

The amount of GFP positive cells appears equal for all siRNA treatment groups. The cells are very confluent and difficult to distinguish from one another. n=3.
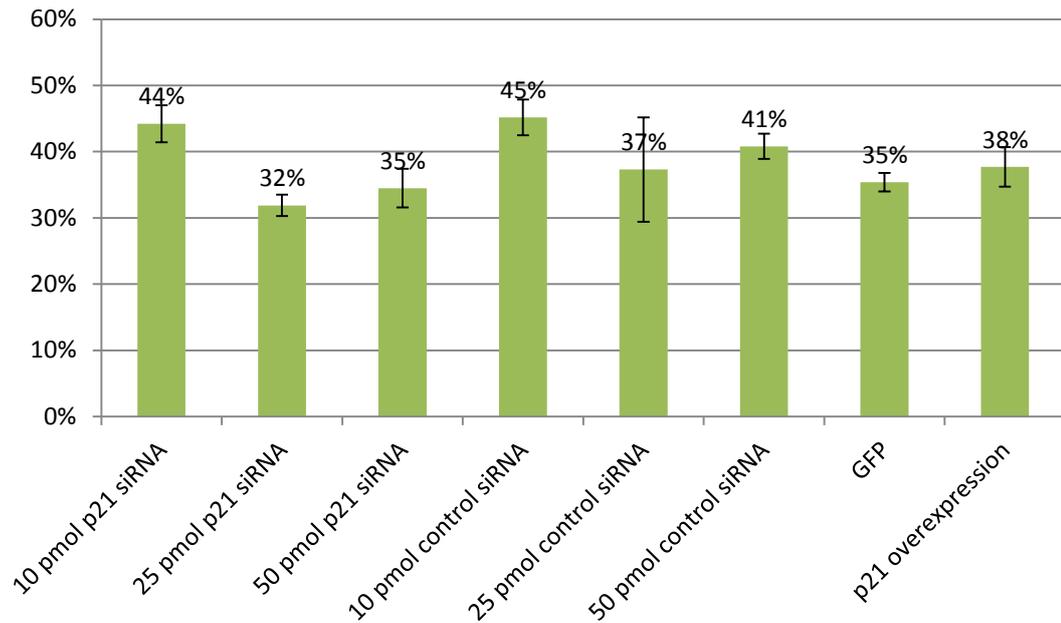
Figure 6.4 - Transfection efficiency in 3T3 fibroblasts

Approximate transfection efficiency shown as the percentage of GFP-positive cells to total nuclei, counted in 3 random fields of views per treatment. The transformation efficiency (%) ranges from 32% to 45%. Error bars are +/-SEM. There is no significant difference between the percentage of GFP-positive cells among treatments (p=0.178; One-way ANOVA).

Due to time constraints and difficulty in finding a cell line that endogenously expressed p57, this analysis was not performed for p57. Nevertheless, the p21 siRNA assay in 3T3 cells serves as a proof of principle for the commercially available siRNAs used in this thesis and the previously published plasmids.

6.2.2 Electroporating the mouse neural plate

All the electroporation experiments were performed at E7.5. Embryos were dissected from the uterus keeping the yolk sac and ectoplacental cone intact, and divided into a treatment and a control group (Figure 6.5, A). siRNA +tagged oligo or overexpressing plasmid(s) +fast green was injected into the amniotic cavity using a handheld mouth pipette. Injected embryos were immediately electroporated through the node region at the base of the embryo (Figure 6.5, B).
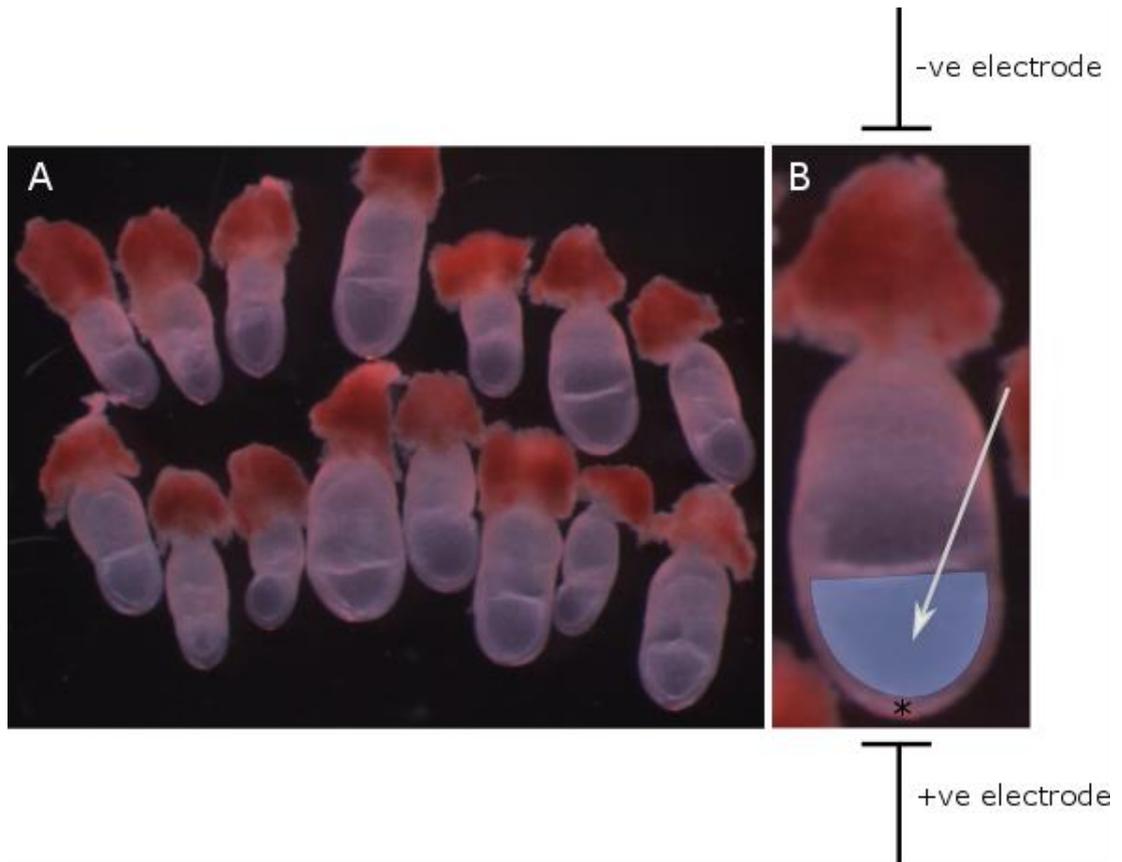
Figure 6.5 - Electroporation of E7.5 embryos

Embryos at E7.5 were dissected and grouped into two identical treatment groups based on developmental stage (A), and subsequently injected with p57 siRNA or GC-matched control together with the tagged oligo. For overexpression experiments, embryos were allocated into three groups: one group was injected with p21 and p57, one group with p21, p27 and p57, and one group with GFP control. In the overexpressing experiments, fast green (0.01%) was used to visualise the plasmid mixture. The amniotic cavity was injected (B; arrow) until the amnion bulged slightly into the exocoelomic cavity. The embryos were subsequently electroporated through the node (*) and cultured for 24 hours in rat serum.

6.2.3 Overexpressing CIP/KIP genes in the neural plate midline

Embryos electroporated with a GFP plasmid exhibit strong GFP expression along the neural tube and PNP after 24 hours of culture (Figure 6.6). The number of embryos with midline GFP expression was approximately 90% and only embryos showing GFP expression in the midline were processed for further analysis. Cross-sections through electroporated embryos reveal that GFP is expressed mainly in the midline (Figure 6.6, C'; arrow), consistent with work showing that the node region gives rise to the embryonic midline (Patten et al., 2003). Some cells in the medial part of the paraxial mesoderm are also GFP-labelled (Figure 6.6, C'; arrowheads). At E7.5, when the embryos were electroporated, neuromesodermal progenitors (NMps) are located in the node streak border in the anterior primitive streak and in the caudal lateral epiblast (Henrique et al., 2015). These NMps give rise to neural progenitors found in the CLE and PNP, and mesoderm progenitors contributing to presomitic mesoderm by E8.5 (Henrique et al., 2015). Consistent with the GFP labelled paraxial mesoderm, it has been suggested that individual NMps are retained caudally in the tail bud and give rise to cells that can contribute to neural as well as mesodermal lineages as the body axis extends (Tzouanacou et al., 2009).

In order to further validate the p21 plasmid, embryos electroporated with p21 + GFP or GFP only were processed for in situ hybridisation following a 24 hour culture period. Five out of five embryos electroporated with the p21 plasmid showed ectopic p21 mRNA expression along the entire mouse midline in a pattern corresponding to the GFP expression observed at the end of culture (Figure 6.7, A-A'). Embryos electroporated with GFP only showed midline GFP expression but none of three embryos displayed ectopic p21 expression (Figure 6.7, B-B'). A cross section through the PNP of a p21 electroporated embryo with subsequent detection of p21 mRNA by in situ hybridisation reveals cells with strong ectopic p21 expression that are centred around the midline (Figure 6.7, A''). This analysis was not done using the p27 and p57 expression plasmids due to time constraints, as these plasmids came into my possession at a very late stage in my PhD. However, I can conclude that the p21 plasmid induces strong ectopic expression of p21 in cell

culture as well as in an intact mouse embryo culture system. The p27 and p57 plasmids have been shown to induce expression of p27 and p57 when electroporated in utero during corticogenesis (Tury et al., 2011).

In order to see if overexpression of the CIP/KIP genes in the neural plate is sufficient to cause an exaggerated midline bend, CD1 embryos were electroporated with p21 and p57, p21, p27 and p57, or the p27 and p57 backbone plasmid expressing EGFP only (Tury et al., 2011). As the p21 expression plasmid does not express GFP, it was assumed that the plasmid would enter the same cells as the EGFP tagged p27 and p57 plasmids. None of the electroporated embryos displayed any morphological MHP changes regardless of treatment (Figure 6.8). Electroporated GFP-positive cells were observed scattered throughout the medial part of the neural plate, and in fact relatively few GFP-positive cells were located in the MHP (Figure 6.8) although quantification revealed that the number of GFP-positive cells on average was higher in the MHP than in the lateral regions (Table 6.1). Hence, my aim of overexpressing the CIP/KIP proteins specifically at high levels in the MHP was not achieved in this experiment.

One embryo that was electroporated with both p21 and p57 expression vectors contained a cluster of GFP-positive cells that coincided with a slight indentation of the lateral neural plate resulting from basal nuclei in that region (Figure 6.8, C and Figure 6.9). This suggests that at high density, p21 and p57 overexpression might be sufficient to induce bending, although this is hard to test in this system due to the scarcity of overexpressing cells. Interestingly, in another embryo electroporated with both p21 and p57, the majority of GFP-positive nuclei were very apical, suggesting that p21 and p57 overexpression does not necessarily result in basal nuclei (Figure 6.8, B-B''; arrows). Triple overexpression did not have any effect on midline bending. This was not due to a lower number of overexpressing cells in the MHP compared to the other treatments (Table 6.1), although electroporated cells are likely to be too few and scattered to induce localised bending (Figure 6.8). This is true for all the treatment groups.

Interestingly, most of the embryos electroporated with CIP/KIP genes exhibited dorsolateral hinge points (DLHPs): this was true of 3 out of 6 embryos electroporated with p21/p57 and 3 out of 3 embryos electroporated with p21/p27/p57. This is something I never observed at this stage in non-electroporated embryos, and only rarely in embryos electroporated with GFP only (1 out of 4) or siRNAs (0 out of 9). It might suggest a role for enhanced CIP/KIP expression in regulating DLHPs, although the dorsal most neural plate, where DLHPs are located, was only rarely GFP-positive in these embryos.
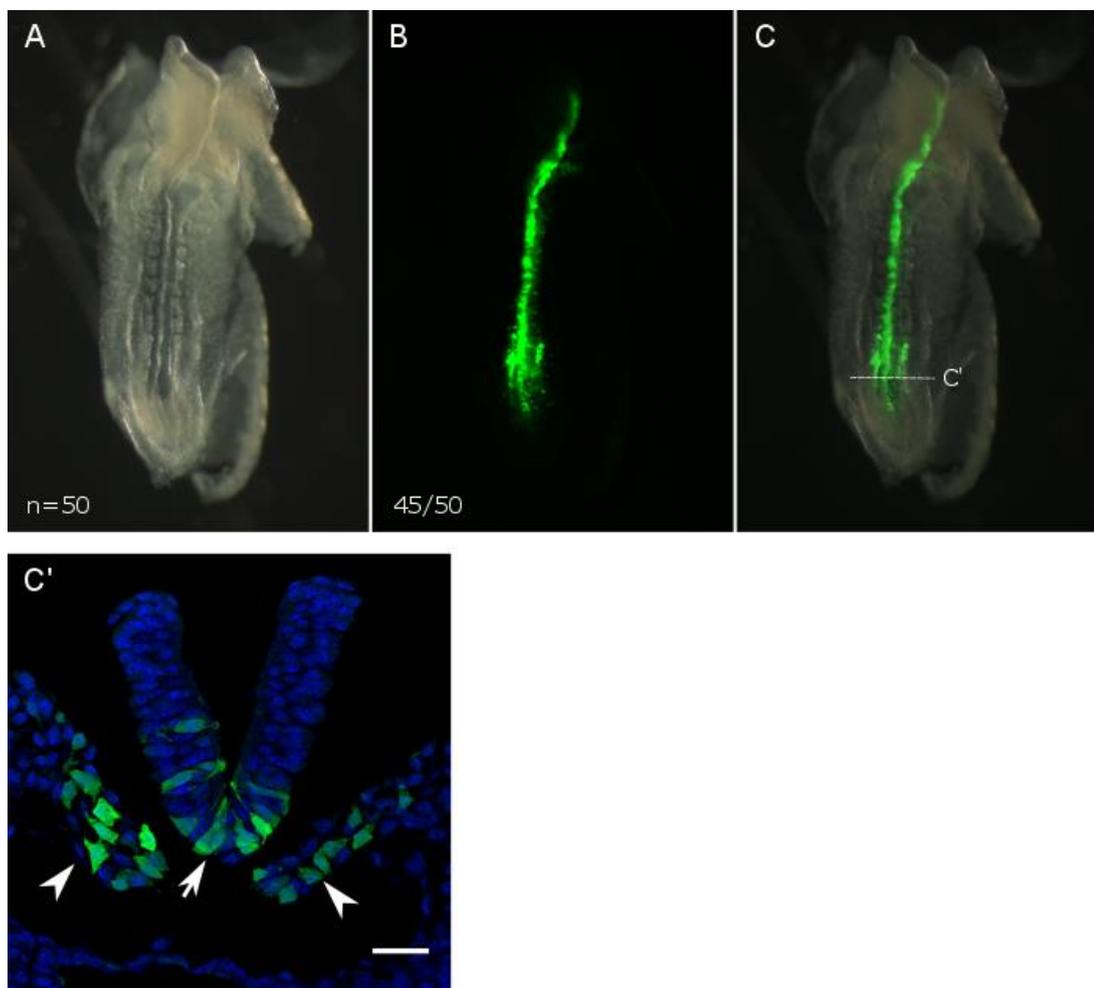
Figure 6.6 - Example of electroporated embryo

Electroporation of a GFP plasmid at E7.5 with a 24 hour subsequent culture period leads to GFP midline expression in approximately 90% of embryos (A-C). Cross-section through the embryo shown in C reveals a number of wedge shaped cells in the MHP (C'; arrow). Note also the GFP labelled cells in the paraxial mesoderm which probably reflects electroporation of the primitive streak (C'; arrowheads), as well as the node. Scale bar = 30 μm.
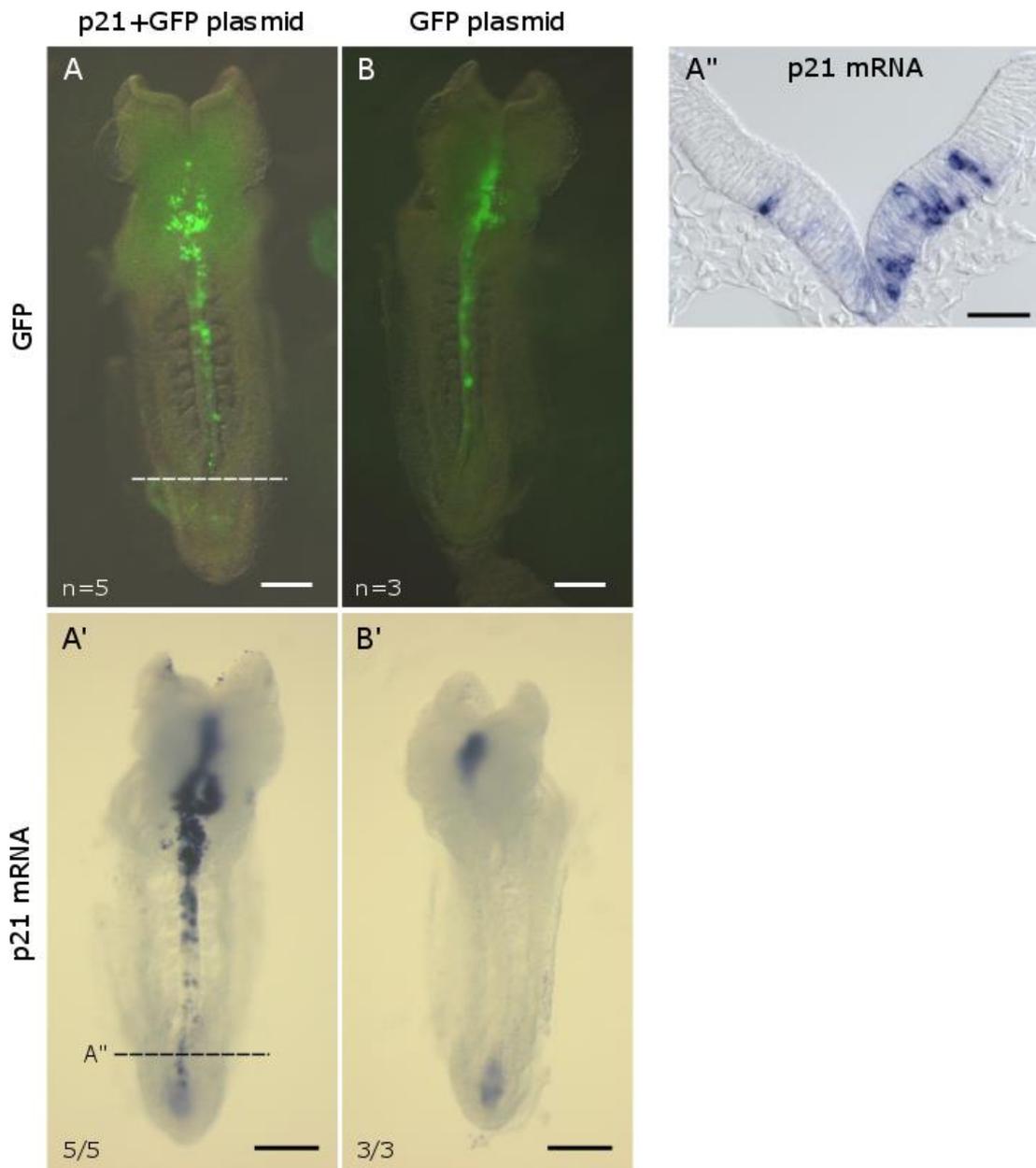
Figure 6.7 - p21 plasmid electroporation causes ectopic expression of p21 mRNA at E8.5

Embryos at E7.5 were electroporated with p21+GFP (A), or GFP only (B) and cultured for 24 hours. Note that both types of embryo show closely similar patterns of GFP expression (compare A and B). However, subsequent analysis by in situ hybridisation reveals dramatically increased expression of p21 along the midline in p21-electroporated embryos, corresponding to the GFP positive region (A-A'). Embryos electroporated with GFP do not show ectopic p21 expression (B-B'). Section through the PNP of an embryo electroporated with p21+GFP shows p21-expressing cells throughout the middle part of the neural plate, and not restricted to the MHP (A''). The level of section A'' is indicated on A'. Scale bars = 500 μm (A-B) and 50 μm (C).
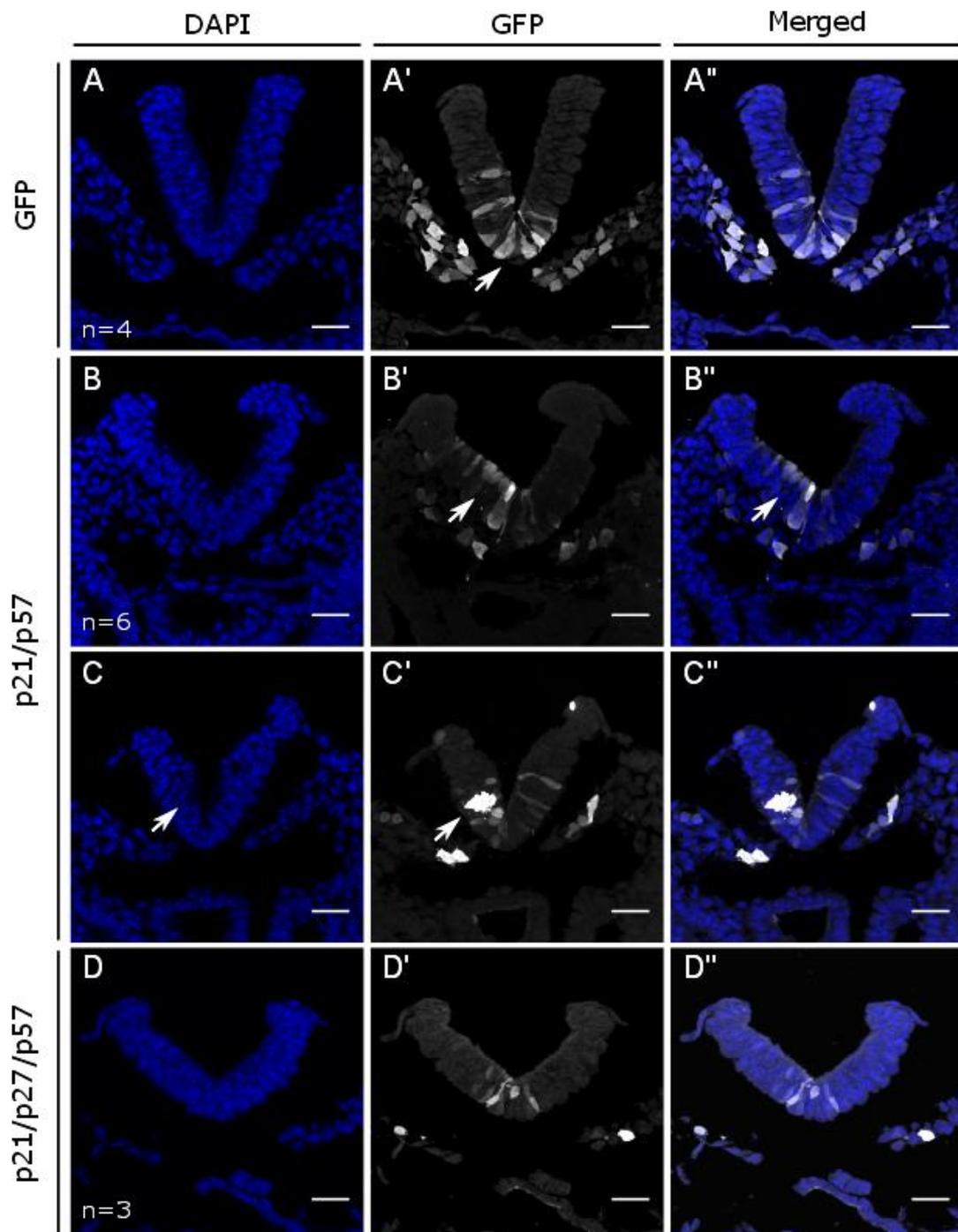
Figure 6.8 - Overexpression of CIP/KIP genes does not affect apparent MHP morphology at E8.5

Embryos electroporated at E7.5 with GFP control (A), or expression plasmids for p21 and p57 (B-C) or p21, p27 and p57 (D) have normal MHPs. Note the amount of wedge shaped cells in the MHP of a control embryo (A'-A''; arrows). Not all cells electroporated with p21 and p57 are basal (B-B''; arrows) but an embryo with a group of cells strongly expressing p21 and p57 shows a distinct indentation in the lateral neural plate (C-C''; arrows). Triple overexpression does not lead to any alteration in MHP appearance (D-D''). Scale bars = 30 µm.
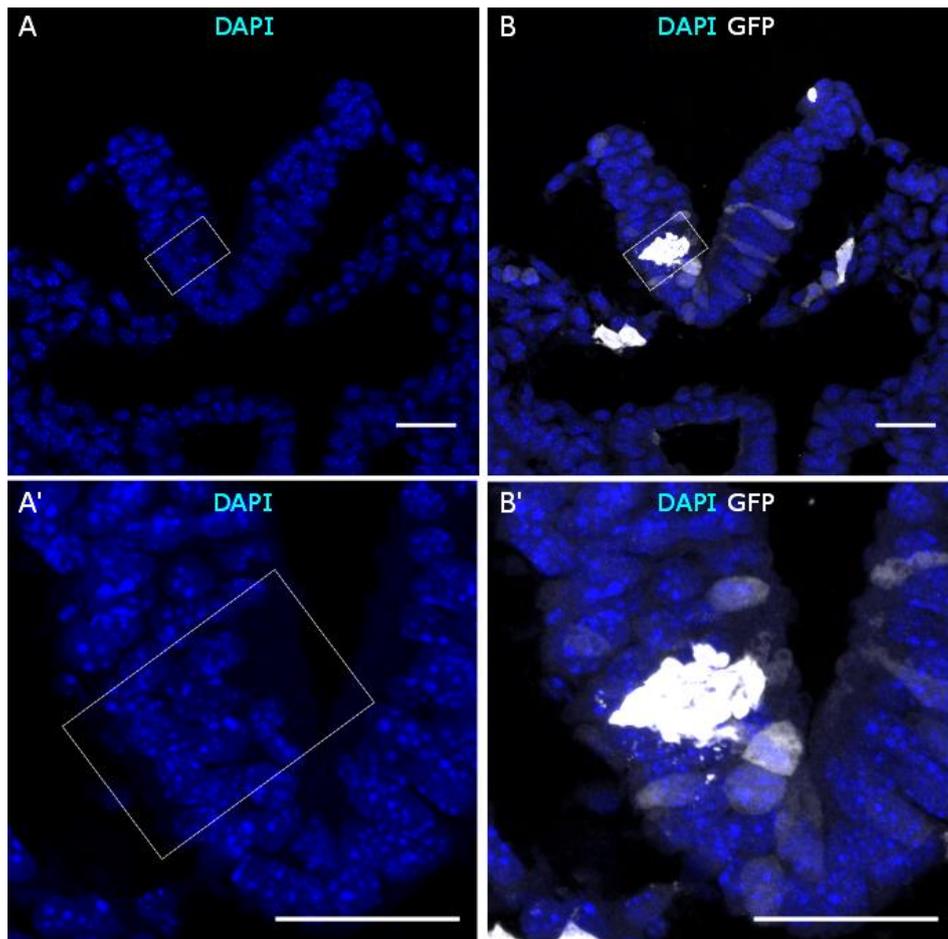
Figure 6.9 - A cluster of p21/p57 overexpressing cells coincides with indentation of neural plate

High density of EGFP indicative of p21 and p57 overexpression coincides with a region of relatively basal nuclei in the lateral neural plate, leading to indentation (inside white dotted box). Scale bars = 30 μm.

Nuclear position was quantified in embryos electroporated with plasmids expressing both p21 and p57; p21, p27 and p57, or GFP control. A region of at least 10 cells (GFP +ve and –ve) in the MHP and in the right and left lateral non-bending region was selected and the distance from the centre of the nucleus to the basal neuroepithelium was measured and presented as a proportion of total neuroepithelial distance (Figure 6.10, top). As in non-electroporated embryos, the MHP has significantly more basal nuclei than lateral regions (Figure 6.10, top). Embryos electroporated with p21 and p57 have significantly more basal nuclei in the MHP compared to embryos electroporated with p21/p27/p57, but not GFP only. In the lateral neural tube there is no difference between treatments.

However, the number of electroporated cells in the neural plate was generally low in this experiment (Table 6.1). Hence, the overexpressing plasmids were perhaps not expressed at high enough levels to cause an overall effect on nuclear localisation in either MHP or lateral regions.

Next, nuclear localisation was quantified in GFP positive (i.e. electroporated) cells only. I expected there to be a trend towards overexpressing cells having more basal nuclei, as the CIP/KIPs are able to inhibit the cell cycle in late G1-/S-/early- G2 phase when nuclei are mostly basal. While MHP cells have significantly more basal nuclei than lateral cells, there is no significant difference in nuclear localisation between the treatments in the MHP or in the lateral neural plate (Figure 6.10, bottom). Triple overexpression in the MHP is, however, again associated with more apical nuclei than double overexpression, suggesting that p27 might serve to counteract the effect of p21 and p57 in inducing a basal nuclear position. p21, p27 and p57 have all been shown to inhibit the cell cycle in G1 phase when they are overexpressed (Fero et al., 1996; Harper et al., 1995; Lee et al., 1995). It is possible that they could have this effect in electroporated embryos, and so inhibit the cell cycle in G1-phase, when nuclei might have a relatively apical position.

In order to examine whether GFP-positive nuclei were more likely to be basal compared to GFP-negative nuclei in the same region, basal nuclear distance of GFP-positive cells was compared to GFP-negative cells in the MHP and lateral regions for each treatment group. No significant difference was found in nuclear position for GFP-positive double overexpressing nuclei or triple overexpression nuclei compared to GFP-negative cells not overexpressing the CIP/KIP genes in the MHP or lateral regions (Table 6.2). Surprisingly, GFP-positive cells in the control group (empty GFP plasmid) were significantly more basal than GFP-negative cells (p=0.003). The reason for this result is unknown. However, as the control plasmid was not sequenced for verification upon arrival, there is a possibility that the plasmid is not empty.

	#Sections	Cells analysed (GFP+)		Cells per section	
		MHP	lat	MHP	lat
p21 and p57	15	171 (39)	197 (22.5)	11.4 (2.6)	13.1 (1.5)
p21, p27, p57	9	133 (47)	111 (0)	14.8 (5.2)	12.3 (0)
GFP control	14	174 (75)	171 (13)	12.4 (5.4)	12.2 (0.9)

Table 6.1 - Quantification of the number of cells analysed for nuclear position at E8.5

The total number of cells analysed per treatment is shown with the number of GFP +ve cells in parentheses. Note that on average, 2.6-5.4 GFP+ve cells were observed in the MHP while the number of GFP+ve cells was very small in the lateral regions analysed.

All cells (GFP +ve and -ve)
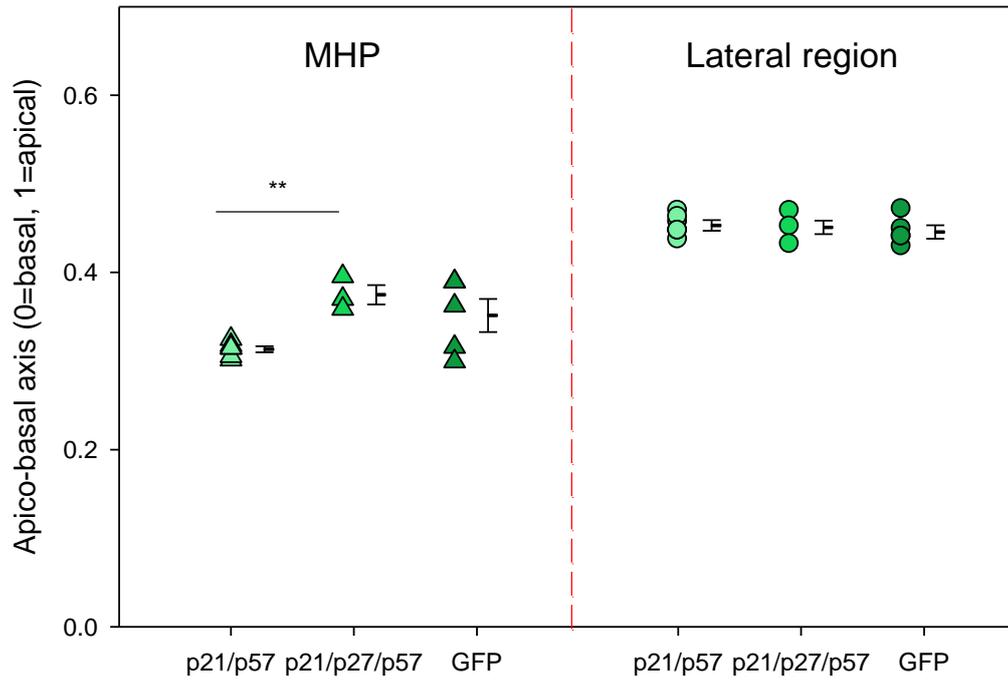
GFP +ve cells
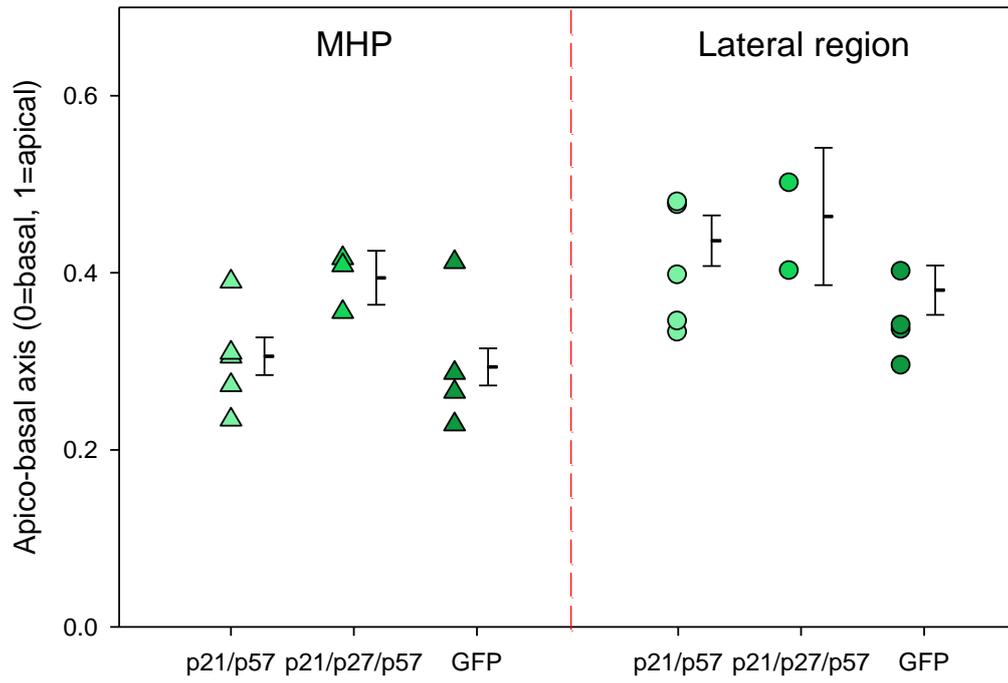
Figure 6.10 – Effect of overexpressing CIP/KIP genes on nuclear position in the neural plate

Embryos electroporated with p21/p57, p21/p27/p57, or GFP control at E7.5 and cultured for 24 hours were analysed for average nuclear position. Basal nuclear distance was measured in >10 cells in the MHP and in right and left lateral non-bending regions regardless of GFP status (top), or only in GFP positive cells (bottom). **Top:** Embryos electroporated with p21/p57 have significantly more basal nuclei than triple overexpression (p<0.001; Two way ANOVA). Comparisons of p21/p57 vs GFP and p21/p27/p57 vs GFP are not significant (Two way ANOVA). There is a significant difference between nuclear position in the MHP and lateral region (p<0.001) but not between treatments in the lateral region (Two way ANOVA). **Bottom:** there is no significant difference between treatments in either region while nuclear position between the MHP and the lateral regions is significantly different (p=0.02; Two way ANOVA). Error bars are +/-SEM.

	GFP +ve (mean +/-SEM)		GFP-ve (mean +/-SEM)	
	MHP	**lateral**	**MHP**	**lateral**
p21 and p57	0.31 (0.06)	0.44 (0.05)	0.31 (0.01)	0.46 (0.01)
p21, p27, p57	0.39 (0.02)	-	0.36 (0.01)	0.45 (0.01)
GFP control*	0.30 (0.04)	0.34 (0.05)	0.37 (0.02)	0.45 (0.01)

Table 6.2 - Basal nuclear distance (mean +/-SEM) for GFP +ve and GFP -ve nuclei

Mean basal nuclear distance of GFP +ve and GFP –ve nuclei measured on 9-15 sections from at least 3 embryos per treatment. Difference between basal nuclear distance is not significant between GFP+ve and GFP-ve cells for p21/p57 (p=0.57; Two-way ANOVA) or p21/p27/p57 (p=0.24; t-test). GFP+ve cells are significantly more basal than GFP–ve cells in the control group (p=0.003; Two way ANOVA). Cells of the MHP are more basal than lateral cells in all treatment groups. This difference is significant for p21 and p57 treated embryos (p<0.001).

6.2.4   p57 knock-down in a p21$^{-/-}$ background

Under the experimental conditions I used, overexpression of the CIP/KIP genes was not found to be sufficient to induce increased 'MHP-like' bending of the neural plate. To test whether CIP/KIP genes are necessary for MHP bending, I electroporated a p57 siRNA into the neural plate of p21$^{+/+}$ and p21$^{-/-}$ embryos to achieve double knock-down of p21 and p57. A tagged oligo was used together with p57 siRNA or the GC-matched siRNA control that could be visualised in the midline of successfully electroporated embryos after 24 hours of culture (Figure 6.11, B; arrow). Only embryos where the tagged oligo could be visualised in the neural tube were analysed. A cross section through an embryo with siRNA in the midline reveals that most of the siRNA is targeted to and around the MHP (Figure 6.11, D).

In order to validate knock-down by the p57 siRNA, CD1 embryos were electroporated with p57 siRNA or siRNA control together with the tagged oligo. After 24 hours of culture, embryos that were labelled in the midline with the tagged oligo were processed for in situ hybridisation with a probe against p57 mRNA. None of the five embryos electroporated with the p57 siRNA display p57 mRNA in the neuroepithelium or the notochord (*) although expression is maintained in the hindgut (arrow) (Figure 6.12, A-C'). In contrast, all 4 embryos electroporated with the control siRNA show the presence of p57 mRNA in the neuroepithelium and notochord as well as in the hindgut (Figure 6.12, D-F'). The loss of p57 mRNA in the neuroepithelium was very consistent between embryos as shown in Figure 6.13. The complete loss of p57 is astonishing considering the low efficiency of GFP electroporated cells shown in Figure 6.8 and the extent of siRNA speckles shown in Figure 6.11. It is possible that the loss of p57 from the neural plate is a secondary effect resulting from the initial knock-down of p57 in the node which could affect several pathways that, in turn, could result in complete loss of p57 in some tissues, e.g. the neural plate.
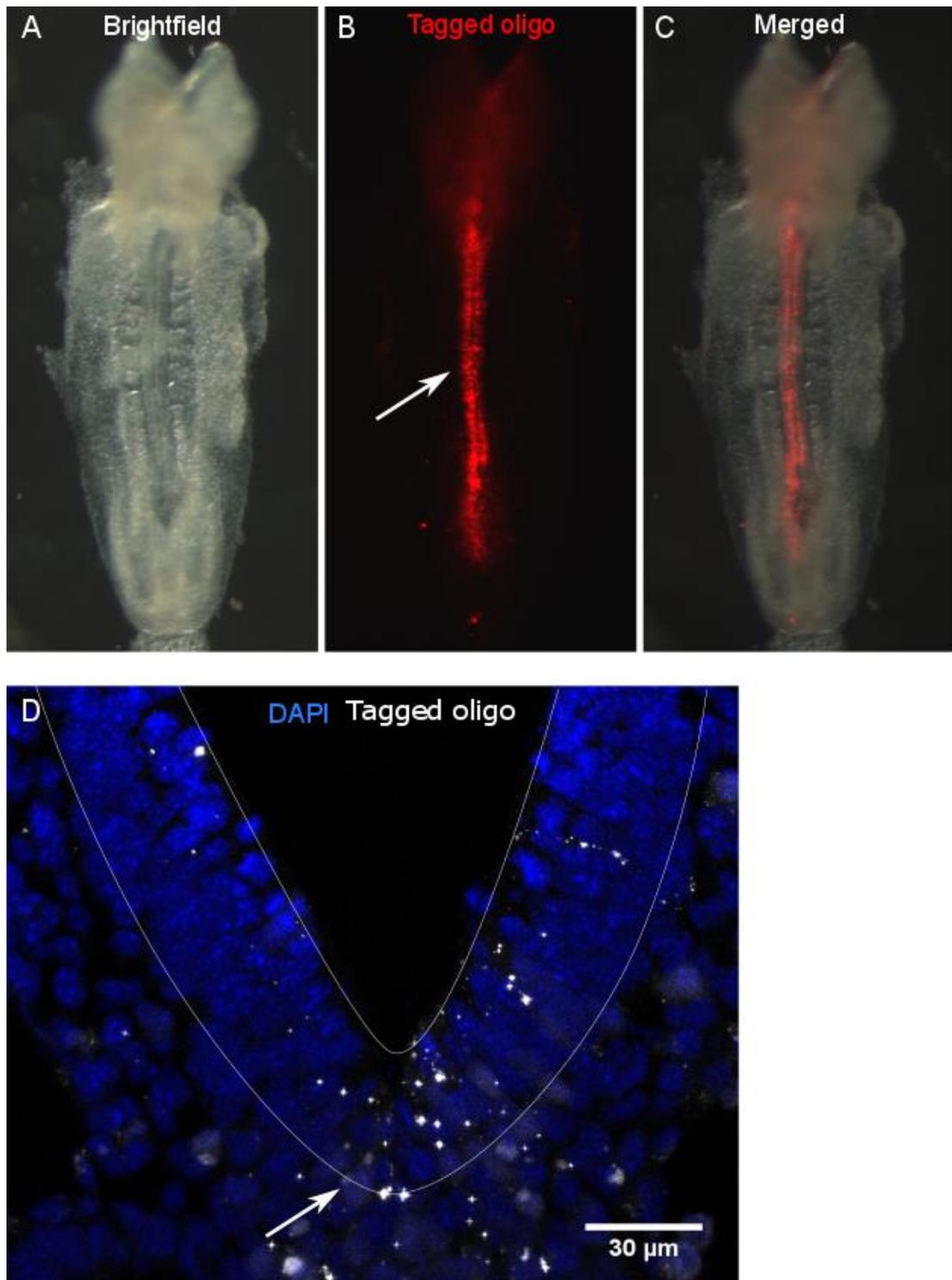
Figure 6.11 - siRNA is targeted to the neural plate midline

Electroporating a tagged siRNA through the node at E7.5 labels the neural plate midline after 24 hours of culture (B; arrow). This uptake can be visualised in cross-sections (D; arrow).

Tagged oligo	Merged	p57 mRNA	p57 mRNA
A	B	C	C´
D	E	F	F´

p57 siRNA

control siRNA

5/5

4/4
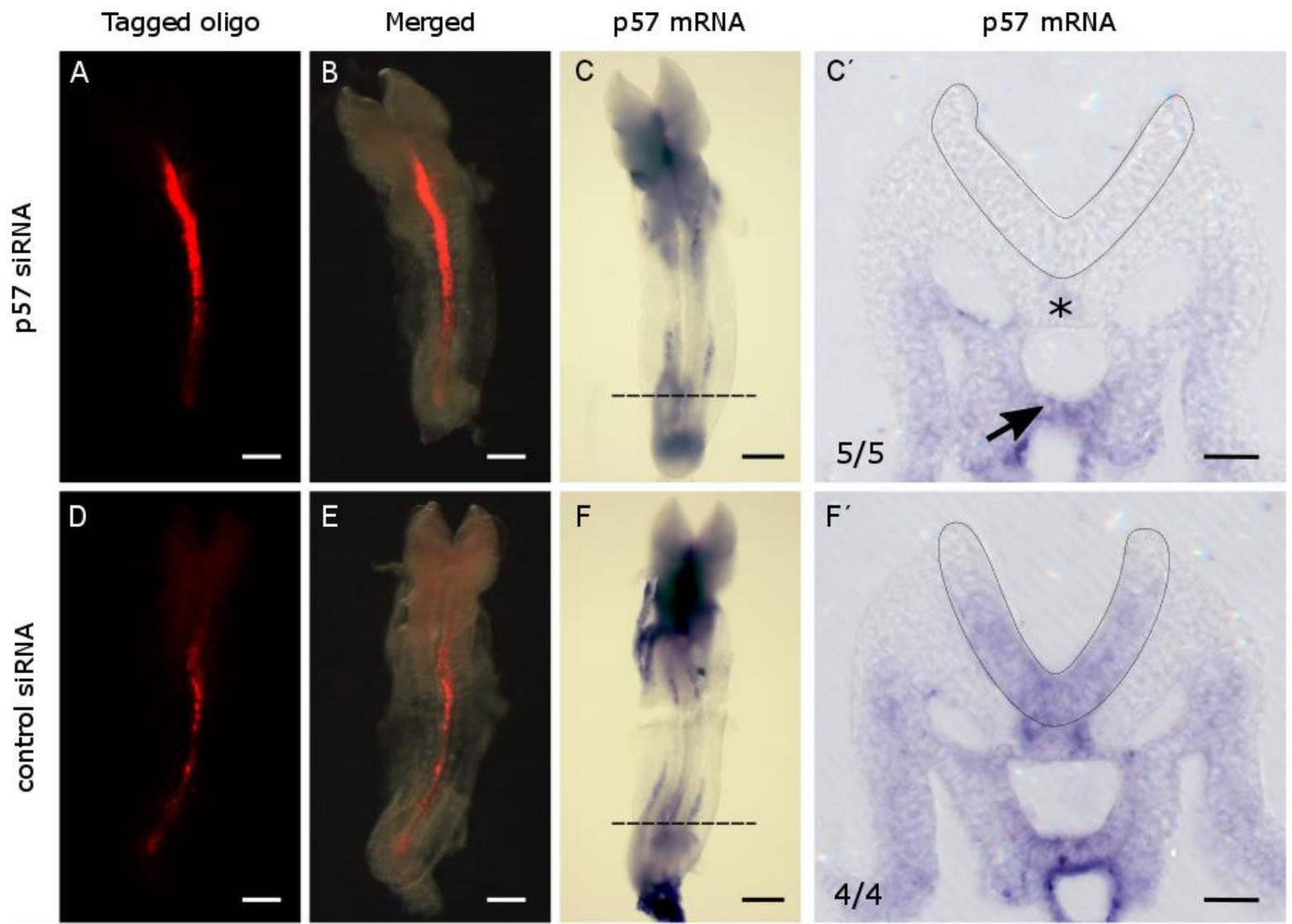
Figure 6.12 - siRNA mediated knockdown of p57 abolishes mRNA in the neuroepithelium at E8.5

Embryos were collected at E7.5 and electroporated with p57 siRNA or a GC control siRNA and cultured for 24 hours. Embryos with midline expression of the tagged oligo were processed for whole mount in situ hybridisation for p57 and sectioned. 5/5 embryos electroporated with p57 siRNA have lost the expression of p57 in the neuroepithelium (inside dotted lines) and the notochord (*), whereas staining is retained in the ventral hindgut (arrow) (A-C'). All 4 controls have retained staining in the neuroepithelium, notochord and hindgut. Scale bars = 500 μm (A-F) and 50 μm (C' and F').
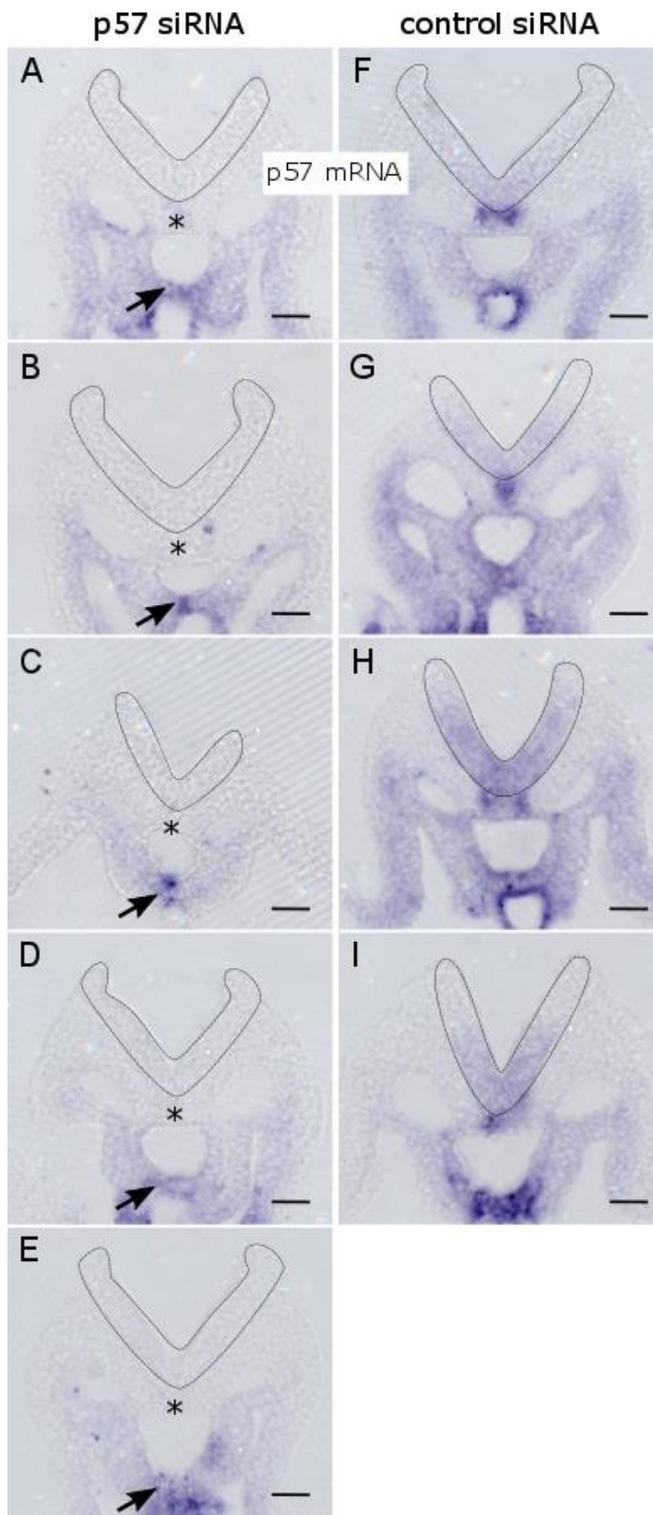
Figure 6.13 - Consistent loss of p57 mRNA upon siRNA treatment

Sections through 5 different embryos (A-E) electroporated with p57 siRNA at E7.5 all show loss of expression of p57 in the neuroepithelium (inside dotted lines) and in the notochord (*) at E8.5 (A-E). Hindgut expression (arrow) is seen in all siRNA-treated embryos. In contrast, sections through 4 different control embryos show p57 mRNA in the neuroepithelium, notochord, and hindgut (F-I). Scale bars 50 = μm.

In order to quantify the knock-down by p57 siRNA, neural tube midlines were dissected from E8.5 CD1 embryos using tungsten needles (Figure 6.14, A; along white dashed lines). The tagged oligo is detected in isolated midlines and is localised to the neural tube rather than the notochord which was not removed from the neural tube (Figure 6.14, B-D; arrows).

6-7 isolated neural midlines were pooled per sample and the level of p57 mRNA as well as p21 and p27 was quantified by qRT-PCR (Figure 6.15). p57 mRNA is reduced following electroporation of p57 siRNA compared to siRNA control, although the reduction does not reach statistical significance (Figure 6.15). p21 and p27 expression in the same midlines is slightly increased although the three replicate samples vary somewhat. Thus, taking together both the embryo in situ hybridisation and qRT-PCR studies of isolated midlines, I can conclude that p57 expression is consistently and specifically reduced in the neural plate of embryos electroporated with p57 siRNA.
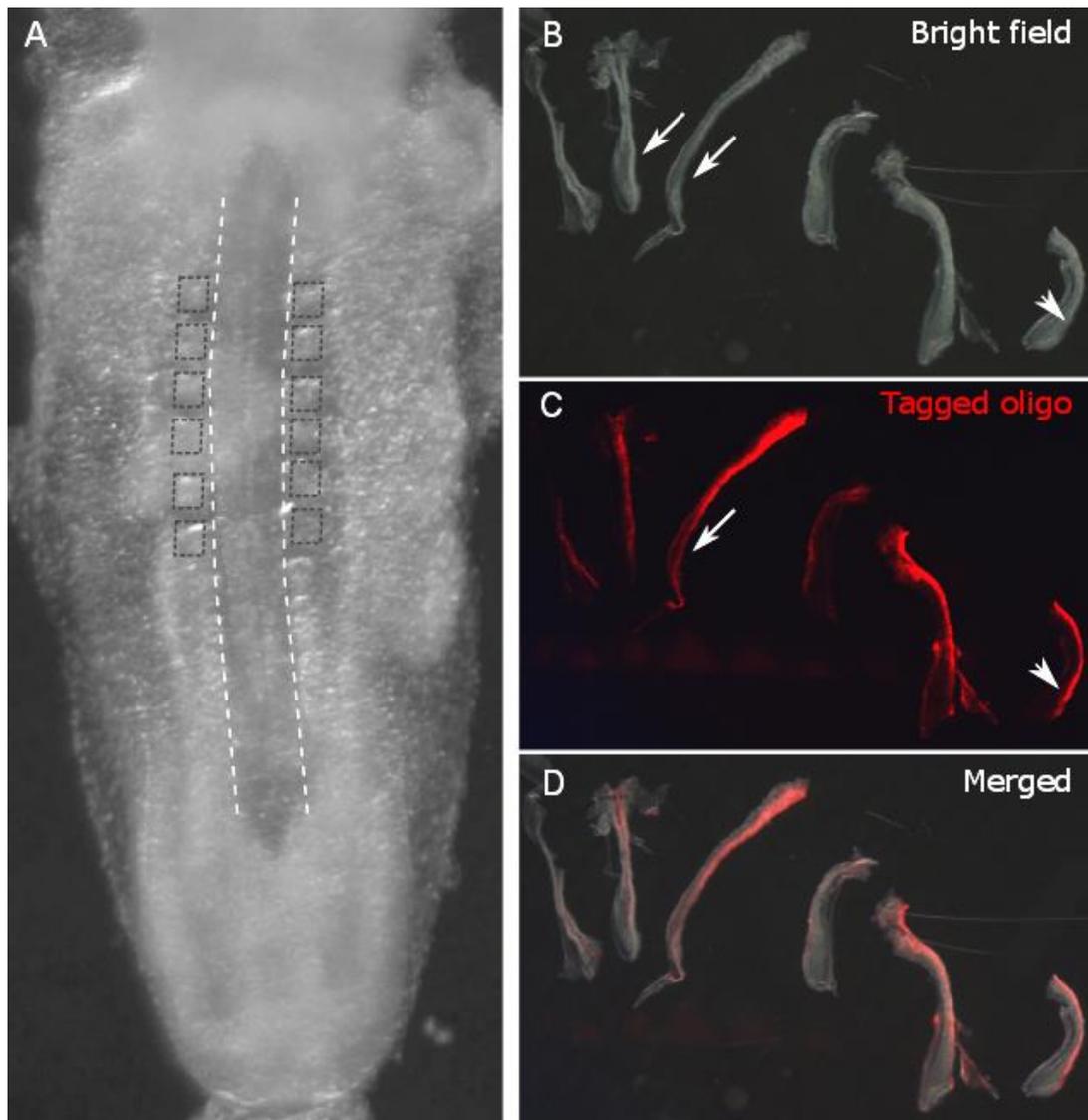
Figure 6.14 - Isolated neural plate midlines specifically express a tagged siRNA

Neural midlines were isolated from embryos at E8.5, 24 hours after electroporation with a tagged siRNA together with p57 siRNA or control siRNA. Embryos were digested in 2% pancreatin before the midline was dissected out with tungsten needles along the indicated lines, taking care not to collect somites (dotted squares) (A). Neural plate midlines were collected along with the most caudal flat neural plate (B; arrows). The tagged siRNA can be visualised specifically along the length of the dissected neural midlines. Note that the strongest expression domain is in the neural tube and not in the underlying region containing the notochord (B-C; arrowhead). 6-7 midlines were pooled per sample. Samples were subsequently quantified for CIP/KIP mRNA by qRT-PCR.
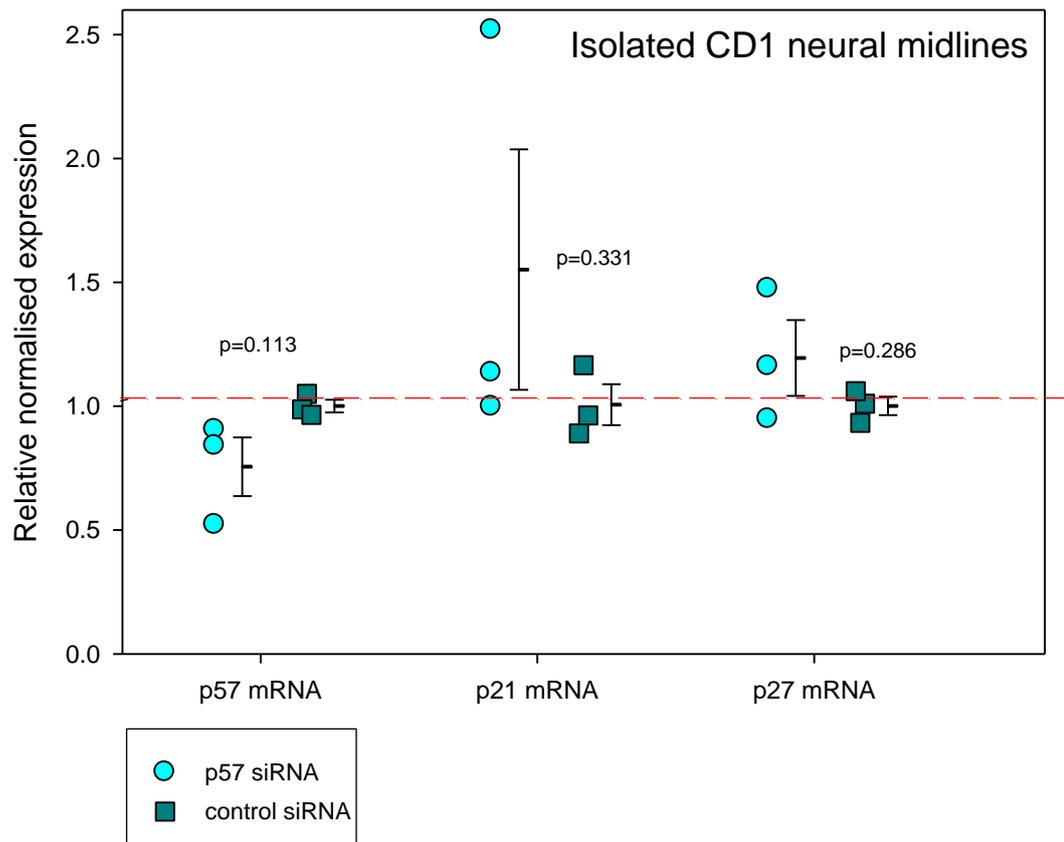
Figure 6.15 - p57 mRNA is reduced in siRNA treated isolated CD1 neural midlines

CD1 embryos at E7.5 were electroporated with CIP/KIP siRNAs or control siRNA followed by a 24 hour culture. CIP/KIP mRNA levels were assayed in three samples of 6-7 pooled midlines from each treatment group. Gene expression was determined by qPCR relative to expression in control siRNA samples. p57 mRNA levels were reduced following p57 siRNA treatment although not statistically significant. p-values, as determined by Student's t-test, are shown on the graph.

I have shown that the p57 siRNA is efficient in abolishing p57 mRNA in the neural plate of mouse embryos. To examine the requirement for CIP/KIP function in midline bending, a few embryos that were wild-type or deficient for p21 were electroporated with p57 siRNA to achieve double knock-down in the mutant embryos. The number of embryos in this analysis is very small and this is therefore a very preliminary result.

$p21^{-/-}$ embryos electroporated with p57 siRNA do not display abnormal MHP bending (Figure 6.16, A-B) compared to $p21^{-/-}$ embryos treated with the control siRNA (Figure 6.16, C-E) although the 'double mutant' MHP looks blunted (especially Figure 6.16, B). p57 knock-down on a p21 deficient background was further examined by measuring the nuclear position of cells in the MHP. There was no statistically significant difference between the nuclear position in the MHP of $p21^{-/-}$ or $p21^{+/+}$ embryos treated with p57 siRNA or control siRNA (Figure 6.17), although one p57 siRNA treated $p21^{-/-}$ embryo had an average nuclear position higher than controls (Figure 6.17).
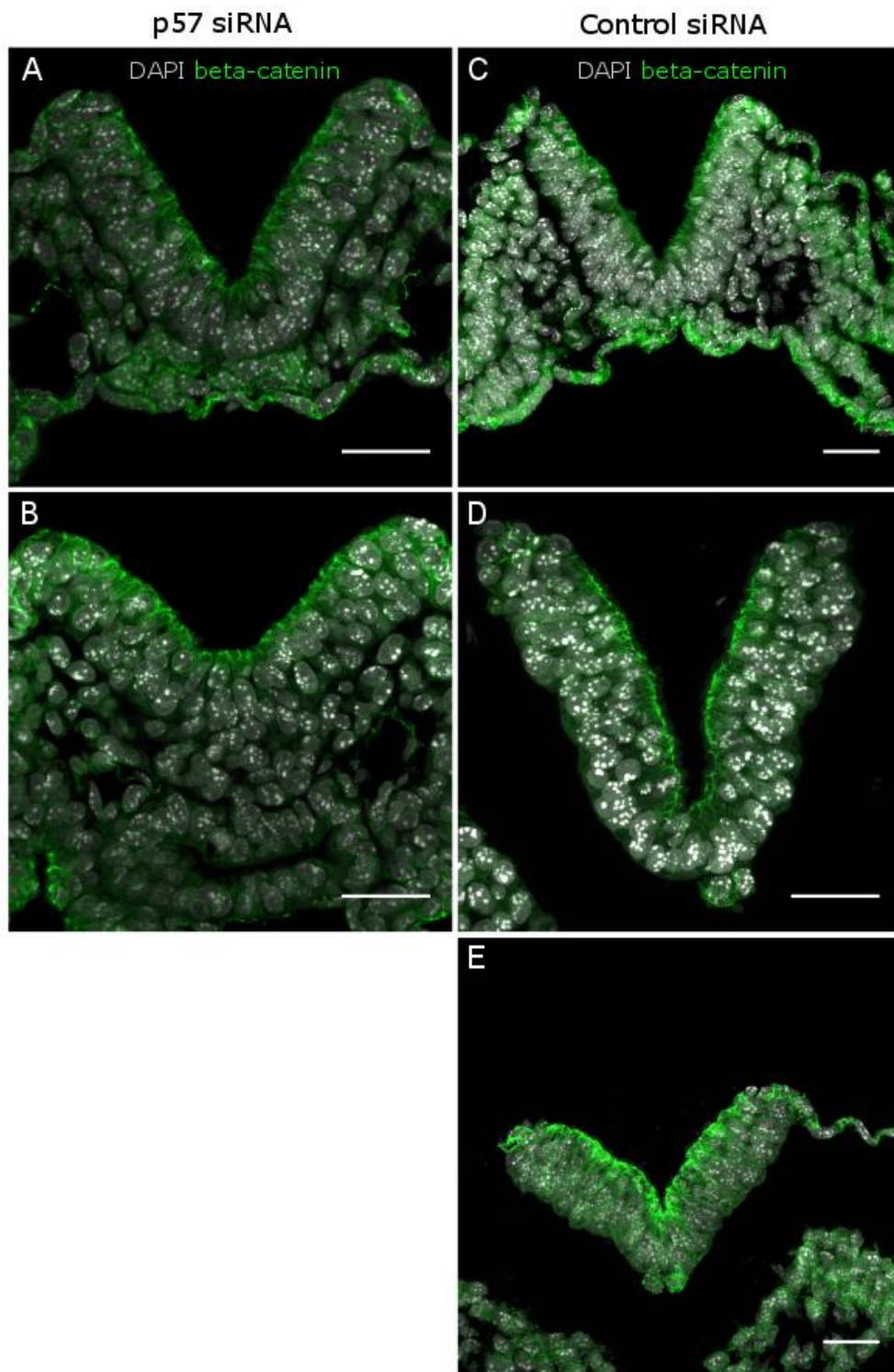
Figure 6.16 - p21/p57 knockout does not abolish the MHP

p21$^{-/-}$ embryos were electroporated with p57 siRNA at E7.5 and cultured for 24 hours. One out of two p21$^{-/-}$ p57 siRNA treated embryos has a blunted MHP (B) compared to the sharp, typical bend in C-E, suggesting that MHP formation might be altered in the absence of p21 and p57. Scale bars = 30 µm.
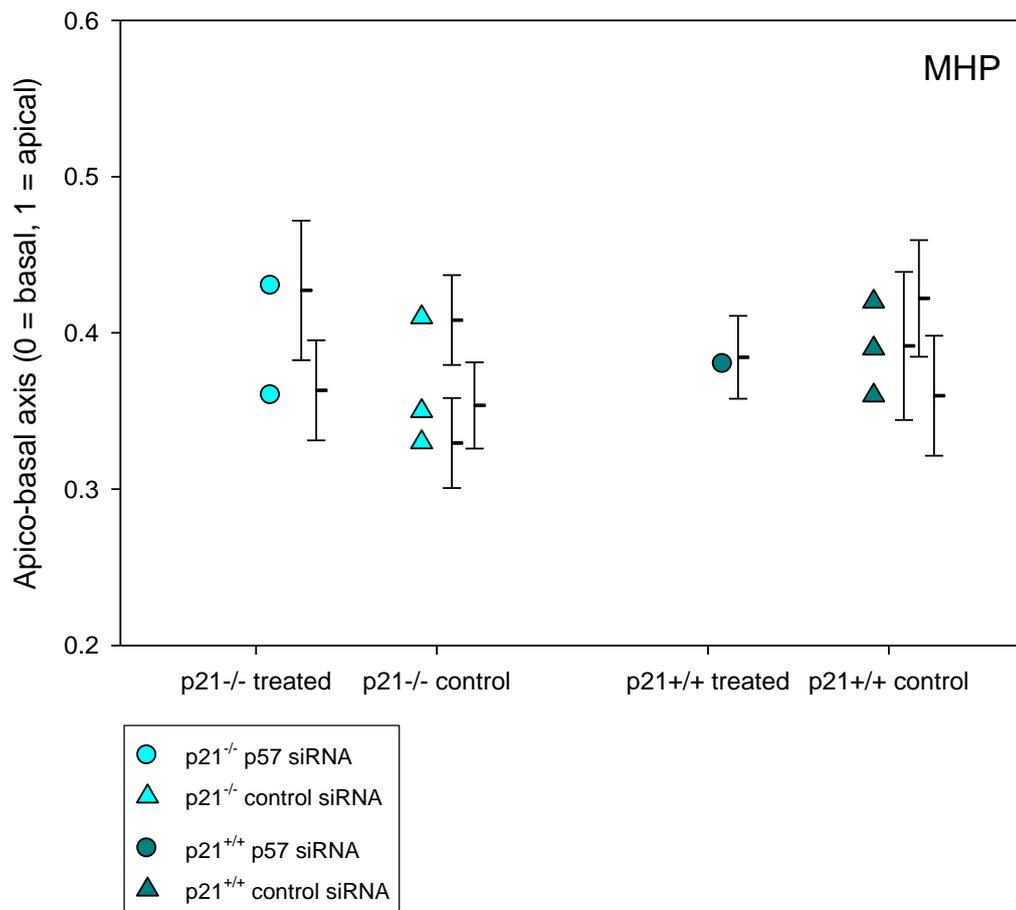
Figure 6.17 – Nuclear position following siRNA mediated knock-down of p57

p21$^{-/-}$ and p21$^{+/+}$ embryos electroporated at E7.5 with p57 siRNA or a control siRNA were analysed for average nuclear position in the MHP after a 24 hour culture. Each point represents an embryo with +/-SEM for each embryo. The difference in the mean values between treatments is not significant after accounting for genotype (p=0.84; Two way ANOVA).

6.3 Discussion

In this chapter I attempted to test the significance of MHP expression of p21, p27 and p57 by testing whether these genes are necessary or sufficient for MHP formation. I used a whole embryo culture system to manipulate CIP/KIP levels in the neural plate of intact mouse embryos. Electroporation of the mouse neural plate was reproducible and reliable, with evident results on p21 and p57 gene expression.

6.3.1 Overexpression of CIP/KIPs

In all overexpressing experiments the number of electroporated cells in the neural tube was sparse as revealed by the number of cells with ectopic expression of p21 (in situ hybridisation), as well as the number of GFP positive nuclei indicating overexpressing CIP/KIP cells.

Overexpression of the CIP/KIP genes did not affect overall MHP morphology. It is difficult to say whether this is due to the low number of GFP-positive cells observed. It is clear, however, that if indentation of the neural plate is the result of simultaneous basal expansion of a group of cells, due to basal nuclear position, then 2-5 scattered overexpressing cells would be unlikely to be sufficient to cause bending. The lack of effect on the apico-basal position of nuclei (GFP +ve and –ve) in the MHP is in line with the low occurrence of overexpressing cells. It is, however, surprising that basal position of GFP-positive nuclei is so similar to that of the total number of nuclei in the MHP or lateral regions, and suggests that overexpression of the CIP/KIP genes is not sufficient to induce basal expansion. In fact, p21 and p57 overexpressing nuclei were particularly apical in one embryo analysed. There was, however, one embryo with a high density of the p21 and p57 overexpressing plasmids that had an ectopic indentation in the lateral neural plate. This suggests that, at high densities, p21 and p57 might be able to induce an ectopic hinge point. The only expression plasmid that had an effect on nuclear position in the MHP was the GFP control plasmid that should not express additional genes. The difference between basal distance of GFP +ve and GFP –ve nuclei of control embryos was statistically significant, suggesting that the plasmid induced basal expansion in the MHP and in the lateral region. The plasmid has not been sequenced for verification. In light of these experiments, that would be important to do.

Electroporated embryos that overexpressed the CIP/KIP genes had a tendency to form premature DLHPs at E8.5. In the mouse, Bmp2 expression in the dorsal neural folds inhibits DLHPs during early neurulation when the neural plate is V-shaped (Ybot-Gonzalez et al., 2007a). As neural tube closure proceeds in the caudal direction, Noggin expressed from the notochord inhibits Bmp2 and DLHPs form

(Ybot-Gonzalez et al., 2007a). In neural stem cells, p21 directly represses Bmp2 at the transcriptional level and loss of p21 leads to upregulation of Bmp2 mRNA and protein (Porlan et al., 2013). Addition of p21 or Noggin prevents Bmp2 upregulation (Porlan et al., 2013). Thus, in p21 overexpressing embryos, Bmp2 in the dorsal neural folds might be inhibited, allowing premature DLHPs to form.

A lot of time was spent on optimising the electroporation technique in order to achieve the maximum number of electroporated cells. In order to target the neural plate midline, the node was electroporated. Because the node lays down cells of the midline, the original population of electroporated cells goes through many rounds of cell division, and, judging by the GFP-positive cells observed on sections, leaves behind between 2.6 and 5.4 cells in the MHP at any one axial level. Hence, although the neural plate midline can be targeted by electroporation, it will be hard to achieve a higher density of GFP-positive cells in the MHP using the current method. The aim was to overexpress the CIP/KIP genes in the lateral neural folds by electroporating this region in E8.5 embryos. This could have led to a concentrated population of overexpressing cells. Unfortunately, this method did not work well.

In the chick midbrain, Noggin overexpression has been shown to cause ectopic hinge point formation even with low electroporation efficiency (Eom et al., 2012). Furthermore, the plasmid concentrations used in that study (0.02-5 µg/µl) (Eom et al., 2012) correspond to the concentrations I have used (3.2 µg/µl). Thus, it is possible that my experiment worked but gave a negative result.

6.3.2 Double CIP/KIP deficiency in the neural plate

Although the number of GFP-positive cells in the overexpressing experiments was very scarce in the neuroepithelium, siRNA knock-down of p57 by the same method resulted in consistent and total abolition of p57 mRNA in the neuroepithelium. The siRNA result is curious, suggesting that the whole neural plate and notochord are targeted, in contrast to what is indicated by the GFP expression in the overexpressing experiments. It could be speculated that the siRNA is smaller and enters cells more easily than the larger plasmids during electroporation. I have,

however, accounted for this: in experiments where the GFP plasmid and the tagged oligo were electroporated together, I found that 94% of cells labelled with the siRNA had also taken up the GFP plasmid. It is more likely that the complete loss of p57 from the neural plate is secondary as a result of p57 knock-down in the node.

Importantly, the p57 in situ hybridisation data following knock-down suggests that $p21^{-/-}$ p57 siRNA treated embryos are in fact double null in the neural plate. The MHP looks blunted in one of the 'double null' embryos, and the other embryo has an average nuclear distance from the basal surface greater than that of $p21^{-/-}$ embryos electroporated with a control siRNA. As the knock-down effect of the p57 siRNA is very striking, it would be very important to repeat these experiments in $p21^{-/-}$ embryos in order to analyse nuclear position and MHP shape in a larger number of embryos.

Interestingly, the embryos electroporated with the p21 and p57 expression plasmids have an average distance from the basal surface of the neural plate of between 3 and 3.2 whereas the two $p21^{-/-}$ embryos electroporated with p57 siRNA have values of 3.6 and 4.3. An interpretation of these results could be that overexpression makes the nuclei more basal and double knock-down more apical. It is, however, worth keeping in mind that CD1 mice were used for the overexpression experiments and p21 mice for the knock-down. Furthermore, the differences observed in apico-basal position are quite small.

6.3.3 Role of p27 in basal expansion?

p27 is expressed in G1 phase and the expression has been suggested to keep cells from entering S-phase. Consequently, p27 levels have to fall for cells to enter S-phase (Moran and Rice, 1976). Thus, it could be that overexpression of p27 prevents the cells from entering S-phase, thereby inhibiting basal expansion and abolishing the effect p21 and p57 seem to have on nuclear position. Furthermore, loss of p57 is associated with increased S-phase entry in cortical precursors (Mairet-Coello et al., 2012) and overexpression leads to G1-phase arrest (Lee et al., 1995; Matsuoka et al., 1995) suggesting that p57 might be preventing cells from entering

236

S-phase in some systems. On the other hand, G1- and S-phase length was reduced in ventricular zone precursors in the absence of p57, suggesting a role for p57 in regulation of S-phase length (Mairet-Coello et al., 2012) although the effect was much more pronounced on G1-phase length. p21 overexpression has also been found to inhibit the cell cycle in G1-phase (Harper et al., 1995) whereas RNA mediated knock-down was suggested to be permissive of S-phase entry (Nakanishi et al., 1995). It could therefore be that a high level of the CIP/KIP genes in general prevents S-phase entry. Thus, high levels of p21, p27 and p57 specifically in the MHP could block cells at the G1/S-phase transition when cells are not necessarily basal.

6.3.4 Analysing the cell cycle in the embryo culture system

The aim was to use thymidine analogues with pHH3 to analyse changes in the cell cycle following overexpression and knock-down of CIP/KIP genes, similar to the analysis in Section 5.2.2. Many attempts were made to make use of thymidine analogues in the embryo culture system. EdU was tested extensively while IdU and BrdU labelling was attempted once. As previously found in our laboratory, BrdU labelling in culture resulted in poor tissue penetrance. The same was found for IdU. EdU worked very well on a couple of occasions, but failed to work in the final experiments despite changing the reagents one by one and re-testing on positive samples. An alternative could have been Ki67 which is expressed in all phases of the cell cycle and is useful as a tool to assign cells to individual phases based on the staining pattern (Braun et al., 1988).

In conclusion, overexpression of CIP/KIP genes does not lead to an exaggerated MHP. Whether this is due to low transfection efficiency or because CIP/KIP overexpression causes G1-phase arrest is unknown. Thymidine labelling would have revealed whether the cells were blocked prior to S-phase. p57 knock-down in a $p21^{-/-}$ background results in a p21/p57 deficient neural plate but does not prevent MHP formation. Further studies are required to assess whether MHP formation is affected in these 'double mutant' neural plates.

Chapter 7 - General discussion

In this thesis I have shown that the cyclin-dependent kinase inhibitor family CIP/KIP is expressed in the MHP during mouse neurulation, in a spatial and temporal pattern that fits with formation of the MHP. p21 was shown to be strongly implicated in being responsible for the prolongation of S-phase that accompanies midline furrowing and the transition of the medial neural plate into a wedge shaped population. In the absence of p21, S-phase in the MHP and lateral region was essentially the same, which is contrary to the wild-type setting where S-phase is prolonged by roughly 30%. Importantly, MHP formation is apparently normal in p21$^{-/-}$ embryos, showing that a prolonged S-phase is not necessary for MHP formation. Overexpression of the CIP/KIPs did not lead to exaggerated bending but rather caused ectopic DLHPs, possibly through p21 mediated inhibition of Bmp2 in the dorsal neural folds. Knock-down of p57 in the neural plate in a p21$^{-/-}$ background did not abolish MHP formation but in a small sample number there seemed to be an effect on the 'sharpness' of the MHP.

7.1 Mechanisms of MHP formation

There has been a lot of focus on basal expansion and cell cycle prolongation regarding MHP formation in the mouse and chick neural plate. I have shown that loss of p21 is sufficient to abolish the regional differences in S-phase length in the MHP. Importantly, a prolonged S-phase in the MHP is not necessary for MHP formation. This is evident in p21$^{-/-}$ neural plates which are morphologically indistinguishable from wild-type embryos.

There is some evidence that cell wedging might precede neural plate bending as discussed in Chapter 3 (McShane et al., 2015; Smith and Schoenwolf, 1987; Smith and Schoenwolf, 1988). However, in light of the findings of this thesis it seems possible that cell cycle driven cell wedging is not responsible for MHP formation. On the other hand it seems unlikely that bending of the neural plate causes cell wedging by compression of the cells by crowding. Firstly because cell wedging has

been reported in neural plate midlines that have been separated from lateral tissues (Alvarez and Schoenwolf, 1992; Schoenwolf, 1988), and secondly, because the high proportion of wedge shaped cells in the MHP is observed in the relatively flat neural plate before a proper bend is found in the midline (Schoenwolf and Franks, 1984). So what other mechanisms could be responsible for MHP formation?

7.1.1   CIP/KIPs as cytoskeletal regulators of MHP formation

As introduced in Chapter 1, all three CIP/KIP genes act on the Rho pathway to regulate actin stress fibre formation. p27 inhibits RhoA, p21 inhibits ROCK, and p57 translocates LIMK from the cytoplasm to the nucleus where it can no longer phosphorylate and inactivate cofilin (Besson et al., 2008). The Rho GTPases are a family of small GTPases that are regulators of actin and microtubule dynamics and, importantly, control cell shape and motility (Etienne-Manneville and Hall, 2002). Thus, the CIP/KIP genes in the neural plate could be involved in cell shape regulation independently of their cell cycle role. In support of this, Rho, F-actin and pMLC, a downstream target of Rho, seem to localise to the forming MHP in chick embryos (Haigo et al., 2003). Furthermore, inhibition of actin, myosin II, Rho or ROCK affects neural tube closure in the chick (Kinoshita et al., 2008). In Drosophila, the inhibition of ROCK perturbs apical migration, suggesting that ROCK might be an upstream activator of actomyosin contraction during IKNM (Meyer et al., 2011). Thus, the CIP/KIP genes could be directly involved in IKNM by regulating the Rho pathway. Interestingly, p57 has been found to be expressed in all the tissues reported to exhibit IKNM in Table 1.1. p21 and p27 have also been reported to be expressed in some of the tissues, as described in Chapter 3. CIP/KIP analysis with antibodies would have revealed whether the proteins are cytoplasmic and thereby possibly involved in regulation of the cytoskeleton.

There are, however, some indications that actomyosin might not be required for MHP formation. First, actin is not localised specifically to the MHP in the mouse but is present in apices in all of the neural plate (Ybot-Gonzalez and Copp, 1999) suggesting that actin is not responsible for regional changes in cell shape. The study in the mouse did, however, not look at the forming MHP region equivalent to the

region in the chick that was enriched for Rho and actin. Furthermore, disruption of actin-microfilaments with Cytochalasin D does not prevent cell wedging and MHP formation in the mouse or chick embryo, suggesting that MHP formation and cell wedging is actin independent (Schoenwolf et al., 1988; Ybot-Gonzalez and Copp, 1999). Even though the early events of neural plate bending, i.e. MHP formation and neural fold elevation, proceed unaffected following Cytochalasin D treatment, embryos consistently fail to complete closure (Schoenwolf et al., 1988). In conclusion, the CIP/KIP proteins can regulate the Rho –ROCK pathway that might be important for IKNM. However, the fact that MHP formation is unperturbed in the absence of actin goes against this theory.

Interestingly, initiation of closure 1 is sensitive to Cytochalasin D treatment (Ybot-Gonzalez and Copp, 1999), suggesting that the force required for the initial point of closure requires actin microfilaments. Considering that this is probably the event that requires the most force as the flat neuroepithelium bends to make a tube, it could be that the subsequent closure of the PNP is a more passive event, unaffected by the loss of microfilaments. This would suggest that the force generated within the closed neural tube drives bending and neural tube closure in the PNP. Interestingly, preliminary data has suggested that disruption of the integrity of the closed neural tube by making an incision some distance rostrally from the closure point halts PNP closure (A.J.Copp, unpublished).

7.1.2 Notochord pulling

If the cytoskeleton is not responsible for MHP formation, and a prolonged cell cycle in dispensable for bending, then what is necessary for MHP formation? It has been argued that forces generated by lateral tissues are important for neural tube closure. However, isolation of the neural tube and plate from lateral tissues does not prevent PNP closure (van Straaten et al., 1993) suggesting that the forces required for spinal neurulation are intrinsic to the neural plate.

The MHP does not form in the absence of the notochord (Smith and Schoenwolf, 1989). This could be due to factors expressed in the notochord that are necessary

for induction of genes with a role in MHP formation, or because of physical attachment of the notochord to the midline that functions as a hinge. In order for the hinge to be effective, there would have to be some sort of downwards pulling of the midline, otherwise the midline would just attach to the notochord and stay in the same formation. In other words, imagine a sheet of paper with a piece of gum attached in a line across the middle of the paper. If there was no pulling at the gum it would just be a flat sheet of paper with the gum attached to it. If I started pulling the gum, then the sheet of paper would become narrow at the point of attachment. Furthermore, if the gum was broad, then the sheet of paper would have a larger bending area than if there was a thin line of pulling gum. Thus, a scenario where a narrow, attached notochord pulls the midline down seems possible. It could be just as likely that the neural plate was pulled away from the notochord, as when the gum is stuck to the table and the paper is pulled. However, the fact that lateral tissues are not necessary for neural plate bending and elevation makes this scenario less likely.

How would the notochord pull on the neural plate in the scenario above? One possibility would be through the very slow proliferative rate in the notochord (McShane et al., 2015). It has been shown in the curly tail mouse, which has a grainyhead-like-3 mutation, that a proliferative defect in the hindgut leads to a growth imbalance between the dorsal and ventral tissues, causing spina bifida through excessive curvature of the PNP (Copp et al., 1988). In the neural plate, the attachment of the notochord, which has a slower proliferative rate than MHP cells (Copp et al., 1988; McShane et al., 2015), could pull on the neural plate by the same mechanism, thereby creating an effective hinge. This would also account for the MHP like characteristics observed in cells of the lateral neural tube that are in contact with transplanted notochordal fragments (Smith and Schoenwolf, 1989). Whether this pulling of the midline would affect the cell cycle, or make the cells basal, is hard to predict.

In PCP mouse mutants, craniorachischisis is observed due to a lack of convergent extension along the body axis, resulting in a broad neural plate midline that is not

permissive of neural fold closure as the neural folds are spaced to wide apart (reviewed by Copp et al., 2003a). It is possible that the broad neural plate arises because of defective convergent extension in the mesoderm underlying the midline, resulting in a broad notochord that no longer functions as an efficient hinge (Copp et al., 2003a). The broad midline resulting from a broad notochord would fit with the theory of notochord pulling described above. In line with this, disruptive MHP formation could be secondary to the primary problem which was a broad notochord. In the notochordal pulling scenario, basal cell expansion regulated by p21 could lead to more efficient midline bending without being necessary.

7.1.3   BMP antagonism in MHP formation

BMP blockade is capable of prolonging the cell cycle at ectopic hinge points in the developing chick neural tube and increase the time cells spend with basal nuclei (Eom et al., 2013). Furthermore, Noggin overexpression in the chick MHP exaggerates bending while BMP overexpression prevents MHP formation (Eom et al., 2012). This suggests that BMP antagonists such as Chordin and Noggin which are expressed in the mouse notochord (Ybot-Gonzalez et al., 2007a) could play a role in MHP formation. p21 has been shown to repress Bmp2 at the transcriptional level in neural stem cells (Burnside, 1971). Furthermore, p21 can be transcriptionally activated by the BMP antagonist Drm/Gremlin in tumour derived cell lines, and Drm/Gremlin, in turn, can be activated by Shh (Chen et al., 2002; Farin et al., 2013). Thus, it could be that p21 in the MHP acts as a BMP antagonist to allow MHP bending. Conversely, a study in keratinocytes has suggested that BMP2 regulates transcription of p57, and upregulates p21 (Gosselet et al., 2007) and in the mouse enamel knot, during tooth development, p21 is induced by BMP4 (Jernvall et al., 1998).

7.2 How does p21 prolong S-phase in the MHP?

p21 interacts directly with PCNA and at low molar ratios p21 is suggested to interfere with the rate of synthesis by polymerase β, possibly interfering with the sliding of the polymerase along the DNA whereby p21 can alter the rates of DNA synthesis (Flores-Rozas et al., 1994). This setting would fit with the long S-phase in p21 expressing MHP cells and is distinct from the G1 arrest caused by DNA damage in which the p53 dependent checkpoint is activated (Flores-Rozas et al., 1994). In other studies it has been suggested that the p21 binding site on PCNA overlaps with the DNA polymerase δ and replication factor C, suggesting that p21 binding to PCNA blocks DNA synthesis by preventing association between PCNA, polδ, and the replication factor (reviewed by Jung et al., 2010). The best known role of p21 is to inhibit DNA replication (Moldovan et al., 2007). My analysis with thymidine analogues shows that DNA synthesis is not blocked in the MHP where p21 expression is high, as most cells incorporate BrdU or IdU. Thus, it is more likely that p21 inhibits the CDK1-cyclin A and/or CDK2-cyclin A complexes that are required for S to G2 transition, keeping the nuclei basal in late S-phase (Deng et al., 1995).

In conclusion, p21 prolongs S-phase in MHP cells. The best known functions of p21 are to inhibit the cell cycle in G1-phase, S-phase or inhibiting S- to G2-phase transition. The number of cells undergoing DNA synthesis in the MHP suggests that the role of p21 is to prolong S-phase or inhibit the transition into G2. Further experiments are required to unravel the mechanism of S-phase prolongation.

The normal MHP morphology of p21$^{-/-}$ embryos suggests that S-phase prolongation is not necessary for MHP formation. It is possible that there is redundancy between CIP/KIP genes in the MHP but S-phase regulation is dependent on p21. Thus, it seems that other mechanisms besides basal expansion are required for MHP formation. The prolongation of S-phase and the basal nuclei could provide a favourable environment for midline bending, but are not required.

Appendix I

p21 -/-	MHP		Left lateral		Right lateral		Lateral comb
	Single/double	S-phase length	Single/double	S-phase length	Single/double	S-phase length	
#B14 A2 I	3/8	5.33	7/3	0.86	3/9	6.00	
#B14 A2 II	6/5	1.67	3/4	2.67	4/4	2.00	
#B14 A2 III	6/6	2.00	5/7	2.80	5/7	2.80	
#B14 A2 IV	4/7	3.50	7/6	1.71	7/11	3.14	
#B14 B1 I	4/6	3.00	12/6	1.00	4/4	2.00	
#B14 B1 II	3/8	5.33	4/10	5.00	4/5	2.50	
#B14 B1 III	4/6	3.00	5/8	3.20	4/4	2.00	
#B14 B1 IV	4/7	3.50	6/6	2.00	2/7	7.00	
#B14 B1 V	2/9	9.00	8/6	1.50	5/8	3.20	
#B14 B1 VI	7/4	1.14	4/8	4.00	6/8	2.67	
#B14 B1 VII	5/8	3.20	6/5	1.67	6/8	2.67	
#B14 B1 VIII	5/9	3.60	11/4	0.73	8/7	1.75	
	53/83	**3.13**	78/73	**1.87**	58/82	**2.83**	**2.35**

Example of the analysis of S-phase length for one embryo (12 sections). Single and double labelled nuclei were counted in the MHP and in two lateral regions for each section, and the total number of single and double labelled nuclei was combined to calculate mean S-phase length per embryo. The lateral regions were combined for the graph while SEM values were calculated on data from both regions.

Appendix II

	Basal dist.		MHP basal dist.		Basal dist.		
#B3 B1 I	0.484	G2	0.455	G2	0.860	late S	
	0.743	G2	0.577	G2	0.498	G2	
	0.274	early/mid S	0.256	G2	0.850	M	
	0.239	G2	0.403	G2	0.504	G2	
	0.581	G2	0.487	G2	0.396	G2	
	0.793	late S	0.246	early/mid S	0.165	G2	
	0.759	G2	0.233	G2	0.792	late S	
	0.494	G2	0.741	late S	0.397	G2	
	0.641	early/mid S	0.358	G2	0.473	G2	
	0.241	early/mid S	0.304	G2	0.695	G2	
	0.872	M			0.773	M	
	0.769	G2			0.295	G2	
	0.369	G2			0.795	late S	
#B3 B1 II	0.362	G2	0.729	S	0.797	M	
	0.751	G2	0.439	S	0.503	late S	
	0.252	early/mid S	0.312	early/mid S	0.292	G2	
	0.468	G2	0.464	G2	0.560	late S	
	0.655	G2	0.390	early/mid S	0.883	M	
	0.856	late S	0.245	early/mid S	0.548	late S	
	0.364	G2	0.622	late S	0.601	G2	
	0.364	G2	0.591	G2	0.330	G2	
	0.804	late S	0.406	late S	0.881	M	
	0.634	G2	0.814	late S	0.447	G2	
#B3 B1 III	0.659	G2	0.584	late S	0.660	late G2/M	
	0.844	M	0.345	early/mid S	0.381	early/mid S	
	0.299	early/mid S	0.567	early/mid S	0.306	early/mid S	
	0.831	M	0.445	G2	0.785	M	
	0.523	early/mid S	0.344	G2	0.516	mid/late S	
	0.307	G2	0.407	late S	0.354	G2	
	0.849	late S	0.264	late S	0.710	G2	
	0.691	G2	0.662	G2	0.609	G2	
	0.277	early/mid S	0.518	G2	0.279	G2	
	0.770	G2	0.330	late S	0.269	G2	
	0.653	G2					
	0.330	G2					
	0.700	G2					
#B3 B1 IV	0.304	G2	0.718	late S	0.385	G2	
	0.844	M	0.418	G2	0.372	G2	
	0.570	late S	0.395	G2	0.827	M	
	0.882	M	0.429	mid S	0.258	G2	
	0.608	late S	0.288	early/mid S	0.610	late S	
	0.651	mid/late S	0.731	G2	0.789	M	
	0.619	early/mid S	0.327	late S	0.338	G2	
	0.751	mid/late S	0.681	G2	0.431	G2	
	0.450	early/mid S	0.236	early/mid S	0.739	G2	
					0.786	M	
					0.498	G2	
Average	**0.582**		**0.455**		**0.551**		**0.566**
SE	0.031		0.026		0.031		

	%	Left #	%	MHP #	%	Right #	
S	24.444	11	28.205	11	6.818	3	**15.631**
late S	13.333	6	25.641	10	15.909	7	**14.621**
G2	51.111	23	46.154	18	54.545	24	**52.828**
M	**11.111**	**5**	**0.000**	**0**	20.455	9	15.783
late G2/M	0.000	0	0.000	0	2.273	1	**1.136**
LateG2/M+M	11.111	5	0.000	0	22.727	10	**16.919**
Total cells	100	45	100	39	100	44	

Example of basal nuclear distances in the left-, MHP- and right regions of 4 sections from one embryo. Each nucleus was assigned to a cell cycle phase based on IdU and pHH3 staining. Mean basal distance and cell cycle distribution is shown at the bottom.

Reference List

Adkins, J. N. and Lumb, K. J. (2002). Intrinsic structural disorder and sequence features of the cell cycle inhibitor p57Kip2. *Proteins* 46, 1-7.

Alvarez, I. S. and Schoenwolf, G. C. (1992). Expansion of surface epithelium provides the major extrinsic force for bending of the neural plate. *J. Exp. Zool.* 261, 340-348.

Bachiller, D., Klingensmith, J., Kemp, C., Belo, J. A., Anderson, R. M., May, S. R., McMahon, J. A., McMahon, A. P., Harland, R. M., Rossant, J. et al. (2000). The organizer factors Chordin and Noggin are required for mouse forebrain development. *Nature* 403, 658-661.

Balint, E., Phillips, A. C., Kozlov, S., Stewart, C. L. and Vousden, K. H. (2002). Induction of p57(KIP2) expression by p73beta. *Proc. Natl. Acad. Sci. U. S. A* 99, 3529-3534.

Bassuk, A. G. and Kibar, Z. (2009). Genetic basis of neural tube defects. *Semin. Pediatr. Neurol.* 16, 101-110.

Bauer, S. and Patterson, P. H. (2005). The cell cycle-apoptosis connection revisited in the adult brain. *J. Cell Biol.* 171, 641-650.

Baye, L. M. and Link, B. A. (2008). Nuclear migration during retinal development. *Brain Res.* 1192, 29-36.

Besson, A., Assoian, R. K. and Roberts, J. M. (2004a). Regulation of the cytoskeleton: an oncogenic function for CDK inhibitors? *Nat Rev. Cancer* 4, 948-955.

Besson, A., Dowdy, S. F. and Roberts, J. M. (2008). CDK inhibitors: cell cycle regulators and beyond. *Dev. Cell* 14, 159-169.

Besson, A., Gurian-West, M., Schmidt, A., Hall, A. and Roberts, J. M. (2004b). p27Kip1 modulates cell migration through the regulation of RhoA activation. *Genes Dev.* 18, 862-876.

Bilodeau, S., Roussel-Gervais, A. and Drouin, J. (2009). Distinct developmental roles of cell cycle inhibitors p57Kip2 and p27Kip1 distinguish pituitary progenitor cell cycle exit from cell cycle reentry of differentiated cells. *Mol. Cell Biol* 29, 1895-1908.

Blagosklonny, M. V., Wu, G. S., Omura, S. and el-Deiry, W. S. (1996). Proteasome-dependent regulation of p21WAF1/CIP1 expression. *Biochem. Biophys. Res. Commun.* 227, 564-569.

Blangy, A., Arnaud, L. and Nigg, E. A. (1997). Phosphorylation by p34cdc2 protein kinase regulates binding of the kinesin-related motor HsEg5 to the dynactin subunit p150. *J. Biol. Chem.* 272, 19418-19424.

Borriello, A., Cucciolla, V., Oliva, A., Zappia, V. and Ragione, F. D. (2007). p27Kip1 Metabolism: A Fascinating Labyrinth. *cc* 6, 1053-1061.

Bort, R., Signore, M., Tremblay, K., Martinez Barbera, J. P. and Zaret, K. S. (2006). Hex homeobox gene controls the transition of the endoderm to a pseudostratified, cell emergent epithelium for liver bud development. *Dev. Biol.* 290, 44-56.

Braun, N., Papadopoulos, T. and Muller-Hermelink, H. K. (1988). Cell cycle dependent distribution of the proliferation-associated Ki-67 antigen in human embryonic lung cells. *Virchows Arch. B Cell Pathol. Incl. Mol. Pathol.* 56, 25-33.

Brugarolas, J., Chandrasekaran, C., Gordon, J. I., Beach, D., Jacks, T. and Hannon, G. J. (1995). Radiation-induced cell cycle arrest compromised by p21 deficiency. *Nature* 377, 552-557.

Burnside, B. (1971). Microtubules and microfilaments in newt neuralation. *Dev. Biol.* 26, 416-441.

Calegari, F. and Huttner, W. B. (2003). An inhibition of cyclin-dependent kinases that lengthens, but does not arrest, neuroepithelial cell cycle induces premature neurogenesis. *J. Cell Sci.* 116, 4947-4955.

Calegari, F., Marzesco, A. M., Kittler, R., Buchholz, F. and Huttner, W. B. (2004). Tissue-specific RNA interference in post-implantation mouse embryos using directional electroporation and whole embryo culture. *Differentiation* 72, 92-102.

Cambray, N. and Wilson, V. (2007). Two distinct sources for a population of maturing axial progenitors. *Development* 134, 2829-2840.

Catala, M., Teillet, M. A., De Robertis, E. M. and Le Douarin, M. L. (1996). A spinal cord fate map in the avian embryo: while regressing, Hensen's node lays down the notochord and floor plate thus joining the spinal cord lateral walls. *Development* 122, 2599-2610.

Cerqueira, A., Martin, A., Symonds, C. E., Odajima, J., Dubus, P., Barbacid, M. and Santamaria, D. (2014). Genetic characterization of the role of the Cip/Kip family of proteins as cyclin-dependent kinase inhibitors and assembly factors. *Mol. Cell Biol.* 34, 1452-1459.

Charrier, J. B., Teillet, M. A., Lapointe, F. and Le Douarin, N. M. (1999). Defining subregions of Hensen's node essential for caudalward movement, midline development and cell survival. *Development* 126, 4771-4783.

Chen, B., Athanasiou, M., Gu, Q. and Blair, D. G. (2002). Drm/Gremlin transcriptionally activates p21(Cip1) via a novel mechanism and inhibits neoplastic transformation. *Biochem. Biophys. Res. Commun.* 295, 1135-1141.

Chiang, C., Litingtung, Y., Lee, E., Young, K. E., Corden, J. L., Westphal, H. and Beachy, P. A. (1996). Cyclopia and defective axial patterning in mice lacking Sonic hedgehog gene function. *Nature* 383, 407-413.

Child, E. S. and Mann, D. J. (2006). The intricacies of p21 phosphorylation: protein/protein interactions, subcellular localization and stability. *cc* 5, 1313-1319.

Coats, S., Flanagan, W. M., Nourse, J. and Roberts, J. M. (1996). Requirement of p27Kip1 for restriction point control of the fibroblast cell cycle. *Science* 272, 877-880.

Cockroft, D. L. (1990). Dissection and culture of post-implantation embryos. In *Postimplantation mammalian embryos. A practical approach* (ed. A.J.Copp and D.L.Cockroft), pp. 15-39. Oxford: Oxford University Press.

Copp, A. J. (1985). Relationship between timing of posterior neuropore closure and development of spinal neural tube defects in mutant (curly tail) and normal mouse embryos in culture. *J. Embryol. Exp. Morphol.* 88, 39-54.

Copp, A. J. (2005). Neurulation in the cranial region--normal and abnormal. *J. Anat.* 207, 623-635.

Copp, A. J., Brook, F. A., Estibeiro, J. P., Shum, A. S. and Cockroft, D. L. (1990). The embryonic development of mammalian neural tube defects. *Prog. Neurobiol.* 35, 363-403.

Copp, A. J., Brook, F. A. and Roberts, H. J. (1988). A cell-type-specific abnormality of cell proliferation in mutant (curly tail) mouse embryos developing spinal neural tube defects. *Development* 104, 285-295.

Copp, A. J., Checiu, I. and Henson, J. N. (1994). Developmental basis of severe neural tube defects in the loop-tail (Lp) mutant mouse: use of microsatellite DNA markers to identify embryonic genotype. *Dev. Biol.* 165, 20-29.

Copp, A. J., Greene, N. D. and Murdoch, J. N. (2003a). Dishevelled: linking convergent extension with neural tube closure. *Trends Neurosci.* 26, 453-455.

Copp, A. J., Greene, N. D. and Murdoch, J. N. (2003b). The genetic basis of mammalian neurulation. *Nat. Rev. Genet.* 4, 784-793.

Copp, A. J., Stanier, P. and Greene, N. D. (2013). Neural tube defects: recent advances, unsolved questions, and controversies. *Lancet Neurol.* 12, 799-810.

Cronkite, E. P., Fliedner, T. M., Bond, V. P., Rubini, J. R., Brecher, G. and Quastler, H. (1959). Dynamics of hemopoietic proliferation in man and mice studied by H3-thymidine incorporation into DNA. *Prog. Nucl. Energy 6. Biol. Sci.* 2, 92-105.

Del, B. F., Wehman, A. M., Link, B. A. and Baier, H. (2008). Regulation of neurogenesis by interkinetic nuclear migration through an apical-basal notch gradient. *Cell* 134, 1055-1065.

Delalande, J. M., Thapar, N. and Burns, A. J. (2015). Dual labeling of neural crest cells and blood vessels within chicken embryos using Chick(GFP) neural tube grafting and carbocyanine dye DiI injection. *J. Vis. Exp.*, e52514.

Deng, C., Zhang, P., Harper, J. W., Elledge, S. J. and Leder, P. (1995). Mice lacking p21CIP1/WAF1 undergo normal development, but are defective in G1 checkpoint control. *Cell* 82, 675-684.

Di, S., V, Giacca, M., Capogrossi, M. C., Crescenzi, M. and Martelli, F. (2011). Knockdown of cyclin-dependent kinase inhibitors induces cardiomyocyte re-entry in the cell cycle. *J. Biol Chem.* 286, 8644-8654.

Downs, K. M. and Davies, T. (1993). Staging of gastrulating mouse embryos by morphological landmarks in the dissecting microscope. *Development* 118, 1255-1266.

el-Deiry, W. S., Tokino, T., Velculescu, V. E., Levy, D. B., Parsons, R., Trent, J. M., Lin, D., Mercer, W. E., Kinzler, K. W. and Vogelstein, B. (1993). WAF1, a potential mediator of p53 tumor suppression. *Cell* 75, 817-825.

el-Deiry, W. S., Tokino, T., Waldman, T., Oliner, J. D., Velculescu, V. E., Burrell, M., Hill, D. E., Healy, E., Rees, J. L., Hamilton, S. R. et al. (1995). Topological control of p21WAF1/CIP1 expression in normal and neoplastic tissues. *Cancer Res.* 55, 2910-2919.

Elms, P., Siggers, P., Napper, D., Greenfield, A. and Arkell, R. (2003). Zic2 is required for neural crest formation and hindbrain patterning during mouse development. *Dev. Biol.* 264, 391-406.

Eom, D. S., Amarnath, S. and Agarwala, S. (2013). Apicobasal polarity and neural tube closure. *Dev. Growth Differ.* 55, 164-172.

Eom, D. S., Amarnath, S., Fogel, J. L. and Agarwala, S. (2011). Bone morphogenetic proteins regulate neural tube closure by interacting with the apicobasal polarity pathway. *Development* 138, 3179-3188.

Eom, D. S., Amarnath, S., Fogel, J. L. and Agarwala, S. (2012). Bone morphogenetic proteins regulate hinge point formation during neural tube closure by dynamic modulation of apicobasal polarity. *Birth Defects Res. A Clin. Mol. Teratol.* 94, 804-816.

Escuin, S., Vernay, B., Savery, D., Gurniak, C. B., Witke, W., Greene, N. D. and Copp, A. J. (2015). Rho-kinase-dependent actin turnover and actomyosin disassembly are necessary for mouse spinal neural tube closure. *J. Cell Sci.* 128, 2468-2481.

Esteve, V., Canela, N., Rodriguez-Vilarrupla, A., Aligue, R., Agell, N., Mingarro, I., Bachs, O. and Perez-Paya, E. (2003). The structural plasticity of the C terminus of p21Cip1 is a determinant for target protein recognition. *Chembiochem.* 4, 863-869.

Etienne-Manneville, S. and Hall, A. (2002). Rho GTPases in cell biology. *Nature* 420, 629-635.

Farin, H. F., Ludtke, T. H., Schmidt, M. K., Placzko, S., Schuster-Gossler, K., Petry, M., Christoffels, V. M. and Kispert, A. (2013). Tbx2 terminates shh/fgf signaling in the developing mouse limb bud by direct repression of gremlin1. *PLoS. Genet.* 9, e1003467.

Fero, M. L., Rivkin, M., Tasch, M., Porter, P., Carow, C. E., Firpo, E., Polyak, K., Tsai, L. H., Broudy, V., Perlmutter, R. M. et al. (1996). A syndrome of multiorgan hyperplasia with features of gigantism, tumorigenesis, and female sterility in p27(Kip1)-deficient mice. *Cell* 85, 733-744.

Firpo, E. J., Koff, A., Solomon, M. J. and Roberts, J. M. (1994). Inactivation of a Cdk2 inhibitor during interleukin 2-induced proliferation of human T lymphocytes. *Mol. Cell Biol.* 14, 4889-4901.

Flores-Rozas, H., Kelman, Z., Dean, F. B., Pan, Z. Q., Harper, J. W., Elledge, S. J., O'Donnell, M. and Hurwitz, J. (1994). Cdk-interacting protein 1 directly binds with proliferating cell nuclear antigen and inhibits DNA replication catalyzed by the DNA polymerase delta holoenzyme. *Proc. Natl. Acad. Sci. U. S. A* 91, 8655-8659.

Fujita, S. (1962). Kinetics of cellular proliferation. *Exp. Cell Res.* 28, 52-60.

Garcia-Fernandez, R. A., Garcia-Palencia, P., Sanchez, M. A., Gil-Gomez, G., Sanchez, B., Rollan, E., Martin-Caballero, J. and Flores, J. M. (2011). Combined loss of p21waf1/cip1 and p27kip1 enhances tumorigenesis in mice. *Lab Invest* 91, 1634-1642.

Gardner, R. L. and Rossant, J. (1979). Investigation of the fate of 4-5 day post-coitum mouse inner cell mass cells by blastocyst injection. *J. Embryol. Exp. Morphol.* 52, 141-152.

Gartel, A. L. and Tyner, A. L. (1999). Transcriptional regulation of the p21((WAF1/CIP1)) gene. *Exp. Cell Res.* 246, 280-289.

Gaston-Massuet, C., Andoniadou, C. L., Signore, M., Jayakody, S. A., Charolidi, N., Kyeyune, R., Vernay, B., Jacques, T. S., Taketo, M. M., Le, T. P. et al. (2011).

Increased Wingless (Wnt) signaling in pituitary progenitor/stem cells gives rise to pituitary tumors in mice and humans. *Proc. Natl. Acad. Sci. U. S. A* 108, 11482-11487.

Ge, X., Frank, C. L., Calderon de, A. F. and Tsai, L. H. (2010). Hook3 interacts with PCM1 to regulate pericentriolar material assembly and the timing of neurogenesis. *Neuron* 65, 191-203.

Georgia, S., Soliz, R., Li, M., Zhang, P. and Bhushan, A. (2006). p57 and Hes1 coordinate cell cycle exit with self-renewal of pancreatic progenitors. *Dev. Biol.* 298, 22-31.

Glaser, O. (1914). THE WATER CONTENT OF THE EMBRYONIC NERVOUS SYSTEM. *Science* 39, 730-731.

Gosselet, F. P., Magnaldo, T., Culerrier, R. M., Sarasin, A. and Ehrhart, J. C. (2007). BMP2 and BMP6 control p57(Kip2) expression and cell growth arrest/terminal differentiation in normal primary human epidermal keratinocytes. *Cell Signal.* 19, 731-739.

Greene, N. D. and Copp, A. J. (2009). Development of the vertebrate central nervous system: formation of the neural tube. *Prenat. Diagn.* 29, 303-311.

Greene, N. D., Gerrelli, D., van Straaten, H. W. and Copp, A. J. (1998). Abnormalities of floor plate, notochord and somite differentiation in the loop-tail (Lp) mouse: a model of severe neural tube defects. *Mech. Dev.* 73, 59-72.

Greene, N. D., Stanier, P. and Copp, A. J. (2009). Genetics of human neural tube defects. *Hum. Mol. Genet.* 18, R113-R129.

Grosse, A. S., Pressprich, M. F., Curley, L. B., Hamilton, K. L., Margolis, B., Hildebrand, J. D. and Gumucio, D. L. (2011). Cell dynamics in fetal intestinal epithelium: implications for intestinal growth and morphogenesis. *Development* 138, 4423-4432.

Gu, Y., Turck, C. W. and Morgan, D. O. (1993). Inhibition of CDK2 activity in vivo by an associated 20K regulatory subunit. *Nature* 366, 707-710.

Haigo, S. L., Hildebrand, J. D., Harland, R. M. and Wallingford, J. B. (2003). Shroom induces apical constriction and is required for hingepoint formation during neural tube closure. *Curr. Biol.* 13, 2125-2137.

Hara, E., Smith, R., Parry, D., Tahara, H., Stone, S. and Peters, G. (1996). Regulation of p16CDKN2 expression and its implications for cell immortalization and senescence. *Mol. Cell Biol.* 16, 859-867.

Harper, J. W., Elledge, S. J., Keyomarsi, K., Dynlacht, B., Tsai, L. H., Zhang, P., Dobrowolski, S., Bai, C., Connell-Crowley, L., Swindell, E. et al. (1995). Inhibition of cyclin-dependent kinases by p21. *Mol. Biol Cell* 6, 387-400.

Harris, M. J. and Juriloff, D. M. (2010). An update to the list of mouse mutants with neural tube closure defects and advances toward a complete genetic perspective of neural tube closure. *Birth Defects Res. A Clin. Mol. Teratol.* 88, 653-669.

Hatada, I. and Mukai, T. (1995). Genomic imprinting of p57KIP2, a cyclin-dependent kinase inhibitor, in mouse. *Nat. Genet.* 11, 204-206.

Hayes, N. L. and Nowakowski, R. S. (2000). Exploiting the dynamics of S-phase tracers in developing brain: interkinetic nuclear migration for cells entering versus leaving the S-phase. *Dev. Neurosci.* 22, 44-55.

Hendzel, M. J., Wei, Y., Mancini, M. A., Van, H. A., Ranalli, T., Brinkley, B. R., Bazett-Jones, D. P. and Allis, C. D. (1997). Mitosis-specific phosphorylation of histone H3 initiates primarily within pericentromeric heterochromatin during G2 and spreads in an ordered fashion coincident with mitotic chromosome condensation. *Chromosoma* 106, 348-360.

Henrique, D., Abranches, E., Verrier, L. and Storey, K. G. (2015). Neuromesodermal progenitors and the making of the spinal cord. *Development* 142, 2864-2875.

Herrmann, B. G. and Kispert, A. (1994). The T genes in embryogenesis. *Trends Genet.* 10, 280-286.

Hirai, H., Roussel, M. F., Kato, J. Y., Ashmun, R. A. and Sherr, C. J. (1995). Novel INK4 proteins, p19 and p18, are specific inhibitors of the cyclin D-dependent kinases CDK4 and CDK6. *Mol. Cell Biol.* 15, 2672-2681.

Hosako, H., Francisco, L. E., Martin, G. S. and Mirkes, P. E. (2009). The roles of p53 and p21 in normal development and hyperthermia-induced malformations. *Birth Defects Research Part B: Developmental and Reproductive Toxicology* 86, 40-47.

Hubaud, A. and Pourquie, O. (2014). Signalling dynamics in vertebrate segmentation. *Nat. Rev. Mol. Cell Biol.* 15, 709-721.

Ishimura, A., Minehata, K., Terashima, M., Kondoh, G., Hara, T. and Suzuki, T. (2012). Jmjd5, an H3K36me2 histone demethylase, modulates embryonic cell proliferation through the regulation of Cdkn1a expression. *Development* 139, 749-759.

Jernvall, J., Aberg, T., Kettunen, P., Keranen, S. and Thesleff, I. (1998). The life history of an embryonic signaling center: BMP-4 induces p21 and is

associated with apoptosis in the mouse tooth enamel knot. *Development* 125, 161-169.

Jung, Y. S., Qian, Y. and Chen, X. (2010). Examination of the expanding pathways for the regulation of p21 expression and activity. *Cell Signal.* 22, 1003-1012.

Kamijo, T., Weber, J. D., Zambetti, G., Zindy, F., Roussel, M. F. and Sherr, C. J. (1998). Functional and physical interactions of the ARF tumor suppressor with p53 and Mdm2. *Proc. Natl. Acad. Sci. U. S. A* 95, 8292-8297.

Kato, J. Y., Matsuoka, M., Polyak, K., Massague, J. and Sherr, C. J. (1994). Cyclic AMP-induced G1 phase arrest mediated by an inhibitor (p27Kip1) of cyclin-dependent kinase 4 activation. *Cell* 79, 487-496.

Kaufmann, L. T., Gierl, M. S. and Niehrs, C. (2011). Gadd45a, Gadd45b and Gadd45g expression during mouse embryonic development. *Gene Expression Patterns* 11, 465-470.

Keller, R. (2002). Shaping the vertebrate body plan by polarized embryonic cell movements. *Science* 298, 1950-1954.

Kinoshita, N., Sasai, N., Misaki, K. and Yonemura, S. (2008). Apical accumulation of Rho in the neural plate is important for neural plate cell shape change and neural tube formation. *Mol. Biol. Cell* 19, 2289-2299.

Kiyokawa, H., Kineman, R. D., Manova-Todorova, K. O., Soares, V. C., Hoffman, E. S., Ono, M., Khanam, D., Hayday, A. C., Frohman, L. A. and Koff, A. (1996). Enhanced growth of mice lacking the cyclin-dependent kinase inhibitor function of p27(Kip1). *Cell* 85, 721-732.

Kosodo, Y., Suetsugu, T., Suda, M., Mimori-Kiyosue, Y., Toida, K., Baba, S. A., Kimura, A. and Matsuzaki, F. (2011). Regulation of interkinetic nuclear migration by cell cycle-coupled active and passive mechanisms in the developing brain. *EMBO J.* 30, 1690-1704.

LaBaer, J., Garrett, M. D., Stevenson, L. F., Slingerland, J. M., Sandhu, C., Chou, H. S., Fattaey, A. and Harlow, E. (1997). New functional activities for the p21 family of CDK inhibitors. *Genes Dev.* 11, 847-862.

Lacy, E. R., Filippov, I., Lewis, W. S., Otieno, S., Xiao, L., Weiss, S., Hengst, L. and Kriwacki, R. W. (2004). p27 binds cyclin-CDK complexes through a sequential mechanism involving binding-induced protein folding. *Nat. Struct. Mol. Biol.* 11, 358-364.

Lammer, E. J., Sever, L. E. and Oakley, G. P., Jr. (1987). Teratogen update: valproic acid. *Teratology* 35, 465-473.

Langman, J., Guerrant, R. L. and Freeman, B. G. (1966). Behavior of neuro-epithelial cells during closure of the neural tube. *J. Comp Neurol.* 127, 399-411.

Langman, J. and Nelson, G. R. (1968). A radioautographic study of the development of the somite in the chick embryo. *J. Embryol. Exp. Morphol.* 19, 217-226.

Lee, H. O. and Norden, C. (2013). Mechanisms controlling arrangements and movements of nuclei in pseudostratified epithelia. *Trends Cell Biol.* 23, 141-150.

Lee, H. Y., Kosciuk, M. C., Nagele, R. G. and Roisen, F. J. (1983). Studies on the mechanisms of neurulation in the chick: possible involvement of myosin in elevation of neural folds. *J. Exp. Zool.* 225, 449-457.

Lee, H. Y. and Nagele, R. G. (1985). Studies on the mechanisms of neurulation in the chick: interrelationship of contractile proteins, microfilaments, and the shape of neuroepithelial cells. *J. Exp. Zool.* 235, 205-215.

Lee, M. H., Reynisdottir, I. and Massague, J. (1995). Cloning of p57KIP2, a cyclin-dependent kinase inhibitor with unique domain structure and tissue distribution. *Genes Dev.* 9, 639-649.

Lee, S. and Helfman, D. M. (2004). Cytoplasmic p21Cip1 is involved in Ras-induced inhibition of the ROCK/LIMK/cofilin pathway. *J. Biol Chem.* 279, 1885-1891.

Leung, L., Klopper, A. V., Grill, S. W., Harris, W. A. and Norden, C. (2011). Apical migration of nuclei during G2 is a prerequisite for all nuclear motion in zebrafish neuroepithelia. *Development* 138, 5003-5013.

Li, X. S., Rishi, A. K., Shao, Z. M., Dawson, M. I., Jong, L., Shroot, B., Reichert, U., Ordonez, J. and Fontana, J. A. (1996). Posttranscriptional regulation of p21WAF1/CIP1 expression in human breast carcinoma cells. *Cancer Res.* 56, 5055-5062.

Liu, X., Hashimoto-Torii, K., Torii, M., Ding, C. and Rakic, P. (2010). Gap junctions/hemichannels modulate interkinetic nuclear migration in the forebrain precursors. *J. Neurosci.* 30, 4197-4209.

Ludtke, T. H., Christoffels, V. M., Petry, M. and Kispert, A. (2009). Tbx3 promotes liver bud expansion during mouse development by suppression of cholangiocyte differentiation. *Hepatology* 49, 969-978.

Luo, Y., Hurwitz, J. and Massague, J. (1995). Cell-cycle inhibition by independent CDK and PCNA binding domains in p21Cip1. *Nature* 375, 159-161.

Macleod, K. F., Sherry, N., Hannon, G., Beach, D., Tokino, T., Kinzler, K., Vogelstein, B. and Jacks, T. (1995). p53-dependent and independent expression of p21 during cell growth, differentiation, and DNA damage. *Genes & Development* 9, 935-944.

Mairet-Coello, G., Tury, A., Van, B. E., Robinson, K., Genestine, M. and Dicicco-Bloom, E. (2012). p57KIP2 regulates radial glia and intermediate precursor

cell cycle dynamics and lower layer neurogenesis in developing cerebral cortex. *Development* 139, 475-487.

Malumbres, M. and Barbacid, M. (2009). Cell cycle, CDKs and cancer: a changing paradigm. *Nat. Rev. Cancer* 9, 153-166.

Mansur, N. R., Meyer-Siegler, K., Wurzer, J. C. and Sirover, M. A. (1993). Cell cycle regulation of the glyceraldehyde-3-phosphate dehydrogenase/uracil DNA glycosylase gene in normal human cells. *Nucleic Acids Res.* 21, 993-998.

Martin, A. and Langman, J. (1965). The development of the spinal cord examined by autoradiography. *J. Embryol. Exp. Morphol.* 14, 25-35.

Martynoga, B., Morrison, H., Price, D. J. and Mason, J. O. (2005). Foxg1 is required for specification of ventral telencephalon and region-specific regulation of dorsal telencephalic precursor proliferation and apoptosis. *Dev. Biol.* 283, 113-127.

Matsuoka, S., Edwards, M. C., Bai, C., Parker, S., Zhang, P., Baldini, A., Harper, J. W. and Elledge, S. J. (1995). p57KIP2, a structurally distinct member of the p21CIP1 Cdk inhibitor family, is a candidate tumor suppressor gene. *Genes & Development* 9, 650-662.

McGrew, M. J., Sherman, A., Lillico, S. G., Ellard, F. M., Radcliffe, P. A., Gilhooley, H. J., Mitrophanous, K. A., Cambray, N., Wilson, V. and Sang, H. (2008). Localised axial progenitor cell populations in the avian tail bud are not committed to a posterior Hox identity. *Development* 135, 2289-2299.

McMahon, J. A., Takada, S., Zimmerman, L. B., Fan, C. M., Harland, R. M. and McMahon, A. P. (1998). Noggin-mediated antagonism of BMP signaling is required for growth and patterning of the neural tube and somite. *Genes Dev.* 12, 1438-1452.

McShane, S. G., Mole, M. A., Savery, D., Greene, N. D., Tam, P. P. and Copp, A. J. (2015). Cellular basis of neuroepithelial bending during mouse spinal neural tube closure. *Dev. Biol.* 404, 113-124.

Megason, S. G. and McMahon, A. P. (2002). A mitogen gradient of dorsal midline Wnts organizes growth in the CNS. *Development* 129, 2087-2098.

Meyer, E. J., Ikmi, A. and Gibson, M. C. (2011). Interkinetic nuclear migration is a broadly conserved feature of cell division in pseudostratified epithelia. *Curr. Biol.* 21, 485-491.

Miller, M. A., Mazewski, C. M., Yousuf, N., Sheikh, Y., White, L. M., Yanik, G. A., Hyams, D. M., Lampkin, B. C. and Raza, A. (1991). Simultaneous immunohistochemical detection of IUdR and BrdU infused intravenously to cancer patients. *J. Histochem. Cytochem.* 39, 407-412.

Minobe, S., Sakakibara, A., Ohdachi, T., Kanda, R., Kimura, M., Nakatani, S., Tadokoro, R., Ochiai, W., Nishizawa, Y., Mizoguchi, A. et al. (2009). Rac is involved in the interkinetic nuclear migration of cortical progenitor cells. *Neurosci. Res.* 63, 294-301.

Mitchell, L. E. (2005). Epidemiology of neural tube defects. *Am. J. Med. Genet. C. Semin. Med. Genet.* 135C, 88-94.

Mlodzik, M. (2002). Planar cell polarization: do the same mechanisms regulate Drosophila tissue polarity and vertebrate gastrulation? *Trends Genet.* 18, 564-571.

Moldovan, G. L., Pfander, B. and Jentsch, S. (2007). PCNA, the maestro of the replication fork. *Cell* 129, 665-679.

Moran, D. and Rice, R. W. (1976). Action of papaverine and ionophore A23187 on neurulation. *Nature* 261, 497-499.

Moran, D. J. (1976). A scanning electron microscopic and flame spectrometry study on the role of Ca2+ in amphibian neurulation using papaverine inhibition and ionophore induction of morphogenetic movement. *J. Exp. Zool.* 198, 409-416.

Morriss-Kay, G., Wood, H. and Chen, W. H. (1994). Normal neurulation in mammals. *Ciba Found. Symp.* 181, 51-63.

Morriss-Kay, G. M. (1981). Growth and development of pattern in the cranial neural epithelium of rat embryos during neurulation. *J. Embryol. Exp. Morphol.* 65 Suppl, 225-241.

Morriss-Kay, G. M., Tuckett, F. and Solursh, M. (1986). The effects of Streptomyces hyaluronidase on tissue organization and cell cycle time in rat embryos. *J. Embryol. Exp. Morphol.* 98, 59-70.

Murciano, A., Zamora, J., Lopez-Sanchez, J. and Frade, J. M. (2002). Interkinetic nuclear movement may provide spatial clues to the regulation of neurogenesis. *Mol. Cell Neurosci.* 21, 285-300.

Murdoch, J. N., Henderson, D. J., Doudney, K., Gaston-Massuet, C., Phillips, H. M., Paternotte, C., Arkell, R., Stanier, P. and Copp, A. J. (2003). Disruption of scribble (Scrb1) causes severe neural tube defects in the circletail mouse. *Hum. Mol. Genet.* 12, 87-98.

Nagahama, H., Hatakeyama, S., Nakayama, K., Nagata, M., Tomita, K. and Nakayama, K. (2001). Spatial and temporal expression patterns of the cyclin-dependent kinase (CDK) inhibitors p27<SMALL><SUP>Kip1</SUP></SMALL> and p57<SMALL><SUP>Kip2</SUP></SMALL> during mouse development. *Anatomy and Embryology* 203, 77-87.

Nagai, T., Aruga, J., Minowa, O., Sugimoto, T., Ohno, Y., Noda, T. and Mikoshiba, K. (2000). Zic2 regulates the kinetics of neurulation. *Proc. Natl. Acad. Sci. U. S. A* 97, 1618-1623.

Nagele, R. G. and Lee, H. (1980). A transmission and scanning electron microscopic study of cytoplasmic threads of dividing neuroepithelial cells in early chick embryos. *Experientia* 36, 338-340.

Nagele, R. G., Pietrolungo, J. F. and Lee, H. (1981). Studies on the mechanisms of neurulation in the chick: the intracellular distribution of Ca++. *Experientia* 37, 304-306.

Nakanishi, M., Adami, G. R., Robetorye, R. S., Noda, A., Venable, S. F., Dimitrov, D., Pereira-Smith, O. M. and Smith, J. R. (1995). Exit from G0 and entry into the cell cycle of cells expressing p21Sdi1 antisense RNA. *Proc. Natl. Acad. Sci. U. S. A* 92, 4352-4356.

Nakayama, K., Ishida, N., Shirane, M., Inomata, A., Inoue, T., Shishido, N., Horii, I., Loh, D. Y. and Nakayama, K. (1996). Mice lacking p27(Kip1) display increased body size, multiple organ hyperplasia, retinal dysplasia, and pituitary tumors. *Cell* 85, 707-720.

Nakayama, K., Nagahama, H., Minamishima, Y. A., Matsumoto, M., Nakamichi, I., Kitagawa, K., Shirane, M., Tsunematsu, R., Tsukiyama, T., Ishida, N. et al. (2000). Targeted disruption of Skp2 results in accumulation of cyclin E and p27(Kip1), polyploidy and centrosome overduplication. *EMBO J.* 19, 2069-2081.

Norden, C., Young, S., Link, B. A. and Harris, W. A. (2009). Actomyosin is the main driver of interkinetic nuclear migration in the retina. *Cell* 138, 1195-1208.

Nourse, J., Firpo, E., Flanagan, W. M., Coats, S., Polyak, K., Lee, M. H., Massague, J., Crabtree, G. R. and Roberts, J. M. (1994). Interleukin-2-mediated elimination of the p27Kip1 cyclin-dependent kinase inhibitor prevented by rapamycin. *Nature* 372, 570-573.

Nowakowski, R. S., Lewin, S. B. and Miller, M. W. (1989). Bromodeoxyuridine immunohistochemical determination of the lengths of the cell cycle and the DNA-synthetic phase for an anatomically defined population. *J. Neurocytol.* 18, 311-318.

O'Rahilly, R. and Muller, F. (2002). The two sites of fusion of the neural folds and the two neuropores in the human embryo. *Teratology* 65, 162-170.

Olson, M. F., Paterson, H. F. and Marshall, C. J. (1998). Signals from Ras and Rho GTPases interact to regulate expression of p21Waf1/Cip1. *Nature* 394, 295-299.

Pagano, M., Tam, S. W., Theodoras, A. M., Beer-Romero, P., Del, S. G., Chau, V., Yew, P. R., Draetta, G. F. and Rolfe, M. (1995). Role of the ubiquitin-proteasome pathway in regulating abundance of the cyclin-dependent kinase inhibitor p27. *Science* 269, 682-685.

Pai, Y. J., Abdullah, N. L., Mohd-Zin, S. W., Mohammed, R. S., Rolo, A., Greene, N. D., Abdul-Aziz, N. M. and Copp, A. J. (2012). Epithelial fusion during neural tube morphogenesis. *Birth Defects Res. A Clin. Mol. Teratol.* 94, 817-823.

Pajalunga, D., Mazzola, A., Salzano, A. M., Biferi, M. G., De, L. G. and Crescenzi, M. (2007). Critical requirement for cell cycle inhibitors in sustaining nonproliferative states. *J. Cell Biol* 176, 807-818.

Parker, S. B., Eichele, G., Zhang, P., Rawls, A., Sands, A. T., Bradley, A., Olson, E. N., Harper, J. W. and Elledge, S. J. (1995). p53-Independent Expression of p21^{Cip1} in Muscle and Other Terminally Differentiating Cells. *Science* 267, 1024-1027.

Parry, D., Bates, S., Mann, D. J. and Peters, G. (1995). Lack of cyclin D-Cdk complexes in Rb-negative cells correlates with high levels of p16INK4/MTS1 tumour suppressor gene product. *EMBO J.* 14, 503-511.

Patten, I., Kulesa, P., Shen, M. M., Fraser, S. and Placzek, M. (2003). Distinct modes of floor plate induction in the chick embryo. *Development* 130, 4809-4821.

Patterson, A. D., Hildesheim, J., Fornace, A. J. and Hollander, M. C. (2006). Neural tube development requires the cooperation of p53- and Gadd45a-associated pathways. *Birth Defects Research Part A: Clinical and Molecular Teratology* 76, 129-132.

Phadke, M. S., Krynetskaia, N. F., Mishra, A. K. and Krynetskiy, E. (2009). Glyceraldehyde 3-phosphate dehydrogenase depletion induces cell cycle arrest and resistance to antimetabolites in human carcinoma cell lines. *J. Pharmacol. Exp. Ther.* 331, 77-86.

Placzek, M. and Briscoe, J. (2005). The floor plate: multiple cells, multiple signals. *Nat. Rev. Neurosci.* 6, 230-240.

Polyak, K., Kato, J. Y., Solomon, M. J., Sherr, C. J., Massague, J., Roberts, J. M. and Koff, A. (1994a). p27Kip1, a cyclin-Cdk inhibitor, links transforming growth factor-beta and contact inhibition to cell cycle arrest. *Genes Dev.* 8, 9-22.

Polyak, K., Lee, M. H., Erdjument-Bromage, H., Koff, A., Roberts, J. M., Tempst, P. and Massague, J. (1994b). Cloning of p27Kip1, a cyclin-dependent kinase inhibitor and a potential mediator of extracellular antimitogenic signals. *Cell* 78, 59-66.

Pomerantz, J., Schreiber-Agus, N., Liegeois, N. J., Silverman, A., Alland, L., Chin, L., Potes, J., Chen, K., Orlow, I., Lee, H. W. et al. (1998). The Ink4a tumor

suppressor gene product, p19Arf, interacts with MDM2 and neutralizes MDM2's inhibition of p53. *Cell* 92, 713-723.

Pyrgaki, C., Trainor, P., Hadjantonakis, A. K. and Niswander, L. (2010). Dynamic imaging of mammalian neural tube closure. *Dev. Biol.* 344, 941-947.

Quelle, D. E., Zindy, F., Ashmun, R. A. and Sherr, C. J. (1995). Alternative reading frames of the INK4a tumor suppressor gene encode two unrelated proteins capable of inducing cell cycle arrest. *Cell* 83, 993-1000.

Quinn, J. C., Molinek, M., Martynoga, B. S., Zaki, P. A., Faedo, A., Bulfone, A., Hevner, R. F., West, J. D. and Price, D. J. (2007). Pax6 controls cerebral cortical cell number by regulating exit from the cell cycle and specifies cortical cell identity by a cell autonomous mechanism. *Dev. Biol.* 302, 50-65.

Roy, S., Kaur, M., Agarwal, C., Tecklenburg, M., Sclafani, R. A. and Agarwal, R. (2007). p21 and p27 induction by silibinin is essential for its cell cycle arrest effect in prostate carcinoma cells. *Mol. Cancer Ther.* 6, 2696-2707.

Sadler, T. W., Greenberg, D., Coughlin, P. and Lessard, J. L. (1982). Actin distribution patterns in the mouse neural tube during neurulation. *Science* 215, 172-174.

Sauer, F. C. (1935). Mitosis in the neural tube. *The Journal of Comparative Neurology* 62, 377-405.

Sauer, M. E. and Walker, B. E. (1959). Radioautographic study of interkinetic nuclear migration in the neural tube. *Proc. Soc. Exp. Biol. Med.* 101, 557-560.

Saunders, T. and Margo, C. E. (2012). Intraocular medulloepithelioma. *Arch. Pathol. Lab Med.* 136, 212-216.

Schenk, J., Wilsch-Brauninger, M., Calegari, F. and Huttner, W. B. (2009). Myosin II is required for interkinetic nuclear migration of neural progenitors. *Proc. Natl. Acad. Sci. U. S. A* 106, 16487-16492.

Schoenwolf, G. C. (1984). Histological and ultrastructural studies of secondary neurulation in mouse embryos. *Am. J. Anat.* 169, 361-376.

Schoenwolf, G. C. (1988). Microsurgical analyses of avian neurulation: separation of medial and lateral tissues. *J. Comp Neurol.* 276, 498-507.

Schoenwolf, G. C., Folsom, D. and Moe, A. (1988). A reexamination of the role of microfilaments in neurulation in the chick embryo. *Anat. Rec.* 220, 87-102.

Schoenwolf, G. C. and Franks, M. V. (1984). Quantitative analyses of changes in cell shapes during bending of the avian neural plate. *Dev. Biol* 105, 257-272.

Schoenwolf, G. C. and Smith, J. L. (1990). Mechanisms of neurulation: traditional viewpoint and recent advances. *Development* 109, 243-270.

Schwaller, J., Koeffler, H. P., Niklaus, G., Loetscher, P., Nagel, S., Fey, M. F. and Tobler, A. (1995). Posttranscriptional stabilization underlies p53-independent induction of p21WAF1/CIP1/SDI1 in differentiating human leukemic cells. *J. Clin. Invest* 95, 973-979.

Selleck, M. A. and Stern, C. D. (1991). Fate mapping and cell lineage analysis of Hensen's node in the chick embryo. *Development* 112, 615-626.

Serrano, M., Lee, H., Chin, L., Cordon-Cardo, C., Beach, D. and DePinho, R. A. (1996). Role of the INK4a locus in tumor suppression and cell mortality. *Cell* 85, 27-37.

Sherr, C. J. and Roberts, J. M. (1999). CDK inhibitors: positive and negative regulators of G1-phase progression. *Genes & Development* 13, 1501-1512.

Shibui, S., Hoshino, T., Vanderlaan, M. and Gray, J. W. (1989). Double labeling with iodo- and bromodeoxyuridine for cell kinetics studies. *J. Histochem. Cytochem.* 37, 1007-1011.

Shum, A. S. and Copp, A. J. (1996). Regional differences in morphogenesis of the neuroepithelium suggest multiple mechanisms of spinal neurulation in the mouse. *Anat. Embryol. (Berl)* 194, 65-73.

Sidman, R. L., Miale, I. L. and Feder, N. (1959). Cell proliferation and migration in the primitive ependymal zone: an autoradiographic study of histogenesis in the nervous system. *Exp. Neurol.* 1, 322-333.

Smith, J. L. and Schoenwolf, G. C. (1987). Cell cycle and neuroepithelial cell shape during bending of the chick neural plate. *Anat. Rec.* 218, 196-206.

Smith, J. L. and Schoenwolf, G. C. (1988). Role of cell-cycle in regulating neuroepithelial cell shape during bending of the chick neural plate. *Cell Tissue Res.* 252, 491-500.

Smith, J. L. and Schoenwolf, G. C. (1989). Notochordal induction of cell wedging in the chick neural plate and its role in neural tube formation. *J. Exp. Zool.* 250, 49-62.

Smith, J. L., Schoenwolf, G. C. and Quan, J. (1994). Quantitative analyses of neuroepithelial cell shapes during bending of the mouse neural plate. *J. Comp Neurol.* 342, 144-151.

Spear, P. C. and Erickson, C. A. (2012a). Apical movement during interkinetic nuclear migration is a two-step process. *Dev. Biol.* 370, 33-41.

Spear, P. C. and Erickson, C. A. (2012b). Interkinetic nuclear migration: a mysterious process in search of a function. *Dev. Growth Differ.* 54, 306-316.

Starostina, N. G. and Kipreos, E. T. (2012). Multiple degradation pathways regulate versatile CIP/KIP CDK inhibitors. *Trends Cell Biol* 22, 33-41.

Stern, C. D., Charite, J., Deschamps, J., Duboule, D., Durston, A. J., Kmita, M., Nicolas, J. F., Palmeirim, I., Smith, J. C. and Wolpert, L. (2006). Head-tail patterning of the vertebrate embryo: one, two or many unresolved problems? *Int. J. Dev. Biol.* 50, 3-15.

Stoll, C., Dott, B., Alembik, Y. and Roth, M. P. (2011). Associated malformations among infants with neural tube defects. *Am. J. Med. Genet. A* 155A, 565-568.

Stone, S., Jiang, P., Dayananth, P., Tavtigian, S. V., Katcher, H., Parry, D., Peters, G. and Kamb, A. (1995). Complex structure and regulation of the P16 (MTS1) locus. *Cancer Res.* 55, 2988-2994.

Susaki, E. and Nakayama, K. I. (2009). Functional similarities and uniqueness of p27 and p57: insight from a knock-in mouse model. *cc* 8, 2497-2501.

Suzuki, T., Higgins, P. J. and Crawford, D. R. (2000). Control selection for RNA quantitation. *Biotechniques* 29, 332-337.

Suzuki-Hirano, A., Ogawa, M., Kataoka, A., Yoshida, A. C., Itoh, D., Ueno, M., Blackshaw, S. and Shimogori, T. (2011). Dynamic spatiotemporal gene expression in embryonic mouse thalamus. *J. Comp Neurol.* 519, 528-543.

Takahashi, T., Nowakowski, R. S. and Caviness, V. S., Jr. (1995). The cell cycle of the pseudostratified ventricular epithelium of the embryonic murine cerebral wall. *J. Neurosci.* 15, 6046-6057.

Tam, P. P. and Behringer, R. R. (1997). Mouse gastrulation: the formation of a mammalian body plan. *Mech. Dev.* 68, 3-25.

Tanaka, H., Yamashita, T., Asada, M., Mizutani, S., Yoshikawa, H. and Tohyama, M. (2002). Cytoplasmic p21(Cip1/WAF1) regulates neurite remodeling by inhibiting Rho-kinase activity. *J. Cell Biol.* 158, 321-329.

Tateishi, Y., Matsumoto, A., Kanie, T., Hara, E., Nakayama, K. and Nakayama, K. I. (2012). Development of mice without Cip/Kip CDK inhibitors. *Biochem. Biophys. Res. Commun.* 427, 285-292.

Toyoshima, H. and Hunter, T. (1994). p27, a novel inhibitor of G1 cyclin-Cdk protein kinase activity, is related to p21. *Cell* 78, 67-74.

Tsai, J. W., Lian, W. N., Kemal, S., Kriegstein, A. R. and Vallee, R. B. (2010). Kinesin 3 and cytoplasmic dynein mediate interkinetic nuclear migration in neural stem cells. *Nat. Neurosci.* 13, 1463-1471.

Tury, A., Mairet-Coello, G. and Dicicco-Bloom, E. (2011). The cyclin-dependent kinase inhibitor p57Kip2 regulates cell cycle exit, differentiation, and migration of embryonic cerebral cortical precursors. *Cereb. Cortex* 21, 1840-1856.

Tzouanacou, E., Wegener, A., Wymeersch, F. J., Wilson, V. and Nicolas, J. F. (2009). Redefining the progression of lineage segregations during mammalian embryogenesis by clonal analysis. *Dev. Cell* 17, 365-376.

Ueno, M., Katayama, K., Yamauchi, H., Nakayama, H. and Doi, K. (2006). Cell cycle progression is required for nuclear migration of neural progenitor cells. *Brain Res.* 1088, 57-67.

Vaccarello, G., Figliola, R., Cramerotti, S., Novelli, F. and Maione, R. (2006). p57Kip2 is induced by MyoD through a p73-dependent pathway. *J. Mol. Biol.* 356, 578-588.

Van Allen, M. I., Kalousek, D. K., Chernoff, G. F., Juriloff, D., Harris, M., McGillivray, B. C., Yong, S. L., Langlois, S., MacLeod, P. M., Chitayat, D. et al. (1993). Evidence for multi-site closure of the neural tube in humans. *Am. J. Med. Genet.* 47, 723-743.

van Straaten, H. W., Hekking, J. W., Consten, C. and Copp, A. J. (1993). Intrinsic and extrinsic factors in the mechanism of neurulation: effect of curvature of the body axis on closure of the posterior neuropore. *Development* 117, 1163-1172.

van Straaten, H. W., Hekking, J. W., Wiertz-Hoessels, E. J., Thors, F. and Drukker, J. (1988). Effect of the notochord on the differentiation of a floor plate area in the neural tube of the chick embryo. *Anat. Embryol. (Berl)* 177, 317-324.

Vega, C. J. and Peterson, D. A. (2005). Stem cell proliferative history in tissue revealed by temporal halogenated thymidine analog discrimination. *Nat. Methods* 2, 167-169.

Wang, D., Moothart, D. R., Lowy, D. R. and Qian, X. (2013). The expression of glyceraldehyde-3-phosphate dehydrogenase associated cell cycle (GACC) genes correlates with cancer stage and poor survival in patients with solid tumors. *PLoS. One.* 8, e61262.

Watanabe, H., Pan, Z. Q., Schreiber-Agus, N., DePinho, R. A., Hurwitz, J. and Xiong, Y. (1998). Suppression of cell transformation by the cyclin-dependent kinase inhibitor p57KIP2 requires binding to proliferating cell nuclear antigen. *Proceedings of the National Academy of Sciences* 95, 1392-1397.

Weber, J. D., Hu, W., Jefcoat, S. C., Jr., Raben, D. M. and Baldassare, J. J. (1997). Ras-stimulated extracellular signal-related kinase 1 and RhoA activities coordinate platelet-derived growth factor-induced G1 progression through the independent regulation of cyclin D1 and p27. *J. Biol. Chem.* 272, 32966-32971.

Westbury, J., Watkins, M., Ferguson-Smith, A. C. and Smith, J. (2001). Dynamic temporal and spatial regulation of the cdk inhibitor p57kip2 during embryo morphogenesis. *Mechanisms of Development* 109, 83-89.

Wilkinson, D. G., Bhatt, S. and Herrmann, B. G. (1990). Expression pattern of the mouse T gene and its role in mesoderm formation. *Nature* 343, 657-659.

Wilson, V., Olivera-Martinez, I. and Storey, K. G. (2009). Stem cells, signals and vertebrate body axis extension. *Development* 136, 1591-1604.

Wu, H., Wade, M., Krall, L., Grisham, J., Xiong, Y. and Van, D. T. (1996). Targeted in vivo expression of the cyclin-dependent kinase inhibitor p21 halts hepatocyte cell-cycle progression, postnatal liver development and regeneration. *Genes Dev.* 10, 245-260.

Wu, X., Gu, X., Han, X., Du, A., Jiang, Y., Zhang, X., Wang, Y., Cao, G. and Zhao, C. (2014). A novel function for Foxm1 in interkinetic nuclear migration in the developing telencephalon and anxiety-related behavior. *J. Neurosci.* 34, 1510-1522.

Xiong, Y., Zhang, H. and Beach, D. (1992). D type cyclins associate with multiple protein kinases and the DNA replication and repair factor PCNA. *Cell* 71, 505-514.

Yan, Y., Fris+®n, J., Lee, M. H., Massagu+®, J. and Barbacid, M. (1997). Ablation of the CDK inhibitor p57Kip2 results in increased apoptosis and delayed differentiation during mouse development. *Genes & Development* 11, 973-983.

Ybot-Gonzalez, P., Cogram, P., Gerrelli, D. and Copp, A. J. (2002). Sonic hedgehog and the molecular regulation of mouse neural tube closure. *Development* 129, 2507-2517.

Ybot-Gonzalez, P. and Copp, A. J. (1999). Bending of the neural plate during mouse spinal neurulation is independent of actin microfilaments. *Dev. Dyn.* 215, 273-283.

Ybot-Gonzalez, P., Gaston-Massuet, C., Girdler, G., Klingensmith, J., Arkell, R., Greene, N. D. and Copp, A. J. (2007a). Neural plate morphogenesis during mouse neurulation is regulated by antagonism of Bmp signalling. *Development* 134, 3203-3211.

Ybot-Gonzalez, P., Savery, D., Gerrelli, D., Signore, M., Mitchell, C. E., Faux, C. H., Greene, N. D. and Copp, A. J. (2007b). Convergent extension, planar-cell-polarity signalling and initiation of mouse neural tube closure. *Development* 134, 789-799.

Yokoo, T., Toyoshima, H., Miura, M., Wang, Y., Iida, K. T., Suzuki, H., Sone, H., Shimano, H., Gotoda, T., Nishimori, S. et al. (2003). p57Kip2 regulates actin dynamics by binding and translocating LIM-kinase 1 to the nucleus. *J. Biol. Chem.* 278, 52919-52923.

Yu, J., Lei, K., Zhou, M., Craft, C. M., Xu, G., Xu, T., Zhuang, Y., Xu, R. and Han, M. (2011). KASH protein Syne-2/Nesprin-2 and SUN proteins SUN1/2 mediate nuclear migration during mammalian retinal development. *Hum. Mol. Genet.* 20, 1061-1073.

Zacksenhaus, E., Jiang, Z., Chung, D., Marth, J. D., Phillips, R. A. and Gallie, B. L. (1996). pRb controls proliferation, differentiation, and death of skeletal muscle cells and other lineages during embryogenesis. *Genes Dev.* 10, 3051-3064.

Zhang, J., Gao, Q., Li, P., Liu, X., Jia, Y., Wu, W., Li, J., Dong, S., Koseki, H. and Wong, J. (2011). S phase-dependent interaction with DNMT1 dictates the role of UHRF1 but not UHRF2 in DNA methylation maintenance. *Cell Res.* 21, 1723-1739.

Zhang, P., Liegeois, N. J., Wong, C., Finegold, M., Hou, H., Thompson, J. C., Silverman, A., Harper, J. W., DePinho, R. A. and Elledge, S. J. (1997). Altered cell differentiation and proliferation in mice lacking p57KIP2 indicates a role in Beckwith-Wiedemann syndrome. *Nature* 387, 151-158.

Zhang, P., Wong, C., DePinho, R. A., Harper, J. W. and Elledge, S. J. (1998). Cooperation between the Cdk inhibitors p27(KIP1) and p57(KIP2) in the control of tissue growth and development. *Genes Dev.* 12, 3162-3167.

Zhang, P., Wong, C., Liu, D., Finegold, M., Harper, J. W. and Elledge, S. J. (1999). p21(CIP1) and p57(KIP2) control muscle differentiation at the myogenin step. *Genes Dev.* 13, 213-224.

Zindy, F., Quelle, D. E., Roussel, M. F. and Sherr, C. J. (1997a). Expression of the p16INK4a tumor suppressor versus other INK4 family members during mouse development and aging. *Oncogene* 15, 203-211.

Zindy, F., Soares, H., Herzog, K. H., Morgan, J., Sherr, C. J. and Roussel, M. F. (1997b). Expression of INK4 inhibitors of cyclin D-dependent kinases during mouse brain development. *Cell Growth Differ.* 8, 1139-1150.

Zohn, I. E., Chesnutt, C. R. and Niswander, L. (2003). Cell polarity pathways converge and extend to regulate neural tube closure. *Trends Cell Biol.* 13, 451-454.

Zwaan, J., Bryan, P. R., Jr. and Pearce, T. L. (1969). Interkinetic nuclear migration during the early stages of lens formation in the chicken embryo. *J. Embryol. Exp. Morphol.* 21, 71-83.